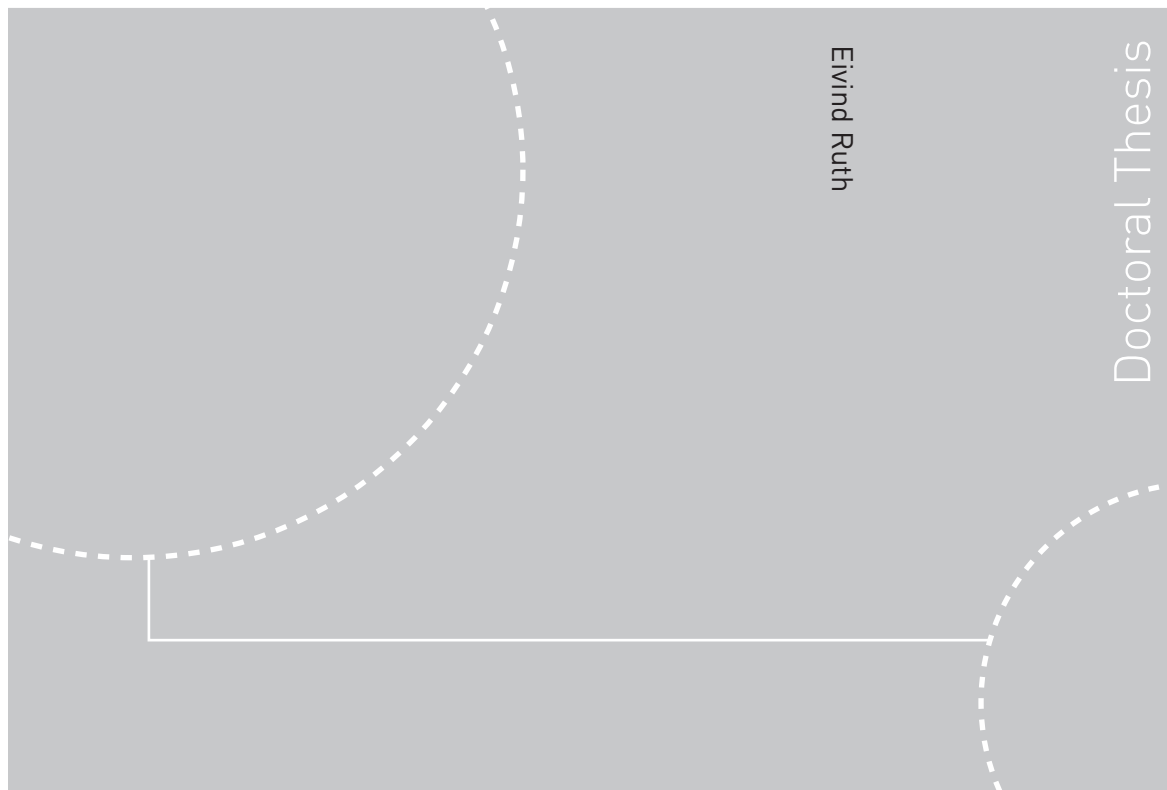


ISBN 978-82-471-1090-4 (printed ver.)
ISBN 978-82-471-1091-1 (electronic ver.)
ISSN 1503-8181



Theses at NTNU, 2008:203

NTNU
Norwegian University of
Science and Technology
Thesis for the degree of
philosophiae doctor
Faculty of Engineering Science and Technology
Department of Marine Technology

Doctoral Theses at NTNU, 2008:203

Eivind Ruth

Propulsion control and thrust allocation on marine vessels

Eivind Ruth

Propulsion control and thrust allocation on marine vessels

Thesis for the degree of philosophiae doctor

Trondheim, October 2008

Norwegian University of
Science and Technology
Faculty of Engineering Science and Technology
Department of Marine Technology



Norwegian University of
Science and Technology

NTNU
Norwegian University of Science and Technology

Thesis for the degree of philosophiae doctor

Faculty of Engineering Science and Technology
Department of Marine Technology

©Eivind Ruth

ISBN 978-82-471-1090-4 (printed ver.)
ISBN 978-82-471-1091-1 (electronic ver.)
ISSN 1503-8181

Theses at NTNU, 2008:203

Printed by Tapir Uttrykk

Abstract

The high demand for oil and gas at the world markets, motivates exploration and exploitation at continuously increasing water depths. A consequence of this development is the increased use of dynamic positioning (DP) systems and thruster assisted position mooring (PM) systems on vessels for maintaining a fixed position. Such systems uses thrusters actively for maintaining position, as opposed to passive mooring systems. The continuous demand for improved positioning accuracy, safety and efficiency in such systems have motivated this thesis. Such improvements may lead to e.g. increased operability in harsh weather, reduced risk of oil spill, reduced bunker costs and reduced CO₂ emissions. This thesis addresses the topics propulsion control and thrust allocation. These are the actuators of the DP controller, and hence vital for the overall station keeping performance. A natural extension of the work on propulsion control has been to include results on propulsion control for ocean crossing merchant vessels, where the efficiency is particularly important to reduce costs and CO₂ emissions.

The efforts on propulsion control are directed towards screw propellers, as this is the most commonly used thrust production device. The environmental, measurement, and modeling differences in the propulsion control problem for surface vessels at low speed maneuvering and in transit are examined. A set of different low level propulsion controllers for surface vessels are compared with regards to efficiency and thrust sensitivity. The thrust sensitivity is the produced to desired thrust ratio, and is important for the positioning accuracy of the vessel. The controller comparison is based on a new proposed nondimensional parameter τ , which makes it possible to compare different propulsion systems producing the same thrust in equal environments (equal advance speed and thrust) as function of this parameter only. This new τ parameter can also be used to determine the optimal propeller diameter and the optimal pitch ratio for a particular propeller.

In severe weather conditions, thrusters may experience large and rapid changes in the propeller loading due to ventilation and in-and-out-of water effects. When a thruster ventilates, air is sucked down from the surface and into the propeller. In more severe cases, part or even the whole propeller can be out of water. These losses vary rapidly with time, and cause increased wear and tear in addition to reduced thrust production performance. This leads to reduced safety, efficiency and positioning accuracy in station keeping operations. Measures to locally counteract these negative effects are denoted anti-spin thruster control. To be able to design and verify such controllers, models of the losses are needed. In

this thesis, experiments with ventilating consolidated controlled propellers are presented. Scaling laws for ventilating propellers are discussed. The results are used to develop a ventilation model for use in simulations. The model is verified by comparing simulations with time series from experiments. As regards anti-spin thruster control, the pitch actuator is found unsuitable for providing rapid response to the ventilation and in-and-out-of water incidents on consolidated controlled propellers. Instead, it is suggested that a slightly modified version of the fixed pitch propeller anti-spin thruster controller is used. It is also found that reducing the pitch ratio (at the sacrifice of increasing the shaft speed) will decrease the likelihood and severity of ventilation on consolidated controlled propellers, hence improving efficiency, safety and positioning accuracy.

Vessels conducting safety critical positioning operations are usually equipped with redundant thruster configurations. This is done in order to reduce the consequences of thruster failures and hence increase the safety. On such vessels, it is common to use a thrust allocation system in order to distribute the control actions determined by the DP controller among the thrusters. A method for thrust allocation based on a linearly constrained quadratic cost function capable of handling rotating azimuths is presented. The problem formulation accounts for convex magnitude and rate constraints on both thruster forces and azimuth directions. Experiments with a model ship are used to validate the thrust allocation system. Suggestions on how to take power constraints on power busses and total power into account are presented. An anti-spin thrust allocation strategy is proposed in order to reduce the effects and the possibility of ventilation and in-and-out-of water events. The proposed strategy results in significant power savings (increased efficiency), major reductions in torque and power fluctuations (improved safety) and improved positioning accuracy. The performance of the proposed allocation strategy is demonstrated by experiments with a model ship. A solution to the thrust allocation problem with nonconvex directional constraints by use of switched thrust allocation is presented. Switched thrust allocation is also used in order to adapt to changing environmental disturbances and handling thruster failures in order to increase both efficiency, accuracy and safety. The presented cases with switched thrust allocation are demonstrated by model scale experiments.

Optimization of the power consumption in thrust allocation tend to rotate the thrusters into near singular configurations. This significantly reduces the ability to rapidly and efficiently produce forces in all directions, hence reducing both positioning accuracy, efficiency and safety. On marine vessels azimuthing thrusters are often capable of producing thrust in positive direction only. It is in this thesis proposed a way to measure the degree of singularity for vessels with one or more thrusters only capable of producing positive thruster forces. A design loop for thruster configurations, focusing on maneuverability is presented. The method takes any single thruster or power bus failure into account. It is further shown how the minimum gain direction can be determined and visualized. A way of doing singularity avoidance in real time is presented. Experimental results demonstrating the theory and singularity avoidance in real time are presented.

Acknowledgements

This thesis is the results of my doctoral studies from August 2005 until July 2008. The work has been carried out at the Centre for Ships and Ocean Structures (CeSOS), sponsored by The Research Council of Norway, at Norwegian University of Science and Technology.

This thesis is a result of many years of collaboration between my main supervisor Professor Asgeir J. Sørensen and myself. Asgeir persuaded me into taking a PhD and has during my education provided excellent guidance. Foremost he has contributed to defining the problems and presenting the solutions in a readable manner. My co-supervisors Dr. Tristan Perez and Professor Mogens Blanke are also acknowledged for help and support. In addition to my supervisors, Dr. Øyvind N. Smogeli has provided excellent guidance, particularly during my Master thesis, giving me a flying start on the PhD.

The work of the lab technicians Torgeir, Kunt Arne and Stefano are greatly appreciated. Without their help, the extensive use of model tests as part of this thesis would not have been possible. In that connection, also Dong should be acknowledged for providing initial parameters for the control system on CyberShip III. His help surely saved me a lot of time when tuning the control system.

Sharing office with Trygve and David has certainly helped me keep up the spirit while working on my PhD. I also highly appreciate the many technical discussions we have had. Certainly I have learned a lot from them. I will also like to thank my colleagues at CeSOS and Department of Marine Technology all contributing to make the Marine Technology Centre an interesting workplace.

I would very much like to thank my parents for providing an excellent foundation for my education. Their continuous support and interest have always been an inspiration. They have also contributed significantly to my basic technical skills, in particular my mother teaching me mathematics and my father teaching me physics.

Last but not least I would like to thank my wife for her continuous and unconditional support throughout the work.

Contents

Abstract	iii
Acknowledgement	v
Nomenclature	xi
1 Introduction	1
1.1 Background	1
1.2 Motivation and objectives	5
1.3 Contributions	6
1.4 List of publications	7
1.5 Outline of thesis	8
2 Propeller models	11
2.1 Scaling laws	11
2.1.1 The non-ventilated regime	15
2.1.2 The fully ventilated regime	15
2.1.3 The partially ventilated regime	16
2.1.4 Effect of Weber's number	16
2.2 Normal operating conditions	17
2.2.1 The τ parameter	17
2.2.2 Experimental propeller with duct	19
2.2.3 Multi quadrant variable pitch models from literature	20
2.3 Ventilation and in-and-out of water effects	26
2.3.1 The stationary model	26
2.3.2 Extension to a dynamic model	28
2.3.3 Simulations verified by open water experiments	30
2.3.4 Implications for control	33
3 Propulsion control for surface vessels	37
3.1 Surface vessels versus underwater vehicles	38
3.2 Low advance speed	39
3.2.1 Advance speed measurement at low advance speeds	39
3.2.2 Optimal control at low advance speeds	40
3.3 Moderate/high advance speeds	41

3.3.1	Advance speed measurements at moderate/high advance speeds	41
3.3.2	Optimal control at moderate/high advance speeds	41
3.4	Propulsion controllers	43
3.4.1	Propellers with one controllable variable	43
3.4.2	Propellers with two controllable variables	46
3.4.3	Low level anti-spin thruster control	51
3.5	Sensitivity functions	53
3.5.1	Shaft speed control	54
3.5.2	Torque control	54
3.5.3	Power control	55
3.5.4	Combined control	56
3.5.5	Pitch control	57
3.5.6	Torque/shaft speed control	57
3.5.7	Comparison of sensitivity functions	58
3.6	Comparison of optimal performance	61
3.7	Simulations	63
4	The thrust allocation problem	67
4.1	Cost functions	68
4.2	Constraints	69
4.3	Previously presented solutions	70
4.4	Convex linearly constrained quadratic thrust allocation	72
4.4.1	The thrust allocation problem with thruster forces in cylindrical coordinates	73
4.4.2	The thrust allocation problem with thruster forces in Cartesian coordinates	74
4.4.3	Power constraints	79
4.5	Experimental validation	82
4.5.1	Run A: Station keeping, convex	82
4.5.2	Run B: Joystick, convex	84
4.5.3	Summary experiments	86
5	Anti-spin thrust allocation	87
5.1	Cost function with $\mathbf{T}^{3/2}$	88
5.2	Modification of the cost due to ventilation and in-and-out of water events	91
5.3	Experimental validation	94
5.3.1	Run C: Anti-spin thrust allocation, thrust redistribution	94
5.3.2	Run D: Anti-spin thrust allocation, power saving	95
5.3.3	Run E: Anti-spin thrust allocation, positioning performance	97
5.3.4	Summary experiments	101

6 Switching in thrust allocation	105
6.1 Controller operating conditions	106
6.2 Supervisory control	107
6.3 Switching	108
6.4 Examples on switched thrust allocation	109
6.4.1 Nonconvex linearly constrained quadratic thrust allocation - Mixed integer solution	109
6.4.2 Switching between fixed and rotating thrusters	113
6.4.3 Thruster failures	114
6.5 Experimental results	114
6.5.1 Run F: Maneuvering, nonconvex	114
6.5.2 Run G: Switching between fixed and rotating thrusters	115
6.5.3 Run H: Thrust failures	117
6.5.4 Run I: Azimuth failures	119
6.5.5 Summary experiments	123
7 Singularity avoidance	125
7.1 Scaling the thruster configuration matrix	126
7.2 Local and global singularity	127
7.3 Fixed bidirectional thrusters	129
7.4 Fixed unidirectional thrusters	130
7.5 Avoiding singularities during design	139
7.5.1 Bidirectional thrusters	140
7.5.2 Unidirectional thrusters	141
7.5.3 During faults	143
7.5.4 Design loop	143
7.6 Example with CyberShip III	145
7.6.1 Fixed bidirectional thrusters	145
7.6.2 Fixed unidirectional thrusters	154
7.6.3 Freely rotating thrusters	154
7.7 Singularity monitoring	158
7.7.1 Monitoring singular direction	159
7.8 Real time singularity avoidance	160
7.8.1 Avoiding small minimum gains	162
7.9 Experimental validation of singularity avoidance in real time	163
7.9.1 Run J: Minimum attainable set	163
7.9.2 Run K: Avoiding small minimum gains	164
7.9.3 Summary experiments	168
8 Conclusions and recommendations	169
8.1 Conclusions	169
8.2 Recommendations for future work	171
Bibliography	173
A Experimental setup: Open water experiments	183

B Experimental setup: CyberShip III	187
B.1 Wave maker	187
B.2 Measurements	187
B.2.1 Position measurement	187
B.2.2 Power measurements	188
B.3 Control systems	189
B.3.1 Position and velocity observer	190
B.3.2 Reference generator	193
B.3.3 PID motion controller	193
B.3.4 Thrust allocator	194
B.3.5 Thruster control	194
B.3.6 Azimuth direction controller	194
B.3.7 Ventilation detection	195
C Experimental Results: CyberShip III	197
C.1 Run A: Station keeping, convex.	198
C.2 Run C: Anti-spin thrust allocation, thrust redistribution	200
C.3 Run D: Anti-spin thrust allocation, power saving	200
C.4 Run E: Anti-spin thrust allocation, positioning performance	202
C.5 Run F: Maneuvering, nonconvex.	204
C.6 Run G: Switching between fixed and rotating thrusters	205
C.7 Run H: Thrust failures	206
C.8 Run I: Azimuth failures	206
C.9 Run J: Minimum attainable set	208
C.10 Run K: Avoiding small minimum gains	210
D Convergence of modified cost function	213
D.1 Finding the equilibrium analytically	213
D.2 The iterative solution	215
D.2.1 Finding the equilibrium	216
D.2.2 Convergence	217

Nomenclature

Abbreviations

c	Combined control
CO ₂	Carbon dioxide
CS3	CyberShip III
D-term	Derivative term
DP	Dynamic positioning
FPP	Fixed pitch propeller
GPS	Global positioning system
I-gain	Integrator gain
I-term	Integrator term
IMO	International Maritime Organization
LQG	Linear quadratic Gaussian
n	Shaft speed control
np	Shaft speed/pitch ratio control
p	Power control
pd	Pitch control
P-term	Proportional term
PhD	Philosophiae doctor
PID	Proportional-integral-derivative
PM	Thruster assisted position mooring
q	Torque control
qn	Torque/shaft speed control
qp	Torque/pitch ratio control
SWATH	Small water plane area twin hull

Lowercase

a	[–]	Constant
a	[–]	Number of inequality constraint
a_+	[–]	Ventilation model parameter
a_-	[–]	Ventilation model parameter
$a_{0.2+}$	[–]	Ventilation model parameter
$a_{0.2-}$	[–]	Ventilation model parameter
$a_{0.8+}$	[–]	Ventilation model parameter

$a_{0.8-}$	$[-]$	Ventilation model parameter
a_Q	$[-]$	Constant
a_T	$[-]$	Constant
a_q	$[-]$	Ventilation model parameter
a	$[-]$	Weighting vector
b	$[-]$	Constant
b_+	$[-]$	Ventilation model parameter
b_-	$[-]$	Ventilation model parameter
$b_{0.2+}$	$[-]$	Ventilation model parameter
$b_{0.2-}$	$[-]$	Ventilation model parameter
$b_{0.8+}$	$[-]$	Ventilation model parameter
$b_{0.8-}$	$[-]$	Ventilation model parameter
b_Q	$[-]$	Constant
b_T	$[-]$	Constant
b_q	$[-]$	Ventilation model parameter
b	$[N]$	Inequality constraint vector
b	$[-]$	Weighting vector
c	$[m]$	Cord length of the propeller blade at $0.7R$
c_1	$[-]$	Constant
c_2	$[-]$	Constant
$d\omega$	$[-]$	Frequency band (used in power and torque spectrum)
f	$[m/s]$	Function
g	$[m/s^2]$	Gravity
g	$[-]$	Mapping from K_{Td} to P/D_{pd}
h	$[m]$	Submergence of propeller shaft
h	$[Nm]$	Mapping from τ to desired torque
h/R	$[-]$	Submergence ratio
h_m	$[m]$	Submergence of propeller shaft in model scale
h_s	$[m]$	Submergence of propeller shaft in full scale
i	$[-]$	Vector element index
j	$[-]$	Vector element index
k	$[kgm]$	Constant
k	$[-]$	Parameter
k	$[-]$	Mapping from τ to P/D_{cqp}
k	$[-]$	Index for different time steps
k	$[-]$	Constant
m	$[Hz]$	Mapping from τ to n_d
m	$[-]$	Number of controlled degrees of freedom
m	$[-]$	Constant
m	$[W/N^{3/2}]$	Constant vector
n	$[Hz]$	Shaft speed in revolutions per second
n	$[-]$	Number of thrusters
n_{min}	$[Hz]$	Minimum shaft speed for detection of ventilation start
n_c	$[-]$	Number of constraints
n_d	$[-]$	Desired shaft speed
n_f	$[-]$	Number of fixed thrusters
n_m	$[Hz]$	Shaft speed in model scale in revolutions per second

n_p	[–]	Number of unidirectional thrusters
n_r	[–]	Number of rotating thrusters
n_s	[Hz]	Shaft speed in full scale in revolutions per second
\mathbf{n}_1	[–]	Thruster force direction when $\alpha_j = 0[\text{deg}]$
\mathbf{n}_2	[–]	Thruster force direction when $\alpha_j = 90[\text{deg}]$
\mathbf{n}_{RAW}	[Hz]	Measured shaft speed vector
p	[s]	Parameter
p	[–]	Percentage error in calculated power
p_{atm}	[Pa]	Atmospheric pressure
p_{cav}	[Pa]	Pressure in cavity
p_{static}	[Pa]	Static water pressure at a given submergence
q	$[(m/kg)^{1/2}]$	Constant
r	[–]	Parameter
\mathbf{r}_j	[m]	Position vector of thruster number j in body frame
s	[N/m]	Surface tension of water
s	[1/s]	Laplace variable
sn_i	[–]	Shaft speed sensitivity for controller i
sp_i	[–]	Power sensitivity for controller i
sq_i	[–]	Torque sensitivity for controller i
st_i	[–]	Thrust sensitivity for controller i
\mathbf{s}	[N]/[Nm]	Slack variable vector
t	[–]	Thrust deduction
t	[s]	Time
t	[s]	Time since previous switching
t_2	[s]	Time σ_{\min} has been larger than σ_{\lim}
t_{\lim}	[s]	Time limit
t_{\lim}	[s]	Dwell time
u	[–]	Variable limiting the thrust
u_d	varies	Desired set point in the propulsion system
w	[–]	Wake fraction
\mathbf{x}_+	[–]	Vector of nonnegative elements
\mathbf{x}_-	[–]	Vector with some negative elements
\mathbf{x}_1	[–]	Vector of nonnegative elements
\mathbf{x}_2	[–]	Vector of nonnegative elements

Uppercase

A_0	[m^2]	Propeller disk area
A_E	[m^2]	Expanded blade area
A_{wet}	[m^2]	Wetted propeller disk area
\mathbf{A}	[–]	Inequality constraint matrix
\mathbf{A}	[–]	Matrix with nonnegative elements
\mathbf{A}	[–]	Directional constraint matrix
B_p	[–]	B_p parameter

\mathbf{B}	$[-]/[m]$	Thruster configuration matrix
\mathbf{B}_A	$[-]/[m]$	Thruster configuration matrix
\mathbf{B}_C	$[-]/[m]$	Thruster configuration matrix in Cartesian coordinates
\mathbf{B}_G	$[-]$	Nondimensional thruster configuration matrix
\mathbf{B}_M	$[-]/[m]$	Modified thruster configuration matrix
\mathbf{B}_S	$[-]$	Scaled thruster configuration matrix
\mathbf{B}_p	$[-]$	Scaled thruster configuration matrix for the unidirectional thrusters
\mathbf{B}_{pn}	$[-]$	Scaled thruster configuration matrix for the bidirectional thrusters
C_Q	$[-]$	Torque coefficient
C_{Tt}	$[-]$	Total thrust coefficient
D	$[m]$	Propeller diameter
$D_{\max O}$	$[m]$	Max. outer diameter of duct
$D_{\min O}$	$[m]$	Min. outer diameter of duct
D_{inner}	$[m]$	Inner diameter of duct
D_m	$[m]$	Propeller diameter in model scale
D_s	$[m]$	Propeller diameter in full scale
F_{nD}	$[-]$	Froude number
F_{nDm}	$[-]$	Froude number model scale
F_{nDs}	$[-]$	Froude number full scale
F_{nh2}	$[-]$	Modified Froude number
$F_{nh2}^{0.2+}$	$[-]$	Ventilation model parameter
$F_{nh2}^{0.2-}$	$[-]$	Ventilation model parameter
$F_{nh2}^{0.8+}$	$[-]$	Ventilation model parameter
$F_{nh2}^{0.8-}$	$[-]$	Ventilation model parameter
H_s	$[m]$	Significant wave height
I	$[-]$	Index of preferred subproblem solution
I_0	$[-]$	Index of preferred subproblem solution in the previous time step
I_{\min}	$[-]$	Index of subproblem with lowest cost
I_τ	$[-]$	Switching flag
$\mathbf{I}_{n \times n}$	$[-]$	Identity matrix with n rows and n columns
J	$[N^2]$	Cost function
J_A	$[-]$	Advance number
J_{Am}	$[-]$	Advance number in model scale
J_{As}	$[-]$	Advance number in full scale
J_M	$[N^{3/2}]$	Modified cost function
J_T	$[N^{3/2}]$	Part of cost function penalizing power consumption
J_{\lim}	$[N^2]$	Hysteresis limit
K_Q	$[-]$	Torque coefficient
K_{Q0}	$[-]$	Nominal torque coefficient at $J_A = 0$
K_{Qc}	$[-]$	Torque coefficient applied in the controllers
K_{Qn}	$[-]$	Nominal torque coefficient
K_{T0}	$[-]$	Nominal total thrust coefficient at $J_A = 0$
K_{Tc}	$[-]$	Total thrust coefficient applied in the controllers

K_{Td}	[–]	Desired total thrust coefficient
K_{Tn}	[–]	Nominal thrust coefficient
K_{Tt}	[–]	Total thrust coefficient
L_D	[m]	Length duct
L_m	[m]	Characteristic length in model scale
L_s	[m]	Characteristic length in full scale
L_{typ}	[m]	Average torque arm for the thrusters
\mathbf{L}_x	[m]	Vector of thruster position in x-direction
\mathbf{L}_y	[m]	Vector of thruster position in y-direction
P	[W]	Power consumption
P/D	[–]	Pitch ratio
P/D_{ci}	[–]	Commanded pitch ratio of controller i
P/D_d	[–]	Desired pitch ratio
$P_{0.7}/D$	[–]	Pitch ratio at $0.7R$
P_2	[W]	Power consumption calculated by quadratic thruster force
P_{AV}	[W]	Available power from the power plant
P_T	[W]	Estimated power consumption
P_{Td}	[W]	Total power requested from the thrust allocation problem
P_{bus}	[W]	Maximum power allowed on the power bus
P_c	[W]	Commanded power consumption from the thrust allocator after power constraints
P_{cost}	[W]	Power consumption calculated by modified approach
P_d	[W]	Desired power
$P_{m,corr}$	[W]	Corrected motor power
P_{meas}	[W]	Measured power consumption
P_m	[W]	Motor power
P_{vent}	[W]	Power consumption of ventilating thruster
\mathbf{P}_d	[W]	Desired thruster power vector
Q_{ci}	[Nm]	Commanded torque of controller i
Q_d	[Nm]	Desired torque
Q_m	[Nm]	Motor torque
Q_n	[N]	Nominal torque
Q_p	[Nm]	Propeller torque
$\dot{Q}_{m,lim}$	[Nm]	Maximum torque change during ventilation start
\mathbf{Q}	[–]/[1/m ²]	Weighting matrix
R	[m]	Propeller radius
R	[N]	Ship resistance
R_m	[m]	Propeller radius in model scale
R_n	[–]	Reynolds' number
R_s	[m]	Propeller radius in full scale
\mathbf{R}	[–]	Weighting matrix
S	[–]	Parameter
\mathbf{S}	[–]/[1/m]	Torque scaling matrix
\mathbf{S}	[–]	Singular value matrix
$\mathcal{S}_{\mathbf{T}}$	[N]	Set of admissible thruster forces

S_α	$[-]$	Set of admissible thrust directions
T	$[N]$	Total thruster force
T_D	$[N]$	Duct thrust
T_d	$[N]$	Desired thrust
T_n	$[N]$	Nominal thrust
T_p	$[N]$	Propeller thrust
T_p	$[s]$	Peak period of wave spectrum
T_t	$[N]$	Total thrust
\bar{T}_{\max}	$[N]$	Average maximum thruster force
\mathbf{T}	$[N]$	Thrust vector
\mathbf{T}_+	$[N]$	Vector of maximum thruster force in the current time step
\mathbf{T}_-	$[N]$	Vector of minimum thruster force in the current time step
\mathbf{T}_0	$[N]$	Vector of thruster force in the previous time step
\mathbf{T}_G	$[N]$	Modified extended thrust vector
\mathbf{T}_{RAW}	$[N]$	Measured thruster force vector
\mathbf{T}_{\max}	$[N]$	Maximum thrust vector
\mathbf{T}_{\min}	$[N]$	Minimum thrust vector
\mathbf{T}_c	$[N]$	Commanded thrust vector
\mathbf{T}_d	$[N]$	Desired thrust vector
$\mathbf{T}_{d,prev}$	$[N]$	Desired thruster force in previous time step vector
\mathbf{T}_f	$[-]$	Vector of maximum required thrusts
\mathbf{T}_x	$[N]$	Thrust in x-direction vector
\mathbf{T}_{xd}	$[N]$	Desired thruster force in x-direction vector
\mathbf{T}_y	$[N]$	Thrust in y-direction vector
\mathbf{T}_{yd}	$[N]$	Desired thruster force in y-direction vector
$\bar{\mathbf{T}}$	$[-]$	Nondimensional thrust vector
$\bar{\mathbf{T}}_G$	$[-]$	Nondimensional thrust vector
$\bar{\mathbf{T}}_i$	$[-]$	Nondimensional thrust vector
$\dot{\mathbf{T}}_{\max}$	$[N/s]$	Maximum rate of change of thrust vector
$\dot{\mathbf{T}}_{\min}$	$[N/s]$	Minimum rate of change of thrust vector
\mathbf{U}	$[-]$	Orthogonal matrix
V_A	$[m/s]$	Advance speed
V_{Am}	$[m/s]$	Advance speed in model scale
V_{As}	$[m/s]$	Advance speed in full scale
V_S	$[m/s]$	Ship speed
V_∞	$[m/s]$	Velocity seen by the propeller blade at $0.7R$
V_d	$[m/s]$	Desired vessel speed
\mathbf{V}	$[-]$	Orthogonal matrix
W	$[-]$	Weber's number
\mathbf{W}_u	$[-]$	Weighting matrix of thruster forces
\mathbf{W}_v	$[1/N^{1/2}]/[1/(N^{1/2}m^2)]$	Weighting matrix of generalized forces
\mathbf{X}	$[-]$	Arbitrary matrix
Y	$[-]$	Set of thrusters
Z	$[-]$	Blade number

Greek

α	[–]	Weighting function
$\alpha_{\sigma_{\min}}$	[–]	Projected direction of the most singular direction
α_i	[–]	Weighting function for controller i
$\boldsymbol{\alpha}$	[–]	Thrust direction vector
$\boldsymbol{\alpha}_+$	[–]	Vector of maximum thrust direction in the current time step
$\boldsymbol{\alpha}_-$	[–]	Vector of minimum thrust direction in the current time step
$\boldsymbol{\alpha}_0$	[–]	Vector of thrust direction in the previous time step
$\boldsymbol{\alpha}_A$	[–]	First thrust direction solution
$\boldsymbol{\alpha}_B$	[–]	Desired thrust direction in second and third step
$\boldsymbol{\alpha}_D$	[–]	Fixed thrust direction vector
$\boldsymbol{\alpha}_{RAW}$	[–]	Measured thrust direction vector
$\boldsymbol{\alpha}_d$	[–]	Desired thrust direction vector
$\boldsymbol{\alpha}_{fixed}$	[–]	Fixed thrust direction vector
$\dot{\boldsymbol{\alpha}}_{\max}$	[1/s]	Maximum rate of change of thrust direction vector
β	[–]	Advance angle
β_Q	[–]	Torque loss factor
$\beta_{Q,off}$	[–]	Torque loss factor for detection of ventilation stop
$\beta_{Q,on}$	[–]	Torque loss factor for detection of ventilation start
β_{Qw}	[–]	Torque loss factor corrected for reduced wetted propeller disk area
β_T	[–]	Total thrust loss factor
β_{Tw}	[–]	Total thrust loss factor corrected for reduced wetted propeller disk area
β_{Tw+}	[–]	Ventilation model parameter
β_{Tw-}	[–]	Ventilation model parameter
$\beta_{Tw \max}$	[–]	Maximum thrust loss factor corrected for reduced wetted propeller disk area
$\beta_{Tw \min}$	[–]	Minimum thrust loss factor corrected for reduced wetted propeller disk area
β_{area}	[–]	Loss factor due to reduced wetted propeller disk area
$\dot{\beta}_{Qw,\max}$	[–]	Maximum rate of change of β_{Qw}
$\dot{\beta}_{Tw,\max}$	[–]	Maximum rate of change of β_{Tw}
β_{Q1}	[–]	Ventilation variable
β_{Q2}	[–]	Ventilation variable
$\dot{\beta}_{lim}$	[–]	Maximum positive rate of change of β_{Q2}
γ	[–]	Gamma parameter in JONSWAP spectrum
γ	[–]	Parameter determining the importance of thrust production compared to energy consumption
$\boldsymbol{\Gamma}$	[–]	Nondimensional generalized force matrix
$\boldsymbol{\Gamma}_i$	[–]	Nondimensional generalized force vector
$\delta \mathbf{T}_+$	[N]	Necessary available positive change in thrust
$\delta \mathbf{T}_-$	[N]	Necessary available negative change in thrust

Δt	[s]	Sampling time
ΔP	[W]	Cost function error
ΔT	[N]	Change in thrust in one time step
$\Delta \mathbf{T}$	[N]	Perturbations in thruster force vector
$\Delta \tau$	[N]/[Nm]	Perturbations in generalized force vector
ε	[–]	Parameter
ε	[N]/[Nm]	Positive constant
ζ	[–]	Ventilation flag
ζ	[W]	Amplitude of power oscillations (used in power and torque spectrum)
η_0	[–]	Propeller efficiency
$\eta_{0\text{optimal}}$	[–]	Optimal propeller efficiency
η_{OBS}	[m]/[–]	Observed vessel position and heading vector
η_d	[m]/[–]	Desired vessel position and heading vector
θ	vaires	Parameter vector
κ_i	[–]	Sensitivity function exponent for controller i
λ	[–]	Scale
ν	[m^2/s]	Kinematic viscosity of the water
ρ	[kg/ m^3]	Density of water
ρ	[–]	Parameter
σ_{\inf}	[–]	Greatest lower bound on σ_{\min}
σ_{\lim}	[–]	Desired minimum gain from thrust to generalized forces
σ_{\min}	[–]	Minimum gain from thrust to generalized forces
$\sigma_{\max, \mathbf{X}}$	[–]	Maximum singular value of \mathbf{X}
$\sigma_{\min, \mathbf{X}}$	[–]	Minimum singular value of \mathbf{X}
σ_{cm}	[–]	Cavitation number model scale
σ_{cs}	[–]	Cavitation number full scale
σ_c	[–]	Cavitation number
σ	[–]	Singular value vector
τ	[–]	τ parameter
τ_{\lim}	[N]	Mean environmental force when switching should be done
τ_d	[–]	τ parameter based on desired thrust
τ_{hyst}	[N]	Hysteresis limit
τ_m	[N]	Desired generalized x-y force
$\bar{\tau}_m$	[N]	Performance measure
$\boldsymbol{\tau}_{RAW}$	[N]/[Nm]	Measured generalized force vector
$\boldsymbol{\tau}_{\sigma_m \min}$	[–]	Most singular generalized force direction
$\boldsymbol{\tau}_c$	[N]/[Nm]	Commanded generalized force
$\boldsymbol{\tau}_d$	[N]/[Nm]	Desired generalized force vector
$\bar{\boldsymbol{\tau}}$	[–]	Nondimensional generalized force
Ψ	[–]	Matrix containing $\bar{\mathbf{T}}_i$'s
ω	[1/s]	Filter frequency
Ω	[–]	Matrix containing $\boldsymbol{\Gamma}_i$'s

Chapter 1

Introduction

Vessels are an important part of today's global society. The two most important areas of use are probably transportation of passengers and goods, and oil and gas exploration and exploitation. The continuous increasing demand for oil and gas motivates exploration and exploitation in increasingly more challenging environments. As a consequence the use of dynamic positioning (DP) systems or thruster assisted position mooring (PM) systems for station keeping are increasing. The recent discovered challenges related to the green house effect, challenge all vessels to become more energy efficient. This includes both vessels used for transportation and in the offshore oil business.

This thesis considers two different levels of control of screw propellers. First the propulsion control problem, which is about how to control the components of the propulsion system is considered. The propulsion system consists of all thrust producing devices e.g. main propellers, tunnel thrusters or azimuthing thrusters. Second, the thrust allocation problem, which determines how the devices in the propulsion system should cooperate in order to fulfill the demands from the motion controller, is investigated. The aim in propulsion control is to achieve high propulsion efficiency and thrust production accuracy. The aim in thrust allocation is to fulfill the demand from the motion controller, reduce power consumption and maintain maneuverability.

1.1 Background

During e.g. drilling, production or diving operations in exploration and exploitation of hydrocarbons, an offshore vessel will be required to maintain a fixed position and a fixed heading. In DP operations the position and heading are maintained by use of thrusters only. In PM systems the thrusters mainly provide heading control and damping to the system, while the mooring takes care of the mean environmental loads. The advantages of a mooring system are reduced energy consumption during long term operation at one site and less complexity in the power, propulsion and automation systems. The energy consumption is reduced, since there is no need for the thrusters to counteract the

mean environmental forces.

At some locations, the seafloor is too crowded to accommodate anchors and mooring lines at the seabed. In that case DP systems are the only choice. Also increasing water depth favours DP systems, since the positioning accuracy of the mooring system becomes insufficient. The start up time of DP operations is considered to be significantly shorter than deployment of a mooring system, due to time consuming anchor handling operations. Hence, DP systems are particularly favorable for vessels only staying in a fixed location for a short amount of time. A challenge for DP systems with increasing water depth is the reduced performance of bottom based position measurement systems, like hydro acoustic positioning reference systems and taut wire.

The consequences of failures in the DP system depend on the tasks performed during DP operation. Hence, the required safety level in a DP system will vary. The International Maritime Organization (IMO) has established three different safety levels in DP operation, called DP classes (IMO 1994). Class 1: "loss of position may occur in the event of single fault". Class 2: "loss of position is not to occur in the event of a single failure in any active component or system". Class 3: loss of position is not to occur in the event of a single failure in any component or system, including fire and flooding in any watertight compartment. The choice of DP class for a particular operation should be based on a risk analysis.

The era of automatic ship control started with "Metal Mike" in 1911. This was a gyroscope-guided autopilot (Fossen 2002). It was not until the 1960's that the DP system was invented in order to make drilling at large water depths possible. The first controllers were PID controllers in cascade with filters which removed wave frequent disturbances. Linear quadratic Gaussian (LQG) control was first introduced into DP systems in Balchen et al. (1976). Their work were followed up by Gimble (1978), Gimble et al. (1979, 1980), Balchen et al. (1980a, b), Sørheim (1981), Fung and Gimble (1983), Sælid et al. (1983) and Gimble and Jonhson (1989). Later results on DP system includes non-linear PID control and passive observers (Fossen 1994, 2002), model based control (Sørensen et al. 1996, Fossen 2002), H_∞ and μ methods (Katebi et al. 1997a, b), roll and pitch damping (Sørensen and Strand 2000), riser shape control (Sørensen et al. 2001), weather optimal positioning (Fossen and Strand 2001), extreme seas (Sørensen et al. 2002), structural reliability concept for DP systems (Leira et al. 2004), system architecture description (Sørensen et al. 2005), and hybrid control (Nguyen 2005, Nguyen et al. 2007, 2008). Recent PhD theses on DP systems includes Strand (1999), Lindegaard (2003) and Nguyen (2005). Design of PM systems are treated in Strand et al. (1998), and a structural reliability concept for PM systems is presented in Berntsen et al. (2008).

Most DP systems are capable of operating in many different modes of operation, where the main modes are:

- Manual control, where the operator determines the desired generalized forces (forces in surge, sway and yaw).
- Set point control, where the vessel is kept in a fixed position with a fixed

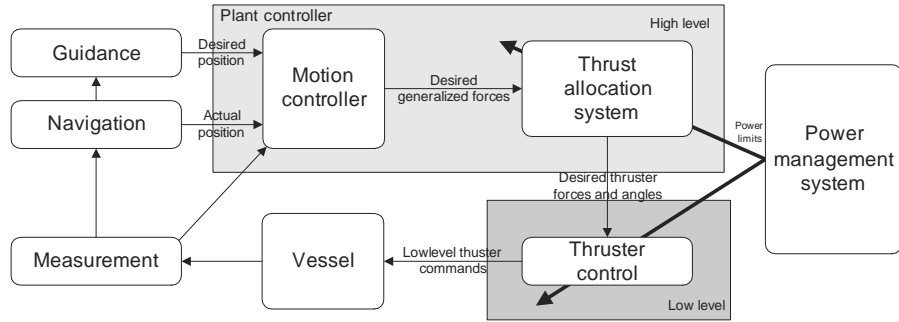


Figure 1.1: Block diagram of DP or PM system.

heading.

- Tracking control, where the vessel follows a path.
- Semi-automatic control, where e.g. position control is manual and heading control is automatic.

DP and PM systems are used on different types of vessels, ranging from shuttle tankers, semi submersibles, offshore service vessels, construction vessels and cruise vessels, to small water plane area twin hull (SWATH) vessels. As a result most DP and PM systems have to be tuned for each installation. The block diagram of a typical DP or PM system is seen in Figure 1.1. The division into different modules are done in order to ease the design, implementation and verification:

- Vessel, constitute the physical system responding to environmental disturbances and thruster forces. The goal of the DP system is to control the position and heading of the vessel. On PM systems this module also includes the mooring system.
- Measurements, include all sensor systems and inputs to the DP or PM system. The measured signals are checked for validity before they are past on to the other modules.
- Navigation, is the task of determining the current position and orientation of the vessel. Usually the wave frequent motion is removed from the measurements in order to reduce the wear and tear, and the power consumption of the DP or PM system. This is usually done by filters or observers.
- Guidance, is to determine the desired set point or path for the vessel to follow. The guidance block should only create trajectories the vessel is capable of carrying out.

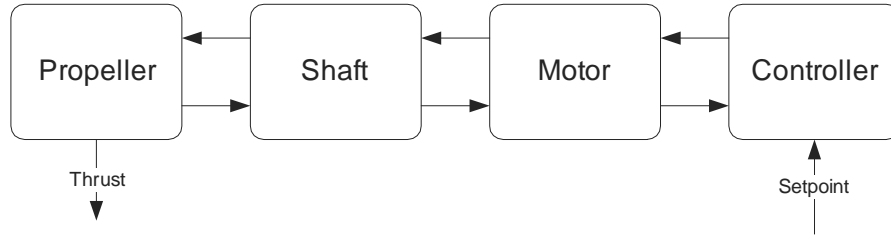


Figure 1.2: Block diagram of propulsion system.

- The motion controller, includes controller logic, feedforward and feedback control actions. The wind measurements are usually used for feedforward control, whereas the position measurements are used for feedback control.
- Thrust allocation, distributes the command from the motion controller on the different thrusters. The outputs are desired thruster force and direction.
- The thrusters, are the actuators in the DP and PM system. Screw propellers are most commonly used. They come in different variants as: fixed pitch propellers, controllable pitch propellers, tunnel thrusters, ducted thrusters, azimuthing thrusters and water jets. Propellers with rudders are considered to be one thrust producing unit. An interesting alternative to the conventional propellers is the Voith Schenider propeller. This propeller is capable of producing thrust in any direction, and the directional changes are much faster than for azimuthing propellers.

The purpose of the propulsion system is to supply the vessel with propulsion and maneuvering forces. Dependent on the vessel, the layout of the propulsion system may vary. However, for each of the propulsors, the block diagram in Figure 1.2 is representative. The goal for any propulsion system is to produce thrust with minimum energy consumption. In this thesis only screw propellers are considered. The choice of propulsion controller depends on whether diesel or electrical motors are used to turn the shaft, whether fixed or controllable pitch propeller are used and the mode of operation. Three categories of controllers are defined: fixed pitch controllers, pitch controllers and consolidated controllers. Fixed pitch controllers control the shaft speed, torque or power delivered to the propeller shaft. Pitch controllers controls the pitch of the propeller blades in order to vary the thrust. Consolidated controllers controls both shaft and pitch. In Schanz (1967) a method for near optimal control of controllable pitch propellers is presented. The method is highlighted in this thesis and compared to other control methods.

Recent advances in electronic power systems have made electrical propulsion more attractive, as the controllability and efficiency are increased, in particular

for vessels with varying operational profile. Compared to direct driven propellers, electrical motors offer the possibility of sudden changes in shaft speed, torque or power. As a result, shaft speed, torque and power control of electrical driven propellers were suggested in Sørensen et al. (1997). More references on propulsion control are found in the propulsion control chapter.

Another important factor when choosing propulsion controller is the mode of operation. In transit operation, efficiency is most important, whereas in station keeping operation, correct thrust production may be equally important. This allows for different control strategies. A subject that has received recent attention is ventilation and in-and-out of water effects on propellers. These effects appear when operating the vessel in heavy seas, and introduce large and sudden load transients in the propulsion system. An extensive discussion of countermeasures, called anti-spin thruster control, for fixed pitch propellers is found in Smogeli (2006).

The purpose of the thrust allocation system is to map the desired generalized forces, determined by the motion controller, into individual thruster forces and directions. This is not done directly in the motion controller in order to ease the design, implementation, verification and fault handling. The thrust allocation problem is a special case of the more general control allocation problem. Examples on solutions to other control allocation problems are found in e.g. Peterson and Bodson (2006). As most vessels using DP or PM systems are over actuated, the sum of the thrusters can still provide the necessary control forces even when subject to a single thruster failure. In that case it is advantageous to only change the thrust allocator, and not the entire motion controller in case of thruster failure. In cases where the vessel is over actuated there exist many solutions to the thrust allocation problem satisfying the demand from the motion controller. This makes for the possibility of also taking power consumption and maneuverability into account. The power consumption is usually accounted for by formulating the problem as a constrained optimization problem, see e.g. Fossen and Johansen (2006). The maneuverability of the vessel can be investigated e.g. by singular value decomposition like in Sørdsalen (1997b). More references on thrust allocation are found in the first chapter on thrust allocation, Chapter 4.

1.2 Motivation and objectives

On vessels conducting DP or PM operations in harsh environment, ventilation and in-and-out-of water effects may lead to unacceptable behavior of the thrusters. This may result in reduced efficiency, accuracy and safety of the DP or PM system. In Smogeli (2006) an extensive study of low level anti-spin control of fixed pitch propellers, which effectively deals with these problems, are presented. The goal of this thesis is to:

- Determine the differences between fixed pitch propellers and consolidated controlled propellers as regards ventilation, in-and-out-of water effects and

anti-spin thruster control.

Propulsion control of DP vessels by use of torque or power control was suggested by Sørensen et al. (1997). The goal of this thesis is to:

- Evaluate the performance of torque and power control, compared to other control methods, in transit operation.

Vessels conducting DP operations are usually over actuated. This should be exploited in the case of ventilation and in-and-out-of water events in order to increase efficiency, safety and positioning accuracy. The goal of this thesis is to:

- Develop an anti-spin thrust allocation system, capable of redistributing thruster force from heavily ventilated to less ventilated thrusters.

Instead of designing one super allocator handling all types of operational requirements and environments, it may be possible to design several simpler ones, and switch among these. The goal of this thesis is to:

- Investigate the possibilities in switched thrust allocation.

On vessels with azimuthing thrusters, the directions of the thrusters significantly affect the maneuverability of the vessel. On vessels with slowly rotating thrusters, this may easily lead to loss of position. The goal of this thesis is to:

- Determine a way of increasing the maneuverability on vessels with slowly rotating azimuths.

1.3 Contributions

To the best of the author's knowledge, the following are believed to be original contributions and extensions to the state of the art.

Chapter 2: a) A summary of scaling laws for screw propellers, including the effects of ventilation and in-and-out of water events, is presented (Ruth 2005, Ruth and Smogeli 2006). b) A new parameter τ is proposed for comparison of propellers under equal operating conditions, meaning equal advance speed and equal produced or desired thrust. The parameter can be used to determine the optimal pitch ratio, determine the optimal propeller diameter, comparing efficiency for different controllers or comparing thrust sensitivity for different controllers (Ruth et al. 2006). c) A dynamic model of propellers subject to ventilation and in-and-out of water effects are developed and verified by experimental results (Ruth and Smogeli 2006). d) On controllable pitch propellers, reduced pitch ratio will reduce the possibility and severity of ventilation (Ruth 2005).

Chapter 3: A review of propulsion control methods for surface vessels, including novel comparisons of efficiency and thrust sensitivity based on the τ parameter, is presented (Ruth et al. 2006).

Chapter 4: a) A convex linearly constrained quadratic thrust allocator is proposed and verified by experimental results (Ruth et al. 2007). b) Different methods for constraining the power consumption of the thrust allocator are proposed.

Chapter 5: a) A modification of the convex linearly constrained quadratic thrust allocator such that the power is proportional to $T^{3/2}$ is proposed (Ruth et al. Accepted). b) An anti-spin thrust allocation strategy is proposed and verified by experimental results. The application of the method results in significant power savings and major reductions in torque and power transients, in addition to improved positioning performance (Ruth et al. Accepted).

Chapter 6: a) A solution to the nonconvex linearly constrained quadratic thrust allocation problem by use of mixed integer solutions is presented and verified by experimental results. b) Switching between different thrust allocators dependent on the environmental condition is demonstrated by experimental results. c) Handling of thruster failures are demonstrated by experimental results.

Chapter 7: a) A method for finding minimum gain from thruster forces to generalized forces for unidirectional thrusters are developed. This gain is a good indicator on the maneuverability of the vessel (Ruth and Sørensen Submitted-b). b) A design loop for thruster configurations based on minimum gain from thruster forces to generalized forces is suggested. The method focus on maneuverability and thrust capability, and is capable of taking thruster or power bus failures into account (Ruth and Sørensen Submitted-a). c) It is proposed how to find and visualize the minimum gain direction (Ruth and Sørensen Submitted-b). d) Different methods for singularity avoidance inn real time are suggested (Ruth and Sørensen Submitted-b).

1.4 List of publications

Journal papers:

1. E. Ruth and A. J. Sørensen. Singularities in marine control allocation with bi- and unidirectional thrusters. *Automatica*, Submitted.
2. E. Ruth, Ø. N. Smogeli, T. Perez, and A. J. Sørensen. Anti-spin thrust allocation for marine vessels. *IEEE Transactions on Control System Technology*, Accepted.
3. E. Ruth and Ø. N. Smogeli. Ventilation of controllable pitch thrusters. *Marine Technology and SNAME news*, 43(4):170–179, October 2006.

Conference papers:

4. E. Ruth and A. J. Sørensen. Design of thruster configurations. In *International Marine Design Conference*, Trondheim, Norway, Submitted.

5. E. Ruth, A. J. Sørensen, and T. Perez. Thrust allocation with linear constrained quadratic cost function. In *Conference on Control Applications in Marine Systems*, Bol, Croatia, September 2007.
6. E. Ruth, Ø. N. Smogeli, and A. J. Sørensen. Overview of propulsion control for surface vessels. In *7th IFAC Conference on Manoeuvring and Control of Marine Craft*, Lisbon, Portugal, September 2006.
7. Ø. N. Smogeli, E. Ruth, and A. J. Sørensen. Experimental validation of power and torque thruster control. In *Joint 2005 International Symposium on Intelligent Control and 13th Mediterranean Conference on Control and Automation*, Limassol, Cyprus, 2005.

1.5 Outline of thesis

Chapter 2: In order to compare and evaluate different propulsion controllers, propeller models are needed. In this chapter both models for normal operation, and ventilation and in-and-out-of water events are presented. This chapter starts by describing the scaling laws for propellers, and continues by describing different nominal models. In connection with the nominal propeller models, a new τ parameter is proposed. The parameter can be used to determine the optimal pitch ratio, determine the optimal propeller diameter, comparing efficiency for different controllers or comparing thrust sensitivity for different controllers. Further, a dynamic model of ventilation and in-and-out-of water events are developed. Based on the developed model, considerations on anti-spin thruster control for consolidated controlled propellers are presented.

Chapter 3: This chapter deals with the topic propulsion control. The focus is on surface vessels. Both low speed (DP) and moderate/high speed (transit) operation are considered. Fixed pitch propellers, controllable pitch propellers and consolidated controlled propellers are compared as regards thrust sensitivity and efficiency. The differences between control of surface vessels and under water vehicles are also elaborated.

Chapter 4: The thrust allocation problem is stated, and an overview of previously published results are presented. A novel formulation of the thrust allocation problem with rotating azimuths is proposed and validated by experiments. Suggestions on how power constraints can be incorporated are also presented.

Chapter 5: On ships conduction station keeping, it is usually redundant thrusters present. It is in this chapter proposed how the redundant thrusters can be used to reduce the loading of a ventilating thruster by redistributing thrust from a ventilating to the nonventilating thrusters (anti-spin thrust allocation). The results are verified by model tests.

Chapter 6: This chapter considers switching in thrust allocation. The idea is that instead of designing one super allocator capable of handling all eventualities, it is switched between several significantly simpler allocators. Solution of the nonconvex linearly constrained quadratic thrust allocation problem by use of mixed integer solution is presented. Further, it is shown how switching can be conducted between different thrust allocators depending on the prevailing environmental condition. Finally, it is demonstrated how the linearly constrained quadratic thrust allocator is capable of handling thruster force and azimuth failures. The results are verified by experiments with a model ship.

Chapter 7: In power optimal thrust allocation, the solutions often tend to near singular configurations. This may result in insufficient thrust capability when subject to sudden changes in the generalized forces. Singularity avoidance can be used as a solution to this problem. It is in this chapter shown how the degree of singularity can be quantized, both for bi- and unidirectional thrusters. A design loop for thruster configurations focusing on the degree if singularity is proposed. An extensive example involving CyberShip III is presented. How singularities and most singular direction can be monitored are shown. Finally, experimental results on singularity avoidance in real time are presented.

Chapter 2

Propeller models

In order to determine the performance of propellers it is common to conduct model tests. To be able to apply the results in full scale, the results have to be scaled. In this chapter the scaling laws for propellers are presented. Further, some models for propellers in normal operating conditions are presented. It is particularly paid attention to variable pitch models found in the literature, covering all combinations of advance speed and shaft speed. These models will be used in the next chapter for comparison of different propulsion controllers with respect to efficiency and thrust production accuracy. In severe weather conditions, ventilation and in-and-out-of water events may deteriorate the performance of the propulsion system. In order to investigate how to deal with this problem, a model of the phenomenon is needed. The ventilation model from Ruth (2005) and Ruth and Smogeli (2006) is presented, and the dynamic performance of the model is verified by open water experiments. The ventilation model is used to draw conclusions about anti-spin thruster control for consolidated controlled propellers, intended to increasing the positioning accuracy, safety and efficiency of vessels in station keeping operation. This chapter is to a large extent taken from Ruth and Smogeli (2006).

2.1 Scaling laws

In this section it is shown how results obtained in model tests can be scaled to full scale. Particular attention is paid to ventilation at low advance speeds. According to Shiba (1953) the two most important parameters when scaling propeller performance from model scale to full scale are:

1. Geometrical similarity:

$$\frac{L_s}{L_m} = \lambda, \quad (2.1)$$

2. Kinematic similarity:

$$J_{Am} = \frac{V_{Am}}{n_m D_m} = \frac{V_{As}}{n_s D_s} = J_{As}, \quad (2.2)$$

where $\lambda[-]$ is the scale, $L[m]$ is any characteristic length, $J_A[-]$ is the advance number, $V_A[m/s]$ is the advance speed, $n[Hz]$ is the shaft speed in revolutions per second, $D[m]$ the propeller diameter, suffix s means full scale, and suffix m means model scale. Further, depending on the operational condition, the following dimensionless parameters have influence on the propeller performance (Shiba 1953, Gutsche 1967, Kruppa 1972, Brandt 1973, ATTC 1974, Scherer 1977, Guoqiang et al. 1989, Olofsson 1996, ITTC 1999b):

3. Submergence ratio:

$$\frac{h}{R}, \quad (2.3)$$

4. Reynolds' number:

$$R_n = \frac{V_\infty c}{\nu}. \quad (2.4)$$

Reynolds' number similarity is not required if $R_n > 5 \cdot 10^5$ (because the drag coefficient is constant in this region), or if corrections for R_n are done according to ITTC (1999a), which requires $R_n > 2 \cdot 10^5$.

5. Froude number:

$$F_{nD} = n \sqrt{\frac{D}{g}}. \quad (2.5)$$

Froude number similarity is not required if $F_{nD} > 3 - 4$ (because gravity forces are dominated by inertial forces). In full scale F_{nD} will typically be between 0 and 1.4 (Shiba 1953).

6. Cavitation number:

$$\sigma_c = \frac{p_{static} - p_{cav}}{\frac{1}{2}\rho V_\infty^2}, \quad (2.6)$$

7. Weber's number:

$$W = nD \sqrt{\frac{\rho}{s} D}. \quad (2.7)$$

Here $h[m]$ is the submergence of the propeller shaft, $R[m]$ is the propeller radius, $V_\infty[m/s]$ is the velocity seen by the propeller blade at $0.7R$, $c[m]$ is the cord length of the propeller blade at $0.7R$, $\nu[m^2/s]$ is the kinematic viscosity of the water, $g[m/s^2]$ is the gravity, $\rho[kg/m^3]$ is the density of the water, $s[N/m]$ is the surface tension of the water which equals 0.072 in fresh water, $p_{static}[Pa]$ is the static water pressure at a given submergence, and $p_{cav}[Pa]$ is the pressure in the cavity.

The total thrust $T_t[N]$ and the propeller torque $Q_p[Nm]$ can be scaled by two different sets of coefficients, the $K_{Tt}[-]$ and $K_Q[-]$ coefficients or the $C_{Tt}[-]$ and $C_Q[-]$ coefficients. In both pairs the coefficients are denoted total thrust coefficient and torque coefficient, and thus ensure geometrical and kinematic

Table 2.1: Relationship between advance angle, advance speed and rotational direction.

Quadrant	β	V_A	n
1	$\langle 0, 90 \rangle$	positive	positive
2	$\langle 90, 180 \rangle$	positive	negative
3	$\langle -180, -90 \rangle$	negative	negative
4	$\langle -90, 0 \rangle$	negative	positive

similarity. Each pair constitutes a propeller characteristics. The $K_{Tt}[-]$ and $K_Q[-]$ coefficients are defined as:

$$T_t = T_p + T_D, \quad (2.8)$$

$$K_{Tt}(J_A, P/D) = \frac{T_t}{\rho D^4 n^2}, \quad (2.9)$$

$$K_Q(J_A, P/D) = \frac{Q_p}{\rho D^5 n^2}, \quad (2.10)$$

$$J_A = \frac{V_A}{nD}, \quad (2.11)$$

where $T_p[N]$ is the propeller thrust, $T_D[N]$ is the duct thrust, and $P/D[-]$ is the pitch ratio. Ducts are commonly used on propellers operating at low advance speeds in order to improve the bollard pull capability. If such a duct is not present $T_D = 0$. The total thrust coefficient and the torque coefficient are normally defined for positive advance speed and positive shaft speed only. The coefficients are commonly expressed as functions of the advance number and the pitch ratio.

The K_{Tt} and K_Q models do not describe the behavior at all combinations of advance speeds V_A and shaft speeds n . To describe all the combinations of advance speeds V_A and shaft speeds n , four quadrant propeller characteristics are needed. The quadrants are defined in Table 2.1. Multi quadrant series are valid in more than one quadrant, based on the advance angle β :

$$\beta = \arctan\left(\frac{V_A}{0.7\pi n D}\right). \quad (2.12)$$

The physical interpretation of β , also called hydro-dynamic pitch angle, is shown in Figure 2.1.

The total thrust and torque coefficients, C_{Tt} and C_Q in the multi quadrant characteristics are defined as (van Lammeren et al. 1969):

$$C_{Tt}(\beta, P/D) = \frac{T_t}{\frac{1}{2}\rho A_0 V_\infty^2} = \frac{T_t}{\frac{1}{2}\rho(V_A^2 + (0.7\pi n D)^2)\frac{\pi}{4}D^2}, \quad (2.13)$$

$$C_Q(\beta, P/D) = \frac{Q_p}{\frac{1}{2}\rho A_0 D V_\infty^2} = \frac{Q_p}{\frac{1}{2}\rho(V_A^2 + (0.7\pi n D)^2)\frac{\pi}{4}D^3}, \quad (2.14)$$

$$A_0 = \frac{\pi}{4}D^2, \quad (2.15)$$

$$V_\infty = \sqrt{V_A^2 + (0.7\pi n D)^2}. \quad (2.16)$$

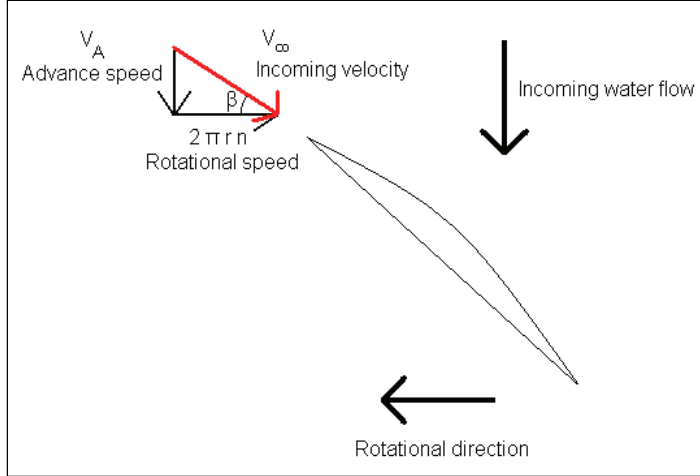


Figure 2.1: Illustration of advance angle, β (2.12) and velocity seen by the propeller, V_∞ (2.16). r is usually chosen to be $0.7\frac{D}{2}$.

where $A_0[m^2]$ is the propeller disc area, and $V_\infty[m/s]$ is the velocity seen by the propeller blade at a distance $0.7\frac{D}{2}$ from the centre of the shaft, see Figure 2.1. For a given propeller it is sufficient to let C_{Tt} and C_Q be functions of pitch ratio P/D and advance angle β (Strom-Tejsen and Porter 1972). The thrust characteristic for a controllable pitch propeller will then consist of the two functions $C_{Tt}(\beta, P/D)$ and $C_Q(\beta, P/D)$.

For the sectors where both the K_{Tt} , K_Q and C_{Tt} , C_Q coefficients are defined the relationships between them are found from (2.9)-(2.11) and (2.13)-(2.14):

$$K_{Tt} = C_{Tt} \frac{\pi}{8} \left(J_A^2 + (0.7\pi)^2 \right), \quad (2.17)$$

$$K_Q = C_Q \frac{\pi}{8} \left(J_A^2 + (0.7\pi)^2 \right). \quad (2.18)$$

Further, the relationship between the advance number and the advance angle are found from (2.11) and (2.12):

$$\beta = \arctan\left(\frac{J_A}{0.7\pi}\right). \quad (2.19)$$

Gutsche (1967), Brandt (1973), Fleischer (1973), Hashimoto et al. (1983) and Guoqiang et al. (1989) divide the operating condition of the propeller into three regions; non-ventilated, partially ventilated and fully ventilated. All these regimes are found in the experimental results presented. The scaling laws described in this thesis are based on experiments with non-ducted propellers, but are assumed to be valid also for ducted propellers, since non-ducted propellers and ducted propellers are scaled in the same way in the non-ventilated regime.

Table 2.2: Scaling requirements in the different regimes at low advance speeds.
Scaling requirement 1-7 refers to (2.1)-(2.7) in the text.

Scaling requirement:	1	2	3	4	5	6	7
Non-ventilated	x	x	x	x			
Fully ventilated	x	x	x	x	x	(x)	
Partially ventilated	x	x	x	x	x	x	

The scaling laws in the different regimes are summarized in Table 2.2 and further commented below. It is important to notice that low advance speeds are considered.

2.1.1 The non-ventilated regime

In this regime, no significant ventilation occurs. This means that the propeller is deeply submerged, or the ventilation is light and not affecting the total thrust or the torque significantly. When both the model scale and the full scale propeller are in the non-ventilated regime, it is possible to scale the results by satisfying the requirements given in Table 2.2. According to Scherer (1977) it is believed that the full scale propeller does not ventilate as easily as the model scale propeller. It is therefore assumed that if the model scale propeller is non-ventilating, then also the full-scale propeller will be non-ventilating. Reynolds' number of $2 \cdot 10^5[-]$ corresponds to a shaft speed of $4[Hz]$ in the model tests presented later. The conclusion is that the non-ventilated model scale results can be scaled to full scale when the shaft speed is $n > 4[Hz]$ in model scale.

2.1.2 The fully ventilated regime

This is when a single ventilated cavity is covering the propeller blade. This means that the pressure on the suction side of the propeller blade is almost atmospheric. If the conditions given in Table 2.2 are satisfied, and both the model scale propeller and the full-scale propeller are fully ventilated, it is possible to scale the results in this regime. It is however not known to the authors how to confirm whether or not the full scale propeller is going to be fully ventilated. Requirement 6, cavitation number similarity, is actually obtained through kinematic similarity, submergence ratio similarity and Froude number similarity. Since $p_{static} = p_{atm} + \rho gh$, where p_{atm} is the atmospheric pressure, the cavitation number becomes:

$$\sigma_c = \frac{p_{atm} + \rho gh - p_{cav}}{\frac{1}{2}\rho V_\infty^2}. \quad (2.20)$$

Since $p_{cav} = p_{atm}$ when the propeller is fully ventilated, the equation can be simplified:

$$\begin{aligned}\sigma_c &= \frac{2gh}{V_\infty^2}, \\ &= \frac{1}{((0.35\pi)^2 + (J_A^2))} \frac{h}{R} \frac{g}{Dn^2}.\end{aligned}\quad (2.21)$$

If $J_{Am} = J_{As}$, $\frac{h_m}{R_m} = \frac{h_s}{R_s}$ and $F_{nDm} = F_{nDs}$, the result is that $\sigma_{cm} = \sigma_{cs}$. The Reynolds' number criterion restricts the scaling to shaft speeds equal to 4[Hz] and larger in model scale. The realistic Froude numbers in full scale corresponds to shaft speeds from 0 to 9[Hz] in model scale.

2.1.3 The partially ventilated regime

This is when only part of the propeller is ventilated. The ventilation is said to be unstable when the propeller's degree of ventilation is not stationary, but is a function of time. The required scaling parameters are summarized in Table 2.2. Although the pressure in the ventilated cavity is nearly atmospheric, there may exist other non-ventilated cavities (Kruppa 1972). These non-ventilated cavities requires cavitation number similarity. It would then require a free surface depressurized cavitation tunnel to do the experiments. The model tests presented in this thesis were all performed at atmospheric pressure, and the test facility has never been used with free surface and depressurization.

The conclusion in this case is that it is not possible to scale the results in the partially ventilated regime to full scale for the experimental results presented later. There is however no reason to believe that the qualitative behavior of a full scale propeller will differ much from the results obtained for a model scale propeller.

2.1.4 Effect of Weber's number

The Weber's number W describes the relationship between surface tension forces and inertial forces. Shiba (1953) and ITTC (1999b) state that W is important when determining the critical advance number, which is the advance number at which ventilation occurs for a given submergence ratio and shaft speed. When working with ventilation in this thesis, low advance numbers are considered, and the results are extrapolated to be valid for zero advance number $J_A = 0$. This means that the critical advance number in this case is irrelevant, since the advance number is always supposed to be small. W will no longer influence the critical advance number when it is larger than 180. This limit is determined in Shiba (1953) by evaluating experimental results. In the model tests presented later W is between 15 and 368, and $n > 12[\text{Hz}] \Rightarrow W > 180$.

2.2 Normal operating conditions

In this section a new parameter for comparison of propeller performance is presented. Then the thrust characteristic of the propeller used in the experiments are presented and multi quadrant controllable pitch thrust characteristics from the literature are commented upon. The applicability of the multi quadrant variable pitch models from the literature for use in simulations will be investigated. The power consumption $P[W]$ and the propeller efficiency $\eta_0[-]$ of a propeller are calculated as follows:

$$P = 2\pi n Q_p, \quad (2.22)$$

$$\eta_0 = \frac{V_A T_t}{P} = \frac{V_A T_t}{2\pi n Q_p}. \quad (2.23)$$

2.2.1 The τ parameter

In this section a non-dimensional parameter $\tau[-]$ first proposed in Ruth et al. (2006) is presented. The τ parameter makes it possible to find the optimal pitch ratio as function of this parameter only. The τ parameter can also be used to compare various propulsion systems producing the same thrust in equal environmental conditions. The propeller efficiency and the thrust sensitivity become functions of τ only for all combinations of thrust and advance speed for a given pitch ratio. The τ parameter is derived by solving (2.9) for n giving:

$$n(J_A, P/D) = \sqrt{\frac{T(J_A, P/D)}{K_T(J_A, P/D)\rho D^4}}. \quad (2.24)$$

Inserting (2.24) in (2.11) gives:

$$\begin{aligned} J_A &= \frac{V_A}{\sqrt{\frac{T(J_A, P/D)}{K_T(J_A, P/D)\rho D^4}}D}, \\ &= \sqrt{\rho D} \frac{V_A}{\sqrt{T(J_A, P/D)}} \sqrt{K_T(J_A, P/D)}. \end{aligned} \quad (2.25)$$

Dividing (2.25) by $\sqrt{K_T(J_A, P/D)}$ gives:

$$\tau = \frac{J_A}{\sqrt{K_T(J_A, P/D)}} = \sqrt{\rho D} \frac{V_A}{\sqrt{T(J_A, P/D)}}. \quad (2.26)$$

The τ parameter is seen to be constant for equal thrust and advance speed, corresponding to equal environmental conditions. Consolidated controlled propellers should then compare efficiencies at equal τ to find the optimal pitch ratio and shaft speed for a given combination of V_A and T .

The τ parameter has similarities with the B_p parameter used in the well known $B_p - \delta$ diagrams (Oosterveld 1970):

$$B_p = 33.07 \frac{\sqrt{K_Q(J_A, P/D)}}{J_A^{5/2}} = \frac{60n\sqrt{P}}{V_A^{5/2}}. \quad (2.27)$$

It is seen that both τ and B_p are modified versions of the advance number. The B_p parameter is a combination of the advance number and the torque coefficient, and can also be connected to the power as in (2.27). The τ parameter is a combination of the advance number and the thrust coefficient, and is then connected to the thrust as in (2.26). The B_p parameter is used in design considerations, typically to find the optimal diameter of the propeller, while τ also can be used to find the optimal operating point (pitch ratio and shaft speed) of an already installed propeller.

The optimal diameter of a propeller can be found by use of the τ parameter as well:

1. Determine the speed (V_S) and resistance (R) of the ship at which the propeller should be optimized.
2. Calculate the advance speed ($V_A = V_S(1 - w)$) and the necessary thrust ($T = R/(1 - t)$) ($w[-]$ is wake fraction and $t[-]$ is thrust deduction).
3. Plot the propeller efficiency as function of τ and pitch ratio based on the thrust characteristic.
4. Find the highest propeller efficiency in the plot. Determine the corresponding τ and P/D values.
5. By rearranging (2.26), the optimal diameter can be found:

$$D = \frac{\tau\sqrt{T}}{V_A\sqrt{\rho}}. \quad (2.28)$$

In Figure 2.2 an propeller efficiency plot for "The Wageningen B4-70 propeller" is shown. Let $V_S = 5.0[m/s]$, $R = 53[kN]$, $w = 0.20[-]$ and $t = 0.10[-]$. Then, $V_A = 4.0[m/s]$ and $T = 59[kN]$. In Figure 2.2 $P/D = 1.4[-]$ and $\tau = 3.05[-]$ is the optimal combination. Then the optimal diameter becomes:

$$D = \frac{3.05\sqrt{59000}}{4.0\sqrt{1025}} = 5.8[m]. \quad (2.29)$$

Since the resistance increases with more than V_S^2 , the faster the ship goes the larger the propeller should be. However, remember that there may be restrictions on the available space for the propeller.

In the case that the optimal diameter is too large, the maximum diameter should be used to calculate the τ parameter and the optimal pitch ratio can be found directly from Figure 2.2. Let the ship design restrict the diameter $D \leq 4.0[m]$ in the above presented example. Then:

$$\tau \leq \sqrt{1025}4.0\frac{4.0}{\sqrt{59000}} = 2.1[-]. \quad (2.30)$$

Using the optimal line in Figure 2.2 it is concluded that $P/D = 1.36[-]$ is the optimal pitch ratio.

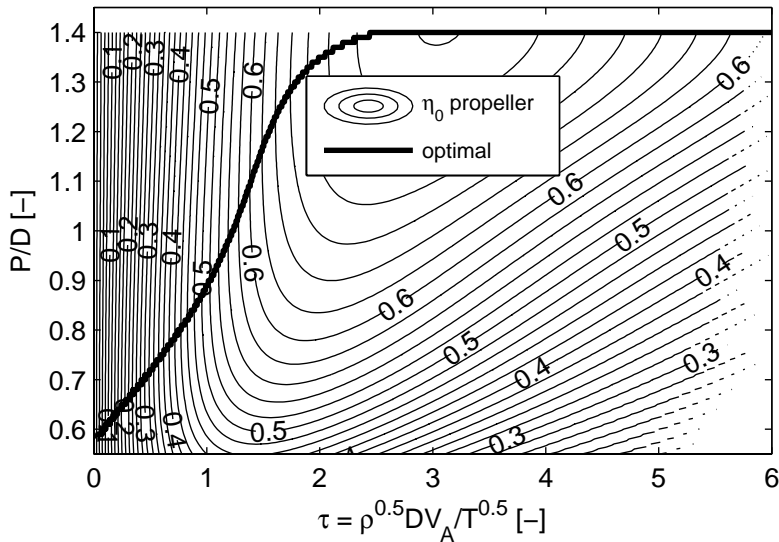


Figure 2.2: Propeller efficiency plot for first quadrant for "The Wageningen B4-70 propeller" based on the K_T and K_Q model.

A modified version of the τ parameter, the τ_d parameter can be used for comparison of different propulsion controllers with equal desired thrust and environmental conditions (advance speed). The τ_d parameter is based on (2.26) with $T = T_d$. Using ($st = T/T_d$) and (2.26) give:

$$\begin{aligned}
 \tau_d &= \sqrt{\rho} D \frac{V_A}{\sqrt{T_d}}, \\
 &= \sqrt{\rho} D \frac{V_A}{\sqrt{stT(J_A, P/D)}}, \\
 &= \frac{\tau}{\sqrt{st}}.
 \end{aligned} \tag{2.31}$$

2.2.2 Experimental propeller with duct

Model tests were carried out in the cavitation tunnel at NTNU. The results are previously presented in Ruth (2005), Ruth and Smogeli (2006). The main particulars of the propeller and the duct are given in Table 2.3 and 2.4. The details of the experimental setup are given in Appendix A. Due to limitations in the experimental equipment the total thrust and torque coefficients at zero advance speed had to be calculated by fitting second order polynomials to the rest of the values. The resulting model is seen in Figure 2.3, where total thrust and torque coefficient are plotted as function of advance number and pitch ratio. As expected, it is seen that increased pitch ratio and/or advance number results

Table 2.3: Propeller dimensions in cavitation tunnel experiments.

Propeller No.	P 1020	
Diameter, D	250	[mm]
Blade number, Z	4	[–]
Pitch ratio, $[P_{0.7}/D]$	0.4 – 1.3	[–]
A_E/A_0	0.55	[–]

Table 2.4: Duct dimensions in cavitation tunnel experiments.

Duct No.	D 143	
Inner diameter, D_{inner}	252.1	[mm]
Max. outer diameter, $D_{max\ O}$	302.4	[mm]
Min. outer diameter, $D_{min\ O}$	267.7	[mm]
Length duct, L_D	118.8	[mm]

in increased values of the total thrust and torque coefficient.

2.2.3 Multi quadrant variable pitch models from literature

In order to do simulations of controllers for consolidated controlled propellers, that is propellers where both shaft speed and pitch are controlled, the following multi quadrant variable pitch models from the literature were evaluated:

- "The Wageningen B4-70 propeller" (van Lammeren et al. 1969).
- "The Wageningen Ka4-70 propeller with nozzle 19A" (Oosterveld 1970).
- "The Wageningen Ka4-70 propeller with nozzle 37" (Oosterveld 1970).
- "The Gutsche 1041 propeller" (Gutsche and Schroeder 1963, Strom-Tejsen and Porter 1972).
- "The CD-CPP 7708 propeller" (Chu et al. 1979).

It will be seen that the surprising conclusion is that none of the models are suitable for simulations in all four quadrants with variable pitch. The details for the different propellers are presented in the following.

"The Wageningen B4-70 propeller"

In van Lammeren et al. (1969) four quadrant measurements with variable pitch ratio are presented for the Wageningen B4-70 propeller with pitch ratios from 0.5 to 1.4. The results are presented as coefficients for polynomials for K_T and K_Q in the first quadrant, and as Fourier coefficients for C_T and C_Q in all four quadrants. It is, however, a problem that the two models differ. As an example propeller efficiency plots are presented. In Figure 2.2 the plot is based on the K_T and K_Q polynomials. Figure 2.4 is based on the C_T and C_Q Fourier series and

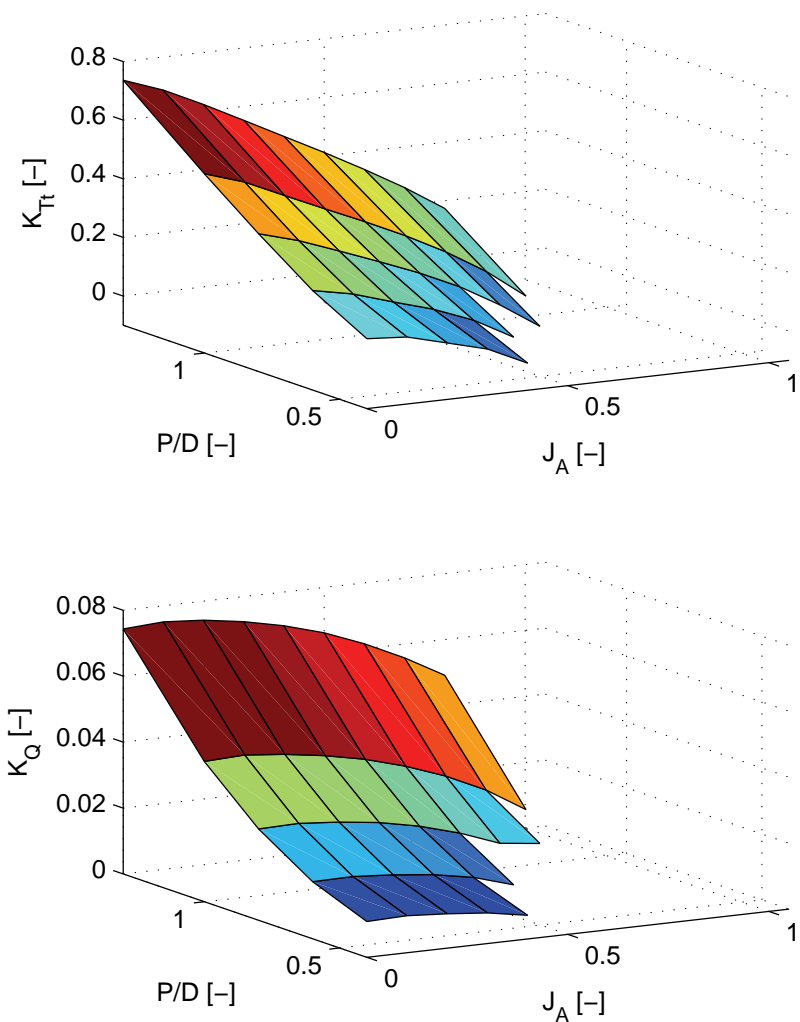


Figure 2.3: Thruster characteristics for experimental propeller with duct, as function of advance number J_A and pitch ratio P/D .

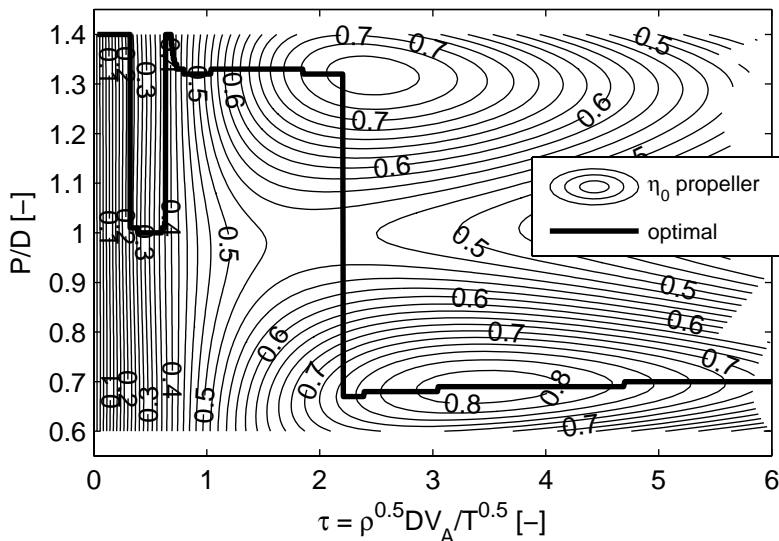


Figure 2.4: Propeller efficiency plot for first quadrant for "The Wageningen B4-70 propeller" based on the C_T and C_Q model.

is obviously unphysical. The following is observed by investigating the complete thrust characteristic (not presented here). The references are to figures and tables in van Lammeren et al. (1969):

- Table 7 is nearly equal to Table 8. When plotting the data from the two tables, the results are nearly identical. The plots we get looks like Figure 37, this is correct for Table 8, but not for Table 7.
- When comparing our plots made from Table 7, with the plots in Figure 39-41 they seems equal, and they should be equal. Hence, this is ok.
- When comparing Figure 39 with $P/D = 0.6$ in Figure 36 they should show the same according to the caption text. However they do not.
- When comparing Figure 41 with $P/D = 1.4$ in Figure 36 they should show the same according to the caption text. However they do not.

It looks like two different versions of Table 8 are given in Table 7 and 8. Since Table 7 is the one with four quadrant data for variable pitch ratio, it is concluded that this model is not usable in four quadrants. The one quadrant model seems, however, appropriate.

"The Wageningen Ka4-70 propeller with nozzle 19A"

In Oosterveld (1970) four quadrant measurements with variable pitch ratio are presented for the Wageningen Ka4-70 propeller with nozzle 19A and pitch ratios

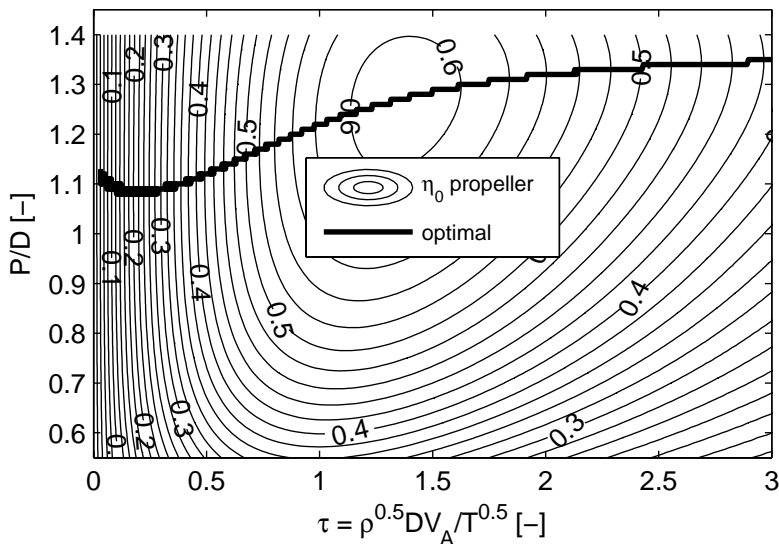


Figure 2.5: Propeller efficiency plot for first quadrant for "The Wageningen Ka4-70 propeller with nozzle 19A" based on the K_T and K_Q model.

from 0.6 to 1.4. The results are presented as coefficients for polynomials for K_T and K_Q in the first quadrant, and as Fourier coefficients for C_T and C_Q in all four quadrants. It is however a problem that the two models differ. As an example propeller efficiency plots are presented. In Figure 2.5 the plot is based on the K_T and K_Q polynomials. Figure 2.6 is based on the C_T and C_Q Fourier series. Again there are significant deviations between the two figures. By investigating the complete thrust characteristics obtained from both the models (not presented here) it is concluded that deviations in the K_Q/C_Q values are the cause of the difference between the first quadrant and four quadrant model. The accuracy of the C_T and C_Q models is considered to be insufficient. However, the K_T and K_Q models seem appropriate.

"The Wageningen Ka4-70 propeller with nozzle 37"

In Oosterveld (1970) four quadrant measurements with variable pitch ratio are presented for the Wageningen Ka4-70 propeller with nozzle 37 and pitch ratios from 0.6 to 1.4. The results are presented as Fourier coefficients for C_T and C_Q . The resulting propeller efficiency plot based on the model is shown in Figure 2.7. It is seen that the highest pitch ratio is the most efficient for all environmental conditions. Hence, the model is unsuitable for investigation of propulsion controllers with respect to optimal performance.

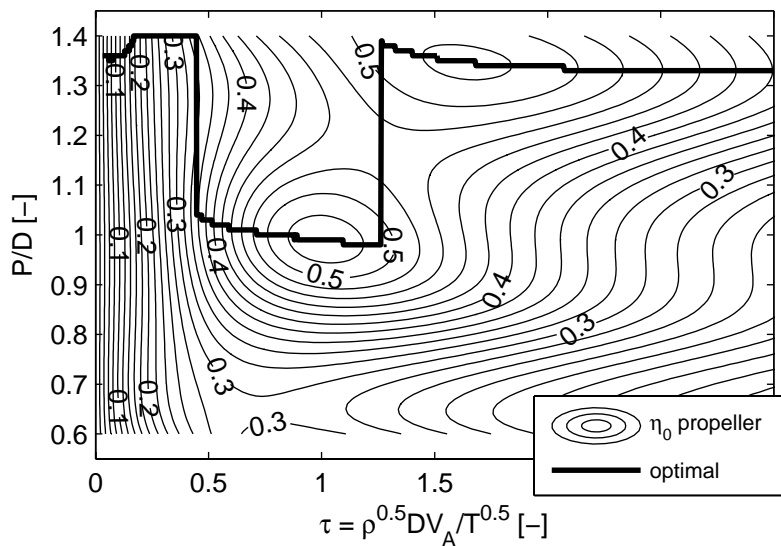


Figure 2.6: Propeller efficiency plot for first quadrant for "The Wageningen Ka4-70 propeller with nozzle 19A" based on the C_T and C_Q model.

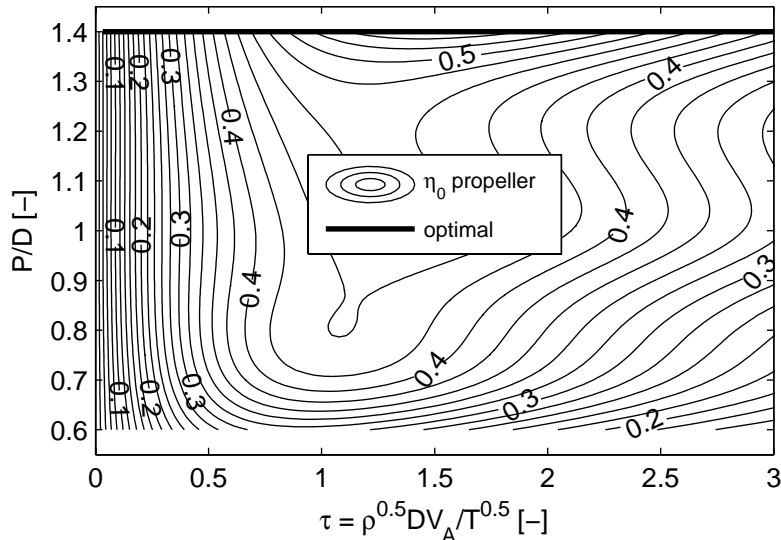


Figure 2.7: Propeller efficiency plot for first quadrant for "The Wageningen Ka4-70 propeller with nozzle 37" based on the C_T and C_Q model.

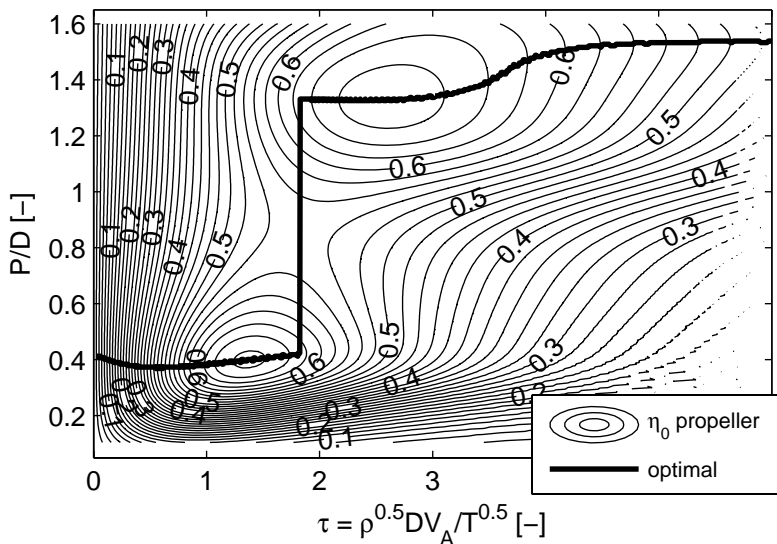


Figure 2.8: Propeller efficiency plot for first quadrant for "The Gutsche 1041 propeller".

"The Gutsche 1041 propeller"

In Strom-Tejsen and Porter (1972) a numerical model of the experimental results obtained by Gutsche and Schroeder (1963) are presented. Both references presents four quadrant results with variable pitch ratio from -1.1 to 1.6 . The propellers used in the Gutsche and Schroeder (1963) experiments are modified versions of the Gawn (1953) propellers, in order to facilitate pitch changes. The resulting propeller efficiency plot based on the numerical model in Strom-Tejsen and Porter (1972) is shown in Figure 2.8. It is seen that the model has two propeller efficiency peaks, one at $P/D = 0.4$ and one at $P/D = 1.3$. This is very strange, and by investigation of the K_Q plots from the numerical model and in Gutsche and Schroeder (1963) it is found a 30% deviation in the numerical model compared to the Gutsche and Schroeder (1963) plot. Hence, it is concluded that the accuracy of the numerical model is insufficient for optimization purposes.

"The CD-CPP 7708 propeller"

In Chu et al. (1979) results on controllable pitch propellers with specific combinations of advance speed and pitch ratio are presented. It is not a complete four quadrant model. Hence, the model is not suitable for comparison of controller performance. The propeller efficiency plot is shown in Figure 2.9. It is seen that the model catches the main characteristics of the propeller for low τ values.

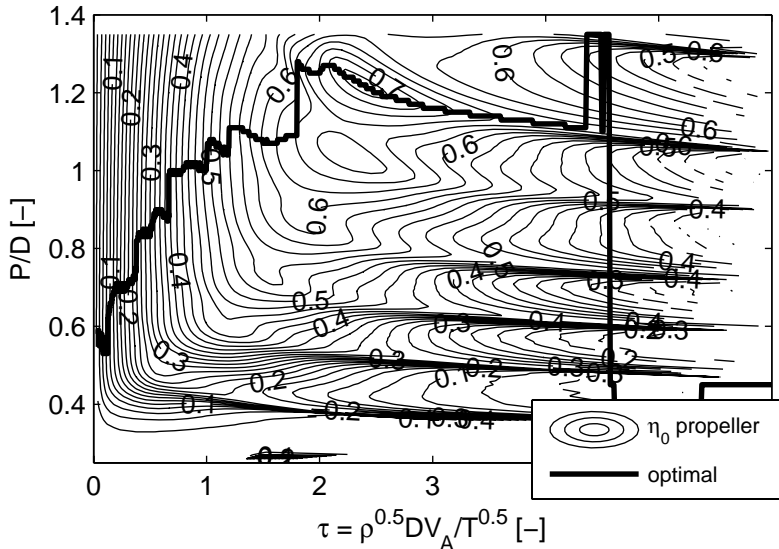


Figure 2.9: Propeller efficiency plot for first quadrant for "The CD-CPP 7708 propeller".

2.3 Ventilation and in-and-out of water effects

A model for thrust and torque losses during ventilation and in-and-out of water effects is found in Ruth (2005) and Ruth and Smogeli (2006). The resulting stationary model is presented here, and the dynamic corrections are developed. The resulting model is simulated and compared with open water experiments. Finally, some considerations on anti-spin thruster control of consolidated controlled propellers are presented.

2.3.1 The stationary model

The thrust loss factor $\beta_T[-]$ and torque loss factor $\beta_Q[-]$ are defined as (Minsaas et al. 1987):

$$\beta_T = \frac{T_t}{T_n}, \quad (2.32)$$

$$\beta_Q = \frac{Q_p}{Q_n}, \quad (2.33)$$

where $T_n[N]$ is the nominal thrust, i.e. the total thrust of a lossless propeller, and $Q_n[Nm]$ is the nominal torque, i.e. the torque of a lossless propeller. The

Table 2.5: Parameters in the static ventilation model.

Parameter	Value	Parameter	Value
$a_{0.8+}$	1.1749	$b_{0.8+}$	-0.4134
$a_{0.8-}$	-0.0832	$b_{0.8-}$	+0.8739
$a_{0.2+}$	1.3173	$b_{0.2+}$	+0.1220
$a_{0.2-}$	-0.8161	$b_{0.2-}$	+2.2007
$\beta_{Tw \text{ max}}$	1.0	$\beta_{Tw \text{ min}}$	0.05
a_q	0.87	b_q	0.13

nominal thrust and torque are defined as:

$$T_n = K_{Tn}(J_A, P/D) \rho D^4 n^2, \quad (2.34)$$

$$Q_n = K_{Qn}(J_A, P/D) \rho D^5 n^2, \quad (2.35)$$

where $K_{Tn}(J_A, P/D)$ is the nominal thrust coefficient, and $K_{Qn}(J_A, P/D)$ is the nominal torque coefficient. The thrust and torque loss factors are used when evaluating the propeller's degree of ventilation. $\beta_T = 1$ means no thrust losses, whereas $\beta_T = 0$ implies total loss of the thrust. Similar reasoning applies to β_Q .

The stationary model has the modified Froude number F_{nh2} and the submergence ratio h/R as input variables. The modified Froude number is defined as:

$$\begin{aligned} F_{nh2} &= \frac{n\sqrt{D}}{\sqrt{(1+h/R)g}}(P/D), \\ &= F_{nD} \frac{P/D}{\sqrt{1+h/R}}. \end{aligned} \quad (2.36)$$

The outputs from the model are the total thrust loss factor β_T and the torque loss factor β_Q . The model is described by the parameters in Table 2.5. The model divides the total thrust and the torque loss factor (β_T and β_Q) into two different contributions: loss factor due to reduced wetted propeller disk area β_{area} , and total thrust or torque loss factor corrected for reduced wetted propeller disk area, $\beta_{Tw}[-]$ or $\beta_{Qw}[-]$. Loosely speaking, the β_{area} represents the losses due to insufficient submergence of the propeller, and the β_{Tw} and β_{Qw} represents the losses caused by air drawing into the submerged parts of the propeller. Mathematically the relationships between the different loss factors are:

$$\beta_T = \beta_{area}\beta_{Tw}, \quad (2.37)$$

$$\beta_Q = \beta_{area}\beta_{Qw}. \quad (2.38)$$

The loss factor due to reduced wetted propeller disk area $\beta_{area}[-]$ can be found

from (Fleischer 1973):

$$\begin{aligned}\beta_{area} &= \frac{A_{wet}}{A_0}, \\ &= \text{real} \left[\begin{array}{l} 1 - \frac{\arccos(h/R)}{\pi} \\ + \frac{h/R}{\pi} \sqrt{1 - (h/R)^2} \end{array} \right],\end{aligned}\quad (2.39)$$

where $A_{wet}[m^2]$ is the wetted area of the propeller, and $A_0[m^2] = \pi R^2$ is the propeller disk area. This loss is present for all shaft speeds and is independent of the shaft speed. β_{Tw} is calculated as follows, with h/R and F_{nh2} as inputs:

$$F_{nh2}^{0.8+} = a_{0.8+}(h/R) + b_{0.8+}, \quad (2.40)$$

$$F_{nh2}^{0.8-} = a_{0.8-}(h/R) + b_{0.8-}, \quad (2.41)$$

$$F_{nh2}^{0.2+} = a_{0.2+}(h/R) + b_{0.2+}, \quad (2.42)$$

$$F_{nh2}^{0.2-} = a_{0.2-}(h/R) + b_{0.2-}, \quad (2.43)$$

$$a_+ = - \left(\frac{F_{nh2}^{0.2+} - F_{nh2}^{0.8+}}{0.2 - 0.8} \right), \quad (2.44)$$

$$a_- = - \left(\frac{F_{nh2}^{0.2-} - F_{nh2}^{0.8-}}{0.2 - 0.8} \right), \quad (2.45)$$

$$b_+ = -0.8a_+ + F_{nh2}^{0.8+}, \quad (2.46)$$

$$b_- = -0.8a_- + F_{nh2}^{0.8-}, \quad (2.47)$$

$$\beta_{Tw+} = \max \left(\frac{\beta_{Tw \min}, \min[\beta_{Tw \max}, }{a_+ F_{nh2} + b_+] \right), \quad (2.48)$$

$$\beta_{Tw-} = \max \left(\frac{\beta_{Tw \min}, \min[\beta_{Tw \max}, }{a_- F_{nh2} + b_-] \right), \quad (2.49)$$

$$\beta_{Tw} = \max (\beta_{Tw+}, \beta_{Tw-}). \quad (2.50)$$

β_{Qw} is calculated from β_{Tw} as:

$$\beta_{Qw} = a_q \beta_{Tw} + b_q. \quad (2.51)$$

Finally the total thrust loss factor β_T and the torque loss factor β_Q are calculated from (2.37) and (2.38). Plots of β_T and β_Q obtained from the model are shown in Figure 2.10.

2.3.2 Extension to a dynamic model

When extending the stationary model to a dynamic model, the stationary model is applied as a quasi-static model. This is reasonable, since the response time of the ventilation phenomenon is slower than the blade frequency, as seen from the measurements presented in the next section. The Wagner effect described

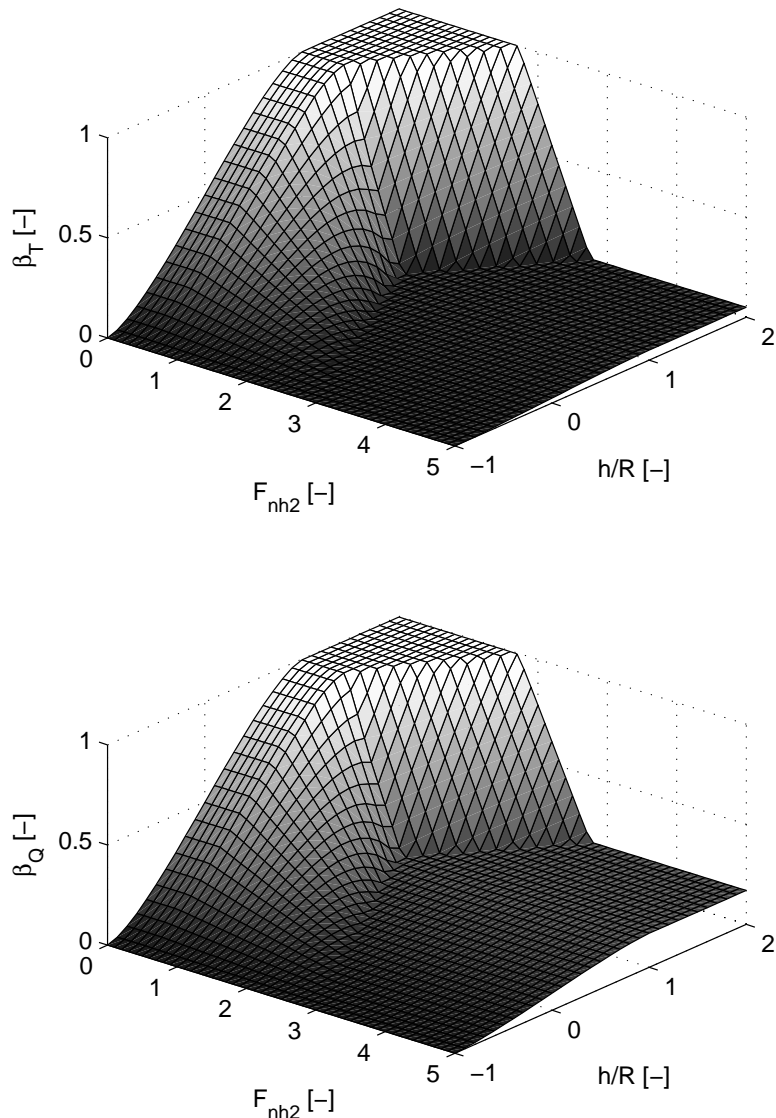


Figure 2.10: Plots of the total thrust loss factor β_T and torque loss factor β_Q obtained from the model as functions of the modified Froude number F_{nh2} and the submergence ratio h/R .

by Wagner (1925) also affects the dynamic model, by creating hysteresis in the thrust production, see Lehn (1992). The propeller uses more time to build up the thrust when going from air to water, than to lose the thrust when going from water to air. This phenomenon causes the thrust to decrease faster than it increases when the degree of ventilation changes. This is modeled by rate limits on β_{Tw} and β_{Qw} :

$$-\infty < \dot{\beta}_{Tw} \leq \dot{\beta}_{Tw,\max}, \quad (2.52)$$

$$-\infty < \dot{\beta}_{Qw} \leq \dot{\beta}_{Qw,\max}. \quad (2.53)$$

where $\dot{\beta}_{Tw,\max}[-]$ is the maximum rate of change of β_{Tw} and $\dot{\beta}_{Qw,\max}[-]$ is the maximum rate of change of β_{Qw} .

The total thrust and the propeller torque are also influenced by the incident water speed on the propeller. Since the water flowing through the propeller can be modeled as a mass, it has a certain response time from thrust and torque are changed until stationary conditions are obtained. This means that when increasing the shaft speed the incident water speed will be lower than at steady state. This implies that the propeller will produce slightly more thrust than in the quasi-static case (since K_T increases with lower advance number). This can be modeled as a forward shift in time from the quasi-static values to the dynamic values. This time shift is also applied to the nominal thrust and torque in the simulations in order to keep the dynamic and nominal values in phase.

2.3.3 Simulations verified by open water experiments

Simulations and experiments are performed to verify the performance of the ventilation model. The simulations are compared to experimental results obtained in the Marine Cybernetics Laboratory (MCLab) at NTNU. The experimental results are obtained with the same propeller as was used to obtain the stationary model. The main particulars of the propeller and duct are found in Table 2.3 and 2.4. In the experiments $V_A = 0$ and $P/D = 1$. To remove measurement noise the results are low-pass filtered at 5[Hz]. It is observed from the raw measurements that the ventilation phenomenon has a response time in order of 0.7[s]. Hence the response time of the filter is 3.5 times faster than the response time of the ventilation, and does not affect the measurements significantly.

In the simulations the total thrust and torque are calculated according to;

$$T_t = \beta_{Tw}\beta_{area}K_{T0}\rho D^4 n^2, \quad (2.54)$$

$$Q_p = \beta_{Qw}\beta_{area}K_{Q0}\rho D^5 n^2, \quad (2.55)$$

where $K_{T0} = K_{Tn}(J_A = 0, P/D)$, $K_{Q0} = K_{Qn}(J_A = 0, P/D)$, and the shaft speed and submergence ratio are functions of time taken from the experiments. In the simulations, the stationary ventilation model is used as a quasi-static model. This is reasonable since the time per revolution is typically less than 0.2[s], and the response time of the ventilation phenomenon is in the order of 0.7[s]. To account for the fact that the total thrust and torque loss factors

decrease faster than they increase, the rise rate limits given in (2.52)-(2.53), with $\dot{\beta}_{Tw,\max} = \dot{\beta}_{Qw,\max} = 1$, are applied to the quasi-static β_{Tw} and β_{Qw} in the simulations. The forward time shift from quasi-static to dynamic values is set to 0.064[s] (8 samples).

The first part of the experiments were performed with shaft speed control, where the thrust reference $T_d[N]$ and the submergence ratio were varied as sine functions. In shaft speed control the desired shaft speed $n_d[Hz]$ was calculated as:

$$n_d = \sqrt{\frac{T_d}{\rho D^4 K_{T0}(P/D = 1)}}, \quad (2.56)$$

and the controller aimed at keeping the shaft speed equal to the desired shaft speed. The thrust reference, and hence also the shaft speed, had a period of 7[s]. The submergence ratio was varied fast with a period of 10[s] (Figure 2.11), and slowly with a period of 100[s] (Figure 2.12). The equations were:

$$T_d = 230 + 160 \sin\left(\frac{2\pi}{7}t\right), \quad (2.57)$$

$$h/R = 1.2 + 1.2 \sin\left(\frac{2\pi}{10}t\right), \quad (2.58)$$

$$h/R = 1.2 + 1.2 \sin\left(\frac{2\pi}{100}t\right), \quad (2.59)$$

where t is the time.

To see the performance of the model under other control schemes than shaft speed control, the thruster was also operated in power control. Power control aims at keeping the power as close as possible to the desired power $P_d[W]$, which was calculated as:

$$P_d = \frac{2\pi K_{Q0}}{\sqrt{\rho} D K_{T0}^{3/2}} T_d^{3/2}. \quad (2.60)$$

Power control reduces the power peaks at high shaft speeds and is further described in Sørensen et al. (1997) and Section 3.4.1. In the power control simulation the submergence ratio was varied sinusoidally with a period of 10[s] (Figure 2.13). The equations were:

$$T_d = 100, 150, 200, \quad (2.61)$$

$$h/R = 1.2 + 1.2 \sin\left(\frac{2\pi}{10}t\right). \quad (2.62)$$

In Figure 2.11, 2.12, and 2.13, start and stop of ventilation are seen as the large transients in the total thrust and torque loss factors. The non-ventilated condition corresponds to $\beta_T = \beta_Q = 1$, where the propeller is lossless. The fully ventilated regime corresponds to the low β_T and β_Q values. The model recreates both the lossless condition and the transients during start and stop of ventilation well. The values obtained in the fully ventilated regime differ a little from the measured values. However, the main importance is that both experiments and simulations show large losses at the same time. Generally the simulated model

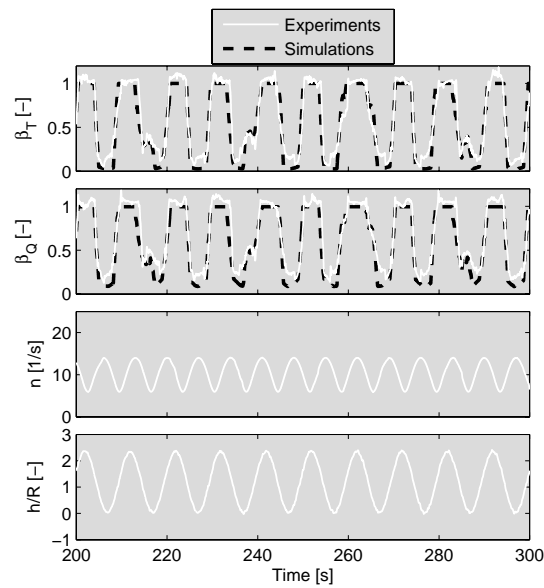


Figure 2.11: Comparison of simulations and experiments in shaft speed control with rapidly varying submergence ratio.

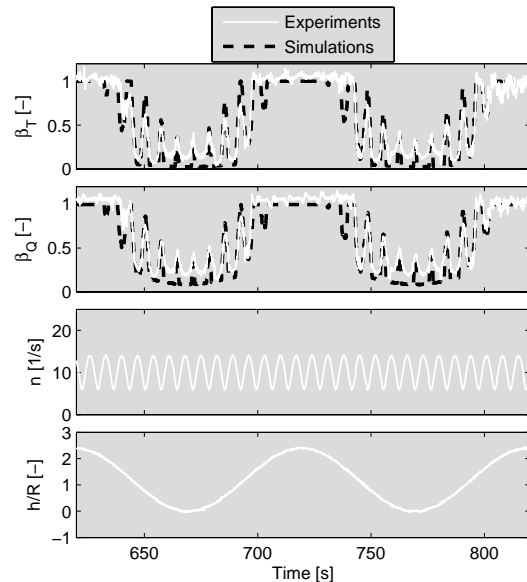


Figure 2.12: Comparison of simulations and experiments in shaft speed control with slowly varying submergence ratio.

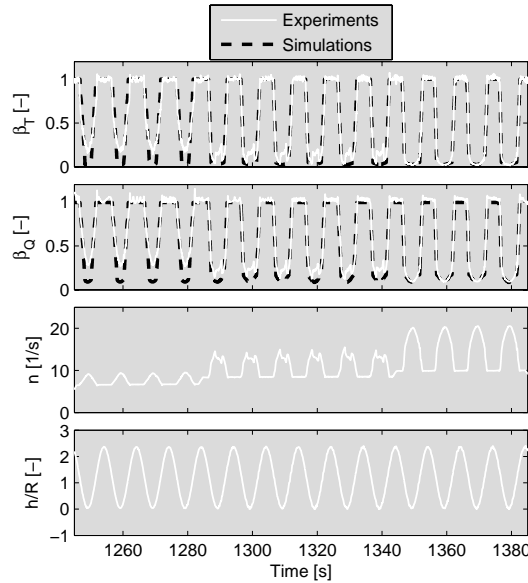


Figure 2.13: Comparison of simulations with experiments in power control.

performs well, reproducing the main characteristics of the ventilation effect. Originally, anti-spin control was invented for torque and power control, as these controllers may cause unacceptable propeller racing in case of ventilation and in-and-out-of water effects. Such propeller racing is clearly seen in Figure 2.13 where the shaft speed has large variations even for constant thrust references. The simulation model is seen to recreate this phenomenon well. In shaft speed control (Figure 2.11 and 2.12), the shaft speed simply follows its reference as intended. In Figure 2.14-2.16 plots of the range of F_{nh2} and h/R in the three open water tests are shown. It is seen that the open water tests cover most of the transition region from the non-ventilated to the fully ventilated condition. This verifies that the model performs well in this region. The model is hence considered accurate enough for control design purposes.

2.3.4 Implications for control

The ventilation model presented is developed in order to investigate the effect of controllable pitch on ventilation. Consider the following simple example where the thrust is modeled as:

$$T = kn^2(P/D)^{1.5}, \quad (2.63)$$

where $k[kgm]$ is a constant. This seems reasonable around $J_A = 0$ by investigating Figure 2.3. Then assume the propeller is operated with two different combinations of pitch ratio and shaft speed at equal thrust. Then:

$$T_1 = kn_1^2(P/D)_1^{1.5} = T_2 = kn_2^2(P/D)_2^{1.5}, \quad (2.64)$$

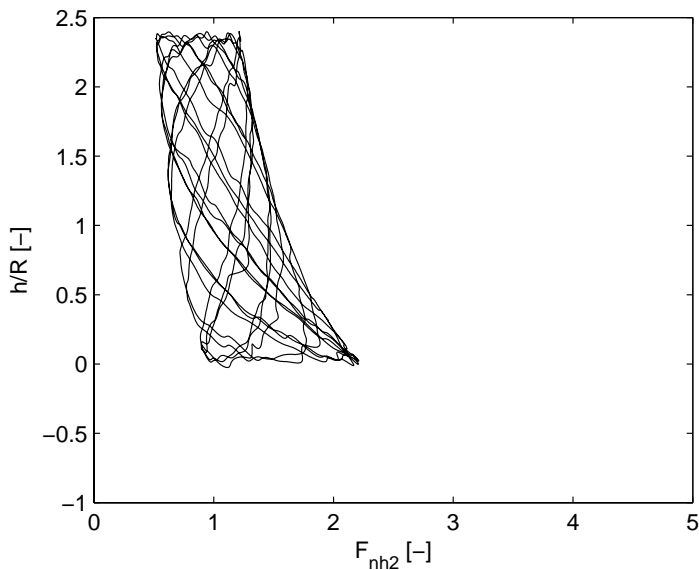


Figure 2.14: Range of F_{nh2} and h/R in the open water test presented in Figure 2.11.

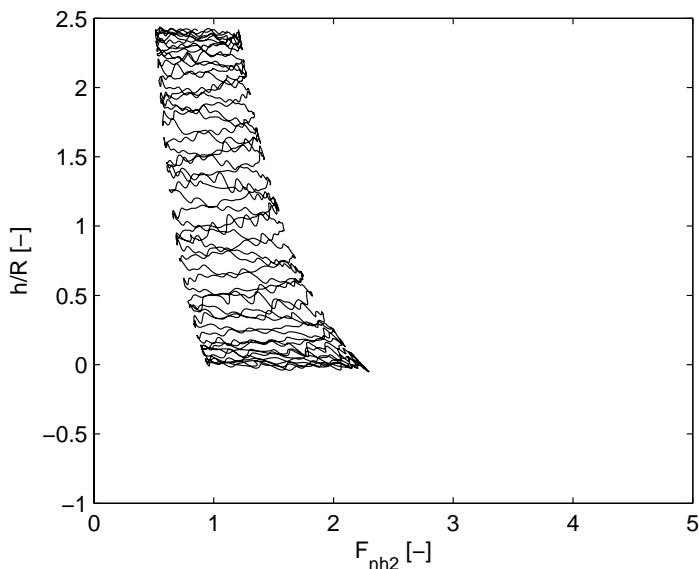


Figure 2.15: Range of F_{nh2} and h/R in the open water test presented in Figure 2.12.

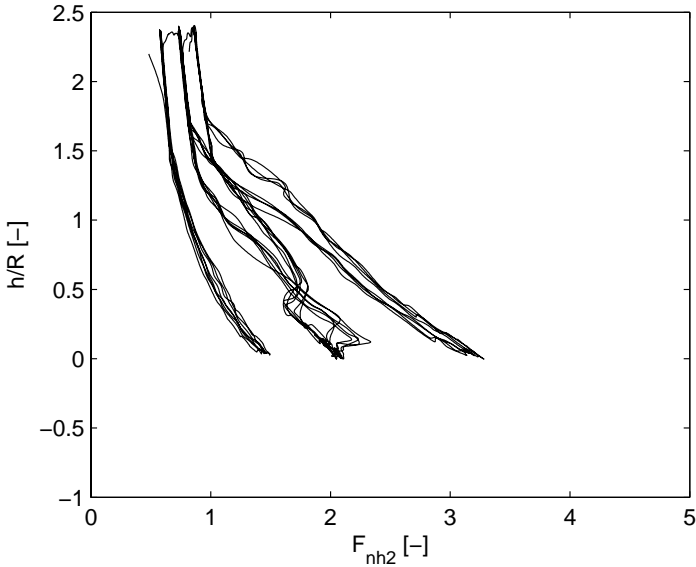


Figure 2.16: Range of F_{nh2} and h/R in the open water test presented in Figure 2.13.

where the subscripts index the two different combinations. Let us assume:

$$(P/D)_2 = a(P/D)_1, \quad (2.65)$$

where $a[-]$ is a constant. This means that the shaft speed of the second combination can be computed:

$$n_2 = \frac{1}{a^{0.75}} n_1. \quad (2.66)$$

The modified Froude number is computed for the two different combinations of pitch ratio and shaft speed:

$$F_{nh2,1} = \frac{\sqrt{D}}{\sqrt{(1 + h/R) g}} n_1 (P/D)_1, \quad (2.67)$$

$$\begin{aligned} F_{nh2,2} &= \frac{\sqrt{D}}{\sqrt{(1 + h/R) g}} n_2 (P/D)_2, \\ &= \frac{\sqrt{D}}{\sqrt{(1 + h/R) g}} \frac{1}{a^{0.75}} n_1 a (P/D)_1, \\ &= a^{0.25} F_{nh2,1}. \end{aligned} \quad (2.68)$$

This means that producing the same thrust with different pitch ratios give different modified Froude numbers. From Figure 2.10 it is seen that smaller modified

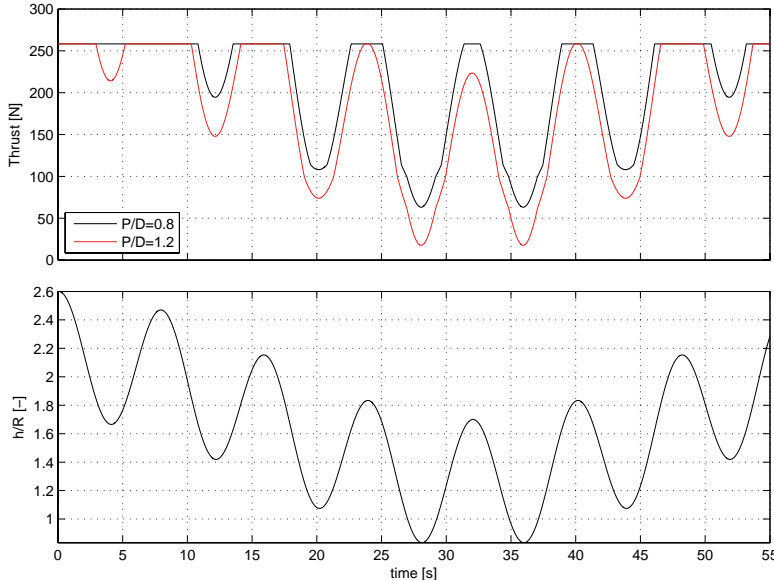


Figure 2.17: Plot of thrust and submergence ratio for two different combinations of shaft speed and pitch ratio, both giving the same thrust fully submerged.

Froude numbers reduces the possibility for ventilation. Hence, it is concluded, as in Ruth (2005), that a smaller pitch ratio reduces the possibility and severity of a ventilation incident.

On electrically driven controllable pitch propellers it is a significant difference in the response time between the pitch actuator and the electric motor. Due to the rapid transients at ventilation start, anti-spin thruster control requires fast actuators. The response time of the pitch actuator, typically in the order of seconds compared to the electric motor which is in the order of tenths of a second. Therefore anti-spin thruster control actions should be put on the electric motor. This means that the excellent results on anti-spin thruster control for fixed pitch propellers found in Smogeli (2006) should be applied. However, it is worth remembering that decreased pitch ratio gives reduced likelihood and severity of ventilation.

Simulations of the propeller used in the model tests, without anti-spin control, at two different combinations of shaft speed and pitch ratio, both giving the same nominal thrust, are seen in Figure 2.17. The black thrust line is with $P/D = 0.8[-]$ and $n = 13.4[Hz]$ and the red line with $P/D = 1.2[-]$ and $n = 10.0[Hz]$. The submergence ratio used on both combinations is seen in the lower subplot. It is seen that the possibility and severity of ventilation is reduced with reduced pitch ratio.

Chapter 3

Propulsion control for surface vessels

This chapter is to a large extent taken from Ruth et al. (2006). Most marine vehicles use screw propellers for thrust production. In this chapter propulsion control of surface vessels with screw propellers, e.g. ships and rigs are elaborated. Rudders are not considered. The differences in the propulsion control problem between surface vessels and underwater vehicles are examined. The two most common operation modes for a surface vessel are low speed maneuvering and transit. The environmental, measurement, and modeling differences between low and moderate/high advance speeds are discussed. A set of different low level propulsion controllers are compared in terms of efficiency, and thrust, torque, power and shaft speed sensitivities subject to varying advance speeds. The sensitivity is the ratio between the actual and the desired value. The comparison is based on the τ parameter, which makes it possible to compare different propulsion systems producing the same thrust in equal environments as function of this parameter only. Based on the comparison, the best controller for a particular task can be chosen in order to maximize positioning accuracy, safety and efficiency.

In Figure 3.1 a schematic drawing of the propulsion controller interfaces is shown. The outputs from the control system to the machinery are in this chapter the commanded pitch ratio and commanded torque. This is because it is a close relationship between torque and current (electrical motors) or fuel rack position (diesel engines). The outputs from the propulsion controller are set points for the governor and the pitch controller. It is important to notice that the controlled variables are not necessarily the outputs from the controller. For e.g. shaft speed control, the controlled variable is the shaft speed. The commanded torque Q_c is then controlled by a PID-controller with desired and measured shaft speed as inputs. Throughout the thesis the term PID-controller will be used, although the D-term may be zero in many cases.

Due to differences in the control objective and in the available measurements, the propulsion control problem for surface vessels is here divided into two differ-

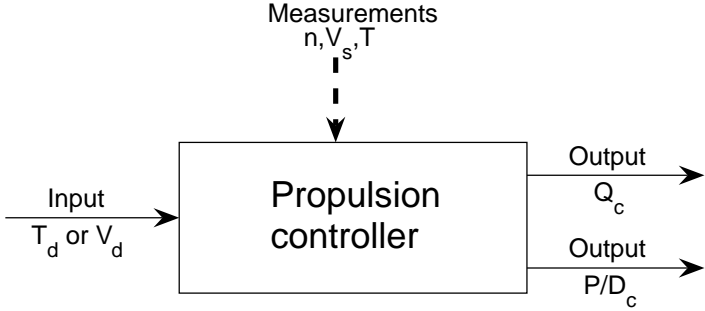


Figure 3.1: Propulsion controller interfaces. V_d is the desired ship speed, V_s is the measured ship speed, Q_c is the commanded torque, and P/D_c is the commanded pitch ratio. Not all the measurements are needed in all the controllers, see Table 3.2.

ent regimes:

- low advance speed (advance speed $< 2[m/s]$),
- moderate/high advance speed (advance speed $> 2[m/s]$).

The control objective of the propulsion controller at low advance speeds is usually to produce the thrust required from the DP system. This means that the mapping from desired to produced thrust is important. At moderate/high advance speeds the objective is usually to maintain a certain ship speed. Hence, the mapping from desired to produced thrust is no longer important as the vessel speed controller simply controls the produced thrust to match the resistance of the vessel.

The propulsion controllers can be divided into three groups: fixed pitch propeller (FPP) controllers, pitch controllers and consolidated controllers. FPP control means that the pitch is fixed, and the commanded torque is varied to produce the desired thrust. Pitch control means to keep a constant shaft speed and vary the thrust by changing the commanded pitch ratio. The most advanced controller is the consolidated controller. This controller varies both the commanded pitch ratio and the commanded torque. Since several combinations of pitch ratio and torque give the same thrust, consolidated control enables optimal control in the entire vessel speed operation range. Here, examples of optimal control with maximization of propeller efficiency are presented.

3.1 Surface vessels versus underwater vehicles

The operational condition of a propeller on a surface vessel is influenced by the load condition, vessel motions, waves and current. An underwater vehicle is

usually operated below the wave zone, and hence only affected by the vehicle motions and current. Further, the vessel motions are usually more violent for a surface vessel than for an underwater vehicle.

The water velocity seen by an underwater vehicle is called the relative velocity, and is the sum of the vehicle velocity and the current velocity, which can relatively accurately be measured by e.g. a Doppler log. The relative velocity is used in the vehicle guidance, navigation, and control system, and is then also available for the propulsion control system. The result of this is that the effects of environmental disturbances on the propellers relatively accurately can be counteracted by the propulsion control system. To further improve the propulsion control system on underwater vehicles Healey et al. (1995), Whitcomb and Yoerger (1995), Whitcomb and Yoerger (1999a), Bachmayer et al. (2000), Blanke et al. (2000), and Bachmayer and Whitcomb (2003) investigate the possibility of modeling the thruster dynamics. Yoerger et al. (1990), Whitcomb and Yoerger (1999b), Fossen and Blanke (2000), Bachmayer and Whitcomb (2001), and Smallwood and Whitcomb (2002) use such models of the thruster dynamics to improve the dynamic performance of the propulsion control system. This is possible since the propeller models are accurate. For surface vessels the same accuracy in these models can not be expected, due to effects like fouling and wake. Blanke et al. (2000) model the propeller dynamics together with the surge dynamics of the vehicle. Fossen and Blanke (2000) use a combination of thruster and surge dynamics of the underwater vehicle to improve the propulsion control system. This is possible since usually there are available accurate models of the vehicle and the propellers. On surface vessels, the surge dynamics is strongly influenced by wind and waves. Then, important unmodelled nonlinear and stochastic dynamics are introduced in to the system. Utilizing the surge model in this case, is then more difficult than for underwater vehicles.

3.2 Low advance speed

3.2.1 Advance speed measurement at low advance speeds

At low advance speeds the ship speed measurements can not be utilized in thruster control, since the ship speed is in the order of (or even smaller) than the water particle velocities induced by waves and current. Water speed measurements at each individual thruster are not common industrial practice. This would require additional sensors and wiring, which are considered unwanted due to increased cost, complexity and maintenance.

In station-keeping operations an additional difficulty is the fact that many thrusters are operated at the same time, and that they are subject to losses like cross coupling (including thruster-thruster interaction), ventilation, in-and-out-of water effects, and thruster-hull interaction (including the Coanda effect). These effects make it difficult to relate the vessel behavior to each individual thruster and vice versa. The thruster-hull interaction does not directly affect the propeller's operational conditions. This means that it is impossible to determine the effect of this loss from measurements done on the thruster. Although this

loss affects the vessel, it is considered to be a thrust loss, since it is strongly dependent on how the thruster is operated.

The conclusion is that currently it is not realistic to utilize advance speed measurements or advance speed observers including the vessel dynamics in thruster control at low advance speeds.

3.2.2 Optimal control at low advance speeds

Optimal control of controllable pitch propellers means to control two variables of the propeller, typically the shaft speed and pitch ratio, simultaneously in an optimal way (e.g. minimization of power), and still produce the desired thrust. For a propeller operating at zero advance speed with positive thrust references there is one optimal pitch ratio regardless of what the thrust reference is. This follows directly from the non-dimensional thrust and torque coefficients K_T , K_Q , and C_T , C_Q . This is because the advance number and the advance angle becomes zero when the advance speed is zero, regardless of what the shaft speed is.

At advance speeds different from zero the propeller efficiency (2.23) is strongly dependent on the advance speed. Hence, information about the advance speed is needed to be able to control the desired shaft speed and pitch ratio optimally. The advance speed have to be estimated from the torque and shaft speed measurements only, since the thrust is commonly not measured. Investigating the behavior of the propeller coefficients at low advance numbers shows that there is not a one-to-one relationship between the coefficients and the advance number. This can be seen in Figure 3.2, showing the torque coefficient of the "The Gutsche 1041 propeller". One might think an observer could be able to track the torque coefficient path if it had a correct starting point. However, it will always be a problem when the observer reaches a local extremum point, maximum or minimum. Thus, an advance speed estimate will be inaccurate under such circumstances. However, at low advance speeds the advance number will also be low, except for very low thrust references. Hence, zero advance speed is a reasonable assumption at low advance speeds.

Since there are no measurements or estimates of the advance speed available, optimal control may be difficult for low advance speeds. However, it is possible to achieve near optimal performance without knowledge of the advance speed. Andresen (2000) controls both the pitch ratio and the shaft speed simultaneously improving the efficiency. The torque/shaft speed controller (Schanz 1967) presented later is also capable of near optimal control at low advance speeds without the advance speed knowledge.

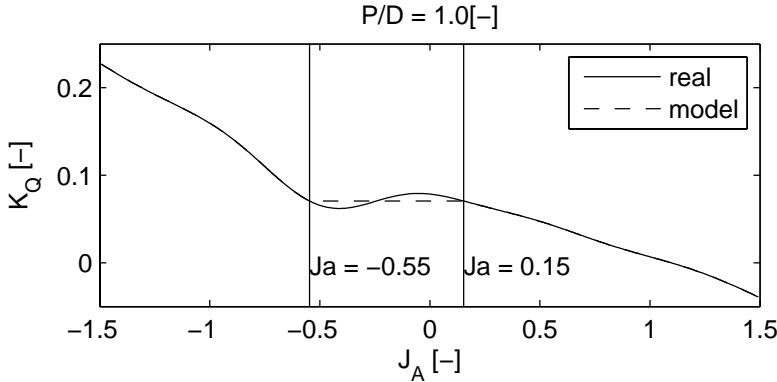


Figure 3.2: $K_Q(J_A, P/D = 1.0)$ for "The Gutsche 1041 propeller".

3.3 Moderate/high advance speeds

3.3.1 Advance speed measurements at moderate/high advance speeds

At moderate/high advance speeds the context of the propulsion control problem is changed since the ship speed dominates the inflow to the propeller. In this case most of the losses mentioned in Section 3.2.1 are minor. There are also rarely more than two propellers operating. This simplifies the relationship between the ship and propeller behavior. Relatively accurate GPS measurements are also available at moderate/high advance speeds. The GPS velocity measurement error is typically in the order of $0.1[m/s]$, independent of the ship speed. While the relative errors at low ship speeds are unacceptable, they are smaller and acceptable at higher advance speeds.

As mentioned before the thrust sensitivity is usually not important in the moderate/high advance speed regime where the goal is to maintain a certain ship speed. The desired set point in the propulsion control system will then typically be set by a PID controller:

$$u_d = \text{PID}(V_s - V_d), \quad (3.1)$$

where $V_s[m/s]$ is the ship speed, and $V_d[m/s]$ is the desired ship speed. u_d is the desired set point in the propulsion system, and can e.g. be the desired thrust T_d , or the desired power $P_d[W]$.

3.3.2 Optimal control at moderate/high advance speeds

The control objective at moderate/high advance speed is to maintain a certain ship speed, and preferable to do such in an optimal way. At the relevant advance numbers (typically $J_A \in [0.3, 1.3]$) the thrust and torque coefficient curves show

nearly linear behavior. However, measurement noise and modeling errors can be significant. Trying to design an observer for the advance speed one will experience that there are no useful innovations or injection terms to construct a corrector. The observer will then correspond to a look-up table from e.g. propeller torque, shaft speed, and pitch ratio to advance speed:

$$V_A = f(Q_p, n, P/D), \quad (3.2)$$

where $f(\cdot)$ is found by solving (2.10) for V_A . This requires detailed knowledge of the full scale propeller characteristics. Another problem is that the model will change during the life cycle and modes of operation due to e.g. changing loading condition and fouling. These problems increase the uncertainty in the model and will degrade the performance of the system. A simpler approach with reasonable accuracy will be to use the ship speed measurements, adjusted by a (constant) wake fraction, as the advance speed.

In the following, seemingly independent efforts to do optimal propulsion control at moderate/high advance speeds will be summarized. Bakoutouzis (1992) assumes measurements of shaft speed, pitch ratio, fuel flow rate, and ship speed or thrust. It is suggested to use a step-wise variation of pitch and shaft speed to determine the optimum settings for the two variables under the prevailing operational conditions and constant ship speed or thrust. Chachulski et al. (1995) use measurements of the torque, the shaft speed, the ship speed and the pitch. The propulsion characteristics are updated by periodical measurements. Based on the propulsion characteristics and measurements, the optimal pitch and shaft speed settings are found. Fukuba et al. (1996) use measurements of the ship speed, the shaft speed, the pitch and the propeller load torque. The system characteristics are identified by neural networks. The optimal pitch and revolution speed for the desired ship speed are then found based on the system characteristics. Morvillo (1996) uses measurements of the ship speed, shaft speed, and propeller pitch ratio, information about the propeller characteristics (K_T and K_Q plots), wake fraction ($w = \frac{V_s - V_A}{V_s}$) and thrust deduction ($t = \frac{T - R}{T}$, where $R[N]$ is the resistance of the ship). Based on this information the resistance of the ship is estimated as:

$$R = (1 - t)\rho D^4 n^2 K_T(J, P/D). \quad (3.3)$$

The estimated resistance is then used in combination with the commanded vessel speed to calculate the desired pitch and shaft speed that minimizes the power. Young-Bok et al. (1998) use state feedback control, and decoupling to do optimal consolidated control. Whalley and Ebrahimi (2002) measure the change of the shaft speed and the change of the turbine torque, linearizes the system about the operation point and minimize the control effort. Ruth (2005) uses measurements of the motor torque and shaft speed, and tries to use extremum seeking in order to find the optimal pitch. The method uses a sinusoidal pitch ratio perturbation to determine whether the pitch ratio should be increased or decreased in order to increase the efficiency. However, it was concluded that the method fails in waves due to the effect of wave frequency of encounter. This is because a ship can be excited by waves at all possible perturbation frequencies due to the effect of

Table 3.1: Comparison of speed regimes and optimality of the different controllers. X means that the controller can be used in this advance speed regime.

Controller	$V_A < 2$	$V_A > 2$	Optimal
Shaft speed	X	X	one J_A
Torque	X	X	one J_A
Power	X	X	one J_A
Combined	X	X	one J_A
Pitch	X	X	No
Torque/pitch ratio		X	Yes
Shaft speed/pitch ratio		X	Yes
Torque/shaft speed	X	X	Nearly

forward speed and frequency of encounter. This makes it impossible to isolate the effect of the perturbation in the output (consumed power), and hence, impossible to determine if the pitch variation actually increases or decreases the efficiency. The work of Blanke et al. (2007) and Pivano (2008) includes a novel approach for increasing the efficiency of fixed pitch propellers operating in waves. They utilize the fact that during a wave cycle, the advance speed seen by the propeller varies. The idea is to produce a little extra thrust when the efficiency is slightly increased due to the advance speed variations.

3.4 Propulsion controllers

The thrust and torque coefficients applied in the controllers are denoted $K_{Tc}[-]$ and $K_{Qc}[-]$. For the FPPs at low advance speeds the following relationship will be applied:

$$K_{Tc} = K_T(J_A = 0), \quad (3.4)$$

$$K_{Qc} = K_Q(J_A = 0). \quad (3.5)$$

At moderate/high advance speeds the controller thrust and torque coefficients can be expressed as linear functions of the advance number J_A (Blanke 1981).

$$K_{Tc} = a_T J_A + b_T, \quad (3.6)$$

$$K_{Qc} = a_Q J_A + b_Q, \quad (3.7)$$

where $a_T[-]$, $b_T[-]$, $a_Q[-]$ and $b_Q[-]$ are constants.

The properties of the different controllers are summarized in Table 3.1 and 3.2. The details of the different controllers are elaborated in the following. The reader is also referred to the work by Pivano (2008) for other recent results on propulsion control.

3.4.1 Propellers with one controllable variable

In this section control of propellers with one controllable variable is considered. This means traditionally that either pitch ratio or shaft speed is fixed, and

Table 3.2: List of required measurements for the different controllers in the two advance speed regimes. Parentheses means that the measurements are needed if K_{Tc} and K_{Qc} are to be varied according to (3.6) and (3.7).

Controller	$V_A < 2$	$V_A > 2$
Shaft speed	n	$n, (V_s)$
Torque	none	(n, V_s)
Power	n	$n, (V_s)$
Combined	n	$n, (V_s)$
Pitch	n	$n, (V_s)$
Torque/pitch ratio	not used	V_s, T
Shaft speed/pitch ratio	not used	n, V_s, T
Torque/shaft speed	n	n

the other variable is varied to achieve the desired thrust or ship speed. The controllers can be used for both low and moderate/high advance speeds. The difference will be that in thruster control (low advance speeds) the desired thrust comes from the DP or PM system, while at moderate/high advance speeds the desired thrust comes from a vessel speed controller like (3.1) with $T_d = u_d$. Propellers with one controllable variable are designed to be optimal at one particular advance number. For thrusters operating at low advance speeds, e.g. during station keeping operations, the propeller is usually optimized for $J_A = 0$. Main propellers used during ocean crossing and transit operations are commonly optimized for a particular advance number dependent on the vessels service speed and resistance. The main properties of the different one controllable variable controllers are given in Table 3.1 and 3.2. The details are given in the following.

Shaft speed control

The shaft speed controller is the most commonly used propulsion controller and aims at keeping the shaft speed constant. The equations are:

$$n_d = \sqrt{\frac{T_d}{K_{Tc}\rho D^4}}, \quad (3.8)$$

$$Q_{cn} = \text{PID}(n - n_d), \quad (3.9)$$

where $n_d[\text{Hz}]$ is the desired shaft speed, and $Q_{cn}[\text{Nm}]$ is the commanded torque.

Torque control

Torque control aims at keeping the motor torque constant. The controller is formulated as:

$$Q_{cq} = Q_d = \frac{K_{Qc}D}{K_{Tc}}T_d, \quad (3.10)$$

where $Q_d[\text{Nm}]$ is the desired torque, and $Q_{cq}[\text{Nm}]$ is the commanded torque. The advantages of torque control are reduced wear and tear, and the most correct

thrust production when the advance speed differs from zero. The references are Sørensen et al. (1997) and Smogeli et al. (2005).

Power control

Power control aims at keeping the motor power constant. The controller is formulated as:

$$P_d = \frac{2\pi K_{Qc}}{\sqrt{\rho} D K_{Tc}^{3/2}} T_d^{3/2}, \quad (3.11)$$

$$Q_{cp} = \frac{P_d}{2\pi n}, n \neq 0, \quad (3.12)$$

where $Q_{cp}[Nm]$ is the commanded torque. The advantages of power control are predictable loading of the power network and improved thrust production at nonzero advance speeds compared to shaft speed control. For DP applications the references are Sørensen et al. (1997) and Smogeli et al. (2005). Blanke and Nielsen (1990) introduced power control on diesel engines with mechanically direct-driven propellers at moderate/high advance speeds. The controller contained no mapping from desired thrust to power, but the desired power was set directly by the operator.

Combined control

The combined controller aims at combining the best properties from the torque and the power controller. It is formulated as:

$$Q_{cc} = \alpha(n) Q_{cq} + (1 - \alpha(n)) Q_{cp}, \quad (3.13)$$

$$\alpha(n) = e^{-k|pn|^r}, \quad (3.14)$$

where $Q_{cc}[Nm]$ is the commanded torque, $\alpha[-]$ is a weighting function, and $k[-]$, $p[s]$, $r[-]$ are parameters. The advantage of combined control is that the torque controller is utilized at low thrust references giving the most correct produced thrust, while the power controller is used at high thrust references to limit the power transients in the power network. The reference is Smogeli et al. (2004b).

Pitch control

Controllable pitch propellers can be used in combination with shaft generators. It is then desirable to keep the shaft speed at a certain value that suits the generators (Carlton 1994). This is called pitch control, since the shaft speed is kept constant, and the pitch is varied to control the thrust:

$$Q_{cpd} = \text{PID}(n - n_d), \quad (3.15)$$

$$\begin{aligned} P/D_{cpd} &= g\left(\frac{T_d}{\rho D^4 n_d^2}\right), \\ &= g(K_{Td}), \end{aligned} \quad (3.16)$$

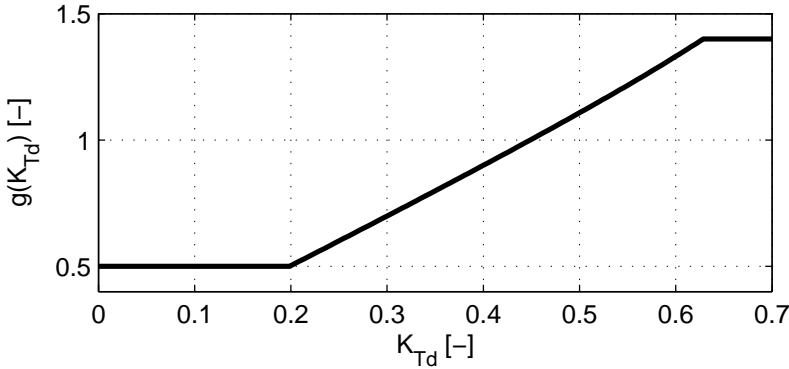


Figure 3.3: Plot of $g(K_{Td})$ for "The Wageningen B4-70 propeller".

where $Q_{cpd}[Nm]$ is the commanded torque, $P/D_{cpd}[-]$ is the commanded pitch ratio, $g(K_{Td})[-]$ is the mapping from K_{Td} to the commanded ratio, and $K_{Td} = \frac{T_d}{\rho D^4 n_d^2} [-]$. The relationship between desired thrust and pitch ratio can e.g. be determined by look-up tables. An example of the $g(K_{Td})$ mapping is shown in Figure 3.3 for "The Wageningen B4-70 propeller".

An advantage of pitch control is that the direct-driven diesel propeller is capable of fulfilling very small thrust references. This may not be possible for all the other controllers, since the engine has to be operated in some kind of shaft speed control at very low shaft speeds. This is because of uncertainties in the friction model. The disadvantage of pitch control is that the power consumption is larger at low loads than for e.g. shaft speed control. This is because the shaft speed is kept at a certain value, increasing the drag and friction forces. The zero load loss may be in the order of 15% of maximum available power (Sørensen 2004). For a DP operated vessel this can result in significantly increased fuel consumption and maintenance cost.

3.4.2 Propellers with two controllable variables

In consolidated control the propulsion system can produce the desired thrust or achieve the desired ship speed at many combinations of the outputs: commanded torque and pitch ratio. This makes it possible to optimize the propulsion system. Usually the system is optimized to maximize the efficiency (2.23). The most commonly used controller is the shaft speed/pitch ratio controller. In this controller the commanded torque is controlled to maintain a certain shaft speed. Hence it is called the shaft speed/pitch ratio controller.

When the propulsion controller consists of a hierarchy of controllers, it is important that a controller at a lower level (closer to the motor or pitch actuator) has a higher bandwidth than the controllers at higher levels in the hierarchy. The main properties of the different two controllable variables controllers are given

in Table 3.1 and 3.2. The details are given in the following.

Torque/pitch ratio controller

This controller is based on the optimal combination of torque and pitch ratio. It is proposed to use the τ parameter to find the optimal combination of torque and pitch ratio. The torque/pitch ratio controller is then formulated as:

$$\begin{aligned} Q_{cqp} &= Q_d, \\ &= \frac{K_Q(\tau)}{K_T(\tau)} DT_d, \end{aligned} \quad (3.17)$$

$$\begin{aligned} P/D_{cqp} &= k(\tau), \\ &= h(\tau) DT_d, \end{aligned} \quad (3.18)$$

where $Q_{cqp}[-]$ is the commanded torque, $h(\tau)[-]$ is the mapping from τ to desired torque, $P/D_{cqp}[-]$ is the commanded pitch ratio, and $k(\tau)[-]$ is the mapping from τ to commanded pitch ratio. A plot of $h(\tau)$ is seen in Figure 3.4 for "The Wageningen B4-70 propeller". The $k(\tau)$ mapping is the solid line in Figure 3.5. To make the controller perform perfect, perfect model and environmental knowledge are needed. In the controller the τ value has to be found. As argued earlier an accurate measurement or estimate of V_A is difficult to obtain. This means that it will be difficult to get accurate measurements or estimates of τ because it is a function of V_A . The complexity of this controller is further increased since an estimate or measurement of the thrust is needed. However, it turns out that the loss of optimality due to errors in the τ value is small. This can be seen from Figure 3.5, which is based on "The Wageningen B4-70 propeller". In Section 3.6 it is seen that the robustness to modeling errors also is good. The FPP torque controller is a special case of this controller. The controllers in Winterbone (1980), Fukuba et al. (1996), and Whalley and Ebrahimi (2002) also use torque and pitch ratio as controlled variables. However, the way of optimization may differ.

Shaft speed/pitch ratio control

Like the torque/pitch ratio controller this controller is based on mappings from the desired thrust to the set points:

$$\begin{aligned} n_d &= \sqrt{\frac{T_d}{K_T(\tau)\rho D^4}}, \\ &= m(\tau) \frac{1}{\sqrt{\rho D^2}} \sqrt{T_d}, \end{aligned} \quad (3.19)$$

$$P/D_{cnr} = k(\tau), \quad (3.20)$$

$$Q_{cnr} = \text{PID}(n - n_d), \quad (3.21)$$

where $m(\tau)[-]$ is the mapping from τ to desired shaft speed, $P/D_{cnr}[-]$ is the commanded pitch ratio, and $Q_{cnr}[Nm]$ is the commanded torque. An example

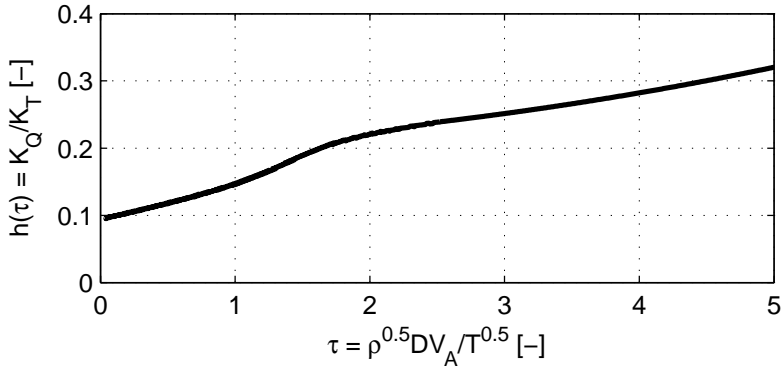


Figure 3.4: Plot of $h(\tau) = \frac{K_Q(\tau)}{K_T(\tau)}$ for "The Wageningen B4-70 propeller".

of $m(\tau)$ is seen in Figure 3.6. The $k(\tau)$ mapping is the solid line in Figure 3.5. In perfect conditions the torque/pitch ratio and the shaft speed/pitch ratio controllers perform equally well. Hence, only the torque/pitch ratio controller is treated in the later comparisons of controllers since this controller is more fundamental and has the same advantages as the FPP torque controller over the shaft speed controller. The shaft speed/pitch ratio controller can be preferred at very low thrust references for diesel engines with mechanically direct-driven propellers, since the diesel engines require a certain minimum shaft speed to operate. The FPP shaft speed controller and the pitch controller are special cases of this controller. The controllers in Parsons and Wu (1985), Bakoutouzis (1992), Chachulski et al. (1995), Morville (1996), and Young-Bok et al. (1998) also use shaft speed and pitch ratio as controlled variables.

Torque/shaft speed control

It is argued that optimal control is difficult without knowledge of the advance speed. However, it turns out that a nearly optimal controller can be achieved, without advance speed knowledge, by controlling the torque and the shaft speed (Schanz 1967). In this controller the pitch ratio is controlled to get the desired shaft speed, while the commanded torque is set to the desired torque. In this type of control the pitch is varied such that the torque coefficient always stays constant at each set point. It turns out that using the same torque coefficient for all set points gives near optimal control. Since the torque coefficient is kept constant, there is a one to one relationship between desired power, and desired torque and desired shaft speed. This means that the resulting controller is a power-torque-shaft speed controller, keeping all these variables constant. The desired shaft speed and the desired torque are calculated from the desired power,

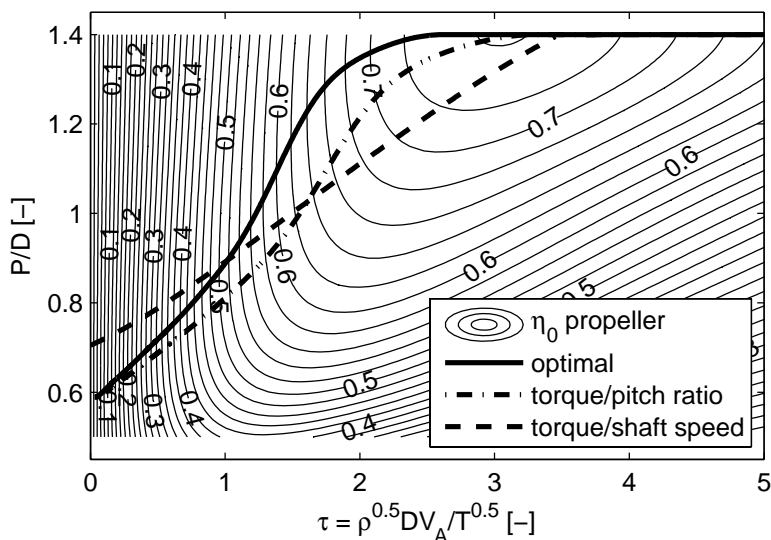


Figure 3.5: Propeller efficiency and controller paths as function of pitch ratio P/D and τ for "The Wageningen B4-70 propeller".

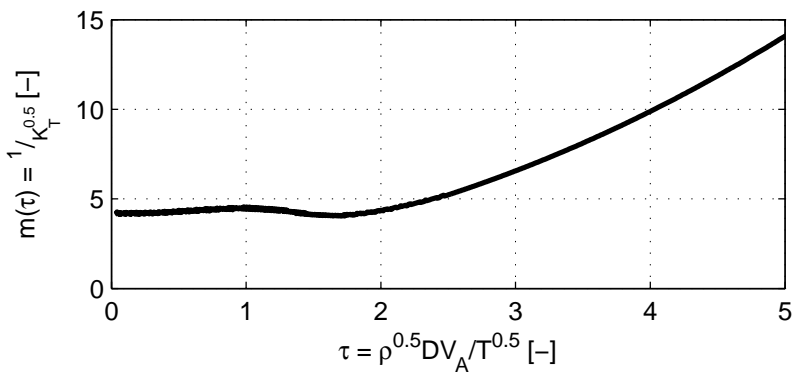


Figure 3.6: Plot of $m(\tau) = \frac{1}{\sqrt{K_T(\tau)}}$ for "The Wageningen B4-70 propeller".

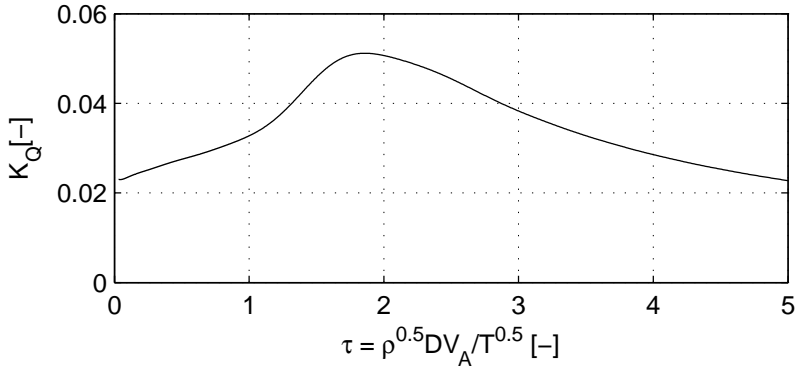


Figure 3.7: Plot of optimal K_Q as function of τ for "The Wageningen B4-70 propeller".

which is the input:

$$Q_{cqn} = Q_d = \sqrt[3]{\frac{K_{Qc}\rho D^5}{(2\pi)^2}} P_d^{2/3}, \quad (3.22)$$

$$n_d = \sqrt[3]{\frac{P_d}{2\pi K_{Qc}\rho D^5}}, \quad (3.23)$$

$$P/D_{cqn} = \text{PID}(n - n_d). \quad (3.24)$$

Here, $Q_{cqn}[Nm]$ is the commanded torque, and $P/D_{cqn}[-]$ is the commanded pitch ratio. K_{Qc} has to be constant or taken from Figure 3.7 if the advance speed should be accounted for. The figure is obtained by finding the torque coefficients corresponding to the optimal pitch ratio and torque combination in (3.17) and (3.18). Since the pitch ratio is allowed to vary here, the K_Q is no longer linear in J_A . It is therefore recommended to use a constant K_{Qc} value, since this requires less model knowledge and gives a simple robust near optimal controller. At low advance speeds P_d is determined as for power control in (3.11). This means that the mapping from T_d to n_d , Q_d , and P_d satisfies (3.8), (3.10) and (3.11), respectively. At moderate/high advance speed P_d is determined from (3.1) with $P_d = u_d$. The input signals to the PID controller determining the pitch ratio should be low-pass filtered to avoid wear and tear of the pitch actuator. The controllers in Schanz (1967), Winterbone (1980) and Parsons and Wu (1985) also use torque and shaft speed as control variables. However, the way of optimization may differ.

The resulting performance for the torque/shaft speed controller as regards propeller efficiency can be seen in Figure 3.8 and 3.9 for "The Wageningen B4-70 propeller". In the first figure the efficiency with $K_{Qc} = 0.033$ is plotted as function of τ and compared with the optimal efficiency. In the second figure the relative error for different K_{Qc} values are plotted as functions of τ . The chosen

K_{Qc} values are:

- $K_{Qc} = 0.0226$, which is the optimal K_Q at zero advance speed.
- $K_{Qc} = 0.033$, which is the K_Q value that gives the least infinity norm of the relative error in efficiency. Mathematically this is expressed $K_{Qc} = \min_{K_Q} \left(\left\| \frac{\eta_0}{\eta_{Optimal}} \right\|_\infty \right)$. A plot of $\frac{\eta_0}{\eta_{Optimal}}$ is seen in Figure 3.9.
- $K_{Qc} = 0.0439$, which is the K_Q value when $P/D = 1.4$ becomes optimal. This is in Figure 3.5 seen to be at $\tau = 2.61$.

It is seen from Figure 3.9 that the propeller efficiency performance is robust with respect to the choice of K_{Qc} .

In addition to the near optimal performance of the propeller, the consolidated control of torque and shaft speed has several other benefits:

- Power, torque and shaft speed limits are included in the controller.
- The controller performs well when the pitch is saturated.
- The K_{Qc} value can be chosen to optimize the total efficiency of the propulsion plant.
- The K_{Qc} value can be chosen such that the maximum continuous rating (MCR) of a diesel engine can be utilized.

The only disadvantage of this controller mentioned by Schanz (1967) is that it will not work in precision maneuvering for diesel engines with mechanically direct-driven propellers. This is because a minimum shaft speed (needed from the diesel engine point of view) not is ensured. This is because the controller can command less torque than necessary to rotate the propeller at zero pitch ratio. It is recommended to switch to pitch control in these cases. Further, it is worth mentioning that the shaft speed limit only works for normal operation, and not for e.g. anti-spin purposes. This is because increasing the pitch ratio may not increase the torque sufficiently to avoid racing during ventilation and in-and-out of water events.

3.4.3 Low level anti-spin thruster control

Anti-spin thruster control was invented as a consequence of the negative behavior of the torque and power controllers in extreme seas. The reason is that in case of e.g. ventilation the shaft speed controller will still keep constant shaft speed, while the torque and power controllers without anti-spin control will race the motor. The racing is caused by large and sudden reductions in the propeller loading. The objective for anti-spin thruster control is first of all to ensure safe operation and reduce the wear and tear, and secondly to reduce the power consumption. Anti-spin thruster control is further described by Smogeli et al. (2003), Smogeli et al. (2004a), Smogeli (2006), and Smogeli et al. (2008). One

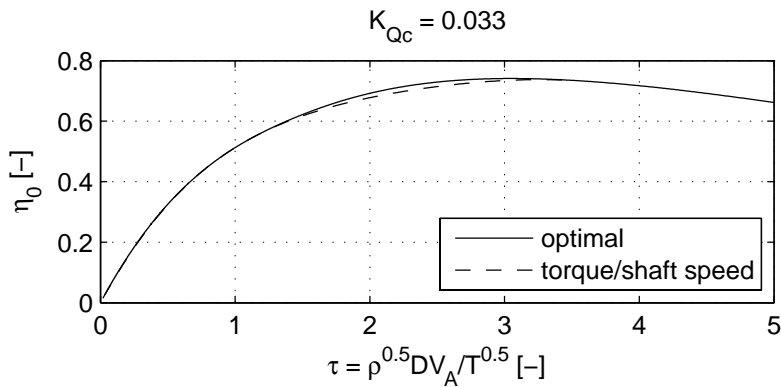


Figure 3.8: Comparison of efficiency of optimal versus torque/shaft speed controller with $K_{Qc} = 0.033$ for "The Wageningen B4-70 propeller".

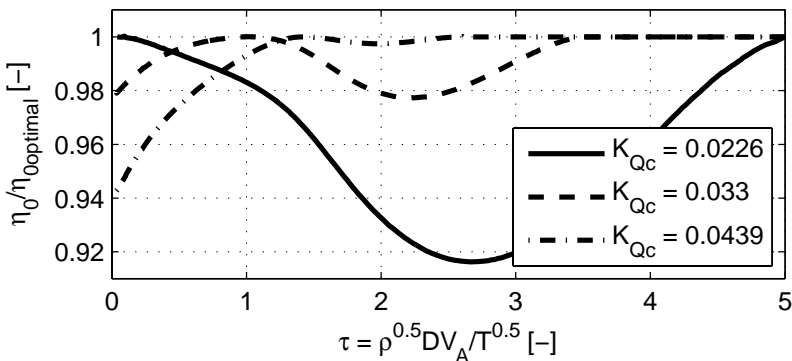


Figure 3.9: Relative error in efficiency of the torque/shaft speed controller for different values of K_{Qc} compared to the optimal controller. "The Wageningen B4-70 propeller" is used.

of the ideas presented in these references is to estimate the propeller torque, calculate the nominal propeller torque based on shaft speed measurements, and compare these values to find out whether the propeller is subject to large losses or not. If large losses are detected, the anti-spin controller can e.g. reduce the thrust reference to limit the shaft speed and the transients in the propeller. Another approach is to simply introduce a shaft speed limit on the motor. This prevents the propeller from racing to unacceptable values. As argued in Section 2.3.4, these results should be applied also to the shaft controller on consolidated controlled propellers. Further, the pitch ratio should be decreased, at the cost of increasing the shaft speed, in order to reduce the likelihood and severity of ventilation in a more long term perspective. Ideas on how anti-spin control can be incorporated in the thrust allocation system in order to improve the over all system efficiency is presented in Chapter 5.

3.5 Sensitivity functions

Following the formulations from Sørensen et al. (1997), a sensitivity function is used to show the deviation of a variable from it's desired value. In this thesis the shaft speed, thrust, torque and power sensitivities are investigated using the τ parameter. The definitions are as follows:

$$sn = \frac{n}{n_d}, \quad (3.25)$$

$$\begin{aligned} st &= \frac{T}{T_d}, \\ &= \frac{K_T(\tau, P/D)\rho D^4 n^2}{K_{Tc}\rho D^4 n_d^2}, \end{aligned} \quad (3.26)$$

$$\begin{aligned} sq &= \frac{Q_p}{Q_d}, \\ &= \frac{K_Q(\tau, P/D)\rho D^5 n^2}{K_{Qc}\rho D^5 n_d^2}, \end{aligned} \quad (3.27)$$

$$\begin{aligned} sp &= \frac{P}{P_d}, \\ &= \frac{2\pi n Q_p}{2\pi n_d Q_d}, \\ &= sn \cdot sq. \end{aligned} \quad (3.28)$$

The thrust sensitivity is important at low advance speeds to avoid degraded performance of e.g. the DP system. This is because the DP system and the thrust allocation in particular relies on the thrusters to fulfill the thrust commands. The sensitivity functions are computed for the shaft speed, torque, power, combined, pitch and torque/shaft speed controller, since these are the controllers applicable at low advance speed.

3.5.1 Shaft speed control

In shaft speed control the shaft speed is kept equal to the desired value:

$$n = n_d. \quad (3.29)$$

Hence, by inserting (3.29) into (3.25), the shaft speed sensitivity is found:

$$sn_n = \frac{n_d}{n_d} = 1. \quad (3.30)$$

Inserting (3.29) into (3.26) gives the thrust sensitivity:

$$\begin{aligned} st_n &= \frac{K_T(\tau)\rho D^4 n_d^2}{K_{Tc}\rho D^4 n_d^2}, \\ &= \frac{K_T(\tau)}{K_{Tc}}. \end{aligned} \quad (3.31)$$

The dependency of the pitch ratio is removed since the propeller is operated as a fixed pitch propeller. The torque sensitivity is found by inserting (3.29) into (3.27):

$$\begin{aligned} sq_n &= \frac{K_Q(\tau)\rho D^5 n_d^2}{K_{Qc}\rho D^5 n_d^2}, \\ &= \frac{K_Q(\tau)}{K_{Qc}}. \end{aligned} \quad (3.32)$$

Using (3.28), (3.30) and (3.32) gives the power sensitivity:

$$sp_n = \frac{K_Q(\tau)}{K_{Qc}}. \quad (3.33)$$

3.5.2 Torque control

In torque control the torque is kept equal to the desired value:

$$Q_p = Q_d. \quad (3.34)$$

Hence, by inserting (3.34) into (3.27), the torque sensitivity is found:

$$sq_q = \frac{Q_d}{Q_d} = 1. \quad (3.35)$$

In order to find the other sensitivity functions (3.27) and (3.35) are solved for n :

$$n = \sqrt{\frac{K_{Qc}}{K_Q(\tau)}} n_d. \quad (3.36)$$

The dependency of the pitch ratio is removed since the propeller is operated as a fixed pitch propeller. The shaft speed sensitivity is found by inserting (3.36) into (3.25):

$$sn_q = \sqrt{\frac{K_{Qc}}{K_Q(\tau)}}. \quad (3.37)$$

Inserting (3.36) into (3.26) gives the thrust sensitivity:

$$\begin{aligned} st_q &= \frac{K_T(\tau)\rho D^4 n^2}{K_{Tc}\rho D^4 n_d^2}, \\ &= \frac{K_T(\tau)}{K_{Tc}} \frac{K_{Qc}}{K_Q(\tau)}. \end{aligned} \quad (3.38)$$

Using (3.28), (3.35) and (3.37) gives the power sensitivity:

$$sp_q = \sqrt{\frac{K_{Qc}}{K_Q(\tau)}}. \quad (3.39)$$

3.5.3 Power control

In power control the power is kept equal to the desired value:

$$P = P_d. \quad (3.40)$$

Hence, by inserting (3.40) into (3.28), the power sensitivity is found:

$$sp_p = \frac{P_d}{P_d} = 1. \quad (3.41)$$

In order to find the other sensitivity functions (3.28) and (3.41) is solved for n :

$$n = \sqrt[3]{\frac{K_{Qc}}{K_Q(\tau)}} n_d. \quad (3.42)$$

The dependency of the pitch ratio is removed since the propeller is operated as a fixed pitch propeller. The shaft speed sensitivity is found by inserting (3.42) into (3.25):

$$sn_p = \sqrt[3]{\frac{K_{Qc}}{K_Q(\tau)}}. \quad (3.43)$$

Inserting (3.42) into (3.26) gives the thrust sensitivity:

$$\begin{aligned} st_p &= \frac{K_T(\tau)\rho D^4 n^2}{K_{Tc}\rho D^4 n_d^2}, \\ &= \frac{K_T(\tau)}{K_{Tc}} \left(\frac{K_{Qc}}{K_Q(\tau)} \right)^{2/3}. \end{aligned} \quad (3.44)$$

The torque sensitivity is found by inserting (3.42) into (3.27):

$$sq_p = \left(\frac{K_Q(\tau)}{K_{Qc}} \right)^{1/3}. \quad (3.45)$$

3.5.4 Combined control

In this case the values will lay in between the values for torque and power control. Further, by letting $\alpha \in [0, 1] \subset \mathbb{R}$ denote the amount of torque control used, the relationships can be approximated by exponents as linear functions of this variable:

$$\kappa = a\alpha + b, \quad (3.46)$$

where a and b are constants varying for the different sensitivities. For a particular sensitivity:

$$\begin{aligned} \kappa_q &= a\alpha_q + b, \\ &= a + b, \\ \kappa_p &= a\alpha_p + b, \\ &= b, \end{aligned}$$

where the indexes q and p denotes torque and power control respectively. Then the a and b coefficients can be calculated as:

$$\begin{aligned} b &= \kappa_p, \\ a &= \kappa_q - b. \end{aligned}$$

This results in the following shaft speed sensitivity:

$$sn_c = \left(\frac{K_{Qc}}{K_Q(\tau)} \right)^\kappa, \quad (3.47)$$

$$\kappa \approx \frac{2+\alpha}{6} \in \left[\frac{1}{3}, \frac{1}{2} \right]. \quad (3.48)$$

The thrust sensitivity becomes:

$$st_c = \frac{K_T(\tau)}{K_{Tc}} \left(\frac{K_{Qc}}{K_Q(\tau)} \right)^\kappa, \quad (3.49)$$

$$\kappa \approx \frac{2+\alpha}{3} \in \left[\frac{2}{3}, 1 \right]. \quad (3.50)$$

The torque sensitivity is approximated by:

$$sq_c = \left(\frac{K_Q(\tau)}{K_{Qc}} \right)^\kappa, \quad (3.51)$$

$$\kappa \approx \frac{1-\alpha}{3} \in \left[0, \frac{1}{3} \right]. \quad (3.52)$$

The power sensitivity is found as:

$$sp_c = \left(\frac{K_Q(\tau)}{K_{Qc}} \right)^\kappa, \quad (3.53)$$

$$\kappa \approx \frac{\alpha}{2} \in \left[0, \frac{1}{2} \right]. \quad (3.54)$$

3.5.5 Pitch control

In pitch control the shaft speed is fixed:

$$n = n_d. \quad (3.55)$$

Inserting (3.55) into (3.25) gives the shaft speed sensitivity:

$$sn_{pd} = \frac{n_d}{n_d} = 1. \quad (3.56)$$

The thrust sensitivity is found by inserting (3.16) and (3.55) into (3.26):

$$\begin{aligned} st_{pd} &= \frac{K_T(\tau, P/D)\rho D^4 n_d^2}{K_{Td}\rho D^4 n_d^2}, \\ &= \frac{K_T(\tau, g(K_{Td}))}{K_{Td}}. \end{aligned} \quad (3.57)$$

Inserting (3.16) and (3.55) into (3.27) gives the torque sensitivity:

$$\begin{aligned} sq_{pd} &= \frac{K_Q(\tau, P/D)\rho D^5 n_d^2}{K_{Qc}(P/D)\rho D^5 n_d^2}, \\ &= \frac{K_Q(\tau, g(K_{Td}))}{K_{Qc}(g(K_{Td}))}. \end{aligned} \quad (3.58)$$

The power sensitivity is calculated by using (3.28), (3.56) and (3.58):

$$sp_{pd} = \frac{K_Q(\tau, g(K_{Td}))}{K_{Qc}(g(K_{Td}))}. \quad (3.59)$$

3.5.6 Torque/shaft speed control

The sensitivity functions are calculated under the assumption that no saturation occur. The shaft speed is then controlled to the desired value:

$$n = n_d. \quad (3.60)$$

Inserting (3.60) into (3.25) gives the shaft speed sensitivity:

$$sn_{qn} = \frac{n_d}{n_d} = 1. \quad (3.61)$$

In order to find the thrust sensitivity (3.60) are inserted into (3.26):

$$\begin{aligned} st_{qn} &= \frac{K_T(\tau, P/D)\rho D^4 n_d^2}{K_{Tc}\rho D^4 n_d^2}, \\ &= \frac{K_T(\tau, P/D)}{K_{Tc}}, \end{aligned} \quad (3.62)$$

where the pitch ratio is found from:

$$K_Q(\tau, P/D) = K_{Qc}. \quad (3.63)$$

Hence the thrust sensitivity are found by solving (3.63) for P/D and inserting the result in (3.62). Since the torque is controlled to the desired value:

$$Q_p = Q_d. \quad (3.64)$$

Inserting (3.64) into (3.27) gives the torque sensitivity:

$$sq_{qn} = \frac{Q_d}{Q_d} = 1. \quad (3.65)$$

The power sensitivity is found by inserting (3.61) and (3.65) into (3.28):

$$sp_{qn} = 1. \quad (3.66)$$

3.5.7 Comparison of sensitivity functions

In order to ensure that the thruster controllers are compared under equal conditions, that is equal advance speed and desired thrust, a modified version of the τ parameter denoted the τ_d parameter is used. This parameter is defined in (2.31).

"The Wageningen B4-70 propeller" is used as an example propeller in order to show the behavior of the sensitivity functions in the first quadrant, that is for positive shaft speed and advance speed. The sensitivity functions for the following controllers are compared:

- Shaft speed control (FPP). $P/D = 0.58$, which is power optimal for zero advance speed.
- Torque control (FPP). $P/D = 0.58$, which is power optimal for zero advance speed.
- Power control (FPP). $P/D = 0.58$, which is power optimal for zero advance speed.
- Pitch control.
- Torque/shaft speed control (Consolidated). $K_{Qc} = 0.0226$, which is power optimal for zero advance speed.

The results for the combined controller will lay in between the torque and the power controller. The position is dependent on the weighting function $\alpha(n)$, and thereby also the shaft speed.

The sensitivity functions for the fixed pitch controllers are single lines in the plots. For the pitch controller the sensitivity functions does not become a single line, but an area in the figure. This is because the same τ value can be reached with different pitch ratios, dependent on the fixed shaft speed. More formally one may say that the choice of the fixed shaft speed at which the thruster operates is an additional variable. The combined torque/shaft speed controller becomes a single line in the diagram, since the shaft speed is a function of the desired

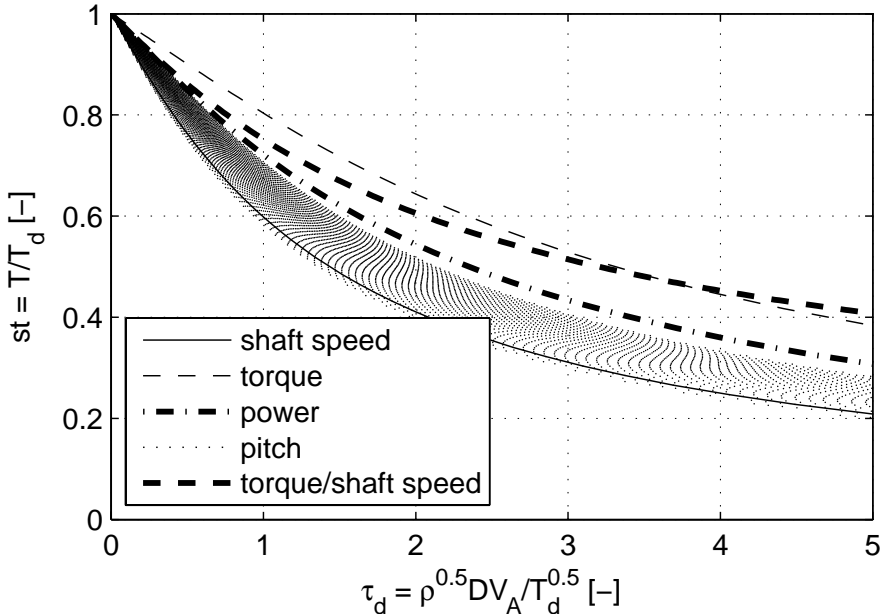


Figure 3.10: Thrust sensitivity for "The Wageningen B4-70 propeller".

thrust and hence, given a desired thrust, τ_d only depends on the advance speed. Further, the pitch ratio is also a function of the desired thrust and the advance speed.

In Figure 3.10 the thrust sensitivity functions are seen. Both the torque and the torque/shaft speed controller are seen to outperform the others with respect to thrust production. The shaft speed controller are the worst with respect to thrust production. The power controller lay approximately in the middle between these. The area of the pitch controller is roughly in between the shaft speed and the power controller. It is, however, worth noting that all controllers have significantly reduced performance with respect to thrust production at high advance speeds or low desired thrusts.

The shaft speed sensitivity functions are seen in Figure 3.11. It is clearly seen that the reason for the improved thrust producing performance of the torque and power controller compared to shaft speed control is caused by the increased shafts speed. For all the other controllers the shaft speed is fixed.

Figure 3.12 shows the torque sensitivity functions. It is here seen that the reduced thrust producing performance also has connections to the motor torque for the controllers. The tendency is clearly that less torque gives less thrust.

In Figure 3.13 the power sensitivities are shown. It is seen that the torque controller increases the power consumption compared to the others. This is important to notice for the power network, and precautions should be taken if the power check is done based on desired thrust only. Generally it is seen

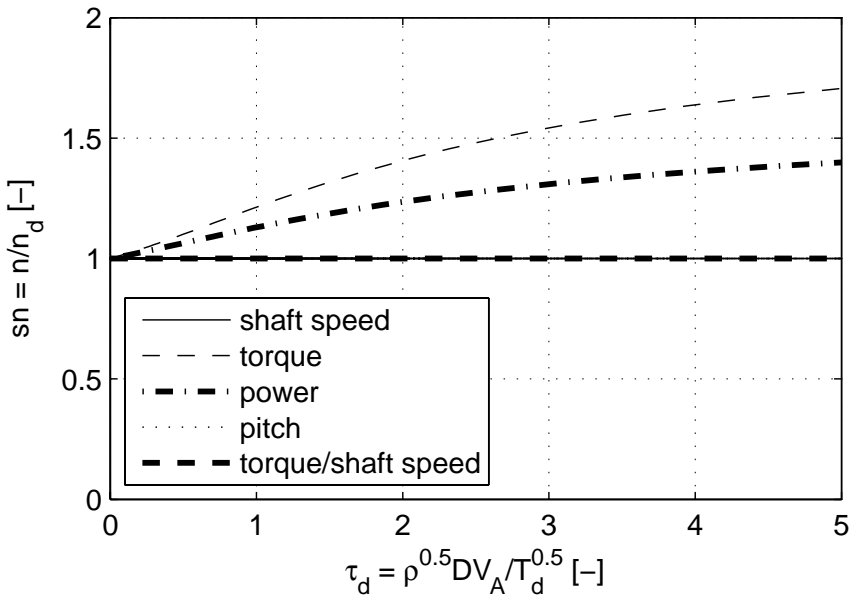


Figure 3.11: Shaft speed sensitivity for "The Wageningen B4-70 propeller".

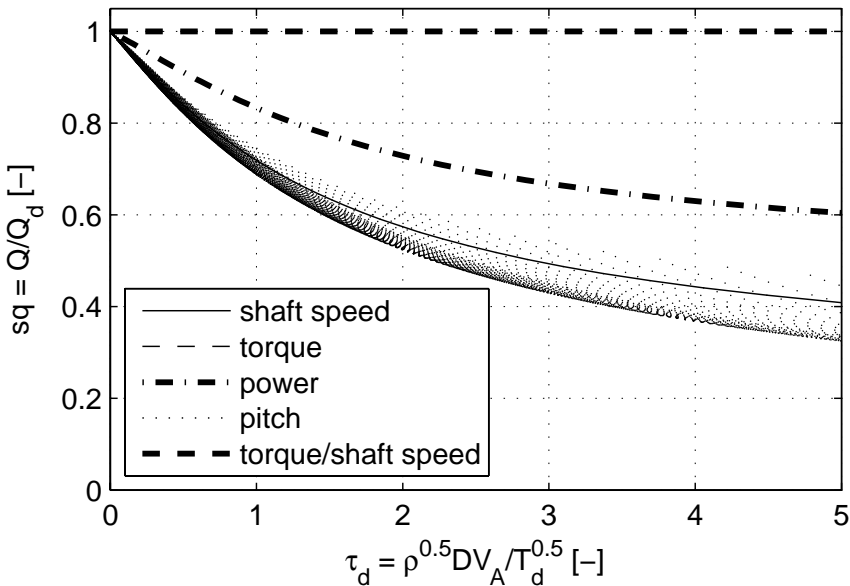


Figure 3.12: Torque sensitivity for "The Wageningen B4-70 propeller".

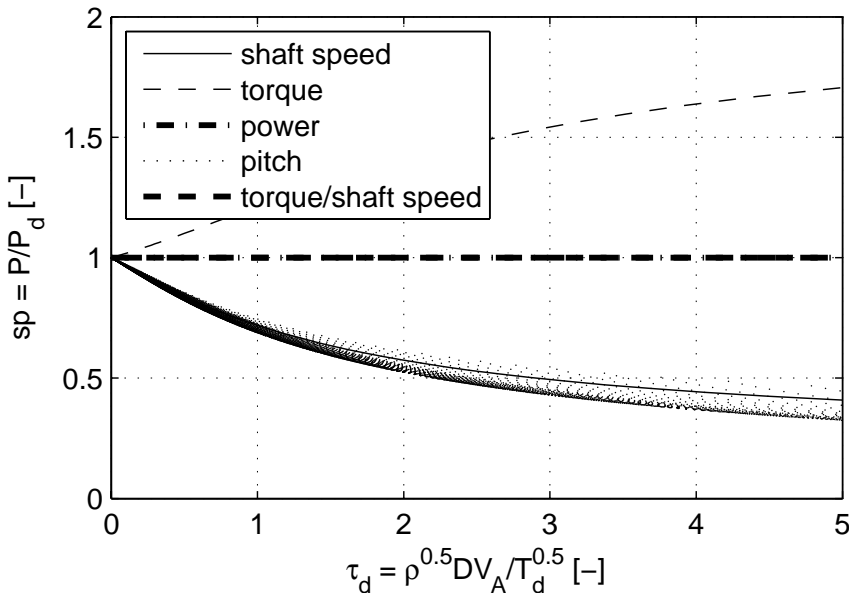


Figure 3.13: Power sensitivity for "The Wageningen B4-70 propeller".

that small thrust sensitivity functions gives small power sensitivity functions, compared to the others.

3.6 Comparison of optimal performance

In Figure 3.5 the propulsion efficiency is plotted as function of pitch ratio and τ for "The Wageningen B4-70 propeller". It is seen that for equal environmental conditions, which corresponds to equal τ , the efficiency is not very dependent on the pitch ratio if one operates to the left in the figure. The optimal pitch ratio from (3.18) and (3.20) is plotted as the solid line in the figure and is to the left in the figure. If the propeller is operated at high τ values, the efficiency is largely affected by the pitch ratio. However, the optimal pitch ratio is in this case always the maximum pitch ratio. In Figure 3.14 the efficiencies of four different controllers are compared to the optimal controller for "The Wageningen B4-70 propeller":

- The torque/pitch ratio controller is based on the optimal path from Figure 3.5. However, the thrust coefficient is modeled 10% to low, the torque coefficient is modeled 10% to high, and the measured advance speed is modeled 20% to high. All errors move the optimal path to the right in the figure (the most unfavorable direction).

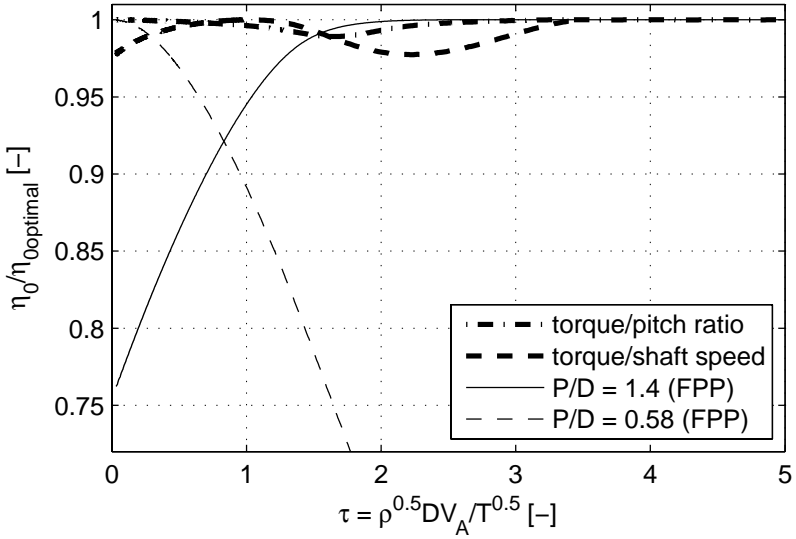


Figure 3.14: Relative error in efficiency of different controllers compared to the optimal controller for "The Wageningen B4-70 propeller".

- The torque/shaft speed controller is taken from Section 3.4.2 with $K_{Qc} = 0.033$.
- A FPP controller with $P/D = 1.4$. It does not matter which FPP controller since if they produce the same thrust at the same pitch ratio, all of them have the same shaft speed and efficiency.
- A FPP control with $P/D = 0.58$. This is the optimal pitch ratio at $\tau = J_A = V_A = 0$.

The path of the consolidated controllers in the propeller efficiency plot can be seen in Figure 3.5. For the fixed pitch controllers these paths are straight lines at the chosen pitch ratio. The absolute ($\|\eta_0 - \eta_{0\text{optimal}}\|_\infty$) and the relative ($\left\|1 - \frac{\eta_0}{\eta_{0\text{optimal}}}\right\|_\infty$) infinity norm errors of the different controllers are compared in Table 3.3. It is seen that the torque/pitch ratio controller performs best, even with severe modeling and measurement errors. However, the torque/shaft speed controller also performs well over the whole range. The FPP controllers can from Figure 3.14 be seen to give satisfactory performance in the highly loaded (low τ value) area and in the lightly loaded (high τ value) area for $P/D = 0.58$ and $P/D = 1.4$, respectively.

Table 3.3: The absolute and relative infinity norm errors of the different controllers applied to "The Wageningen B4-70 propeller".

	Absolute	Relative
Torque/pitch ratio	0.7%	1.1%
Torque/shaft speed	1.6%	2.3%
$P/D = 1.4$ (FPP)	4.5%	24%
$P/D = 0.58$ (FPP)	46%	73%

3.7 Simulations

"The Wageningen B4-70 propeller" is simulated 5[m] submerged under the mean water surface. The advance speed in on the propeller is the sum of a constant current of 1.0[m/s] and the water particle velocity from undisturbed waves generated by a JONSWAP spectrum with parameters $H_s = 2.0[m]$, $T_p = 5.9[s]$, and $\gamma = 3.3[-]$. The resulting advance speed of the propeller is shown in Figure 3.15. The propeller diameter is 4.0[m], the inertia of the propulsion system (from Q_m to n) is 5000[Nm/s²], and the pitch ratio change rate is restricted to $\pm 0.2[1/s]$. In equation (3.9) and (3.15) the PID gain is set to $1 \cdot 10^6$, the integration time constant is set to $\frac{1}{2\pi}[s]$, and no derivative action is included. In equation (3.8), (3.10), (3.11), and (3.13) $K_{Tc} = 0.2394$ and $K_{Qc} = 0.0226$ are used. In (3.14) the parameters are set to $k = 1.0$, $p = 0.5[s]$, and $r = 20$. The mapping $g(K_{Td})$ used in (3.16) is shown in Figure 3.3. In the shaft speed and the combined controller the pitch ratio is fixed at 0.58[–]. In the pitch controller the shaft speed is fixed at 2.0[Hz]. In the torque/shaft speed controller the PID gain and integration time constant are set to -1 and $\frac{3}{2\pi}[s]$ respectively in equation (3.24). In equation (3.22) and (3.23) $K_{Tc} = 0.2394$ and $K_{Qc} = 0.0226$ are used.

From Table 3.4 and Figure 3.16 and 3.17 it is seen that the controllers perform as expected from the static relationships in Figure 3.9, 3.10 and 3.14. The desired and produced thrusts are seen in Figure 3.16. The thrust sensitivity is seen in Figure 3.17 in order to elaborate the differences in thrust production accuracy between the different controllers. It is seen that the combined controller and the torque/shaft speed controller have the most correct thrust production, while it is seen in Table 3.4 that the torque/shaft speed controller uses the least amount of power. $P_{m,corr}$ are the corrected mean power such that all the controllers produce the same average thrust. It is calculated from:

$$P_m = 2\pi n Q_m, \quad (3.67)$$

$$P_{m,corr} = \text{mean}(P_m) \left(\frac{\text{mean}(T_d)}{\text{mean}(T)} \right)^{3/2}, \quad (3.68)$$

where P_m is the motor power and Q_m is the motor torque. In the simulations the desired thrust and the advance speed are restricted to positive values only since this is the valid area for the simulated propeller model. The presented simulations are only examples at given environmental conditions and a particular thrust demand. Other combinations of environment and thrust demand can

Table 3.4: Corrected average power consumption of the different controllers applied to "The Wageningen B4-70 propeller" in the simulations.

Controller	$P_{m,corr}$ [MW]
Shaft speed	3.00
Combined	2.98
Pitch	3.39
Torque/shaft speed	2.94

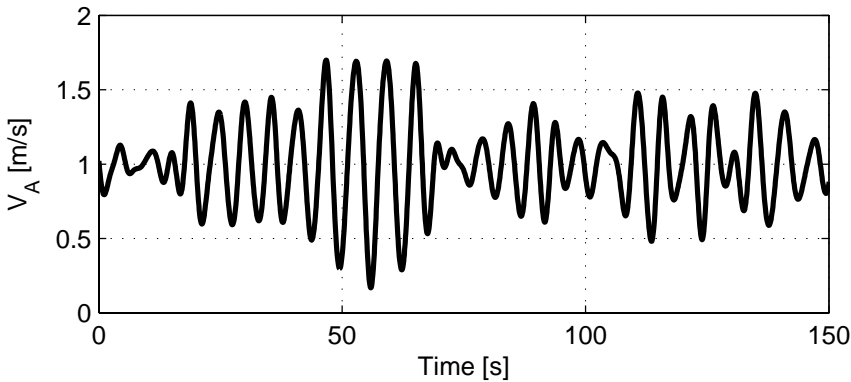


Figure 3.15: The advance speed in the simulation.

produce significantly different results. Due to lack of sufficiently accurate four quadrant models, the performance in four quadrants is not verified.

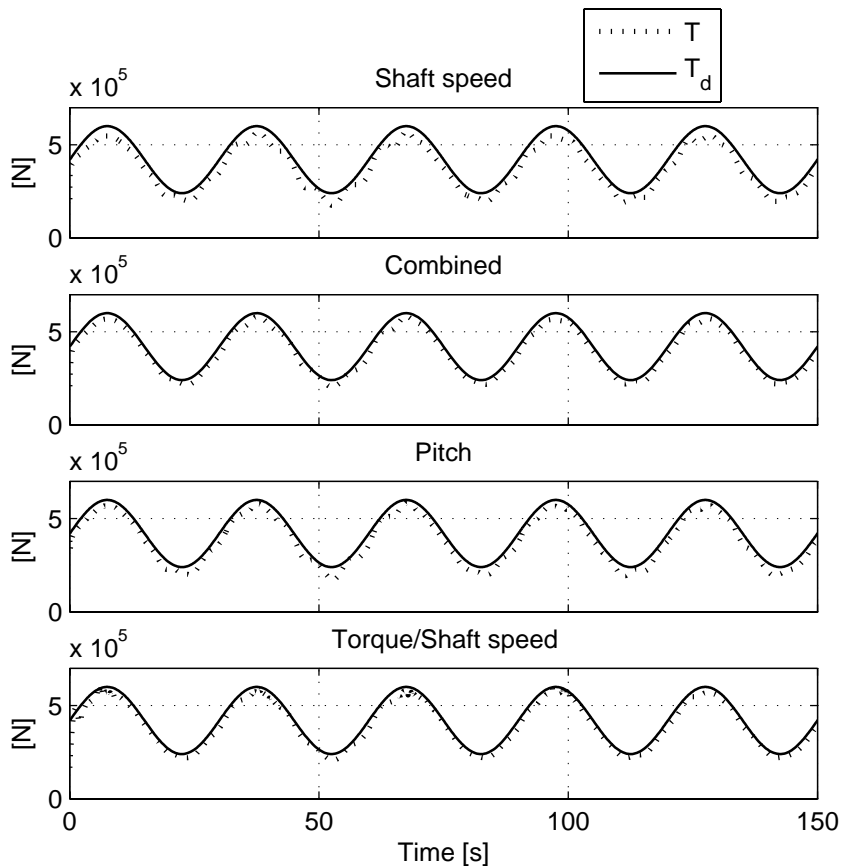


Figure 3.16: Measured and desired thrust during simulations of different controllers applied to the "The Wageningen B4-70 propeller".

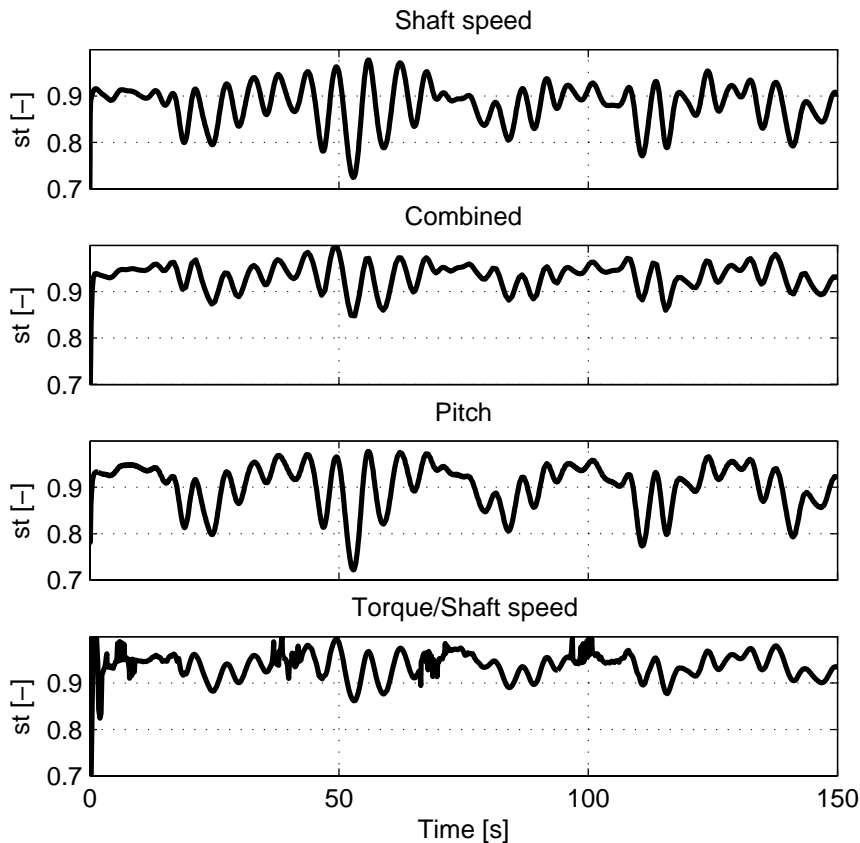


Figure 3.17: Thrust sensitivity during simulations of different controllers applied to the "The Wageningen B4-70 propeller".

Chapter 4

The thrust allocation problem

The thrust allocation problem is a special case of the more general control allocation problem, which also includes control allocation in flight control, space crafts and cars. The thrust allocation system or thrust allocator in a DP or PM system can be seen in Figure 1.1. The purpose of the thrust allocation system is to distribute among the thrusters the desired generalized forces computed by the motion controller. The output from the thrust allocator is the desired thruster forces and directions. Thrust allocation is used instead of finding the desired thruster forces and directions directly in the motion controller, since this enables modular design, and the same motion controller can be used despite of changes in the thruster configuration. For the thrust allocator, an important feature of the vessel is whether it is under actuated, fully actuated or over actuated. Under actuated means that there are not enough actuators present to produce any reasonable generalized force command. In this case it should be considered to redesign the motion controller such that it only gives reasonable commands, or to change the layout of the thruster system. Design of motion controllers for underactuated vessels are treated in e.g. Pettersen et al. (2004) and references therein. If the vessel is fully actuated it is capable of producing any reasonable generalized force command. The vessel is over actuated if there exist many, often infinitely many, different solutions to the problem, all producing the desired generalized force. Over actuated systems are commonly used in order to increase the safety against thruster failures. In order to choose one particular solution, it is usual to apply some kind of optimization criterion. This may be to reduce the power consumption, reduce the wear and tear or maximization of maneuverability. In this thesis the focus is on power optimal thrust allocation, in order to increase the overall efficiency of the thrusters.

To ensure safe operation it is important that a thrust allocator always provide a solution and provide the solution in time. Further the thrust allocator should try its best to produce the desired generalized force. Failure to satisfy these demands may have severe consequences like loss of position or black out.

The general thrust allocation problem is in this thesis formulated as an optimization problem:

$$[\mathbf{T}_d, \boldsymbol{\alpha}_d] = \underset{\mathbf{T} \in \mathcal{S}_{\mathbf{T}}, \boldsymbol{\alpha} \in \mathcal{S}_{\boldsymbol{\alpha}}}{\operatorname{argmin}} (J(\mathbf{T}, \boldsymbol{\alpha}, \mathbf{s}, \boldsymbol{\tau}_d, \boldsymbol{\theta})), \quad (4.1)$$

subject to:

$$\mathbf{B}(\boldsymbol{\alpha}_d)\mathbf{T}_d + \mathbf{s} = \boldsymbol{\tau}_d, \quad (4.2)$$

where J in (4.1) is the cost function, (4.2) is the constraint satisfying the desired generalized force, $\mathbf{T}_d \in \mathbb{R}^n$ is a vector of desired thruster forces taking values in the set of admissible thrusts $\mathcal{S}_{\mathbf{T}} \subset \mathbb{R}^n$, $\boldsymbol{\alpha}_d \in \mathbb{R}^n$ is a vector of desired thrust directions taking values in the set of admissible directions $\mathcal{S}_{\boldsymbol{\alpha}} \subset \mathbb{R}^n$, $\mathbf{s} \in \mathbb{R}^m$ is a vector of slack variables introduced in order to make sure there always exist a solution, $\boldsymbol{\tau}_d \in \mathbb{R}^m$ is a vector of desired generalized forces, $\boldsymbol{\theta} \in \mathbb{R}^l$ is a vector of parameters, $n \in \mathbb{R}$ is the number of thrusters, $m \in \mathbb{R}$ is the number of controlled degrees of freedom, and $\mathbf{B} \in \mathbb{R}^{m \times n}$ is the thruster configuration matrix determined by the position of the individual thrusters. The j 'th column in \mathbf{B} corresponds to the generalized force produced by one unit thruster force from the j 'th thruster. In 6 degrees of freedom the j 'th column of \mathbf{B} , $\mathbf{B}_j \in \mathbb{R}^6$ becomes:

$$\mathbf{B}_j = \begin{bmatrix} \mathbf{n}_1 \cos \boldsymbol{\alpha}_j + \mathbf{n}_2 \sin \boldsymbol{\alpha}_j \\ \mathbf{r}_j \times (\mathbf{n}_1 \cos \boldsymbol{\alpha}_j + \mathbf{n}_2 \sin \boldsymbol{\alpha}_j) \end{bmatrix}, \quad (4.3)$$

where $\mathbf{n}_1 \in \mathbb{R}^3$ is a unit vector determining the force direction when $\boldsymbol{\alpha}_j = 0[\text{deg}] \in \mathbb{R}$, $\mathbf{n}_2 \in \mathbb{R}^3$ is a unit vector determining the force direction when $\boldsymbol{\alpha}_j = 90[\text{deg}]$, and $\mathbf{r}_j \in \mathbb{R}^3$ is the position vector of the thruster in the body frame.

In this chapter normal operating conditions are considered. A solution to the problem when ventilation and in-and-out of water effects are present on the propellers, are shown in the next chapter. The solution to the thrust allocation problem is in this thesis found by use of quadratic programming. If the problem is formulated as a convex problem, quadratic programming provides an efficient method for obtaining the global minimum. Other solution methods based on more complicated problem formulations usually results in locally minimum solutions (Nocedal and Wright 1999). Therefore, in order to ensure that the global solution is found, quadratic programming is used. However, this imposes constraints on the mathematical formulation of the problem, since it has to be convex, and the cost function quadratic. In the cases where the problem is nonconvex, it is proposed to use a mixed integer approach. This is presented in a later chapter. The present chapter also includes considerations on power constraints, and ends with validation of the proposed strategy for thrust allocation by model scale experiments.

4.1 Cost functions

The cost function is used to mathematically describe the cost of different solutions. When over-actuated thrust allocation problems are solved as optimization

problems, the cost function is used to determine the particular solution with the lowest cost. In power optimal thrust allocation the cost function is typically quadratic in thrust and slack variables:

$$J(\mathbf{T}, \boldsymbol{\alpha}, \mathbf{s}, \boldsymbol{\tau}_d, \boldsymbol{\theta}) = \mathbf{T}^T \mathbf{R} \mathbf{T} + \mathbf{s}^T \mathbf{Q} \mathbf{s}, \quad (4.4)$$

where $\mathbf{R} \in \mathbb{R}^{n \times n}$ and $\mathbf{Q} \in \mathbb{R}^{m \times m}$ are weighting matrices, usually constant and diagonal, and their elements are members of $\boldsymbol{\theta}$. There are mainly two reasons for using quadratic cost functions:

1. The problem becomes easy to solve.
2. The cost function increases with the magnitude of \mathbf{T} and \mathbf{s} , as compared to negative \mathbf{T} 's and \mathbf{s} 's in linear cost functions.

Further, the power consumption of a propeller is proportional to $T^{3/2}$, see (3.11). This means that T^2 is a reasonable approximation. The literature also contains examples of linear and nonlinear cost functions. E.g. Sinding and Anderson (1998) have a $T^{3/2}$ term in the cost function, Liang and Cheng (2004) have $\sum_j (T_{x,j} + T_{y,j})$ in the cost function, and Johansen et al. (2004) have a singularity avoidance term $\frac{\rho}{\varepsilon + \det(\mathbf{B}(\boldsymbol{\alpha})\mathbf{B}^T(\boldsymbol{\alpha}))}$, where $\rho \in \mathbb{R}$ and $\varepsilon \in \mathbb{R}$ are constant parameters. Sinding and Anderson (1998) and Liang and Cheng (2004) solve their problems by nonlinear methods, while Johansen et al. (2004) linearize the expression before using quadratic programming (QP). Typically the weight of the slack variables are significantly larger, in the order of 1000 times, than the other weights in order to force the thrust allocator to produce the desired generalized force. This is because the slack variable should ideally be zero all the time, but it has to be allowed to differ from zero if there does not exist a solution, i.e. $\#\mathbf{T}_d|\mathbf{B}\mathbf{T}_d = \boldsymbol{\tau}_d$.

4.2 Constraints

The most important constraint in thrust allocation is the equality constraint on generalized force given in (4.2). This constraint ensures that the desired generalized force is produced.

There are physical limitations on the thrusters that restrict the set of admissible thrusts $\mathcal{S}_{\mathbf{T}}$ and directions $\mathcal{S}_{\boldsymbol{\alpha}}$. These limitations can be expressed as constraints. The physical limitations on the thruster force are in terms of maximum $\mathbf{T}_{\max} \in \mathbb{R}^n$ and minimum $\mathbf{T}_{\min} \in \mathbb{R}^n$ produced thrust, maximum $\dot{\mathbf{T}}_{\max} \in \mathbb{R}^n$ and minimum $\dot{\mathbf{T}}_{\min} \in \mathbb{R}^n$ rate of change of produced thrust:

$$\mathbf{T}_{\min} \leq \mathbf{T} \leq \mathbf{T}_{\max}, \quad (4.5)$$

$$\dot{\mathbf{T}}_{\min} \leq \dot{\mathbf{T}} \leq \dot{\mathbf{T}}_{\max}. \quad (4.6)$$

Power limitations are imposed by the power network. The power limitations can be on individual thrusters, groups of thrusters (on the same power bus) or on the total power consumption. In many industrial DP systems the power

constraints are checked after the thrust allocation by imposing power limitations directly on the thrusters. In Section 4.4.3 it is shown how the power constraints can be included in the presented thrust allocator.

A rotating thruster can rarely produce thrust in any direction without disturbing other thrusters or submerged equipment on the vessel. Therefore limitations on thrust directions, such as forbidden zones, are common. These limitations are implemented as sector constraints like e.g.:

$$\boldsymbol{\alpha}_j \in \left[0, \frac{\pi}{4}\right] \cup \left[\frac{\pi}{2}, \frac{3\pi}{2}\right]. \quad (4.7)$$

These constraints may be caused by e.g. the desire to avoid flushing other thrusters or disturbing the hydro acoustic position reference system. There are also restrictions on how fast the direction of the thruster force can change. This is expressed as:

$$|\dot{\boldsymbol{\alpha}}_j| \leq \dot{\boldsymbol{\alpha}}_{\max,j}, \quad (4.8)$$

where $\dot{\boldsymbol{\alpha}}_{\max} \in \mathbb{R}^n$ is the maximum rate of change vector.

For fixed thrusters the constraint on thrust direction is simply:

$$\boldsymbol{\alpha}_j = \boldsymbol{\alpha}_{fixed,j}, \quad (4.9)$$

where $\boldsymbol{\alpha} \in \mathbb{R}^n$ is the thrust direction vector, $\boldsymbol{\alpha}_{fixed} \in \mathbb{R}^n$ is the vector of fixed thrust directions, and j indexes the different thrusters.

4.3 Previously presented solutions

A good survey of previously published methods for thrust allocation is found in Fossen and Johansen (2006). They divide the thrust allocation problem into three main categories: linear quadratic unconstrained thrust allocation, linear quadratic constrained thrust allocation, and nonlinear constrained thrust allocation. Further, the problems are characterized by fixed or rotating thrusters, and the solution method. A simple classification of the contributions is found in Figure 4.1.

Solutions to the unconstrained quadratic thrust allocation problem are proposed by Sørdalen (1996, 1997a, b), Berge and Fossen (1997) and Garus (2004). Although the problems are formulated as unconstrained quadratic optimization problems, the solutions in Sørdalen (1996, 1997a, b) and Berge and Fossen (1997) includes singularity handling. This means that infinite thrust commands due to singular thruster configurations are avoided. The work of Sørdalen (1996, 1997a, b) calculates the thrust directions from a low pass filtered extended thrust vector. Singularities are handled by modifying the singular value decomposition, obtained by use of the previously obtained thrust directions, in order to calculate the thruster forces. In Sørdalen (1997b) it is also shown how the problem of rotational thrusters both capable of producing positive and negative thrust can be handled. In Berge and Fossen (1997) the thrust directions are calculated from a low pass filtered desired generalized force. The singularites are

	Linear	Quadratic	Other nonlinear
Constrained	Lindfors (1993)	Swanson (1992) Johansen et. al. (2003,2005,2007) Lindegaard and Fossen (2003) Ruth et. al. (2007)	Sinding and Anderson (1998) Webster and Sousa (1999) Liang and Cheng (2004) Johansen (2004) Johansen et. al. (2004) Tjønnås and Johansen (2005,2007)
Unconstrained		Sørdaalen (1996,1997 a,b) Berge and Fossen (1997) Garus (2004)	

Figure 4.1: Classification of thrust allocation methods. Linear means linear cost function and linear constraints. Quadratic means linear quadratic cost function and linear constraints. All other combinations of cost function and constraints are denoted other nonlinear.

handled by using a damped least squares method when calculating the thruster forces based on the previously calculated thrust directions. In the work of Garus (2004) different solutions to the unconstrained quadratic thrust allocation problem for fixed thrusters are presented. This work also includes a way of taking failure of one of the thrusters into account.

The linear quadratic constrained thrust allocation problem is solved by Swanson (1982), Johansen et al. (2003, 2005, 2007), Lindegaard and Fossen (2003) and Ruth et al. (2007). In Swanson (1982) a blending coefficient based on power consumption is used to weight between a fixed and a rotating thruster solution. Johansen et al. (2003, 2005, 2007) solve the problem by multiparametric quadratic programming leading to piecewise linear functions which are precomputed and solved in real time. Johansen et al. (2005) solve the problem for fixed directions of the thrusters only and sketches solutions to problems with dynamic thrust constraints. The results are extended in Johansen et al. (2003, 2007) to include rotating thrust producing devices and decomposition of nonconvex problems. Lindegaard and Fossen (2003) solve the problem with sector constraints on one thruster only. The solution is explicit and does not include other inequality constraints. The approach of Ruth et al. (2007) is presented in detail later in this chapter.

The work of Sinding and Anderson (1998), Webster and Sousa (1999), Liang and Cheng (2004), Johansen (2004), Johansen et al. (2004) and Tjønnås and Johansen (2005, 2007) solve nonlinear constrained thrust allocation problems. Sinding and Anderson (1998) take limitations on thruster force and direction, rate limitations on thrust directions, reversing rotating thrusters, thruster hull and thruster-thruster interaction into account. Subroutines for nonlinear constrained optimization introduced by Madsen and Tingleff (1990) are used to solve the problem. The method may reach local minima instead of global ones. In Webster and Sousa (1999) rate limitations on direction, and magnitude and rate limitations on thruster force are taken into account. The problem is linearized

before it is solved by linear programming. Due to linearization the stationary solution may scatter between two solutions. Small time steps are needed in order to limit the allowed change in the variables during each time step. Sequential quadratic programming (SQP) is used in Liang and Cheng (2004) and Johansen et al. (2004) to solve the thrust allocation problem. Johansen et al. (2004) formulates a nonlinear optimization problem with power consumption proportional to $|T|^{3/2}$ and singularity avoidance. Constraints on thruster force magnitude, and directional magnitude and rate of change are included. Solutions are found by expanding the power consumption in the cost function to the second order and linearizing the other nonlinearities. They assume that the thrust directions are changed at a maximum speed of $1[\text{deg}/\text{s}]$. Local optimal solutions may be found instead of global ones. The paper does not say how the system handles going through singular configurations, particularly in combination with sector constraints. This would be important and interesting to investigate in future work. In Johansen (2004) and Tjønnås and Johansen (2005, 2007) the problem is solved by Lyapunov methods. The examples presented on vessel applications seem not to fully satisfy the assumptions of the theory. This applies to the mapping from actuator commands to generalized forces, denoted $h(t, x, u)$ in the paper. The suggested $h(t, x, u)$ function is not twice differentiable as assumption 3 requires, and $\frac{\partial h}{\partial u}(t, x, 0) = 0$ and thereby not satisfying assumption 2. One solution to this problem may be to formulate a linear mapping from thrust to generalized forces and use barrier functions to handle constraints. However, the Lyapunov methods are not subject to further research in this thesis.

Lindfors (1993) formulates a nearly linear thrust allocation problem where the optimization criterion is minimization of the sum of the thruster forces. The only nonlinearity is in the magnitude constraint on the azimuthing thrusters. The problem is linearized and solved as a linear programming problem. The cost function is modified in order to favor the current direction of the azimuth thrusters, and hence reducing the oscillations and cycle-to-cycle variations in thrust direction.

4.4 Convex linearly constrained quadratic thrust allocation

In this section it is proposed to formulate the thrust allocation problem as a convex linearly constrained quadratic optimization problem. The constraints are on thrust force, azimuth angle and commanded generalized force. The solution is found by quadratic programming (QP), as opposed to Johansen et al. (2007) which solves the problem by piecewise linear functions. By solving the problem as a quadratic programming problem the flexibility in on-line reconfiguration is larger as compared to solutions based on piecewise linear functions. This means that the thrusters can be turned on and off, the constraints of the different thrusters can be varied, the cost of the different thrusters can be varied, and the thrust directions can vary between fixed and free. By use of a QP solver it is guaranteed that the solution is found within a certain number of iterations,

and that the cost is nonincreasing during these iterations. This means that the iterative solver can deliver a reasonable solution without finding the final solution, if the iteration sequence takes longer than allowed. The use of quadratic programming also ensures the existence of only one minimum. Further, the unmodified thruster configuration matrix is used, as compared to using a linearized one, which is common in the nonlinear methods. E.g. Johansen et al. (2004) linearize with respect to thrust directions and use increments on thrust directions as variables in the QP problem. A contribution of the approach presented in this section is that the azimuth angles are solved for as a part of the quadratic programming problem, without any approximations. The solution as presented here does not include singularity handling as compared to Sørørdalen (1997b). Results on singularity avoidance is found in Chapter 7. The results in this chapter can also be found in Ruth et al. (2007).

To make sure the linearly constrained quadratic thrust allocation finds the global minimum, the formulation has to be convex without rate constraints. In order to find the local minimum when the rate constraints are included, also this problem has to be convex. If the problem is nonconvex, typically by sector constraints on the azimuth angle, the nonconvex problem can be divided into a set of convex sub problems as in Johansen et al. (2003, 2007). Like in these references the nonconvex problem can then be solved by a mixed-integer-like approach based on the convex sub problems. The solution to the mixed-integer-like nonconvex problem can be obtained in real time without the use of piecewise linear functions for a reasonable number sub problems. This is shown in Section 6.4.1.

4.4.1 The thrust allocation problem with thruster forces in cylindrical coordinates

Since the constraints on the thruster forces are on magnitude and direction, the thrust allocation problem is formulated with use of cylindrical coordinates on the thruster forces. The thrust allocator is optimized with respect to power consumption, and mathematically formulated as:

$$[\mathbf{T}_d, \boldsymbol{\alpha}_d] = \arg \left(\min_{\mathbf{T}, \boldsymbol{\alpha}} (\|\gamma \mathbf{W}_v \mathbf{s}\|_2^2 + \|\mathbf{W}_u \mathbf{T}_d\|_2^2) \right), \quad (4.10)$$

subject to:

$$\mathbf{B}(\boldsymbol{\alpha}_d) \mathbf{T}_d + \mathbf{s} = \boldsymbol{\tau}_d, \quad (4.11)$$

$$\begin{bmatrix} \mathbf{I}_{n \times n} \\ -\mathbf{I}_{n \times n} \end{bmatrix} \mathbf{T}_d \leq \begin{bmatrix} \mathbf{T}_+ \\ -\mathbf{T}_- \end{bmatrix}, \quad (4.12)$$

$$\begin{bmatrix} \mathbf{I}_{n \times n} \\ -\mathbf{I}_{n \times n} \end{bmatrix} \boldsymbol{\alpha}_d \leq \begin{bmatrix} \boldsymbol{\alpha}_+ \\ -\boldsymbol{\alpha}_- \end{bmatrix}, \quad (4.13)$$

where $\gamma \in \mathbb{R}$ is a parameter determining the importance of thrust production compared to energy consumption, $\mathbf{W}_v \in \mathbb{R}^{m \times m}$ is a matrix determining the

weight between the different generalized forces, $\mathbf{W}_u \in \mathbb{R}^{n \times n}$ is a matrix determining the weights between the different thrusters, $\mathbf{I}_{n \times n}$ is the identity matrix, $\mathbf{T}_+ \in \mathbb{R}^n$ is a vector of maximum thrust in the current time step, taking both absolute and rate constraints into account, $\mathbf{T}_- \in \mathbb{R}^n$ is a vector of minimum thrust in the current time step, taking both absolute and rate constraints into account, $\boldsymbol{\alpha}_+ \in \mathbb{R}^n$ is a vector of maximum azimuth angle in the current time step, taking both absolute and rate constraints into account, and $\boldsymbol{\alpha}_- \in \mathbb{R}^n$ is a vector of minimum azimuth angle in the current time step, taking both absolute and rate constraints into account. The γ parameter is usually selected as large as possible without causing numerical problems in order to ensure that the allocator always tries its best to produce the desired generalized force. Since the thrust allocator is implemented as a discrete controller, rate saturations are converted to absolute constraints in each time sample. The constraints are implemented as follows:

$$\mathbf{T}_+ = \max \left(\min \left(\mathbf{T}_{\max}, \mathbf{T}_o + \dot{\mathbf{T}}_{\max} \Delta t \right), \mathbf{T}_o + c_1 \dot{\mathbf{T}}_{\min} \Delta t \right), \quad (4.14)$$

$$\mathbf{T}_- = \min \left(\max \left(\mathbf{T}_{\min}, \mathbf{T}_o + \dot{\mathbf{T}}_{\min} \Delta t \right), \mathbf{T}_o + c_1 \dot{\mathbf{T}}_{\max} \Delta t \right), \quad (4.15)$$

$$\boldsymbol{\alpha}_+ = \max \left(\min \left(\boldsymbol{\alpha}_{\max}, \boldsymbol{\alpha}_o + \dot{\boldsymbol{\alpha}}_{\max} \Delta t \right), \boldsymbol{\alpha}_o - c_1 \dot{\boldsymbol{\alpha}}_{\max} \Delta t \right), \quad (4.16)$$

$$\boldsymbol{\alpha}_- = \min \left(\max \left(\boldsymbol{\alpha}_{\min}, \boldsymbol{\alpha}_o - \dot{\boldsymbol{\alpha}}_{\max} \Delta t \right), \boldsymbol{\alpha}_o + c_1 \dot{\boldsymbol{\alpha}}_{\max} \Delta t \right), \quad (4.17)$$

where $\Delta t \in \mathbb{R}$ is the sample time, $\mathbf{T}_0 \in \mathbb{R}^n$ is the commanded thrust in the previous time step, and $c_1 \in [0, 1] \in \mathbb{R}$ is a constant. The $\mathbf{T}_o + c_1 \dot{\mathbf{T}}_{\min} \Delta t$ term ensures that if the current operating point is outside the current maximum bound, a solution is still found. This solution approaches the legal values at c_1 of maximum speed. $c_1 = 0.9$ is used instead of 1.0 in order to avoid numerical problems when solving the inequality constraints and is a value that works well. Another solution could have been to introduce an equality constraint instead, but this will significantly increase the complexity of the allocator.

4.4.2 The thrust allocation problem with thruster forces in Cartesian coordinates

To be able to solve the problem (4.10)-(4.13) by quadratic programming (QP), the thrust vectors are converted to Cartesian coordinates, also called extended thrust formulation in Sørdsalen (1997b), to form a convex linearly constrained quadratic programming problem. Define:

$$\mathbf{T}_{xd,j} = \mathbf{T}_{d,j} \cos(\boldsymbol{\alpha}_{d,j}), \quad (4.18)$$

$$\mathbf{T}_{yd,j} = \mathbf{T}_{d,j} \sin(\boldsymbol{\alpha}_{d,j}), \quad (4.19)$$

where $j \in \mathbb{N}$ indexes the different thrusters, and $\mathbf{T}_{xd} \in \mathbb{R}^n$ and $\mathbf{T}_{yd} \in \mathbb{R}^n$ are the thruster force in body x and y direction. The Cartesian formulation of the thrust allocation problem is written:

$$[\mathbf{T}_{xd}, \mathbf{T}_{yd}] = \arg \left(\min_{\mathbf{T}_x, \mathbf{T}_y} (\|\gamma \mathbf{W}_v \mathbf{s}\|_2^2 + \|\mathbf{W}_u \mathbf{T}_x\|_2^2 + \|\mathbf{W}_u \mathbf{T}_y\|_2^2) \right), \quad (4.20)$$

subject to:

$$\mathbf{B}_C \begin{bmatrix} \mathbf{T}_{xd} \\ \mathbf{T}_{yd} \end{bmatrix} + \mathbf{s} = \boldsymbol{\tau}_d, \quad (4.21)$$

$$\mathbf{A} \begin{bmatrix} \mathbf{T}_{xd} \\ \mathbf{T}_{yd} \end{bmatrix} \leq \mathbf{b}, \quad (4.22)$$

where $\mathbf{B}_C \in \mathbb{R}^{m \times 2n}$ is the thruster configuration matrix in Cartesian coordinates, $\mathbf{A} \in \mathbb{R}^{a \times 2n}$ is the inequality constraint matrix, $\mathbf{b} \in \mathbb{R}^a$ is the inequality constraint vector, and $a \in \mathbb{N}$ is the number of inequality constraints. If \mathbf{W}_u is a diagonal matrix, which is common, there are no differences in value of the cost functions (4.10) and (4.20). This can be shown by considering the contribution to $\|\mathbf{W}_u \mathbf{T}_d\|_2^2$ from thruster number j :

$$\mathbf{W}_{u,j}^2 \mathbf{T}_{d,j}^2 = \mathbf{W}_{u,j}^2 (\mathbf{T}_{xd,j}^2 + \mathbf{T}_{yd,j}^2). \quad (4.23)$$

The thruster mapping (4.11) is also unchanged due to the reformulation in Cartesian coordinates. This means that \mathbf{B}_C is defined as:

$$\mathbf{B}_C = \begin{bmatrix} \mathbf{1}_{1 \times n} & \mathbf{0}_{1 \times n} \\ \mathbf{0}_{1 \times n} & \mathbf{1}_{1 \times n} \\ -\mathbf{L}_y & \mathbf{L}_x \end{bmatrix}, \quad (4.24)$$

where $\mathbf{1}_{1 \times n}$ and $\mathbf{0}_{1 \times n}$ are vectors of ones and zeros, respectively, and $\mathbf{L}_x \in \mathbb{R}^n$ and $\mathbf{L}_y \in \mathbb{R}^n$ are vectors of the thruster positions in body x and y direction, respectively.

Constraints on fixed thrusters

If a thruster is said to be fixed it means that the thrust direction is fixed. The directional constraints then becomes:

$$\boldsymbol{\alpha}_{+,j} = \boldsymbol{\alpha}_{-,j} = \boldsymbol{\alpha}_{D,j}, \quad (4.25)$$

where $\boldsymbol{\alpha}_{D,j}$ is the fixed thrust direction. When converting to Cartesian coordinates (4.13) becomes:

$$-\sin(\boldsymbol{\alpha}_{D,j}) \mathbf{T}_{xd,j} + \cos(\boldsymbol{\alpha}_{D,j}) \mathbf{T}_{yd,j} \geq 0, \quad (4.26)$$

$$\sin(\boldsymbol{\alpha}_{D,j}) \mathbf{T}_{xd,j} - \cos(\boldsymbol{\alpha}_{D,j}) \mathbf{T}_{yd,j} \geq 0. \quad (4.27)$$

In order to avoid numerical difficulties the two inequality constraints above are substituted by one equality constraint, without any loss of information. The equality constraint is the solution to the above inequality constraints:

$$-\sin(\boldsymbol{\alpha}_{D,j}) \mathbf{T}_{xd,j} + \cos(\boldsymbol{\alpha}_{D,j}) \mathbf{T}_{yd,j} = 0. \quad (4.28)$$

Inserting (4.18) and (4.19) into (4.28) gives:

$$-\sin(\boldsymbol{\alpha}_{D,j}) \mathbf{T}_{d,j} \cos(\boldsymbol{\alpha}_{D,j}) + \cos(\boldsymbol{\alpha}_{D,j}) \mathbf{T}_{d,j} \sin(\boldsymbol{\alpha}_{D,j}) = 0, \quad (4.29)$$

and it is easily seen that the equation is satisfied.

In Cartesian coordinates the constraint on minimum thrust becomes:

$$\cos(\alpha_{D,j})\mathbf{T}_{xd,j} + \sin(\alpha_{D,j})\mathbf{T}_{yd,j} - \mathbf{T}_{-,j} \geq 0, \quad (4.30)$$

inserting (4.18) and (4.19) gives:

$$\begin{aligned} \cos(\alpha_{D,j})\mathbf{T}_{d,j} \cos(\alpha_{D,j}) \\ + \sin(\alpha_{D,j})\mathbf{T}_{d,j} \sin(\alpha_{D,j}) - \mathbf{T}_{-,j} \end{aligned} \geq 0, \quad (4.31)$$

$$\Downarrow \quad (4.32)$$

$$\mathbf{T}_{d,j} \geq \mathbf{T}_{-,j}, \quad (4.33)$$

Similar as for the minimum thrust constraint, the maximum thrust constraint in Cartesian Coordinates is:

$$-\cos(\alpha_{D,j})\mathbf{T}_{xd,j} - \sin(\alpha_{D,j})\mathbf{T}_{yd,j} + \mathbf{T}_{+,j} \geq 0, \quad (4.34)$$

when inserting (4.18) and (4.19) this gives:

$$\begin{aligned} -\cos(\alpha_{D,j})\mathbf{T}_{d,j} \cos(\alpha_{D,j}) \\ - \sin(\alpha_{D,j})\mathbf{T}_{d,j} \sin(\alpha_{D,j}) + \mathbf{T}_{+,j} \end{aligned} \geq 0, \quad (4.35)$$

$$\Downarrow \quad (4.36)$$

$$\mathbf{T}_{+,j} \geq \mathbf{T}_{d,j}, \quad (4.37)$$

For a fixed thruster the Cartesian constraints are given by (4.28), (4.30) and (4.34).

Constraints on rotating thrusters

As a simplification it is in this thesis chosen to let the rotating thrusters only produce positive thruster force. Otherwise, the convexity of the formulation is lost. An alternative could be a two step procedure where the first step determines the azimuth angles for positive thruster forces only, the thrusters rotate only if the desired thrust direction has deviated from the current direction for some time, and the second step solves the fixed thruster directions allocation problem allowing both positive and negative thruster force. In practical implementations different factors affect the choice between these two methods: mechanical design, power supply, response time of azimuth compared to bandwidth of the DP system, thrust efficiency and risk of cavitation. In the mechanical design it may not have been taken into account that the thruster should be reversed. In that case the structural strength of the gears may be insufficient for reverse operation. The durability of the azimuth mechanism will also affect the ability to let the azimuth thruster change direction frequently and fast. If an electrical motor drives the propeller shaft, the thrust direction can be reversed much faster than if the propeller is driven directly by e.g. a diesel engine. The main reason for using only positive thruster forces are that most propellers (except for tunnel thrusters) are optimized for operation with one particular direction

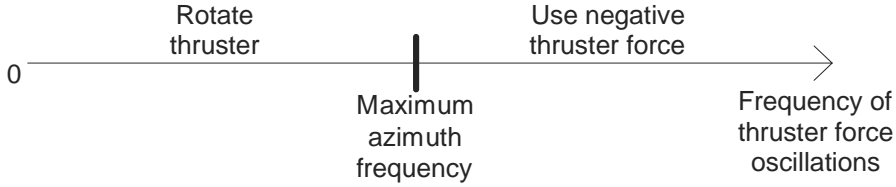


Figure 4.2: When to rotate or use negative thrust.

of thrust production. Hence, usually the efficiency and the maximum capability of the negative thrusts are much smaller than for the positive thrusts. Also the risk for cavitation during the reversion should be taken into account. To avoid use of negative thrusts, the response time of the azimuth mechanism should be significantly smaller than of the DP system. If it is chosen to let the thrusters produce negative force and the oscillations in thrust is smaller than the mean value, such that no zero crossing of the thruster force occur, no special precautions are needed. However, if the mean load of the thruster is smaller than the oscillations, zero crossing will occur, and the desired action will depend on the relationship between the frequency of the thruster force oscillations and the maximum azimuth frequency. This is illustrated in Figure 4.2. On DP vessels the thrusters counteract a mean environmental disturbance, and hence operates around a mean value different from zero. On PM vessels, this is not the case, as the mooring takes care of the mean loads and the thrusters only provides damping. This means that the thrusters are operated around zero mean thrust on PM vessels, and hence both positive and negative thrusts should be allowed on all thrusters.

Three approximations are made when converting the constraints of rotating thrusters from cylindrical to Cartesian coordinates. First a little region about zero is allowed in order to facilitate rotation with zero thrust to a new more optimal direction. This affects the directional constraints, which are rechecked after optimization. If the minimum thrust is zero, it should instead be given a small negative value to allow for the small area about zero. The directional constraints are beyond the small area about zero identical in cylindrical and Cartesian coordinates. The equations becomes:

$$-\sin(\alpha_{-,j})\mathbf{T}_{xd,j} + \cos(\alpha_{-,j})\mathbf{T}_{yd,j} + c_2 |\cos(\alpha_{-,j})| (\mathbf{T}_{+,j} - \mathbf{T}_{-,j}) \geq 0, \quad (4.38)$$

$$\sin(\alpha_{+,j})\mathbf{T}_{xd,j} - \cos(\alpha_{+,j})\mathbf{T}_{yd,j} + c_2 |\cos(\alpha_{+,j})| (\mathbf{T}_{+,j} - \mathbf{T}_{-,j}) \geq 0, \quad (4.39)$$

where $c_2 \in \mathbb{R}$ is a small constant. It is the $c_2 |\cos(\alpha_-)| (\mathbf{T}_+ - \mathbf{T}_-)$ term that enables a small area about $\mathbf{T}_j = 0$, such that the thruster can rotate with zero thrust. The value of c_2 should be as large as possible without affecting the solution noticeably. It is suggested to use $c_2 = 0.001$. In Figure 4.3 these equations are illustrated as line 1 and 2, respectively. After solving the QP

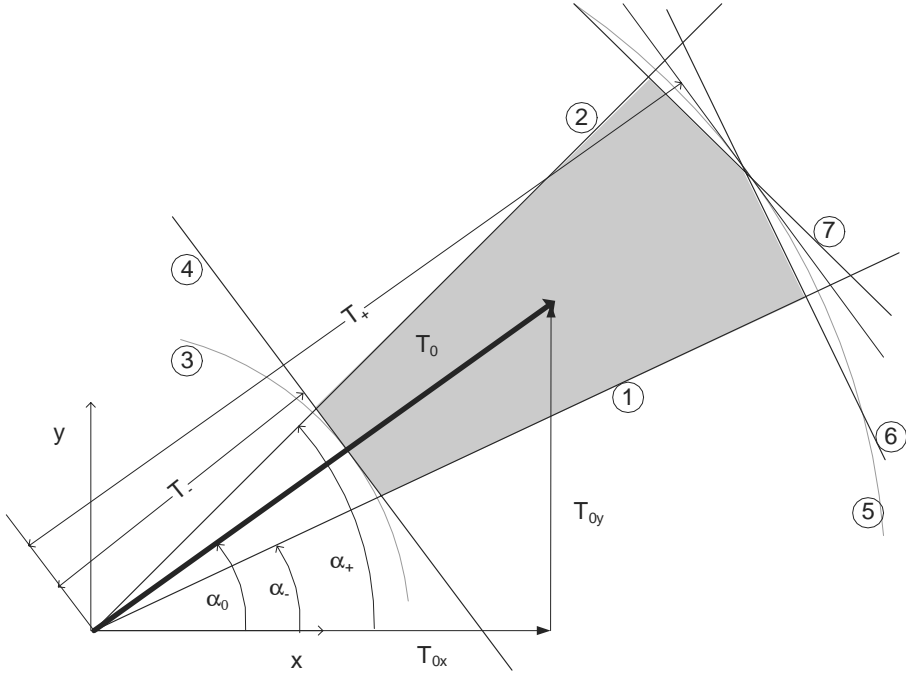


Figure 4.3: Constraints in Cartesian coordinates. \mathbf{T}_0 is the desired thrust from the last time step.

problem the constraints on $\boldsymbol{\alpha}_j$ is rechecked, and T_j is set to zero if $T_j < 0$.

The minimum thrust constraint is approximated by a line instead of an arc. The cylindrical constraint is line number 3 in Figure 4.3 and the Cartesian constraint are line number 4 given by:

$$\cos(\boldsymbol{\alpha}_j)\mathbf{T}_{xd,j} + \sin(\boldsymbol{\alpha}_j)\mathbf{T}_{yd,j} - \mathbf{T}_{-,j} \geq 0. \quad (4.40)$$

The maximum thrust constraint is approximated by two lines. The inspiration to this approach came from Lindfors (1993). Two lines are used instead of one in order to favour the current operating direction in case of saturation. The cylindrical constraints is line 5 in Figure 4.3. The Cartesian maximum thrust constraint equations are given as:

$$\begin{aligned} -\cos(\boldsymbol{\alpha}_{-,j})\mathbf{T}_{xd,j} - \sin(\boldsymbol{\alpha}_{-,j})\mathbf{T}_{yd,j} \\ + \cos(\boldsymbol{\alpha}_{-,j} - \boldsymbol{\alpha}_{0,j})\mathbf{T}_{+,j} \end{aligned} \geq 0, \quad (4.41)$$

$$\begin{aligned} -\cos(\boldsymbol{\alpha}_{+,j})\mathbf{T}_{xd,j} - \sin(\boldsymbol{\alpha}_{+,j})\mathbf{T}_{yd,j} \\ + \cos(\boldsymbol{\alpha}_{+,j} - \boldsymbol{\alpha}_{0,j})\mathbf{T}_{+,j} \end{aligned} \geq 0. \quad (4.42)$$

The equations correspond to line 6 and 7 in Figure 4.3, respectively.

The benefits of this formulation are that the exact thruster mapping is used, there exist one global minimum, the thrusters are constraint in both absolute

value and rate for both thruster force and direction, real time reconfiguration is easily accommodated, and that the problem can efficiently be solved by a standard QP solver. The use of quadratic cost functions and linear constraints are a prerequisite for using the QP solver. The error when converting the constraints from cylindrical coordinates to Cartesian is small due to the rate constraints on thrust directions.

4.4.3 Power constraints

Power constraints are always checked in real industrial applications. However, the only reference we have found is Jenssen and Realfsen (2006). It is in this thesis proposed other ways of taking power constraints into account in power optimal thrust allocation. Two types of constraints are treated: constraints on total power consumption and power bus constraints.

Constraint on total power

In case of power optimal thrust allocation, which is presented in this thesis, limitations on total power consumption can easily be taken into account. The approach presented here is very similar with the percentage phase back approach in Jenssen and Realfsen (2006). Since the power optimal solution is found in the optimization problem, the thrusts have to be reduced and the generalized force can no longer be produced if the power optimal solution violates the power constraint. Usually, in station keeping operations, control of heading is more important than control of position. This is because the forces on the ship increase significantly if the bow is not kept against the weather. Hence, the first approach may be to resolve the thrust allocation problem with increased weights on fulfillment of yaw command. If the solution still does not satisfy the power constraints, or the initial weight of the yaw command was high enough, it is proposed to reduce all the generalized forces with the same percent. This approach preserves the desired generalized force direction. Let $P_{Td} \in \mathbb{R}$ be the total power requested from the thrust optimization problem. By inserting in (3.11):

$$P_{Td} = \sum_j \frac{2\pi \mathbf{K}_{Qc,j}}{\sqrt{\rho} \mathbf{D}_j \mathbf{K}_{Tc,j}^{3/2}} \mathbf{T}_{d,j}^{3/2}, \quad (4.43)$$

where j indexes the different thrusters, $\mathbf{K}_{Tc,j}$ and $\mathbf{K}_{Qc,j}$ are the controller thrust and torque coefficient, respectively, $\rho \in \mathbb{R}$ is water density, and \mathbf{D}_j is the propeller diameter.

The estimate of the power consumption can be improved by prediction from the measured power consumption:

$$P_{T,k} = P_{meas,k-1} \frac{P_{Td,k}}{P_{c,k-1}}, \quad (4.44)$$

where $P_T \in \mathbb{R}$ is the estimated power consumption, $P_{meas} \in \mathbb{R}$ is the measured power consumption, $P_c \in \mathbb{R}$ is the commanded power consumption from the

thrust allocator after the power constraints, and k indexes the current time step.

Let $P_{AV} \in \mathbb{R}$ be the total available power from the power plant. Then, if $P_{AV} \geq P_T$, there is no problem. However, if $P_{AV} < P_T$, there is not enough power available to fulfill the commands, and the desired thrust has to be reduced. Assume it is desirable to maintain the weighting between the different generalized forces, as argued above. The desired generalized force should then be reduced to:

$$\boldsymbol{\tau}_c = u\boldsymbol{\tau}_d, \quad (4.45)$$

$$= u\mathbf{B}\mathbf{T}_d, \\ = \mathbf{B}(u\mathbf{T}_d), \quad (4.46)$$

where $\boldsymbol{\tau}_c$ is the commanded generalized force, and $u \in [0, 1] \in \mathbb{R}$ is a variable limiting the thrust and hence also the power consumption. This means that, if none of the thrusters are saturated, the power optimal solution is to reduce the desired thrust equally on all the thrusters, that is the commanded thrust $T_{c,j}$ equals $uT_{d,j}$. The variable u is determined from:

$$P_{AV} = P_{T,k}, \quad (4.47)$$

$$= \frac{P_{meas,k-1}}{P_{c,k-1}} \sum_j \frac{2\pi \mathbf{K}_{Qc,j}}{\sqrt{\rho} \mathbf{D}_j \mathbf{K}_{Tc,j}^{3/2}} (u\mathbf{T}_{d,j})^{3/2}, \\ = u^{3/2} \frac{P_{meas,k-1}}{P_{c,k-1}} \sum_j \frac{2\pi \mathbf{K}_{Qc,j}}{\sqrt{\rho} \mathbf{D}_j \mathbf{K}_{Tc,j}^{3/2}} \mathbf{T}_{d,j}^{3/2},$$

$$= u^{3/2} \frac{P_{meas,k-1}}{P_{c,k-1}} P_{Td} \Rightarrow \quad (4.48)$$

$$u = \left(\frac{P_{AV}}{P_{Td}} \frac{P_{c,k-1}}{P_{meas,k-1}} \right)^{2/3}. \quad (4.49)$$

This will reduce the commanded generalized force to $\boldsymbol{\tau}_c = u\boldsymbol{\tau}_d$, and $P_{c,k} = u^{3/2} P_{Td,k}$, and the constraint on total power consumption will be satisfied. It is however important to tell the power plant that the demand for power is $P_{T,k}$ such that more generators can be started if possible and necessary. In cases where the thruster are saturated, this method still satisfy the power constraint, but the solution may no longer be the perfectly power optimal solution.

Constraint on the power bus

Constraints on maximum power outtake on a single power bus can be included by the constraints:

$$\sum_{j \in Y} \mathbf{P}_{d,j} = \sum_{j \in Y} \mathbf{m}_j |\mathbf{T}_{d,j}|^{3/2} \leq P_{bus}, \quad (4.50)$$

where $Y = \{j | \text{thruster number } j \text{ is on the power bus}\}$, $\mathbf{P}_d \in \mathbb{R}^n$ is the desired thruster power, $\mathbf{m} \in \mathbb{R}^n$ is a constant vector that is determined from (3.11) and

$P_{bus} \in \mathbb{R}$ is the maximum power consumption allowed on the bus. Linearizing with respect to \mathbf{T}_{xd} and \mathbf{T}_{yd} gives:

$$\begin{aligned} \sum_{j \in Y} P_{d,j} &= \sum_{j \in Y} \mathbf{m}_j \left(\sqrt{\mathbf{T}_{x,d,j}^2 + \mathbf{T}_{y,d,j}^2} \right)^{3/2}, \\ &= \sum_{j \in Y} \mathbf{m}_j (\mathbf{T}_{x,d,j}^2 + \mathbf{T}_{y,d,j}^2)^{3/4}, \end{aligned} \quad (4.51)$$

$$\approx \sum_{j \in Y} \frac{\mathbf{m}_j (\mathbf{T}_{0x,j}^2 + \mathbf{T}_{0y,j}^2)^{3/4}}{\frac{3}{4}\mathbf{m}_j (\mathbf{T}_{0x,j}^2 + \mathbf{T}_{0y,j}^2)^{-1/4} 2\mathbf{T}_{0x,j} (\mathbf{T}_{x,j} - \mathbf{T}_{0x,j}) + \frac{3}{4}\mathbf{m}_j (\mathbf{T}_{0x,j}^2 + \mathbf{T}_{0y,j}^2)^{-1/4} 2\mathbf{T}_{0y,j} (\mathbf{T}_{y,j} - \mathbf{T}_{0y,j})} \quad (4.52)$$

Inserting (4.52) in (4.50) gives:

$$\begin{aligned} &\sum_{j \in Y} \frac{3}{2}\mathbf{m}_j (\mathbf{T}_{0x,j}^2 + \mathbf{T}_{0y,j}^2)^{-1/4} (\mathbf{T}_{0x,j} \mathbf{T}_{x,j} + \mathbf{T}_{0y,j} \mathbf{T}_{y,j}) \\ &\leq P_{bus} - \sum_{j \in Y} \left(\frac{\mathbf{m}_j (\mathbf{T}_{0x,j}^2 + \mathbf{T}_{0y,j}^2)^{3/4}}{\frac{3}{2}\mathbf{m}_j (\mathbf{T}_{0x,j}^2 + \mathbf{T}_{0y,j}^2)^{-1/4} (\mathbf{T}_{0x,j}^2 + \mathbf{T}_{0y,j}^2)} \right) \quad (4.53) \\ &\Downarrow \end{aligned}$$

$$-\sum_{j \in Y} \frac{\frac{3}{2}\mathbf{m}_j (\mathbf{T}_{0x,j}^2 + \mathbf{T}_{0y,j}^2)^{-1/4}}{(\mathbf{T}_{0x,j} \mathbf{T}_{x,j} + \mathbf{T}_{0y,j} \mathbf{T}_{y,j})} \geq -\frac{1}{2} \sum_{j \in Y} \mathbf{m}_j (\mathbf{T}_{0x,j}^2 + \mathbf{T}_{0y,j}^2)^{3/4} \quad (4.54)$$

$$-\sum_{j \in Y} \frac{\frac{3}{2}\mathbf{m}_j (\mathbf{T}_{0d,j}^2)^{-1/4}}{(\mathbf{T}_{0x,j} \mathbf{T}_{x,j} + \mathbf{T}_{0y,j} \mathbf{T}_{y,j})} \geq -P_{bus} - \frac{1}{2} \sum_{j \in Y} \mathbf{m}_j (\mathbf{T}_{0d,j}^2)^{3/4}. \quad (4.55)$$

Since there are rate constraints on the magnitude of the thruster force, the inaccuracy in the linearization should be acceptable. Assume the rate constraint on the thrust magnitude is 20% of the maximum thrust \mathbf{T}_{max} . For small values of \mathbf{T}_0 the inaccuracy in the linearization may be large. However, if \mathbf{T}_0 is let say 50% of maximum thrust, the accuracy of the linearization should be acceptable. If the thrust is increased by 20% of the maximum thrust, the thrust becomes 70%. This gives an increase in power by 66%. The linearization gives an increase of 60%. This should be sufficiently accurate, especially since the accuracy will increase significantly in the next sample. Power limitations are also usually a problem at high thrusts. It is also an option to reduce the value of $\dot{\mathbf{T}}_{max}$ and increase the values of $\dot{\mathbf{T}}_{min}$ in order to improve the accuracy of the power constraints. This may particularly be desirable if there are few generators running, and the instantly maximum available power is low compared to the available power when more generators are running.

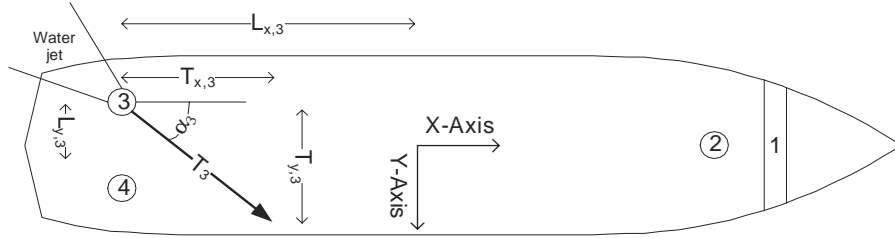


Figure 4.4: Layout of CyberShip III.

Table 4.1: Main dimensions of CyberShip III.

Parameter	Model	Ship	Unit
Length	1.97	59	[m]
Beam	0.44	13.2	[m]
Draught	0.16	4.8	[m]
Mass	89	$2.4 \cdot 10^6$	[kg]

4.5 Experimental validation

The convex linearly constrained quadratic thrust allocator without power constraints are validated by experiments with a model ship. The ship is a 1:30 scale version of an offshore service vessel, and is called CyberShip III (CS3). A sketch of the layout of CS3 is shown in Figure 4.4, the main particulars of the vessel are given in Table 4.1, and the key parameters of the thrusters are shown in Table 4.2. It should be noted that rotating thrusters are only allowed to give positive thrust force, while fixed thrusters can produce both positive and negative thrust force. The rotating thrusters are constrained to positive thrust force only, to always chase the optimal solution. The rotating speed of the azimuth directions are $12.0[\text{deg}/\text{sample}]$, corresponding to $11[\text{deg}/\text{s}]$ in full scale. The details of the experimental setup is given in Appendix B. Only a selection of figures are presented in the text. A complete collection of figures for the presented runs are found in Appendix C. The sample time of the control system, including the thrust allocator was $0.20[\text{s}]$, corresponding to $1[\text{Hz}]$ in full scale.

4.5.1 Run A: Station keeping, convex

In this case CS3 was operated in DP operation. Disturbances in terms of regular waves with amplitude $0.06[\text{m}]$ and period $0.8[\text{s}]$ were applied (corresponds moderate seas with amplitude $1.8[\text{m}]$ and period $4.4[\text{s}]$ in full scale). The first $100[\text{s}]$ are with all the thrusters fixed, and the last $100[\text{s}]$ are with three rotating thrusters. From Figure 4.5 it is seen that the convex linearly constrained quadratic thrust allocator performs well for both fixed and rotating thrusters. In

Table 4.2: Key parameters of thrusters on CyberShip III.

Thruster No.	1	2	3	4
Type	Tunnel	Azimuth	Azimuth	Azimuth
Max. thrust [N]	0.58	8.7	13.5	13.0
Fixed direction [deg]	90	90	45	-45
Max. thrust full scale [kN]	16	235	365	351
Approximate power delivered to propeller full scale [MW]	0.031	1.2	2.6	2.4

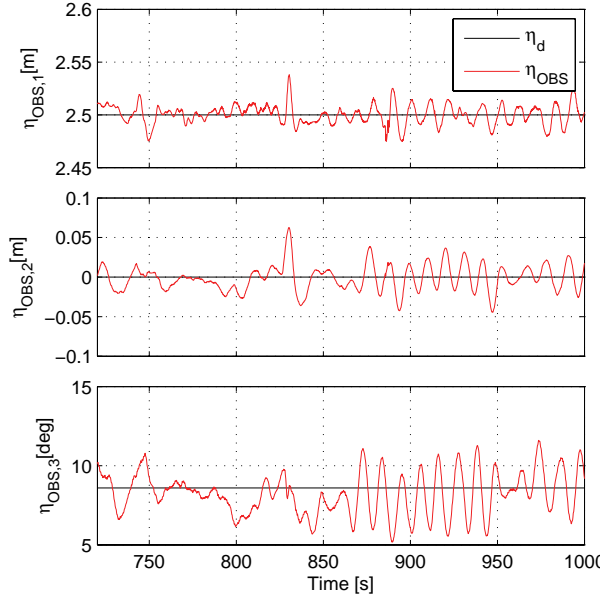


Figure 4.5: Plot of position and heading during station keeping operation in head seas, Run A. Fixed thrusters until 820[s], and rotating thrusters from 900[s].

Figure 4.6 the power consumption is plotted. The power consumption is reduced by 44% by use of rotating compared to fixed thrusters. The power consumption in the case of fixed thrusters are dependent on the chosen fixed directions. The directions used here are chosen in order to get high maneuverability. The saving in power is expected since the thrusters work against a mean force. This means that the rotating thrusters do not miss the ability to produce negative thrust. However, in conditions without mean disturbances the fixed solution with fixed thrust directions outperform the solution letting the thrusters rotate. The reason for the increased power consumption of rotating thrusters in conditions without a mean environmental force is that a minor unbalance will trigger the thrusters to work against each other. This is consistent with the findings of Swanson (1982) which solved the problem by switching between the two solutions. An suggestion to how this can be done in our case is shown in Section 6.4.2.

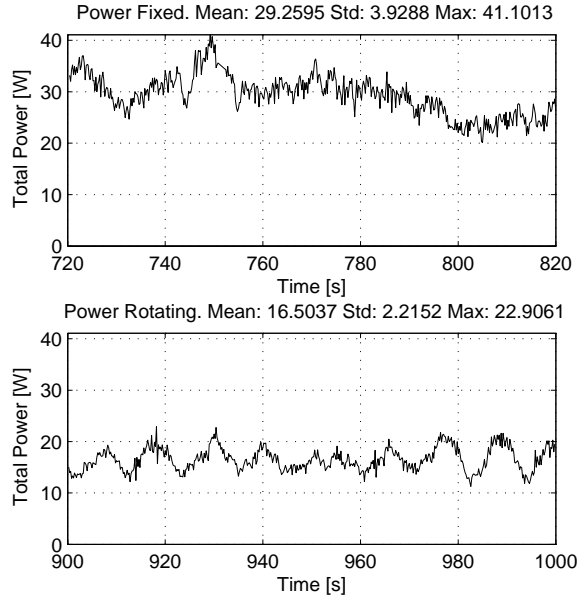


Figure 4.6: Plot of power consumption during station keeping operation in head seas, Run A. Fixed thrusters in upper plot and rotating thrusters in lower plot.

4.5.2 Run B: Joystick, convex

In order to demonstrate that the presented thrust allocator with rotating azimuths is capable of handling rapidly varying generalized force commands, the input command from the joystick was varied in steps. No waves were present. The resulting desired τ_d , commanded τ_c and measured τ_{RAW} generalized forces are shown in Figure 4.7. The variable τ_{RAW} is computed based on the measured thrust direction α_{RAW} and the measured thrust T_{RAW} , which again is computed from the measured shaft speed n_{RAW} . For details see Appendix B. From the figure it is seen that the commanded generalized force approaches the desired value. In short periods after the changes in the desired value, the commanded forces differ from the desired values. This is because the allocator during transition to the new setting passes through singular configurations. From Figure 4.8 and 4.9 it is seen that the desired and measured thrust direction and force varies smoothly. It is also seen in the figures that it is a small time lag between the commanded and measure quantities. This is caused by the response time of the actuators. The time lag is in the order of a few samples. When all the thrusters are rotated simultaneously, about e.g. 1555[s], it is seen that the time lag causes the measured generalized force to deviate from the commanded one. This is caused by the time lag in the azimuths.

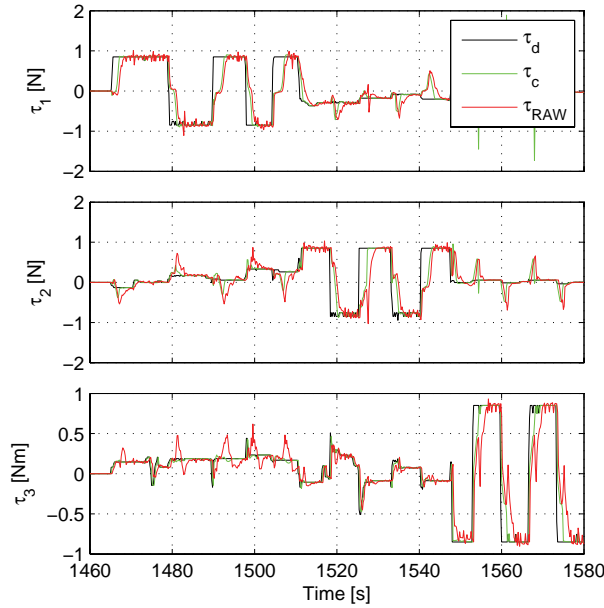


Figure 4.7: Plot of generalized forces during joystick operation, Run B. The ripples on τ_{RAW} are caused by noise in the shaft speed measurements.

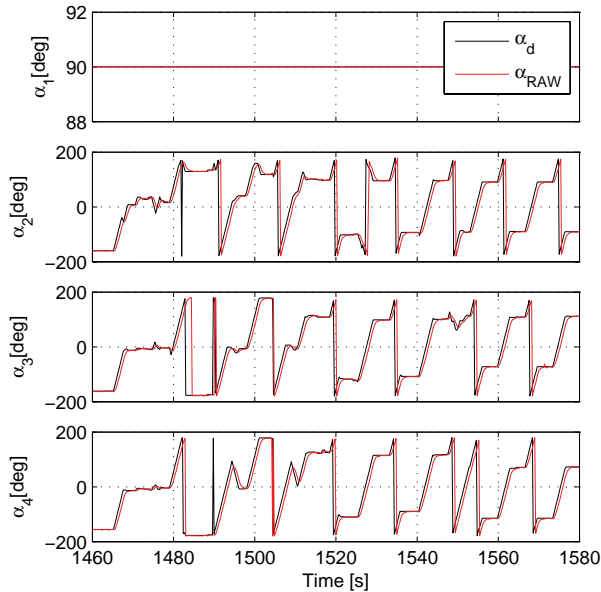


Figure 4.8: Plot of thrust directions during joystick operation, Run B. The vertical lines are caused by transitions between $\pm 180[\text{deg}]$.

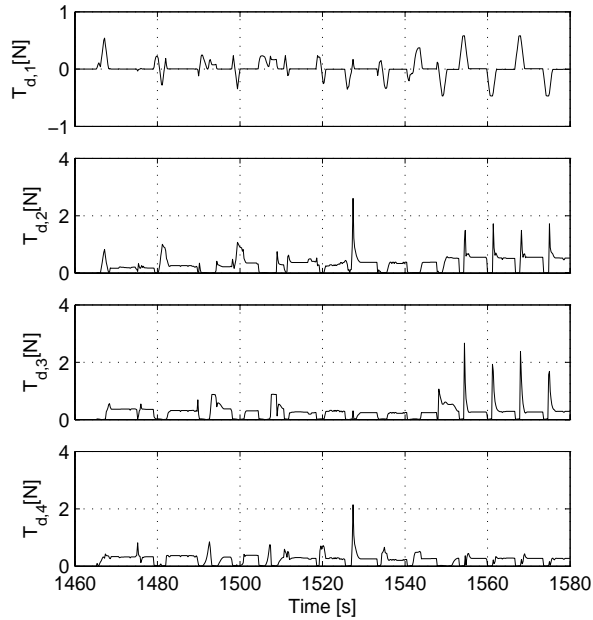


Figure 4.9: Plot of thruster forces during joystick operation, Run B.

4.5.3 Summary experiments

Satisfactory performance of the thrust allocator during station keeping operations was observed. Rotating thrusters had a significant power saving compared to fixed ones, if the thrusters were counteracting a mean environmental force. When subject to rapidly varying desired generalized forces, the measured generalized forces were somewhat delayed, due to the limited rotational speed of the azimuths.

Chapter 5

Anti-spin thrust allocation

In oil and gas exploration and exploitation, ships and rigs conduct all-year operation in extreme environmental conditions. These vessels include shuttle tankers, drilling rigs, and offshore service, construction and production vessels. Harsh weather conditions with high waves, large ship motions, and high thrust demands can cause ventilation and in-and-out-of water events on the thrusters. A thruster ventilates when air is sucked down from the surface and into the propeller. Ventilation can cause the produced thruster force to decrease to 5-20% of the nominal value, in a few seconds (Ruth and Smogeli 2006). Ventilation and in-and-out-of water events hence affect the vessel's positioning accuracy, because they give large differences between the commanded thruster force and the produced thruster force. Both ventilation and in-and-out of water effects cause rapid variations in thrust, torque, power and shaft speed, and thus causes mechanical wear and tear of the thrusters and transients in the power network, leading to reduced safety. In the case with torque or power controlled thrusters, as suggested in Smogeli (2006) and Smogeli et al. (2005), ventilation and in-and-out-of water events may cause unacceptable propeller racing.

Anti-spin control is used in the car industry, see e.g. Borrelli et al. (2006), and in local thruster controllers Smogeli et al. (2004a), Smogeli (2006), Smogeli et al. (2008), and Bakkeheim et al. (Accepted). The idea of anti-spin control is to detect the reduced performance of the actuator and do something about it. On cars, the wheel speed is monitored, and the brakes are applied if the wheel spins. This is because spinning wheels have much lower friction between tire and road than non spinning wheels. The same principle is used in thruster controllers. However, in this case brakes are not applied, but instead the output torque from the motor is reduced. Further, the main goal is no longer to increase the force, but to reduce the wear and tear and ensure safe operation. It is also a goal to get more predictable thrust production in order to increase the positioning accuracy.

Motivated by similar challenges with controlling wheel spin on cars, it is proposed in Smogeli (2006) to apply anti-spin control also to the thrust allocator, which will enable thrust redistribution. In this thesis, it is proposed to use the

performance measures in Smogeli (2006) to distribute the generalized forces to the most efficient thrusters. This is denoted anti-spin thrust allocation. The idea pursued in this chapter is to modify the cost in the thrust allocation problem to disfavor the thrusters subject to large losses. The possibility of modifying the thruster configuration matrix was also investigated. Results from simulations (not presented here) showed that modifying the thruster configuration matrix was unfavorable. This is because modifying the thruster configuration matrix by use of the instant thrust losses will result in large changes in the allocated thrusts in between the different time steps, and actually increase the wear and tear compared to no action at all. Further, applying filtered values of the thrust losses will result in a wrong mapping from thruster forces to generalized forces. This is because ventilation is a short term incident, and the propeller will actually be non-ventilated most of the time. The conclusion about thruster configuration matrix modification was that the matrix should not be modified. Instead the cost of using a ventilating thruster should be increased sufficiently to avoid ventilation. This will give $\beta_T \approx 1$, and hence, it is no need for thrust modifications.

For safe operation of the individual thrusters, it is proposed to use a simple shaft speed limit. This is normally already included and will not affect the constraints on thruster force in the thrust allocator. The anti-spin thrust allocation action will take effect in the time step after detection. The detection can either be done locally on the thrusters, usually operating at a high frequency, or by the thrust allocator usually operating at 1.0[Hz]. A proper designed anti-spin thrust allocator is expected to reduce the wear and tear (increase safety), reduce power consumption (increase efficiency) and increase the positioning accuracy. The theory are verified by model scale experiments. This chapter is to a large extent based on (Ruth et al. Accepted).

5.1 Cost function with $T^{3/2}$

In order to get a more correct penalty of the power consumption and hence make it easier to quantify the efficiency loss due to ventilation, it is proposed to replace the cost function in (4.10) with:

$$[\mathbf{T}_d, \boldsymbol{\alpha}_d] = \arg \left(\min_{\mathbf{T}, \boldsymbol{\alpha}} (\|\gamma \mathbf{W}_v \mathbf{s}\|_2^2 + \left\| \frac{\mathbf{W}_u}{\sqrt[4]{|\mathbf{T}_{d,prev}|}} \mathbf{T} \right\|_2^2) \right), \quad (5.1)$$

where $\mathbf{T}_{d,prev} \in \mathbb{R}^n$ is the desired thrust from the previous time step. For diagonal \mathbf{W}_v and \mathbf{W}_u (5.1) can also be written as:

$$[\mathbf{T}_d, \boldsymbol{\alpha}_d] = \arg \min_{\mathbf{T}, \boldsymbol{\alpha}} \left(\sum_{j=1}^m (\gamma \mathbf{W}_{v,jj}^2 \mathbf{s}_j^2) + \sum_{j=1}^n \left(\frac{\mathbf{W}_{u,jj}^2}{\sqrt[4]{|\mathbf{T}_{d,prev,j}|}} \mathbf{T}_j^2 \right) \right). \quad (5.2)$$

The novelty of this formulation is in how the thrusters are penalized in terms of power consumption using QP solvers. Traditionally, in the literature, the power consumption of a thruster is penalized by the term $\|\mathbf{W}_u \mathbf{T}_d\|_2^2$. However, since the

power is proportional to $|T_d|^{3/2}$, the power should be modeled as $|T_d|^{3/2}$ in the cost function. This has been done by Sinding and Anderson (1998), Johansen (2004), Johansen et al. (2004), and Tjønnås and Johansen (2005, 2007) using nonlinear solvers, sequential quadratic programming and Lyapunov methods. It will be shown here how this can be done with a standard QP solver. The reasons for using a standard QP solver is that it provides reliable solutions efficiently. By formulating convex problems, the solution is guaranteed to be the global solution. First an example of the error by use of T_d^2 is investigated.

Example 5.1 Assume the power is penalized by T_d^2 , and the actual power consumption is $P = |T_d|^{3/2}$. Then the power penalty should be modified by a constant k , such that $P_2 = kT_d^2$, to give the least percentage error p , in the calculated power. That is to minimize p which gives:

$$p = \min_k \left\| \frac{P_2 - P}{P} \right\|_\infty, \quad (5.3)$$

$$\begin{aligned} &= \min_k \left\| \frac{kT_d^2 - |T_d|^{3/2}}{|T_d|^{3/2}} \right\|_\infty, \\ &= \min_k \left\| k\sqrt{|T_d|} - 1 \right\|_\infty. \end{aligned} \quad (5.4)$$

On a typical real ship $|T_d| \in [1 \cdot 10^3, 1 \cdot 10^6]$ [N]. Solving (5.3) with $|T_d| \in [1 \cdot 10^3, 1 \cdot 10^6]$ gives $k = 1.94 \cdot 10^{-3}$ and $p = 0.94$. This means that the old cost function can over and under predict the cost by 94%. This example is illustrated in Figure 5.1.

The correct formulation with $|T_d|^{3/2}$ is normally not used in order to make the thrust allocation problem easier to solve. It is proposed here to use the desired thrust from the previous time step to modify the cost in such a way that the cost approaches $|T_d|^{3/2}$. The cost term then becomes:

$$J_T = \left\| \frac{\mathbf{W}_u}{\sqrt[4]{|\mathbf{T}_{d,prev}|}} \mathbf{T}_d \right\|_2^2, \quad (5.5)$$

where J_T is the part of (5.1) penalizing the power consumption of the thrusters. If $T_d \rightarrow T_{d,prev}$, then the new cost function $P_{\text{cost}} = \frac{T_d^2}{\sqrt[4]{|T_{d,prev}|}} \rightarrow P = |T_d|^{3/2}$. This can be seen by taking the limit:

$$\begin{aligned} \lim_{T_d \rightarrow T_{d,prev}} P_{\text{cost}} &= \lim_{T_d \rightarrow T_{d,prev}} \frac{T_d^2}{\sqrt[4]{|T_{d,prev}|}}, \\ &= |T_d|^{3/2}. \end{aligned} \quad (5.6)$$

The convergence ($T_d \rightarrow T_{d,prev}$) of (4.10)-(4.11) in the special case with two actuators ($a = 2$), one controlled direction ($b = 1$) and a constant generalized force $\boldsymbol{\tau}_d$ is shown analytically in Appendix D. That is, to show that if $T_{d,prev}$

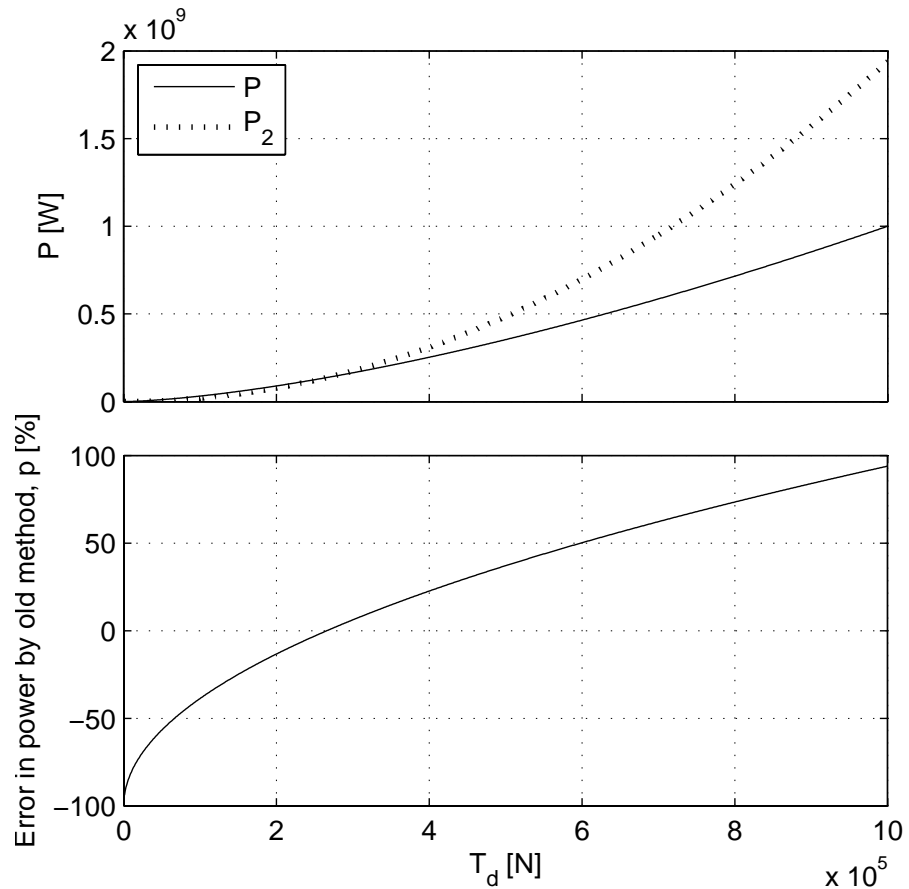


Figure 5.1: Comparison of power consumption computed from $P_{old} = 1.94 \cdot 10^{-3} T_d^2$ and $P = |T_d|^{3/2}$ when $|T_d| \in [1 \cdot 10^3, 1 \cdot 10^6]$.

differs from the true solution to the problem, the solution will converge to the true solution during the next time steps. At this stage no analytical proof for the more general case has been found. This is a topic for further research. Simulation studies, however, indicate convergence for problems with more actuators and more controlled directions. Moreover, the convergence turns out to be quite fast, in the matter of typically 5 – 10 samples. The conditions for convergence are positive definite matrices \mathbf{W}_v and \mathbf{W}_u , $|\mathbf{T}_{d,prev}| > 0$, $\gamma > 0$ and convex constraints. In the case with dynamic τ_d one might experience that P_{cost} is delayed compared to the actual power P . However, since the convergence of the cost function is faster than the typical variations in thrust, $\Delta P = P_{cost} - P$ will be small. Let $\Delta T = T_d - T_{d,prev}$ and approximate P_{cost} by a first order Taylor expansion:

$$P_{cost} = |T_d|^{3/2} + \frac{1}{2}\sqrt{|T_d|}\text{sign}(T_d)\Delta T + h.o.t.. \quad (5.7)$$

Then the typical relative error in the cost function will be:

$$\begin{aligned} \frac{\Delta P}{P} &\approx \frac{\frac{1}{2}\sqrt{|T_d|}\text{sign}(T_d)\Delta T}{|T_d|^{3/2}}, \\ &\approx \frac{\Delta T}{2T_d}, \end{aligned} \quad (5.8)$$

where ΔT is the change in desired thruster force since the last time step, and T_d is the desired thruster force. One way to reduce the convergence time is to run the thrust allocator at a higher frequency than the motion controller. This is not believed to be strictly necessary, but will improve the performance of the thrust allocator.

5.2 Modification of the cost due to ventilation and in-and-out of water events

In order to redistribute thrust from ventilating to nonventilating thrusters, it is proposed to increase the cost of the ventilating thrusters in the thrust allocator based on the number of ventilation incidents and the torque loss factor β_Q . We state the following requirements for the modification of the cost when ventilation is detected:

- The cost should be increased sufficiently to stop ventilation immediately.
- The cost should be increased on a long term basis to reduce the risk of ventilation.
- The cost should be reduced during some time such that the thruster can go back to normal operation.

An advantage of modifying the cost is that the desired thrust is only changed if redundant thrusters are available. If there are no redundant thrusters the

allocator will automatically prioritize fulfillment of the desired generalized force, although the cost is high. Looking at the thrust allocation problem formulated in (4.20)-(4.22), it is seen that as long as the slack variables dominate the cost function, the thrust mapping in (4.21) will hardly be affected by changes in the cost of using the different thrusters. This means that the thrust allocator will continue to use inefficient thrusters if it is impossible to obtain the desired generalized forces without them. On the other hand, if there are many solutions to the thrust mapping problem (4.21) subject to (4.22), increasing the cost of one redundant thruster will reduce the amount of thrust allocated to this thruster. This is an example of thrust redistribution. Also, modifying the cost does not affect the stability of the vessel control system because if the system is fully actuated, with or without anti-spin, (4.11) ensures that the allocator commands the desired generalized force. However, degraded actuator performance due to ventilation and in-and-out-of water events will influence the performance and may influence the stability of the DP system as well. The intention of the anti-spin thrust allocator is to make the thrust production of the actuators more predictable, hence improving the actuator performance and vessel performance.

The cost of thrust is modeled as a quadratic cost function, which is common and necessary to be able to use quadratic solvers. The proposed cost J_j for thruster number j is:

$$\begin{aligned} J_j &= q \frac{2\pi \mathbf{K}_{Qc,j}}{\sqrt{\rho} \mathbf{D}_j \mathbf{K}_{Tc,j}^{3/2}} \frac{1}{\sqrt{\mathbf{T}_{d,prev,j}}} \mathbf{T}_{d,j}^2, \\ &= \mathbf{W}_{u,j,j}^2 \frac{1}{\sqrt{\mathbf{T}_{d,prev,j}}} \mathbf{T}_{d,j}^2, \end{aligned} \quad (5.9)$$

where $q \in \mathbb{R}$ is a constant equal for all the thrusters. The q parameter is chosen such that:

$$\frac{1}{q} = \frac{1}{n} \sum_{j=1}^n \left[\frac{2\pi \mathbf{K}_{Qc}}{\sqrt{\rho} D \mathbf{K}_{Tc}^{3/2}} \right]_j^2, \quad (5.10)$$

where n is the number of thrusters. The parameter q is included to get at consistent relationship between the cost of the thrusters $\left\| \frac{\mathbf{W}_u}{\sqrt{\mathbf{T}_{d,prev}}} \mathbf{T}_d \right\|_2^2$ and the cost of not producing the correct thrust $\|\gamma \mathbf{W}_v \mathbf{s}\|_2^2$. The term $\frac{2\pi \mathbf{K}_{Qc,j}}{\sqrt{\rho} \mathbf{D}_j \mathbf{K}_{Tc,j}^{3/2}}$ is found in (3.11) and ensures that there is a correct relationship between the power consumption of the different thrusters.

Based on the cost function in (5.1) with $|T_d|^{3/2}$ representing the power consumption, the change in cost due to ventilation and in-and-out of water events

can be calculated as:

$$P_{vent} = sp_t P_d, \quad (5.11)$$

$$\begin{aligned} &= sp_t \frac{2\pi K_{Qc}}{\sqrt{\rho} D K_{Tc}^{3/2}} T_d^{3/2}, \\ &= \frac{\beta_Q}{\beta_T^{3/2}} \frac{2\pi K_{Qc}}{\sqrt{\rho} D K_{Tc}^{3/2}} T_d^{3/2}, \\ &\approx \beta_Q^{1-\frac{3}{2m}} \frac{2\pi K_{Qc}}{\sqrt{\rho} D K_{Tc}^{3/2}} T_d^{3/2}, \end{aligned} \quad (5.12)$$

where sp_t is the power sensitivity function for thrust control (Smogeli 2006), $\beta_T \approx \beta_Q^m$, and m is a constant. For more information about the β_T , β_Q relationship see Smogeli (2006). In this thesis $m = 0.65$ is used. The relationship in (5.11) apply for all the different thruster controllers, since this is the cost of producing the desired thrust.

Since the power consumption of a thruster is increased by $\beta_Q^{1-\frac{3}{2m}}$ due to losses, the cost of that j 'th thruster should be modified similarly in the modified cost function $J_{M,j}$:

$$J_{M,j} = \beta_{Q,j}^{1-\frac{3}{2m}} J_{T,j}. \quad (5.13)$$

One should notice that, if a different cost function is used, e.g. with power penalized by T_d^2 , another cost modification will be needed.

If the β_Q estimate only included losses due to ventilation, the above actions due to changes in β_Q could be implemented directly. However, in a real case, the value of β_Q will be significantly affected by the advance speed of the propeller and other loss effects. Since we only want to change the cost function due to ventilation and in-and-out of water effects, we have to separate these incidents from the advance speed effects. This is done by using a modified version of the ventilation detection method in (Smogeli 2006). A ventilation incidence is detected if:

$$\beta_Q < \beta_{Q,on} \cap sign(Q_m) \dot{Q}_m < \dot{Q}_{m,\lim} \cap |n| > n_{\min}, \quad (5.14)$$

where $\beta_{Q,on}$ and n_{\min} are tuning parameters used to avoid detection of ventilation due to variations in the advance speed, and $\dot{Q}_{m,\lim}$ is a tuning parameter to avoid detection of ventilation when the motor torque is rapidly increased. The ventilation incidence is turned off when:

$$\beta_Q > \beta_{Q,off}, \quad (5.15)$$

where $\beta_{Q,off}$ is a tunable parameter. The ventilation flag ζ is changed to 1 if (5.14) is true and changed to 0 if (5.15) is true. Else the value of the ventilation parameter is held. The following logic is included to enable fast response to a ventilation incident, and reduce the risk of ventilation in a more long term

perspective:

$$\beta_{Q1,j} = \begin{cases} 1, & \text{if } \zeta_j = 0, \\ \beta_{Q,j}, & \text{if } \zeta_j = 1, \end{cases} \quad (5.16)$$

$$\dot{\beta}_{Q2,j} = \begin{cases} \dot{\beta}_{Q1,j}, & \text{if } \beta_{Q2,j} = \beta_{Q1,j} \wedge \dot{\beta}_{Q1,j} < \dot{\beta}_{\lim,j}, \\ \dot{\beta}_{\lim,j}, & \text{if } \beta_{Q2,j} < \beta_{Q1,j}, \\ -\infty, & \text{else,} \end{cases} \quad (5.17)$$

$$\mathbf{W}_{u,j} = \beta_{Q2,j}^{\frac{S}{2}} \mathbf{W}_{u,normal,j}. \quad (5.18)$$

where $S = 1 - \frac{3}{2m} \in \mathbb{R}$. Equation (5.17) is also known as a rate limiting function. In practice this means that the cost is suddenly reduced when ventilation is detected, and that the cost slowly decreases to its normal value when the thruster is nonventilated. Hence, all the requirements listed in the beginning of the section are satisfied.

5.3 Experimental validation

Experiments were conducted with CyberShip III (CS3). Only a selection of figures are presented in the text. A complete collection of figures for the presented runs are found in Appendix C. The sample time of the control system, including the thrust allocator was 0.20[s], corresponding to approximately 1[Hz] in full scale. In order to facilitate ventilation of the stern thrusters, the ship is trimmed forward and the directions of the aft thrusters are fixed. This significantly reduces the ability to redistribute forces, but still demonstrates the principles. The ventilation detection algorithm used in the experiments differs slightly from the one presented previously. This is because hardware limitations forced the torque observer to run at the same frequency as the DP system. On a real ship the ventilation detection algorithm should be placed at the individual thrusters, and run at the same frequency as the local thruster controller. Details on the implemented ventilation detection algorithm is found in the Appendix B.

5.3.1 Run C: Anti-spin thrust allocation, thrust redistribution

In this case CS3 was operated in station keeping using a DP system. Disturbances in terms of regular waves with amplitude 0.04[m] and period 0.8[s] were applied. The desired heading of the ship was 135[deg] during the run. This means that the ship experienced quartering seas from port. In Figure 5.2 the thruster forces are seen in combination with the β_{Q2} values. In the upper subplot, the anti-spin on/off flag is shown instead of the β_{Q2} value for thruster number 1. This is because it was assumed that the tunnel thruster was fully submerged all the time, and hence, $\beta_{Q2,1} = 1$ all the time. The flag is 1 if anti-spin thrust allocation is turned on, and 0 otherwise. The anti-spin control is turned on and off in order to demonstrate the effect of the anti-spin action.

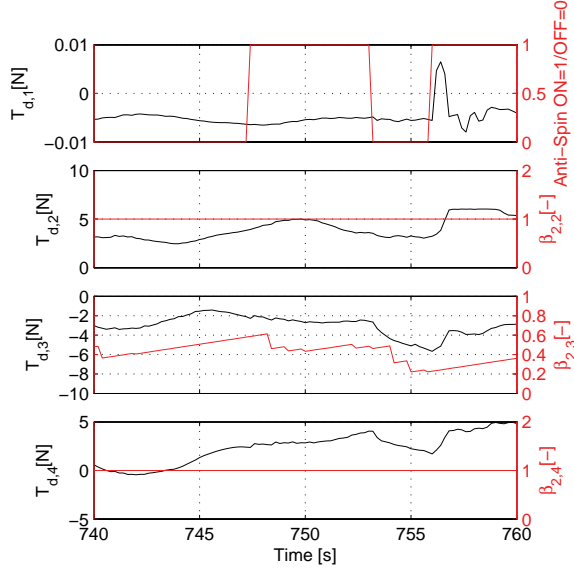


Figure 5.2: Plot of thruster forces during Run C.

The anti-spin control is turned on at 747[s] and 756[s]. At the first incident it is not possible to see any traces of the anti-spin actions on the thruster forces. This is because the cost of redistributing is higher than the cost of using the ventilating thruster. It is important to notice that the ability to redistribute is very dependent on the desired generalized force. This is illustrated the next time the anti-spin control is turned on, where significant redistribution can be seen. It is probably the sign change on the desired yaw force, see Figure 5.3, that allows the allocator to redistribute in this case. It is clearly seen from the plots that the thruster force on thruster number 3 is redistributed to thruster number 1, 2 and 4 the second time the anti-spin thrust allocation is turned on. It is also seen that the response of the anti-spin thrust allocator is very fast when the ventilation incident is detected. In Figure 5.3 it is seen that the allocator commands the desired generalized force when subject to anti-spin action, and that the anti-spin thrust allocator gives no significant transients in the generalized force.

5.3.2 Run D: Anti-spin thrust allocation, power saving

In this case CS3 was operated in station keeping using a DP system. Regular waves with amplitude 0.06[m] and period 0.8[s] were applied. The desired heading is following seas $\eta_{d,3} = 180[\text{deg}]$, since this facilitates redistribution from the aft thrusters to the forward azimuth in case of ventilation. In Figure 5.4 the vessel position and heading during the run are shown. It is seen that the performance of the DP system is satisfactory. In Figure 5.5 the thruster forces are seen

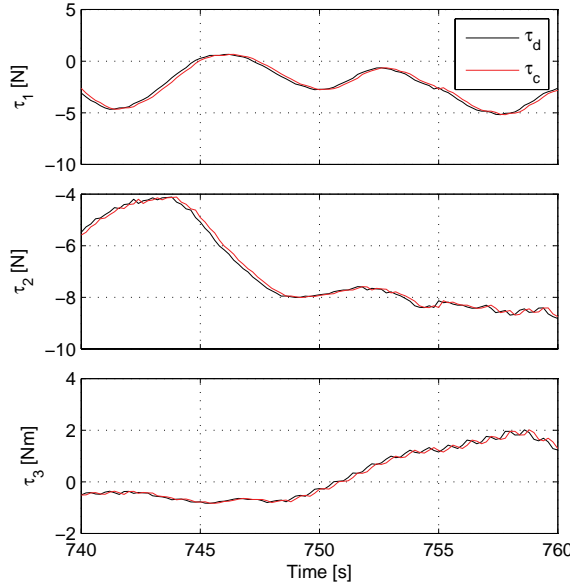


Figure 5.3: Plot of generalized forces during Run C.

together with the β_{Q2} values for thruster number 2, 3 and 4. A controller flag is shown together with thrust on thruster number 1. By comparing the controller flag with the positions in Figure 5.4, it is seen that the largest position errors occur right after the switching incidents. This is caused by the integrator in the DP controller and will be further elaborated and demonstrated in the next run. By looking at Figure 5.5 it is seen that when anti-spin thrust allocation is turned on, the thrust on thruster number 2 is significantly increased, and the magnitude of the thrusts on thruster 3 and 4 are decreased. This means that thrust from thruster number 3 and 4 are redistributed to thruster 2. Further, it is seen in the figure that the operating conditions for the aft thrusters are improved when anti-spin thrust allocation is turned on. This can be seen from the higher β_{Q2} values, indicating that the propeller losses are smaller.

The anti-spin thrust allocation also results in significant reduction in the power consumption and in the fluctuations on power and motor torque. In Figure 5.6 the total power consumption is plotted. It is seen that there is a 23% reduction in power consumption by use of anti-spin thrust allocation. This is because thrust is redistributed from thruster 3 and 4 to thruster number 2, since the efficiency of this thruster is significantly larger when the others are subject to ventilation and in-and-out-of water effects. From the figure it is also possible to see that the anti-spin thrust allocation reduces the fluctuations in the power. In order to investigate this the power spectrum of the total power consumption is presented in Figure 5.7. It is here clearly seen that there are significant energy at the wave frequency (1.25[Hz]) without anti-spin thrust allocation. This is

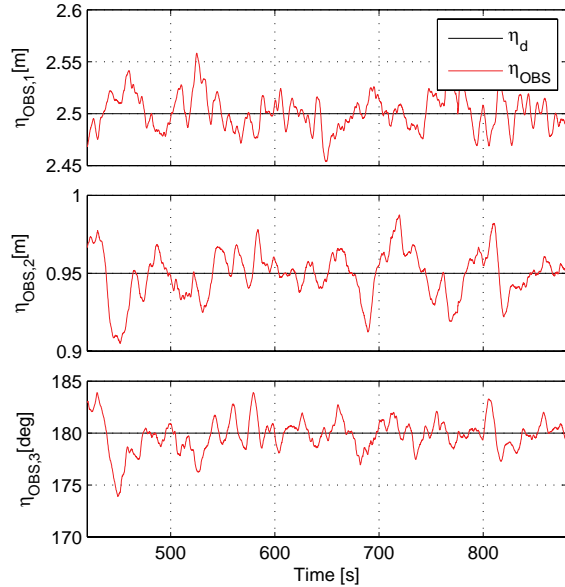


Figure 5.4: Plot of position and heading during Run D.

because when the thrusters are operated in shaft speed control as here, the torque has to be adjusted when the propeller ventilates in order to maintain the same shaft speed when the loading of the propeller is varied. It is seen that the anti-spin thrust allocation reduces the energy spent at the wave frequency by approximately 20 times. Since the ventilation phenomenon is highly nonlinear, it is also significant energy present at the higher harmonics, e.g. 2.5[Hz]. In Figure 5.8 the power spectrums of the motor torques for the individual thrusters are presented. It is here seen that the anti-spin thrust allocation significantly reduces the wave frequency fluctuations of the motor torque, which in turn will reduce the wear and tear of the propulsion system (Smogeli 2006). The repeatability of the results are verified by Figure 5.6, 5.7 and 5.8.

5.3.3 Run E: Anti-spin thrust allocation, positioning performance

In this case CS3 was operated in slow speed maneuvering using a DP system. Disturbances in terms of regular waves with amplitude 0.03[m] and period 0.8[s] were applied. The vessel made four 360[deg] turns in order to demonstrate the effect of the anti-spin thrust allocation on the integration term in the DP controller. The vessel was turned clock-wise with and without anti-spin. One turn took approximately 70[s]. The position and heading errors ($\tilde{\eta} = \eta_{OBS} - \eta_d$) are shown in Figure 5.9. The time scale is seconds after initiation of yaw change. It is seen that the positioning performance is slightly improved with anti-spin

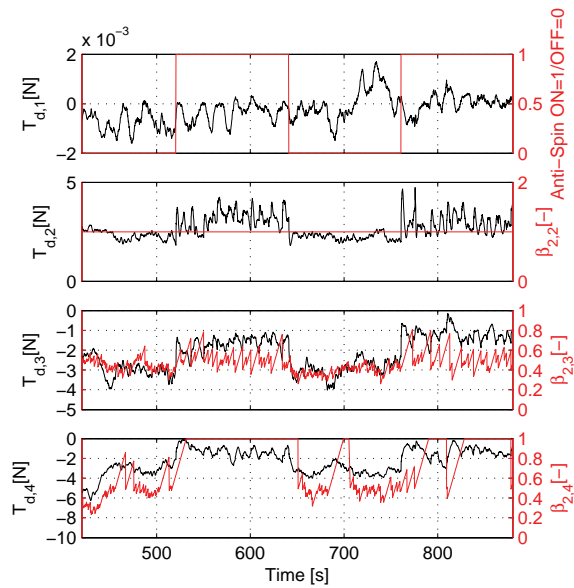


Figure 5.5: Plot of thruster forces during Run D.

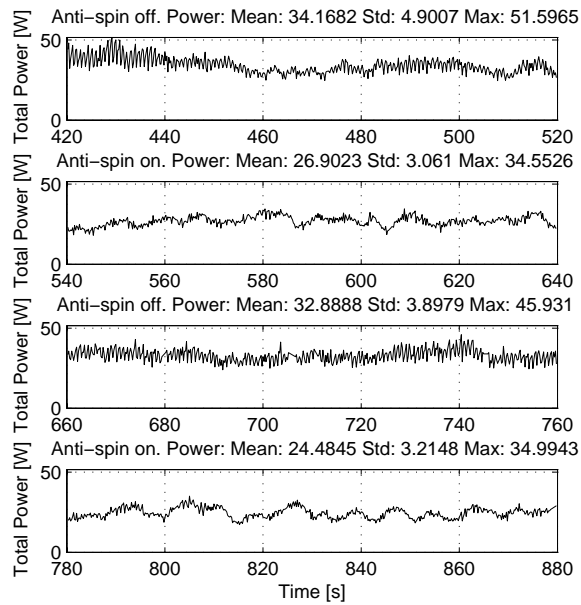


Figure 5.6: Plot of total power during Run D.

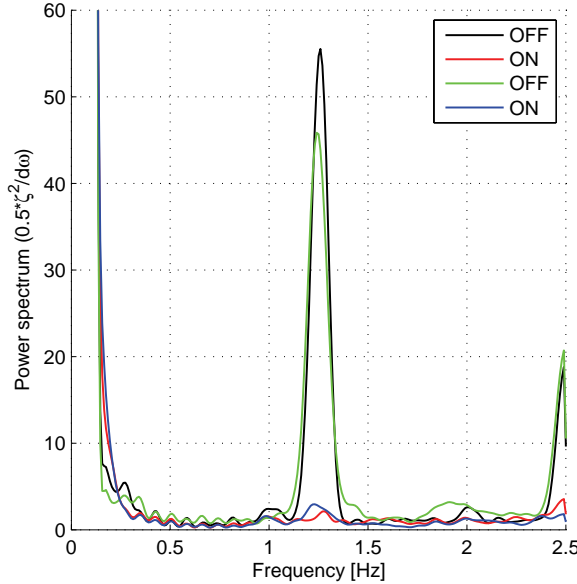


Figure 5.7: Plot of power spectrum from Run D. Two series with (ON) and without (OFF) anti-spin thrust allocation.

thrust allocation. Due to the rotation, the vessel leaves the ventilation regime rather fast such that the improved positioning accuracy is only limited in this case. In order to show repeatability, two runs both with and without anti-spin thrust allocation are presented. As the results are repeatable, it may be difficult to distinguish the runs in the figures. In Figure 5.10 the thrusts and the β_{Q2} value for thruster number 3 is shown. The other β_{Q2} values are not presented since they were all equal to one. Significant thrust redistribution from thruster number 3 to thruster number 2 and 4 can be seen.

Assume a thruster is ventilated. The produced thruster force will then differ from the desired thruster force. This will cause the integrator in the DP controller to increase the desired generalized force in order to achieve the necessary disturbance rejection force. In this case both the P- and the I-term in the DP controller counteracts the disturbances. If the disturbance direction now changes from positive to negative, the I term will work with the disturbances, and the P-term will have to counteract both the I-term and the disturbances. This will cause overshoot and reduced positioning performance.

By use of anti-spin thrust allocation the difference between desired and produced thruster force in case of ventilation will be reduced, and hence, the size of the I-term. This can be seen in Figure 5.11, where the I-terms for the clockwise turns are compared. Reducing the size of the I-term will lead to improved positioning performance. This can be seen in Figure 5.12 where the P-terms (proportional to the position error in body coordinates) are plotted. By com-

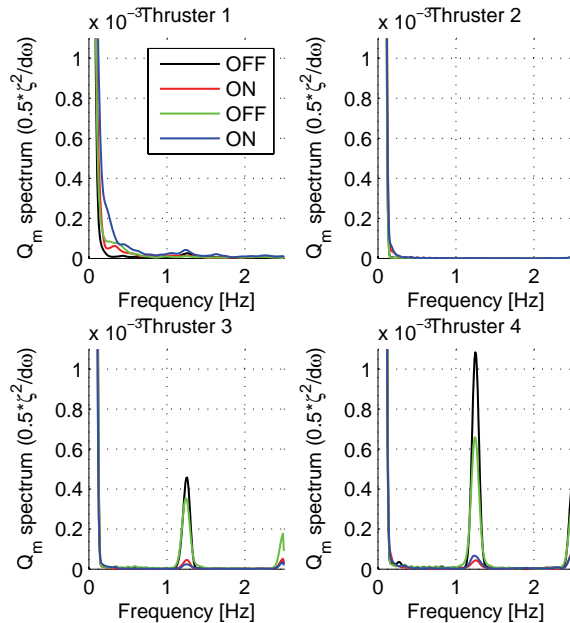


Figure 5.8: Plot of power spectrum of motor torque from Run D. Two series with (ON) and without (OFF) anti-spin thrust allocation.

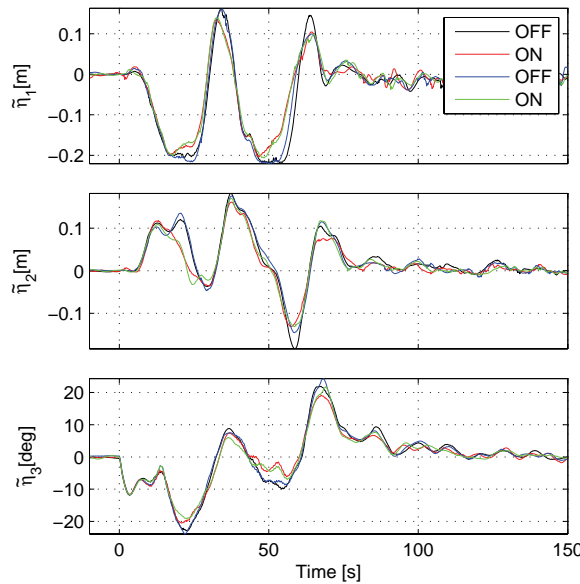


Figure 5.9: Position and heading error during Run E. Two series with (ON) and without (OFF) anti-spin thrust allocation.

paring Figure 5.11 with Figure 5.12 is it seen that in the surge direction, the P-term changes sign at approximately the same time with and without anti-spin thrust allocation. However, the zero crossing of the I-term is significantly delayed in the case without anti-spin thrust allocation. This means that the I-term counteracts the P-term for a smaller period of time with use of anti-spin thrust allocation. By looking at Figure 5.12 it is also seen that the overshoot in surge is significantly reduced by use of anti-spin thrust allocation. The two sets of time series in the figures show that the results are repeatable.

In DP controllers the size of the I-gain is a trade-off between response time and stability. A large I-gain will give rapid response to changes in the mean disturbance, but can easily cause oscillations in position. Usually a low I-gain is preferred in order to reduce the oscillations and the power consumption. In the cases with low I-gains, the anti-spin thrust allocation will be more important than with high I-gains. This is because the with high I-gains the response of the PID controller to permanent changes in the mean disturbance is faster, and the I-term will then go faster to the new value.

5.3.4 Summary experiments

It was demonstrated that the anti-spin thrust allocator only redistributed forces, if redundant thruster were available. The positioning performance of a DP system with an anti-spin thrust allocator was shown to be satisfactory. It was shown

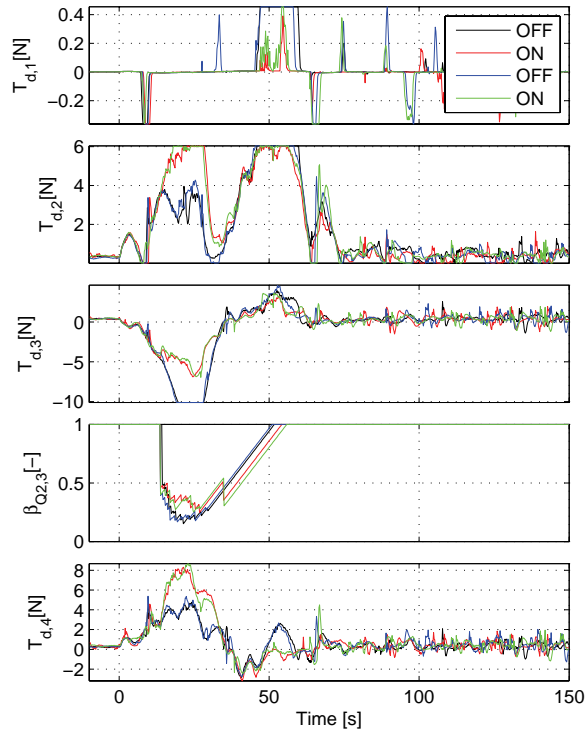


Figure 5.10: Thruster forces and β_{Q2} value for thruster number 3 during Run E. Two series with (ON) and without (OFF) anti-spin thrust allocation.

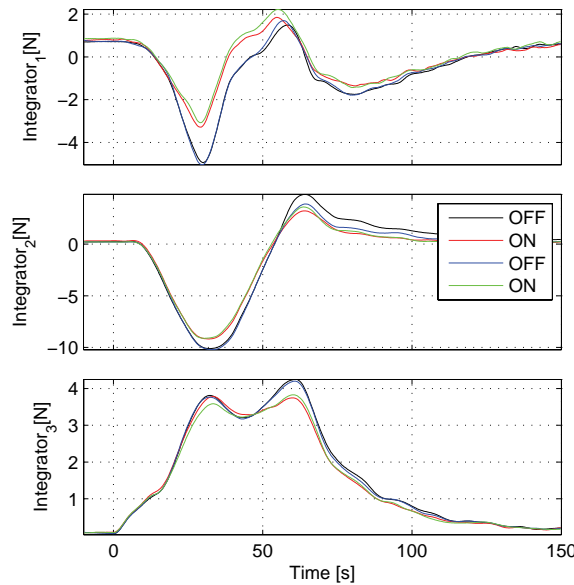


Figure 5.11: Plot of integrator (I) term in the DP controller during Run E. Two series with (ON) and without (OFF) anti-spin thrust allocation.

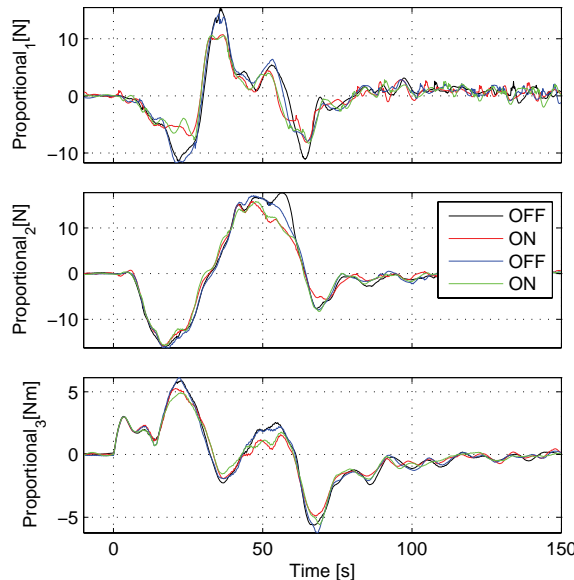


Figure 5.12: Plot of proportional (P) term in the DP controller during Run E. Two series with (ON) and without (OFF) anti-spin thrust allocation.

that the anti-spin thrust allocator can eliminate wave frequent power fluctuations caused by the ventilation incidents and significantly reduce the power consumption. It was also seen that the anti-spin thrust allocator reduced the integration terms in the motion controller, leading to improved positioning performance.

Chapter 6

Switching in thrust allocation

When designing thrust allocators there are trade-offs between robustness and performance. One way of improving both the robustness and performance is to design several thrust allocators, specialized at particular operational and environmental conditions, and switch among these. The switched thrust allocation system can be used to handle mixed-integer solutions, changing operating conditions, faults, and changing actuator configurations. The structure of a switched thrust allocator is shown in Figure 6.1. The supervisory controller is responsible for deciding which of the thrust allocators to use. The supervisory controller can be automatic, or take input from the operator. The switching block handles the actual transition between the different thrust allocators.

Changes in the thrust allocator are denoted switching incidents regardless of whether the changes are in the cost function, the constraints or the choice of solver. The challenges in switched thrust allocation are "when" and "how" to switch without increasing the complexity more than necessary. When to switch can be decided by a supervisory controller, always telling which of the individual thrust allocators that are best suited for the task. Previous work on design of supervisory controllers includes Blanke et al. (2003), Hespanha et al. (2003) and Morse (1996). The actual switching in itself is also a challenge, since safe operation is important also during the switching operation. Theory on switching between stabilizing linear controllers is treated in e.g. Hespanha and Morse (2002) and Margaliot (2006). The results in these references ensure that the switched system approaches the origin, but do not say anything about the smoothness of the control signal. The control allocation problem is a mapping and not a dynamic system. Hence, other stability results will be more appropriate. Especially, it is desirable that the switching does not create rapid changes in the controller signal. Results on switching applied to DP systems are found in Nguyen (2005) and Nguyen et al. (2007).

The idea of switched thrust allocation for marine applications is previously proposed by Swanson (1982). In this reference the reason for doing switched

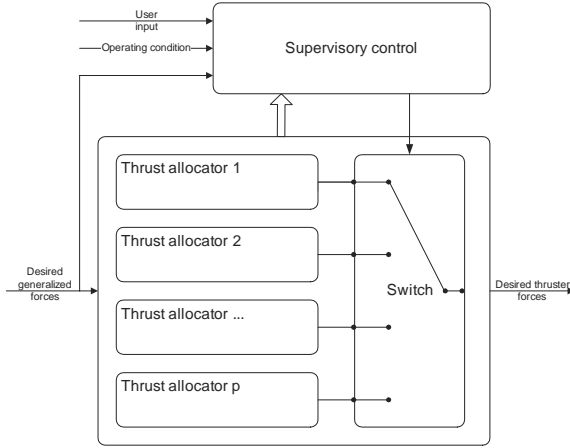


Figure 6.1: Block diagram of internal structure of switched thrust allocation system.

thrust allocation is to exploit the best properties of two different thrust allocators in calm and heavy seas, respectively. The weight between the different strategies is decided by the power consumption, which is a good indicator of the prevailing environmental disturbances. The work in this thesis extends the idea of Swanson (1982) to switching between several thrust allocators accounting for varying environmental and operational conditions.

In the following controller operating conditions, supervisory control, and switching are discussed. Further, a mixed-integer solution to the nonconvex constrained quadratic thrust allocation problem is presented. Switching between fixed and rotating thrusters are presented to exemplify that switching can increase both the efficiency and accuracy in station keeping operations. Examples of thruster fault handling are presented in order to show how switching can be used to increase the operational safety. Experimental results on mixed-integer solution, switching between fixed and rotating thrusters, handling of thrust failures and handling of azimuth faults are presented.

6.1 Controller operating conditions

The operating condition of a controller is defined by all the properties affecting the choice of controller. The controller operating conditions are divided into four main categories according to cause, and how the conditions affect the controller. These are:

- **Objectives.** The objectives are what the controller should achieve. This can for instance be: power optimal control, maximum maneuverability, guarantee of solution or use of only the main propellers. Changes in the objectives are caused by the user or a supervisory controller.

- **Structure** changes require the need for either another controller or another set of parameters in the controller. The need for structural changes are caused by changes in the physical properties of the vessel. Changes in propeller efficiency, thrust direction of fixed thrusters, or deactivation of a thruster can cause the need for structural changes in the thrust allocator.
- **Disturbances** are caused by the environment. It is the task of the controller to somehow counteract these disturbances. Usually it is expected that moderate changes in the environment should not require changes in the controller. However, significant changes of the environment may induce the need for changes in the controller. Usually, it is not the task of the thrust allocation to counteract disturbances. However, in the case of anti-spin thrust allocation the thrust allocator is used to counteract the ventilation and in-and-out of water effects.
- **Faults** in actuators may affect the ability to generate forces. This might require significant changes in the control system. Typical faults in a thrust allocator will be loss of thrust or azimuth capability.

6.2 Supervisory control

In switched thrust allocation the task of the supervisory controller is to decide which of the different thrust allocators to use. Inputs to the supervisory controller can be measurements, operating condition and user inputs. The supervisory controller should, based on this information, determine which of the thrust allocators that are best suited for the task, and secondly determine if switching should take place. The first problem is solved by means of a performance measure, which differs from case to case. Theory on how to design supervisory controllers are found in Hespanha et al. (2003). The particular case of fault-tolerant control is treated in Blanke et al. (2003). The second problem usually requires both hysteresis switching and dwell time switching in order to avoid scattering, resulting in increased wear and tear. Hysteresis switching are treated in Hespanha et al. (2003), Middleton et al. (1988) and Morse et al. (1992). The idea is to require a certain minimum exceeding of the prescribed limit before switching is performed. Dwell time switching is considered in e.g. Morse (1996) and Morse (1997). In this method, fast chattering is avoided by requiring a certain minimum time between each switching incident.

Since the thrust allocation is a mapping from desired generalized forces to thruster forces, the stability of the switching can be ensured by the new allocator. The supervisory controller can choose to change the cost function, the constraints or the solution method.

The cost function is used to weight different variables against each other. In this thesis the power consumption of the different thrusters, and the error between the desired and commanded generalized force are weighted. The weights are used to command most thrust from the hydrodynamic most efficient thruster, and to prioritize the different generalized forces. Changes in the cost function

will typically be initiated by changes in the efficiency of the different thrusters, e.g. caused by ventilation and in-and-out of water effects, Coanda effect or thruster-thruster interaction. It can also be initiated by changes in the priority between the generalized forces.

The constraints are not allowed to be violated in the solver. Hence, the constraints have to be sufficiently loose to ensure that a solution exist. All thrusters have constraints on their maximum and minimum thrust and maximum rate of change in thrust. Azimuth thrusters also have constraints on azimuth rate, and in some cases azimuth angles. Loss of azimuthing capability can be implemented by treating the thruster as a fixed one. Loss of thrust producing capability can be incorporated by changing the maximum and minimum thrust. If all thrust producing capability is lost, the column in the \mathbf{B} matrix, corresponding to the lost thruster, should be set to zeros. This is done to avoid numerical problems due to the maximum and minimum constraints. A thruster can of course also be turned off e.g. in order to perform maintenance. In the implementations presented here, the new allocator is responsible for satisfying the constraints as fast as possible. This means that if the current solution is outside the constraint limits, due to a recent switching incident, the solution is forced as fast as allowed by the rate constraints to the legal region.

Most thrust allocators solve the instant thrust allocation problem. Changing to e.g. model predictive control will require changes in the size of the problem, although the same solver can be used. This is characterized as a change in the solution method.

6.3 Switching

In the industry switching using different ad-hoc methods for phasing in and out controllers have been used with success for many years. The implementations presented in this chapter are based on the principle that the new controller is responsible for "stability". This means that the switching is done abruptly, the new thrust allocator is initiated by the current physical values, and after that, the new allocator is handling the transition automatically. When changing the cost function, only the optimum will shift and no special precautions have to be taken. If the magnitude constraints are changed, it is still the task of the new thrust allocator to handle the transition. However, in this case more care has to be exercised. It is then important that the solver is capable of finding a new solution within its rate constraints. Otherwise the thrusters will fail to provide the desired forces. This means that the constraints sent to the solver are changed if the rate constraints have to be violated in order to reach the new magnitude constraints. In the allocator presented in Section 4.4 the thruster force and direction are set to approach the area within the magnitude constraints at c_1 of maximum speed. In (4.14) the maximum thrust at the current sample \mathbf{T}_+ is found. This is done by first finding the minimum of the maximum allowed thrust and the maximum allowed increase in thrust from the previous sample ($\min(\mathbf{T}_{\max}, \mathbf{T}_o + \dot{\mathbf{T}}_{\max}\Delta t)$). This is the upper limit for \mathbf{T}_+ .

Secondly, the max operation in (4.14) ensures that the thruster is capable of satisfying the rate constraints in the current time step. If $\mathbf{T}_{\max} \geq \mathbf{T}_o + c_1 \dot{\mathbf{T}}_{\min} \Delta t$, $\mathbf{T}_+ = \min(\mathbf{T}_{\max}, \mathbf{T}_o + \dot{\mathbf{T}}_{\max} \Delta t)$. However, if $\mathbf{T}_{\max} < \mathbf{T}_o + c_1 \dot{\mathbf{T}}_{\min} \Delta t$, that means the thruster is incapable of fulfilling \mathbf{T}_{\max} due to rate constraints, \mathbf{T}_+ is set to $\mathbf{T}_o + c_1 \dot{\mathbf{T}}_{\min} \Delta t$. This ensure that the rate constraints are satisfied, and the thruster approaches the magnitude constraints at minimum c_1 of maximum speed. Similar reasoning applies to (4.15)-(4.17).

When going from rotating to fixed thrusters, the method explained above handles the problem well. However, in the implementation, the thrusters are allowed to rotate with maximum speed to their fixed direction. When going from fixed to rotating thrusters additional precautions have to be included. This is because in this work, negative thrusts are allowed for the fixed thrusters, but not for the rotating ones. When going from fixed to rotating thrusters, the included logic sets the minimum thrust limit \mathbf{T}_{\min} close to zero ($-c_2(|T_{\max}| + |T_{\min}|)$) and forces the thruster to stay as a fixed thruster until $\mathbf{T}_0 > -c_2(|T_{\max}| + |T_{\min}|)$. When \mathbf{T}_0 exceeds the limit, the thruster is released as a rotating thruster. The delay in the switching is in the order of a few time steps by this approach.

6.4 Examples on switched thrust allocation

This section contains examples of switched thrust allocation systems. First a solution to nonconvex problems by use of switching is presented. Further on, an example with switching between fixed and rotating thrusters is presented. Switching is conducted in order to exploit the properties of fixed thrusters at small environmental disturbances, and the properties of rotating thrusters when a significant mean environmental force is present. Finally, how to do fault handling by use of switched thrust allocation is shown.

6.4.1 Nonconvex linearly constrained quadratic thrust allocation - Mixed integer solution

In practical cases the thrust allocation problem is rarely convex in nature. This is typically caused by e.g. sector constraints as illustrated in Figure 6.2. The forbidden sectors are in red, and are introduced to avoid the thrusters flushing on others. This means that e.g. thruster number 3 is not allowed to produce thrust between -110 and $-70[\text{deg}]$ in order to avoid flushing on thruster number 4. It is in this section proposed to overcome the nonconvex problem by dividing the nonconvex problem into convex subproblems, like in Johansen et al. (2003, 2007), and use a supervisory controller to switch among the solutions. For the given nonconvex problem illustrated in Figure 6.2 the convex subproblems are defined in Table 6.1, and the lay out of the switched system is shown in Figure 6.3. On thruster number 3 the sector from -70 to $159[\text{deg}]$ can not be covered by one subproblem, since the subproblem has to be convex, which imply that the sector in the subproblem should be less than $180[\text{deg}]$. Therefor the sector is split into two subproblems $[-70, 109]$ and $[-20, 159][\text{deg}]$. The overlap

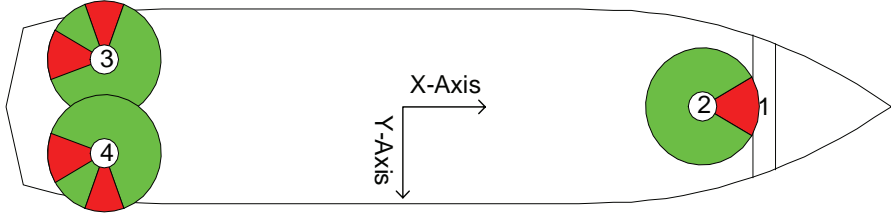


Figure 6.2: Illustration of sector constraints used on CyberShip III. Red means that thrust production in that direction is forbidden. The numbers given in Table 6.1 correspond to the green sectors.

from -20 to $109[\text{deg}]$ is introduced in order to avoid unnecessary switching. In total the allowed thrust directions on thruster number 2 are divided into two subproblems, the allowed thrust directions on thruster number 3 are divided into three subproblems and the allowed thrust directions on thruster number 4 are divided into three subproblems. This means that there is a total of 18 subproblems covering any combination of allowed sectors on thruster 2, 3 and 4. At every time step, the solutions for all the subproblems are found, with the previous solution in the particular subproblem as the initial condition. In case of switching, the current physical values are used as initial conditions in the next time step for the subproblem it is switched to. Simulations on a computer with a 2GHz processor and 1.5GB RAM show that there should be possible to solve at least some thousand subproblems simultaneously in real time ($1[\text{Hz}]$).

In the supervisory controller a combination of hysteresis switching (Middleton et al. 1988, Morse et al. 1992, Hespanha et al. 2003) and dwell time switching (Morse 1996, 1997) are used. The values of the cost functions (4.4) for the individual convex subproblems are used as switching parameters. For each sample time, the supervisory controller starts by checking if the time from the previous switching incident is large enough to allow for a new switching incident. This is called dwell time switching. Secondly, if the dwell time limit is exceeded, that means the dwell time limitation allow switching, it is checked if the reduction in cost is sufficient to favour switching. This is done to avoid chattering, where the supervisory controller continuously switches between two solutions, only limited by the dwell time. This is called hysteresis switching. It is desirable to only allow switching if it is a significant reduction in cost. This is because the switching may take the thrusters through forbidden zones, and that should only be done if the improvement in efficiency is higher than a certain value to be defined. By letting $J_j \in \mathbb{R}$ be the costs in the j 'th subproblem solutions, see (4.4), the supervisory controller can mathematically be expressed

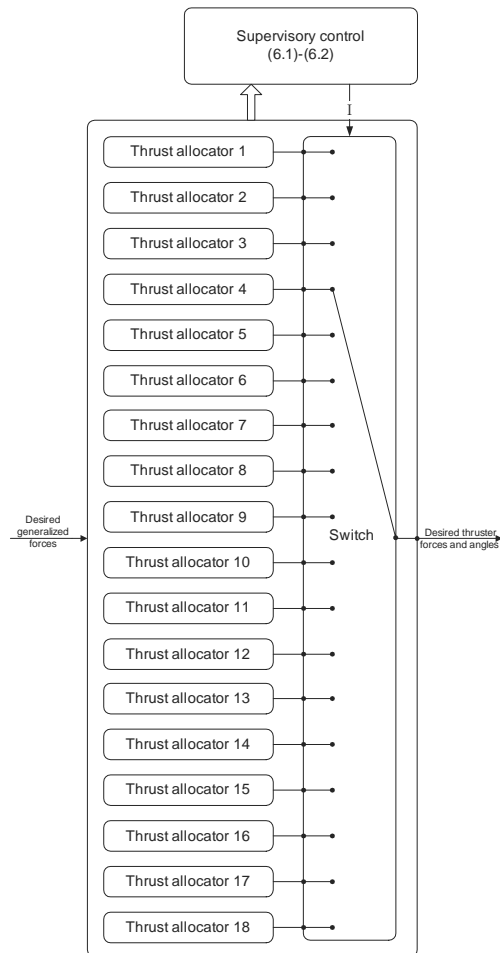


Figure 6.3: Switched thrust allocator applied to the mixed integer solution of the nonconvex problem.

Table 6.1: Constraints in convex subproblems. Corresponding to Figure 6.2.

Subproblem number	α_2 [deg]	α_3 [deg]	α_4 [deg]
1	[30, 209]	[-70, 109]	[-109, 70]
2	[30, 209]	[-70, 109]	[-159, 20]
3	[30, 209]	[-70, 109]	[110, 150]
4	[30, 209]	[-20, 159]	[-109, 70]
5	[30, 209]	[-20, 159]	[-159, 20]
6	[30, 209]	[-20, 159]	[110, 150]
7	[30, 209]	[-150, -110]	[-109, 70]
8	[30, 209]	[-150, -110]	[-159, 20]
9	[30, 209]	[-150, -110]	[110, 150]
10	[-209, -30]	[-70, 109]	[-109, 70]
11	[-209, -30]	[-70, 109]	[-159, 20]
12	[-209, -30]	[-70, 109]	[110, 150]
13	[-209, -30]	[-20, 159]	[-109, 70]
14	[-209, -30]	[-20, 159]	[-159, 20]
15	[-209, -30]	[-20, 159]	[110, 150]
16	[-209, -30]	[-150, -110]	[-109, 70]
17	[-209, -30]	[-150, -110]	[-159, 20]
18	[-209, -30]	[-150, -110]	[110, 150]

as:

$$I_{\min} = \arg \left(\min_j (\log_{10} (J_j)) \right), \quad (6.1)$$

$$I = \begin{cases} I_{\min}, & \text{if } t \geq t_{\lim} \wedge \log_{10} (J_{I_{\min}}) < \log_{10} (J_{I_0}) - J_{\lim}, \\ I_o, & \text{else,} \end{cases}, \quad (6.2)$$

where $I_{\min} \in \mathbb{N}$ is the index of the subproblem (see Table 6.1) with the lowest cost, $I \in \mathbb{N}$ is the preferred subproblem solution, $t \in \mathbb{R}$ is the time since the previous switching, $t_{\lim} \in \mathbb{R}$ is the dwell time limit, $I_0 \in \mathbb{N}$ is the preferred subproblem solution in the previous time step, and $J_{\lim} \in \mathbb{R}$ is the hysteresis limit. The \log_{10} function is applied to the costs in order to get smaller differences (in numerical value) between the costs in the different subproblems, and in order to be able to specify a percentile reduction of the cost as opposed to a fixed amount, e.g. $100[N^2]$. When going through a forbidden sector the thrusters are allowed to produce thrust, but they pass through the forbidden sector as fast as possible. Logics can be included to reduce the thrust magnitude in the forbidden sectors. This will reduce the available thrust when passing through forbidden sectors, but also reduce the magnitude of the losses caused by e.g. thruster-thruster interactions and thruster-hull interactions.

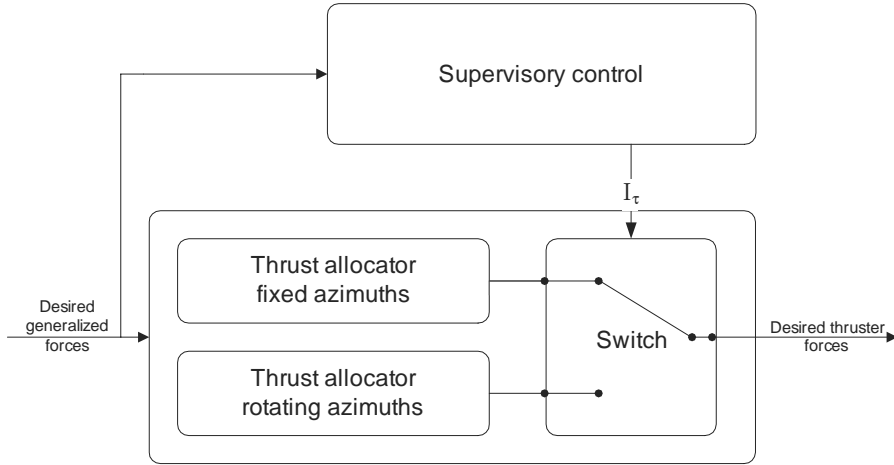


Figure 6.4: Switched thrust allocator when varying between fixed and rotating azimuths due to changes in the environmental disturbances.

6.4.2 Switching between fixed and rotating thrusters

For the thrust allocator presented in Chapter 4.4 fixed thrusters are preferred in case of small environmental disturbances, and rotating thrusters are preferred in case of large ones. This is because the fixed thrusters respond faster to changes in the desired generalized force direction than the rotating ones. At large environmental disturbances rotating thrusters are preferred since the power consumption may be significantly reduced by proper allocation, and since the maximum generalized force is significantly increased. An example of such a switched thrust allocation system is seen in Figure 6.4.

It is proposed to use a low pass filtered magnitude of the desired generalized force in the x-y plane as performance measure in the supervisory controller. The performance measure $\bar{\tau}_m$ is defined as:

$$\bar{\tau}_m = \frac{\omega}{s + \omega} \tau_m, \quad (6.3)$$

$$\tau_m = \left\| \begin{bmatrix} \tau_{d,1} \\ \tau_{d,2} \end{bmatrix} \right\|, \quad (6.4)$$

where s is the Laplace variable, ω is the filter frequency, τ_m is the desired generalized x-y force, and $\tau_{d,1}$ and $\tau_{d,2}$ are the desired generalized force in x and y direction, respectively.

Let I_τ be the switching flag. Then, the following switching rule is proposed:

$$I_\tau = \begin{cases} 1, & \text{if } t \geq t_{\lim} \wedge \bar{\tau}_m > \tau_{\lim} + \tau_{hyst}, \\ 0, & \text{if } t \geq t_{\lim} \wedge \bar{\tau}_m < \tau_{\lim} - \tau_{hyst}, \\ I_\tau(t - \Delta t), & \text{else,} \end{cases} \quad (6.5)$$

where t is the time since the previous switching, t_{lim} is the dwell time, τ_{lim} is the mean environmental force when switching should be done, τ_{hyst} is the hysteresis, and $I_\tau(t - \Delta t)$ is the previous value of the switching flag. This means that the thrusters are set to rotate if the low pass filtered generalized force exceeds the threshold τ_{lim} by a certain amount τ_{hyst} , fixed if the low pass filtered generalized force is lower than the threshold τ_{lim} by a certain amount τ_{hyst} , and else the current state (fixed or rotating) is kept.

6.4.3 Thruster failures

The thrust producing capability of a thruster might be reduced due to mechanical failures, e.g. gear failure or electrical failures, e.g. loss of fuse. If the thrust producing capability is reduced, the maximum T_{\max} and minimum T_{\min} thrust can be changed to new appropriate values. This is done in Strømquist (2007). He also performed a simplified failure modes and effect analysis (FMEA) for the thruster system on CyberShip III. If the thrust producing capability is completely lost, the column in the thruster configuration matrix corresponding to that particular thruster should be set to zero. This is a better solution than setting $T_{\max} = T_{\min} = 0$, since this problem is numerically difficult to solve without changing from inequality to equality constraints. This is similar to the approach of Garus (2004) which uses a readiness matrix.

If it is experienced difficulties with the azimuth capabilities of a thruster, the allowed azimuth rate can be reduced. If the azimuth capability is completely lost, the thruster should be considered a fixed thruster in order to avoid numerical difficulties in the solution of the thrust allocation problem.

6.5 Experimental results

Experiments were conducted with CyberShip III (CS3) in the MCLab. Supplementary figures for the presented runs are found in Appendix C. The sample time of the control system, including the thrust allocator was 0.20[s], corresponding to approximately 1[Hz] in full scale.

6.5.1 Run F: Maneuvering, nonconvex

In this case CS3 was maneuvered by changing the reference position. This was done in order to get switching between the different convex thrust allocators. The switched thrust allocator described in Section 6.4.1 was used. The parameters in the supervisory controller are given in Table 6.2. The dwell time was set to 3[s] such that the thrusters should have time to rotate to the new subsolution, before another switching was conducted. The hysteresis limit was set to 0.04[N²] as this corresponds to a 10% improvement of the cost function. The ship was operated in regular waves with 0.03[m] amplitude and a period of 0.8[s]. A DP system was used, and the yaw set point was varied in order to get changing thrust directions. The switching signal are shown together with the resulting thrust directions from the thrust allocator in Figure 6.5. In the upper plot, the

Table 6.2: Parameters in supervisory controller in the experiments with the nonconvex thrust allocator, Run F.

Parameter	Value	Unit
t_{\lim}	3	[s]
J_{\lim}	0.04	[N^2]

switching signal corresponding to the sectors in Table 6.1 is shown. This signal determines which of the individual subsolutions that is used. In the three lower plots, it is seen that the thrusters go through the forbidden zones as fast as possible and stay in the allowed region the rest of the time. Between 300[s] and 330[s] it is seen that the solution is jumping back and forth through the forbidden sector on thruster number three. This scattering could be reduced by increasing either the hysteresis or the dwell time. At approximately 364[s] in the figure, it is seen that it is switched between two subproblems without any forbidden zone in between. This causes the dwell time constraint to delay the switching back. This can be avoided if dwell time only has effect if one is about to switch through a forbidden zone. In Figure 6.6 it is seen that most switching incidents are hardly detectable on the commanded generalized force. On the other hand, the directional constraints make it difficult to command the desired generalized force. This is particularly seen in surge at 260[s] where the commanded surge force differs significantly from the desired one. The duration of the deviation is approximately 5[s]. Deviations of this duration should be expected due to the azimuth speed of the propellers which is 180[deg] in 3[s]. In a more refined DP system, there should be feedback from the thrust allocator telling the controller, particularly the integrator, that it is not capable of producing the desired force. It is worth noticing that the ship does not lose control during this incident.

6.5.2 Run G: Switching between fixed and rotating thrusters

In Run G CS3 was operated in station keeping by use of a DP system. Disturbances in terms of regular waves with amplitude 0.04[m] and period 0.8[s] were turned on and off to simulate changing environmental conditions. The ship was operated in head seas. The thrust allocator switched between fixed and rotating thrusters, according to the method in Section 6.4.2, depending on the low pass filtered generalized surge-sway force. The parameters in the supervisory controller are given in Table 6.3. The parameters were chosen to match the environment in the basin. In Figure 6.7 the desired and measured generalized forces are shown. It is seen that the thrust allocator was capable of providing the desired generalized forces during the switching incidents. In Figure 6.8 the performance measure $\bar{\tau}_m$ is shown together with the thrust directions. In the upper plot, the green area is the hysteresis area. The sudden changes in the performance measure are caused by the waves being turned on and off. The waves result in a mean drift force, which again gives a mean desired generalized force. The waves reach the ship at approximately 257[s] and 343[s], and leaves the ship at approximately 302[s] and 391[s]. Switching was conducted when the perfor-

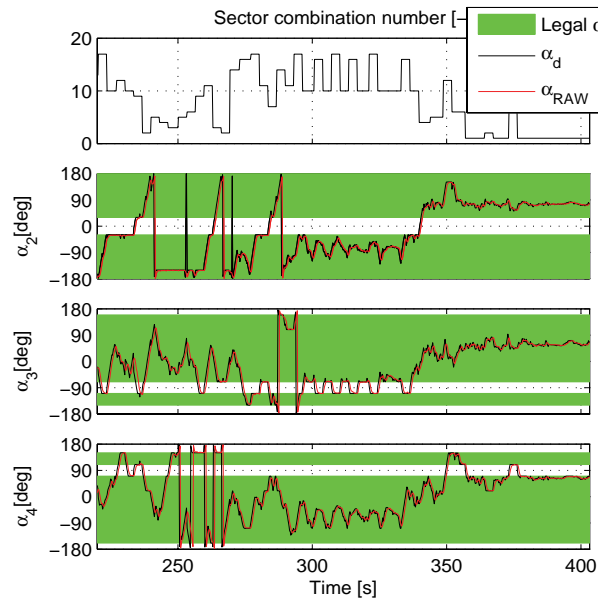


Figure 6.5: Plot of thrust directions during the experiments with nonconvex thrust allocator, Run F

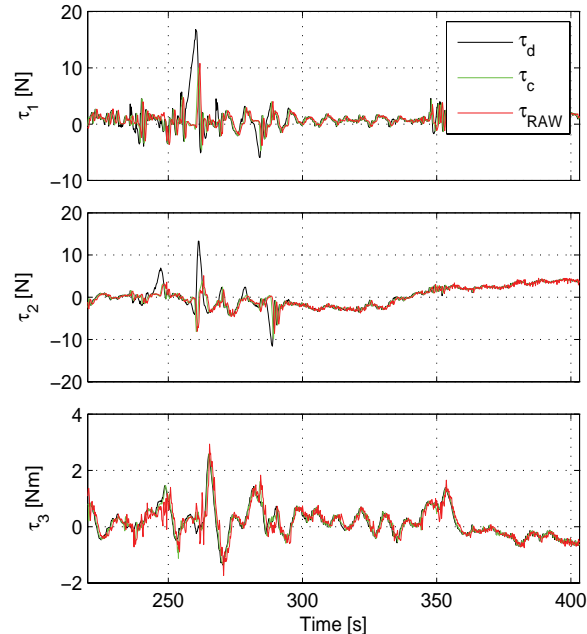


Figure 6.6: Plot of generalized forces during the experiments with nonconvex thrust allocator, Run F.

Table 6.3: Values of parameters in the supervisory controller when switching between fixed and rotating thrusters, Run G.

Parameter	Symbol	Value
Dwell time	t_{lim}	5[s]
Generalized force limit	τ_{lim}	1.5[N]
Hysteresis	τ_{hyst}	0.2[N]

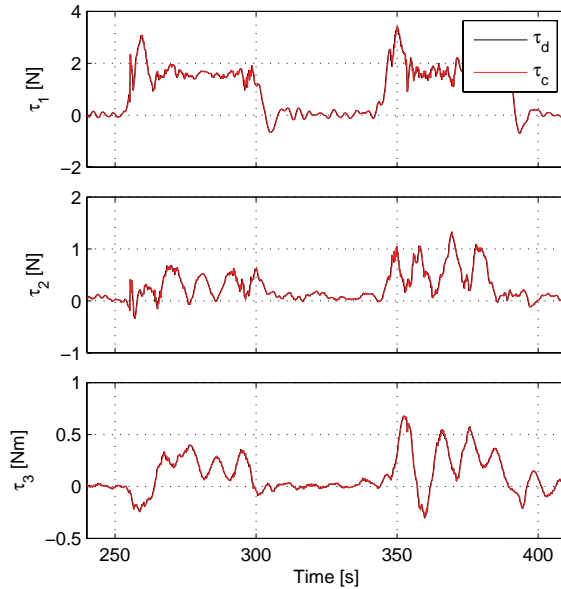


Figure 6.7: Plot of generalized forces when switching between fixed and rotating thrusters, Run G.

mance measure left the green area and the dwell time limit was exceeded. From the desired thrust directions it is easily seen when switching was conducted. In Figure 6.9 the thrust forces are shown to be smooth during the switching.

6.5.3 Run H: Thrust failures

In this experiment CS3 was operated in station keeping by use of a DP system. Disturbances in terms of regular waves with amplitude 0.03[m] and period 0.8[s] were applied. The ship was operated in head seas. Thruster failures with a 5 sample, 1.0[s] time detection time was introduced by the operator. By looking at Figure 6.10, 6.11 and 6.12 it is seen that the thrust allocator was capable of handling any single thruster failure without loss of position. The red areas in the second figure corresponds to when the thrusters were in faulty condition. The different fault scenarios are named by the numbers of the enabled thrusters.

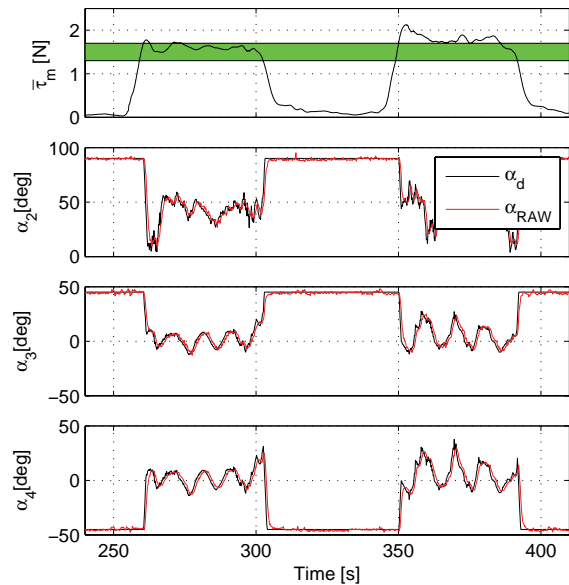


Figure 6.8: Plot of thrust directions when switching between fixed and rotating thrusters, Run G. The green area represent the hysteresis in the supervisory controller. Leaving the green area upwards means that rotating azimuths are enabled, and leaving the green area downwards means that fixed azimuths are enabled.

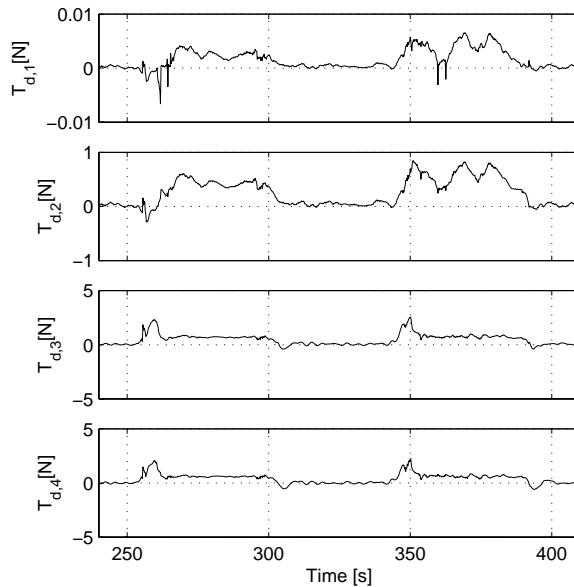


Figure 6.9: Plot of thrust forces when switching between fixed and rotating thrusters, Run G.

E.g. if thruster number 3 is faulty and thruster number 1, 2 and 4 are enabled, the configuration is named 124. By investigating the figures it is seen that for the 14 and 12 configuration, position was lost. Further, for the 34 configuration, performance was significantly reduced, however, without loss of position. In Figure 6.11 it is seen that the thrust allocator was capable of providing the necessary generalized forces during the switching incidents.

6.5.4 Run I: Azimuth failures

In this experiment CS3 was operated in station keeping by use of a DP system. Disturbances in terms of regular waves with amplitude 0.03[m] and period 0.8[s] were applied. The ship was operated in head seas. Azimuth failures with a 5 sample, 1.0[s] time detection time was introduced by the operator. In Figure 6.13, 6.14 and 6.15 it is seen that position was lost when both the aft thrusters fail. In the figures it is seen that the allocator was capable of handling the faults smoothly. The red areas in the second figure corresponds to when the thrusters were in faulty condition. Note that the results as regards positioning performance depend heavily on the directions in which the azimuths were fixed. However, the purpose of the experiment was to show that the thrust allocator was capable of providing the desired generalized force during the switching.

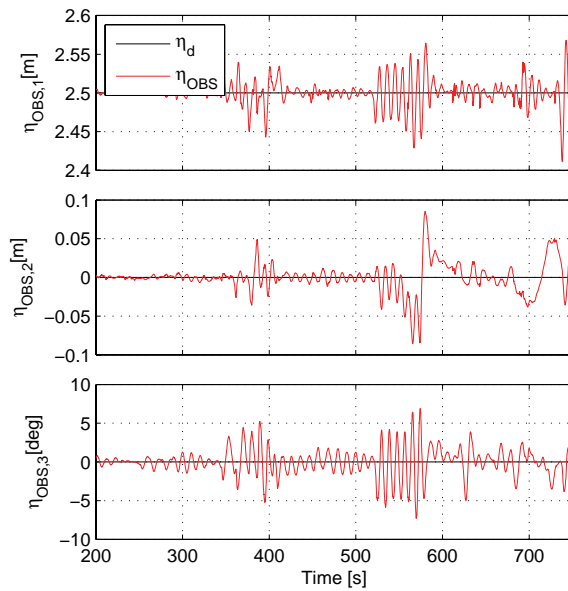


Figure 6.10: Plot of position and heading when subject to thrust failures, Run H.

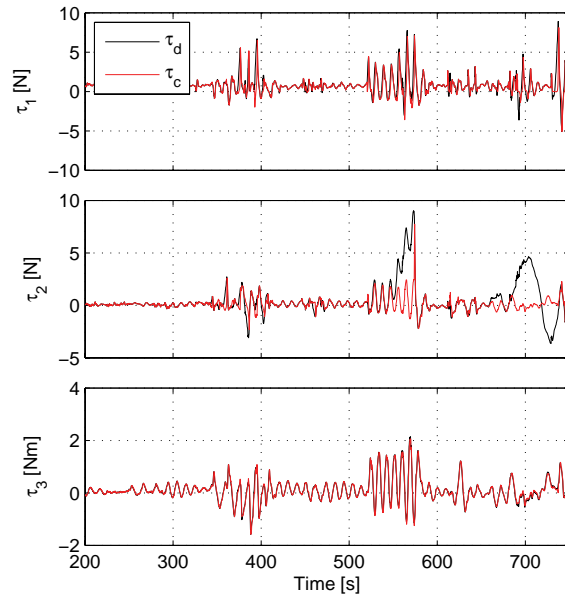


Figure 6.11: Plot of generalized forces when subject to thrust failures, Run H.

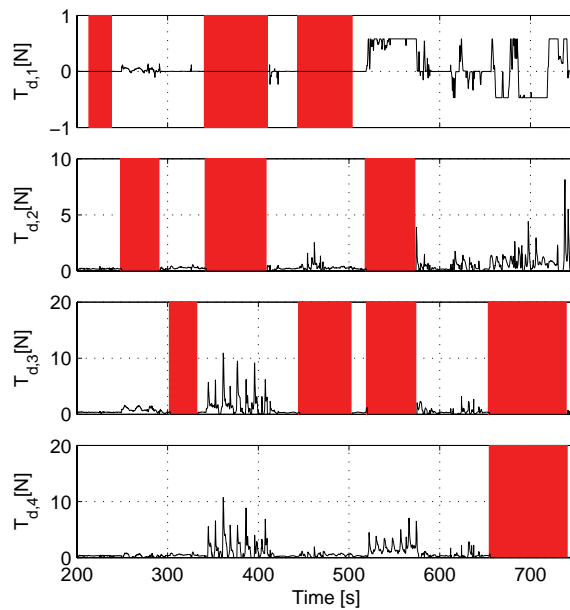


Figure 6.12: Plot of thrust forces when subject to thrust failures, Run H.

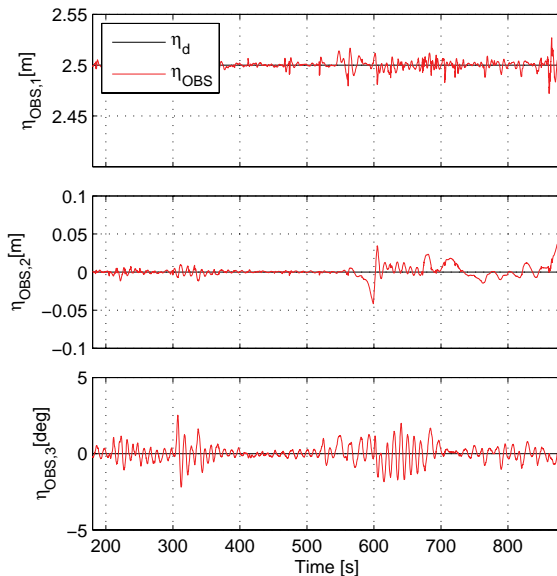


Figure 6.13: Plot of position and heading when subject to azimuth failures, Run I.

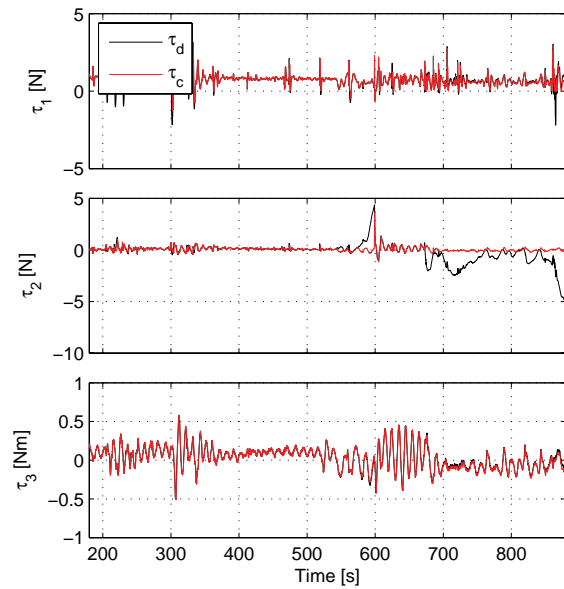


Figure 6.14: Plot of generalized forces when subject to azimuth failures, Run I.

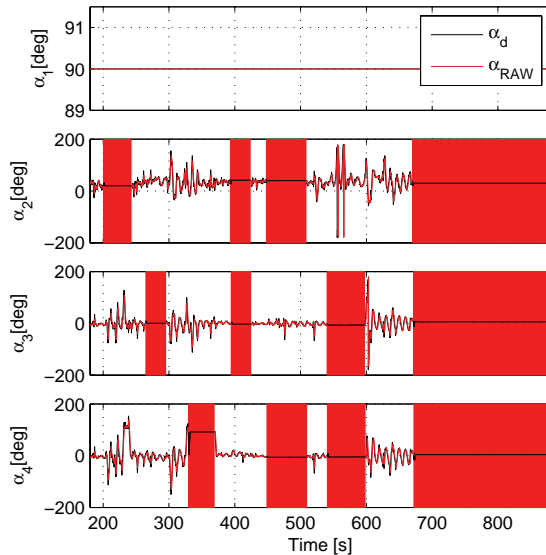


Figure 6.15: Plot of thrust directions when subject to azimuth failures, Run I.

6.5.5 Summary experiments

The nonconvex linearly constrained quadratic thrust allocator was demonstrated by experiments. Switching between fixed and rotating azimuths, depending on the mean environmental force, was shown to give stable positioning performance. The consequences of different thrust and azimuth failures were demonstrated. The model ship was capable of handling any single thruster failure without loss of position.

Chapter 7

Singularity avoidance

In thrust allocation, a singular configuration is when the orientation of the thrusters makes it impossible to produce generalized forces in all directions. Mathematically the thrust allocation problem is said to be singular if:

$$\forall (\boldsymbol{\tau} \in \mathbb{R}^m \wedge \|\boldsymbol{\tau}\| \leq \varepsilon) \nexists (\mathbf{T} \in \mathcal{S}_T | \mathbf{B}(\boldsymbol{\alpha})\mathbf{T} = \boldsymbol{\tau}), \quad (7.1)$$

where ε is a positive constant. Singularity is particularly a problem for vessels with rotating thrusters that change direction slowly. This is because the response time of the thrusters to changes in the desired generalized force may be too slow. If all the thrusters are fixed, singularity avoidance is equally important, but the problem is solved once and for all during the vessel design, since none of the thrusters are allowed to rotate. For thrusters with rapid directional changes, singularity avoidance may not be a problem, since the thrusters can quickly move out of a singular configuration. Solutions to power optimal thrust allocation problems tends to singular configurations, since these often appear to be the energy optimal solutions where e.g. all thrusters points in the same direction against the dominating environmental loads. Hence, under certain operational conditions with rapidly changing environmental disturbances singular or near singular configurations may cause large power demands and even loss of position. Therefore singularity avoidance is important in order to maintain an acceptable efficiency, positioning performance and level of safety.

In the first section of this chapter, suggestions on how the thruster configuration matrix can be scaled in order to be able to compare forces, moments and different thrusters are presented. Further, the terms local and global singularity are defined. Then, it is shown how the singular value decomposition can be used to say something about the minimum gain from thruster forces to generalized forces for the special case with only fixed thrusters, all capable of producing both positive and negative thrust. Further, a solution to the problem with only fixed thrusters, and one or more thrusters only capable of producing positive thruster force is proposed. In the next section design considerations on thruster configurations by use of minimum gain from thruster forces to generalized forces are presented. This includes generalization of the theory for fixed thrusters to

problems with convex directional constraints. A design loop for evaluation of the thruster configuration is presented. This is followed by an extensive example with application of the presented theory to CyberShip III. The next section then presents a way of how the minimum gain direction can be found and how the minimum gain and minimum gain direction can be monitored. Then a method for singularity avoidance in real time is proposed. Finally, experimental results verifying theory and the real time singularity avoidance method are shown. This chapter is to a large extent based on (Ruth and Sørensen Submitted-b).

7.1 Scaling the thruster configuration matrix

One way of investigating the singularity of a thruster configuration is by looking at the thruster configuration matrix (Sørdalen 1996). The elements giving moments (yaw) may be one or two orders of magnitude larger than the force elements (surge, sway), due to the torque arm. It is therefore necessary to scale the moments such that they are comparable in size with the other elements of the thruster configuration matrix. In this thesis the average torque arm $L_{typ} \in \mathbb{R}$ is used:

$$L_{typ} = \frac{1}{n} \sum_{j=1}^n \sqrt{\mathbf{L}_{x,j}^2 + \mathbf{L}_{y,j}^2}. \quad (7.2)$$

The standard thruster configuration matrix does not reflect the thrusters ability to produce thrust. In order to take the maximum thrusts into consideration, the thruster configuration matrix is scaled by the maximum thrusts. This is done by multiplying each column of the thruster configuration matrix with its corresponding maximum thrust, and dividing all elements in the matrix by the average maximum thrust. The average maximum thrust $\bar{T}_{max} \in \mathbb{R}$ is defined as:

$$\begin{aligned} \bar{T}_{max} &= \frac{1}{n} \sum_{j=1}^n |\mathbf{T}_{max,j}|, \\ &= \frac{1}{n} \|\mathbf{T}_{max}\|_1. \end{aligned} \quad (7.3)$$

When comparing different thruster configurations on the same vessel, it is important that the same values of the average torque arm and the average maximum thrust are used. The resulting scaled thruster configuration matrix $\mathbf{B}_S \in \mathbb{R}^{m \times n}$ is defined as:

$$\mathbf{B}_S(\alpha) = \frac{1}{\bar{T}_{max}} \mathbf{S} \mathbf{B}(\alpha) \text{diag}(\mathbf{T}_{max}), \quad (7.4)$$

where $\mathbf{S} \in \mathbb{R}^{m \times m}$ is the torque scaling matrix, which is diagonal with 1's for forces, and $\frac{1}{L_{typ}}$'s for moments. For the surge, sway and yaw case where $m = 3$:

$$\mathbf{S} = \begin{bmatrix} 1 & 0 & 0 \\ 0 & 1 & 0 \\ 0 & 0 & \frac{1}{L_{typ}} \end{bmatrix}.$$

This results in the following relationship between the scaled thrust and generalized force vectors:

$$\bar{\tau} = \mathbf{B}_S \bar{\mathbf{T}}, \quad (7.5)$$

$$\bar{\tau} = \frac{1}{T_{\max}} \mathbf{S} \tau, \quad (7.6)$$

$$\bar{\mathbf{T}} = \text{diag}(\mathbf{T}_{\max})^{-1} \mathbf{T}, \quad (7.7)$$

where $\bar{\tau} \in \mathbb{R}^m$ is the nondimensional generalized force, and $\bar{\mathbf{T}} \in \mathbb{R}^n$ is the nondimensional thrust.

7.2 Local and global singularity

From an operational point of view it is interesting to look at both local and global singularity. In order to explain the difference, the terms bi- and unidirectional thrusters have to be defined. Bidirectional thrusters are thrusters capable of producing both positive and negative thrust. Unidirectional thrusters (Swanson 1982) are thrusters only capable of producing positive thrust. This is illustrated in Figure 7.1 where the allowed thrust region of the bi- and unidirectional thrusters are shown. In order to investigate the behavior of the thrusters about the current thrust value the terms locally bi- and unidirectional thrusters are defined. A thruster is locally bidirectional if it can change thruster force in both positive and negative direction:

$$\mathbf{T}_{\min,j} - \delta \mathbf{T}_{-,j} \leq \mathbf{T}_j \leq \mathbf{T}_{\max,j} - \delta \mathbf{T}_{+,j}, \quad (7.8)$$

where $\delta \mathbf{T}_- \in \mathbb{R}^n \leq 0$ and $\delta \mathbf{T}_+ \in \mathbb{R}^n \geq 0$ are the necessary available negative and positive, respectively, change in thrust for thruster number j . The thruster is said to be positively locally unidirectional if:

$$\mathbf{T}_{\min,j} - \delta \mathbf{T}_{-,j} \not\leq \mathbf{T}_j \leq \mathbf{T}_{\max,j} - \delta \mathbf{T}_{+,j}. \quad (7.9)$$

This will typically be thrusters operated close to zero thrust, only capable of producing positive thrust. If a thruster is close to saturation, that is close to its maximum thrust, it is only capable of changing thrust in negative direction. This is an example of a negatively unidirectional thruster. Mathematically, a thruster is said to be negatively unidirectional if:

$$\mathbf{T}_{\min,j} - \delta \mathbf{T}_{-,j} \leq \mathbf{T}_j \not\leq \mathbf{T}_{\max,j} - \delta \mathbf{T}_{+,j}. \quad (7.10)$$

The necessary available change in thrust vector is a parameter that can be set by the user, computed by some kind of statistics, determined by the current mode of operation, or computed based on expected generalized force perturbations.

Global singularity is defined as in (7.1). It indicates something about the capability of the vessel to produce generalized forces in any direction. However, it is also important to investigate the thruster configuration's capability to produce small perturbations in generalized force in any direction about the current

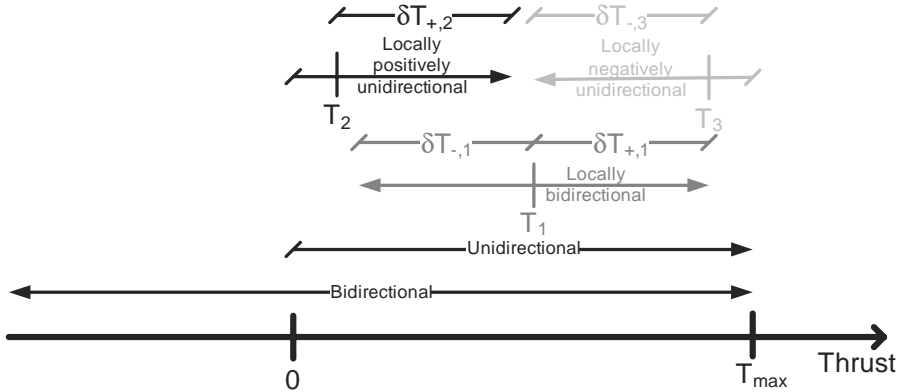


Figure 7.1: Thrust range for bidirectional, unidirectional, locally bidirectional, locally positively unidirectional, and locally negatively unidirectional thrusters. \mathbf{T}_j is the current thrust on thruster number j , and $\delta\mathbf{T}_j$ is the necessary available change in thrust on thruster number j .

operating point. Mathematically a thruster configuration is locally singular if:

$$\forall (\Delta\boldsymbol{\tau} \in \mathbb{R}^m \wedge \|\Delta\boldsymbol{\tau}\| \leq \varepsilon) \nexists \left((\mathbf{T} + \Delta\mathbf{T}) \in \mathcal{S}_T \mid \frac{\mathbf{B}(\boldsymbol{\alpha})(\mathbf{T} + \Delta\mathbf{T})}{(\boldsymbol{\tau} + \Delta\boldsymbol{\tau})} \right), \quad (7.11)$$

where $\Delta\boldsymbol{\tau} \in \mathbb{R}^m$ and $\Delta\mathbf{T} \in \mathbb{R}^n$ are perturbations in generalized force vector and thruster force vector, respectively. It is worth noting that for bidirectional thrusters operated away from their limits, there are no difference between global and local singularity. However, a unidirectional thruster satisfying (7.8) is considered to be locally bidirectional. Hence, it can change its thrust locally in both positive and negative direction. This is illustrated in Figure 7.1. A locally bidirectional thruster is considered to be bidirectional when evaluating local singularity. In the following bi- and unidirectional thrusters gives global singularity results, while locally bi- and unidirectional thrusters gives local singularity results.

As regards global singularity, only perturbations not causing the thrusters to saturate are included. In the case of saturating thrusters, the local singularity approach will be more appropriate. However, this is an extreme situation. If a thruster is saturated, or close to being saturated (at its maximum limit), it is to be considered to be a negatively unidirectional thruster. Hence, saturation can be accounted for by considering the saturating thruster as a negatively unidirectional thruster. In order to ease the presentation in this chapter, it is chosen to constrain unidirectional thrusters to positive values only. However, negatively unidirectional thrusters can then be incorporated by flipping the sign

in the corresponding column in the thruster configuration matrix:

$$\begin{aligned}\boldsymbol{\tau}_j &= \mathbf{B}_j \mathbf{T}_j^-, \quad \mathbf{T}_j^- \leq 0, \\ &= \mathbf{B}_j (-\mathbf{T}_j^+), \quad \mathbf{T}_j^+ = -\mathbf{T}_j^-, \\ &= (-\mathbf{B}_j) \mathbf{T}_j^+, \quad \mathbf{T}_j^+ \geq 0,\end{aligned}\tag{7.12}$$

where $\boldsymbol{\tau}_j \in \mathbb{R}^m$ is the contribution from thruster number j to the generalized force vector.

One way of computing the necessary available change in thrust for a given combination of bi and unidirectional thrusters is by requiring a necessary available change in generalized forces. Assume the minimum gain from thrusts to generalized forces σ_{\min} is known (how to obtain this gain will be shown later). Then the following equations hold:

$$\frac{\|\Delta\bar{\boldsymbol{\tau}}\|_2}{\|\Delta\bar{\mathbf{T}}\|_2} \geq \sigma_{\min} \Rightarrow \tag{7.13}$$

$$\|\Delta\bar{\mathbf{T}}\|_\infty \leq \|\Delta\bar{\mathbf{T}}\|_2 \leq \frac{\|\Delta\bar{\boldsymbol{\tau}}\|_2}{\sigma_{\min}} \Rightarrow \tag{7.14}$$

$$|\Delta\mathbf{T}_j| \leq \frac{\|\Delta\bar{\boldsymbol{\tau}}\|_2}{\sigma_{\min}} \mathbf{T}_{\max,j}, \tag{7.15}$$

$$\leq \mathbf{T}_{\max,j} \frac{\min(1, L_{typ})}{\sigma_{\min} \bar{T}_{\max}} \|\Delta\boldsymbol{\tau}\|_2, \tag{7.16}$$

where j indexes the different thrusters. This means that the system can handle any perturbation $\|\Delta\boldsymbol{\tau}\|_2$ if $|\delta\mathbf{T}_{-,j}| \geq |\Delta\mathbf{T}_j| \leq \delta\mathbf{T}_{+,j}$ for bidirectional thrusters, $|\Delta\mathbf{T}_j| \leq |\delta\mathbf{T}_{+,j}|$ for positively unidirectional thrusters, and $|\delta\mathbf{T}_{-,j}| \geq |\Delta\mathbf{T}_j|$ for negatively unidirectional thrusters.

7.3 Fixed bidirectional thrusters

For fixed bidirectional thrusters, the singularity of the thruster configuration can be investigated by looking at the singular values of the thruster configuration matrix as in Sørdsalen (1996, 1997a, b). He uses a thruster configuration matrix normalized with respect to the desired generalized force. The details of how the normalization is done is not presented. However, it is stated that the singular values can be viewed as gain from thrust to generalized force. This correlates well with Skogestad and Postlethwaite (2007) which use singular value decomposition to evaluate similar properties of multivariable control systems.

By investigating the rank of \mathbf{B}_S the controllability of the configuration can be investigated. The minimum requirement for controllability is to have $\text{rank}(\mathbf{B}_S) = m$. By taking the singular value decomposition of the \mathbf{B}_S matrix, the order of magnitude of the gains in the different directions can be found (Sørdsalen 1996, 1997a, b, Skogestad and Postlethwaite 2007). According to Skogestad and Postlethwaite (2007) the following applies for the singular values

of a matrix:

$$\sigma_{\min, \mathbf{B}_S} \leq \frac{\|\mathbf{B}_S \mathbf{T}\|_2}{\|\mathbf{T}\|_2} \leq \sigma_{\max, \mathbf{B}_S}, \quad (7.17)$$

where $\sigma_{\min, \mathbf{B}_S} \in \mathbb{R}$ and $\sigma_{\max, \mathbf{B}_S} \in \mathbb{R}$ are the minimum and maximum singular values of \mathbf{B}_S . In order to show that the singular values actually represent gains from thrust to generalized force (7.17) can be rewritten as:

$$\sigma_{\min, \mathbf{B}_S} \|\mathbf{T}\|_2 \leq \|\boldsymbol{\tau}\|_2 \leq \sigma_{\max, \mathbf{B}_S} \|\mathbf{T}\|_2. \quad (7.18)$$

For comparison of different thruster configurations it is advised to look at the minimum singular value. This is because this can be seen as a minimum gain from thruster force to any generalized force in the system.

7.4 Fixed unidirectional thrusters

The approach in the previous section by use of singular value decomposition assumes that the thrusters are bidirectional. This is reasonable when the thrusters are operated far away from their constraints. However, in the cases where the thrusters are operated close to their constraints, they are considered to be unidirectional, and therefore another approach is required. In this thesis a new method for calculating a minimum gain from thruster forces to generalized forces, taking the unidirectional constraints on \mathbf{T} into account, is proposed.

The idea of the proposed method is to find $\bar{\mathbf{T}}_i$ vectors (i indexing different vectors), satisfying the unidirectional constraints, such that any generalized force $\bar{\boldsymbol{\tau}}$ can be found as the sum $\sum_{i=1}^{2m} \mathbf{B}_S \mathbf{a}_i \bar{\mathbf{T}}_i$ where the weights $\mathbf{a}_i \geq 0$ is the elements of $\mathbf{a} \in \mathbb{R}^{2m}$. The minimum of:

$$\frac{\left\| \sum_{i=1}^{2m} \mathbf{B}_S \mathbf{a}_i \bar{\mathbf{T}}_i \right\|_2}{\left\| \sum_{i=1}^{2m} \mathbf{a}_i \bar{\mathbf{T}}_i \right\|_2} \forall \mathbf{a}_i, \quad (7.19)$$

is then found, representing the minimum gain from thruster forces to generalized forces. The following problem is formulated to find the appropriate $\bar{\mathbf{T}}_i$'s:

$$\min \|\bar{\mathbf{T}}_i\|_2, \quad (7.20)$$

$$\boldsymbol{\Gamma}_i = \mathbf{B}_S \bar{\mathbf{T}}_i, \quad (7.21)$$

$$\mathbf{B}_S = [\mathbf{B}_p \mathbf{B}_{pn}], \quad (7.22)$$

$$\bar{\mathbf{T}}_{i,j} \geq 0 \forall j = 1 \dots n_p, \quad (7.23)$$

where $\boldsymbol{\Gamma}_i \in \mathbb{R}^m$ is a generalized force vector (input to the problem), $\mathbf{B}_p \in \mathbb{R}^{m \times n_p}$ and $\mathbf{B}_{pn} \in \mathbb{R}^{m \times (n-n_p)}$ are the scaled thruster configuration matrices for the unidirectional thruster and bidirectional thrusters (inputs to the problem), respectively, and n_p is the number of unidirectional thrusters. The matrix \mathbf{B}_S

is then ordered such that the unidirectional thrusters are in the first columns. The solutions are indexed by i and the different thrusters by j .

In order to find $\bar{\mathbf{T}}_i$ vectors such that any vector $\bar{\boldsymbol{\tau}}$ is \mathbb{R}^m can be written as $\sum_{i=1}^{2m} \mathbf{B}_S \mathbf{a}_i \bar{\mathbf{T}}_i$, the chosen Γ_i 's at least have to span \mathbb{R}^m . One such basis is the orthogonal basis $\mathbf{I}_{m \times m}$. During later deviations, it will be evident that using $\mathbf{I}_{m \times m}$ as basis simplifies the mathematics. Since some of the thrusters are restricted to positive values (equivalent with $\bar{\mathbf{T}}_{i,j} \geq 0, \mathbf{a}_i \geq 0$), one can not simply take $-\bar{\mathbf{T}}_i$ to get the negative Γ_i 's. Therefore, it is necessary also to solve for $-\mathbf{I}_{m \times m}$. We therefore propose to define the m by $2m$ matrix $\Gamma \in \mathbb{R}^{m \times 2m}$:

$$\Gamma = [\Gamma_1 \dots \Gamma_{2m}] = [\mathbf{I}_{m \times m} \ -\mathbf{I}_{m \times m}]. \quad (7.24)$$

Then, if there exist solutions to (7.20)-(7.23) for all $\Gamma_i, i = 1..2m$ given in (7.24), any vector $\bar{\boldsymbol{\tau}}$ can be written as:

$$\begin{aligned} \bar{\boldsymbol{\tau}} &= \sum_{i=1}^{2m} \mathbf{a}_i \Gamma_i, \\ &= \sum_{i=1}^{2m} \mathbf{B}_S \mathbf{a}_i \bar{\mathbf{T}}_i, \end{aligned} \quad (7.25)$$

where $\bar{\mathbf{T}}_i$ are the solutions to (7.20)-(7.23), and \mathbf{a}_i is the weight of the different generalized force solutions.

Example 7.1 In order to have a simple example, a traveling crane as shown in Figure 7.2 is considered. Assume the hoist has a bidirectional actuator in y direction producing one unit force per input, an unidirectional actuator in positive x direction producing one unit force per input, and an unidirectional actuator in negative x direction producing 0.5 unit force per input. This means that there are two controlled degrees of freedom $m = 2$, three actuators $n = 3$, and two actuators that are positive only $n_p = 2$. The first column in the \mathbf{B}_S matrix represents the unidirectional actuator in positive x direction. The second column is the unidirectional actuator in negative x direction. The third column is the bidirectional actuator in y direction. The result is:

$$\mathbf{B}_S = \begin{bmatrix} 1 & -0.5 & 0 \\ 0 & 0 & 1 \end{bmatrix}. \quad (7.26)$$

Using (7.24) and $m = 2$ gives:

$$\Gamma = \begin{bmatrix} 1 & 0 & -1 & 0 \\ 0 & 1 & 0 & -1 \end{bmatrix}. \quad (7.27)$$

The solutions to (7.20)-(7.23) with (7.26) and (7.27) as inputs are found by quadratic programming:

$$[\mathbf{T}_1 \ \mathbf{T}_2 \ \mathbf{T}_3 \ \mathbf{T}_4] = \begin{bmatrix} 1 & 0 & 0 & 0 \\ 0 & 0 & 2 & 0 \\ 0 & 1 & 0 & -1 \end{bmatrix}. \quad (7.28)$$

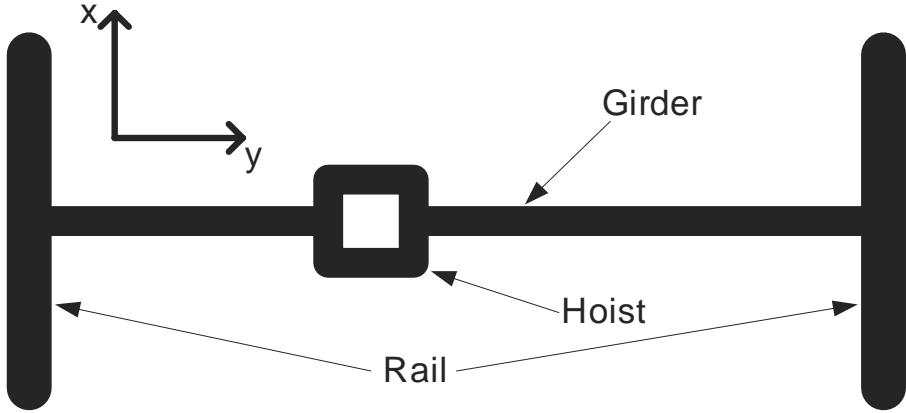


Figure 7.2: Traveling crane seen from above.

Theorem 7.1 If there exist solutions to (7.20)-(7.23) for all Γ_i , $i = 1..2m$ in (7.24), a lower bound on the minimum gain from thruster forces to generalized forces is:

$$\frac{\|\bar{\tau}\|_2}{\|\bar{T}\|_2} \geq \frac{1}{\sqrt{m} \|\mathbf{T}_f\|_2} = \sigma_{\min}, \quad (7.29)$$

where $\mathbf{T}_{f,j} = \max_i(|\bar{\mathbf{T}}_{i,j}|)$, $i = 1..2m$.

Proof. Without loss of generality it is required that:

$$\sum_{i=1}^{2m} (\mathbf{a}_i^2) = 1, \quad (7.30)$$

$$\mathbf{a}_i \geq 0, \quad (7.31)$$

$$\mathbf{a}_i \vee \mathbf{a}_{i+m} = 0 \quad \forall i \in 1..m. \quad (7.32)$$

The last requirement does not affect the solution since it is meaningless to apply both positive and negative force in the same direction. The requirement in (7.30) is equivalent to requiring that:

$$\begin{aligned} \|\bar{\tau}\|_2 &= \left\| \sum_{i=1}^{2m} \mathbf{a}_i \Gamma_i \right\|_2, \\ &= 1, \end{aligned} \quad (7.33)$$

since the Γ_i vectors with $\mathbf{a}_i \neq 0$ are orthonormal. The thrust vector becomes:

$$\bar{\mathbf{T}} = \sum_{i=1}^{2m} \mathbf{a}_i \bar{\mathbf{T}}_i. \quad (7.34)$$

The norm of the thrust vector is:

$$\begin{aligned}\|\bar{\mathbf{T}}\| &= \left\| \sum_{i=1}^{2m} \mathbf{a}_i \bar{\mathbf{T}}_i \right\|, \\ &\leq \left\| \left(\sum_{i=1}^{2m} \mathbf{a}_i \right) \mathbf{T}_f \right\|, \\ &\leq \left\| \sum_{i=1}^{2m} \mathbf{a}_i \right\| \|\mathbf{T}_f\|. \end{aligned} \quad (7.35)$$

The value of $\|\mathbf{T}_f\|$ is known from the solutions of (7.20)-(7.23). Hence, by finding an upper limit on $\left\| \sum_{i=1}^{2m} \mathbf{a}_i \right\|$ an upper limit on $\|\bar{\mathbf{T}}\|$ is found.

Let:

$$\mathbf{b}_i = \mathbf{a}_i + \mathbf{a}_{i+m}, \quad (7.36)$$

where \mathbf{b}_i are the elements of $\mathbf{b} \in \mathbb{R}^m$. This way \mathbf{b}_i is the weight in the i 'th direction, either in positive or negative direction. Due to (7.32):

$$\begin{aligned}\sum_{i=1}^{2m} \mathbf{a}_i &= \sum_{i=1}^m (\mathbf{a}_i + \mathbf{a}_{i+m}), \\ &= \sum_{i=1}^m \mathbf{b}_i. \end{aligned} \quad (7.37)$$

Hence, maximizing $\left\| \sum_{i=1}^{2m} \mathbf{a}_i \right\|$ subject to (7.30)-(7.32) is equivalent with maximizing:

$$\max \left(\sum_{i=1}^m \mathbf{b}_i \right) = \max (\|\mathbf{b}\|_1), \quad (7.38)$$

subject to:

$$\sum_{i=1}^m (\mathbf{b}_i)^2 = 1 \Rightarrow \|\mathbf{b}\|_2 = 1, \quad (7.39)$$

$$\mathbf{b}_i \geq 0. \quad (7.40)$$

According to Khalil (2000) the following relationship exist between the 1- and 2-norm:

$$\|\mathbf{b}\|_1 \leq \sqrt{m} \|\mathbf{b}\|_2. \quad (7.41)$$

Hence, it is concluded that:

$$\|\mathbf{b}\|_1 \leq \sqrt{m}, \quad (7.42)$$

since $\|\mathbf{b}\|_2 = 1$. By taking the particular choice $\mathbf{b}_i = \frac{1}{\sqrt{m}}, i = 1..m$ the 1-norm of \mathbf{b} becomes:

$$\begin{aligned}\|\mathbf{b}\|_1 &= \sum_{i=1}^m |\mathbf{b}_i|, \\ &= \sum_{i=1}^m \frac{1}{\sqrt{m}}, \\ &= m \frac{1}{\sqrt{m}}, \\ &= \sqrt{m}.\end{aligned}\tag{7.43}$$

By (7.37), (7.42) and (7.43) it is therefore concluded that:

$$\begin{aligned}\max \left(\sum_{i=1}^{2m} \mathbf{a}_i \right) &= \max \left(\sum_{i=1}^m \mathbf{b}_i \right), \\ &= \sqrt{m}.\end{aligned}\tag{7.44}$$

Inserting (7.44) into (7.35) gives:

$$\|\bar{\mathbf{T}}\| \leq \sqrt{m} \|\mathbf{T}_f\|. \tag{7.45}$$

Dividing (7.33) by (7.45) gives:

$$\frac{\|\bar{\boldsymbol{\tau}}\|_2}{\|\bar{\mathbf{T}}\|_2} \geq \frac{1}{\sqrt{m} \|\mathbf{T}_f\|_2} = \sigma_{\min}. \tag{7.46}$$

If (7.20)-(7.23) do not have solutions for all $\mathbf{T}_i, i = 1..2m$, the system is not controllable. In that case $\sigma_{\min} = 0$.

The minimum bound on the gain from thrust to generalized force is very conservative for highly controllable systems. However, for systems with low gains, the bound gives a better estimate (in absolute value). It is also a general property of the norms that the less thrusters and the less freedoms to control, the better the lower bound will be. However, for the cases in this thesis with $m = 2$ and 3 the minimum bound catches the main behavior of the gain from $\bar{\mathbf{T}}$ to $\bar{\boldsymbol{\tau}}$.

Example 7.2 \mathbf{T}_f is found by taking the absolute value of all the elements in (7.28) and finding the largest element in each row. In our example \mathbf{T}_f becomes:

$$\mathbf{T}_f = \begin{bmatrix} 1 \\ 2 \\ 1 \end{bmatrix}. \tag{7.47}$$

By applying Theorem 7.1, σ_{\min} becomes:

$$\begin{aligned}\sigma_{\min} &= \frac{1}{\sqrt{m} \|\mathbf{T}_f\|_2}, \\ &= \frac{1}{\sqrt{2}\sqrt{6}}, \\ &\approx 0.29.\end{aligned}\tag{7.48}$$

This means that one unit input can produce at least 0.29 unit force in any direction, $0.29 \|\bar{\mathbf{T}}\|_2 \leq \|\bar{\tau}\|_2$.

Using Theorem 7.1 requires a small amount of computations. However, the result is often very conservative. In order to improve the accuracy of the minimum gain from thruster forces to generalized forces, a more computational demanding approach is proposed:

Theorem 7.2 *If there exist solutions to (7.20)-(7.23) for all Γ_i , $i = 1..2m$ in (7.24), a lower bound on the minimum gain from thruster forces to generalized forces is:*

$$\frac{\|\bar{\tau}\|_2}{\|\bar{\mathbf{T}}\|_2} \geq \min_k \left(\frac{1}{\sigma_{\max, \Psi_k}} \right) = \sigma_{\min},\tag{7.49}$$

where $\Psi_k \in \mathbb{R}^{n \times m}$ is a matrix who's column number i is either $\bar{\mathbf{T}}_i$ or $\bar{\mathbf{T}}_{i+m}$, and k indexes all the different combinations.

Proof. Let \mathbf{b} vector be the weight of the different solutions like in (7.36). Then, since the Γ_i 's are orthonormal vectors, $\|\bar{\tau}\|_2 = 1$ if $\|\mathbf{b}\|_2 = 1$. Let Ω_k be the matrix corresponding to Ψ_k , containing Γ_i 's. Then:

$$\|\bar{\tau}_k\|_2 = \|\Omega_k \mathbf{b}\|_2.\tag{7.50}$$

According to Strang (1988):

$$\|\Omega_k \mathbf{b}\|_2 = \|\mathbf{b}\|_2,\tag{7.51}$$

since Ω_k is orthogonal. Then:

$$\|\bar{\tau}_k\|_2 = \|\mathbf{b}\|_2 = 1.\tag{7.52}$$

The vector $\bar{\mathbf{T}}$ can be written as:

$$\bar{\mathbf{T}}_k = \Psi_k \mathbf{b}.\tag{7.53}$$

Then:

$$\begin{aligned}\|\bar{\mathbf{T}}_k\|_2 &= \|\Psi_k \mathbf{b}\|_2, \\ &\leq \|\Psi_k\|_2 \|\mathbf{b}\|_2, \\ &\leq \sigma_{\max, \Psi_k} \|\mathbf{b}\|_2, \\ &\leq \sigma_{\max, \Psi_k}.\end{aligned}\tag{7.54}$$

Further:

$$\frac{\|\bar{\tau}_k\|_2}{\|\bar{\mathbf{T}}_k\|_2} \geq \frac{1}{\sigma_{\max, \Psi_k}} = \sigma_{\min, k}. \quad (7.55)$$

By computing $\sigma_{\min, k}$ for all k , the minimum gain in all directions has been found, and hence the global minimum is the smallest of the $\sigma_{\min, k}$'s:

$$\begin{aligned} \frac{\|\bar{\tau}\|_2}{\|\bar{\mathbf{T}}\|_2} &\geq \min_k \left(\frac{\|\bar{\tau}_k\|_2}{\|\bar{\mathbf{T}}_k\|_2} \right), \\ &\geq \min_k \left(\frac{1}{\sigma_{\max, \Psi_k}} \right) = \sigma_{\min}. \end{aligned} \quad (7.56)$$

■

Remark 7.1 Pay attention to the fact that Theorem 7.2 does not require $\mathbf{b}_i \geq 0$. It is true for any $\mathbf{b}_i \in \mathbb{R}$. The computational burden of this approach is small. It is required to solve the quadratic programming problem (7.20)-(7.23) $2m$ times, and to compute the singular values for 2^m different Ψ_k 's. For $m = 6$, which is the maximum in motion control, the QP problem has to be solved $2 \cdot 6 = 12$ times, and the singular values have to be found for $2^6 = 64$ different matrices.

Example 7.3 We continue on our example. The following Ψ_k 's are then found:

$$\Psi_1 = [\bar{\mathbf{T}}_1 \quad \bar{\mathbf{T}}_2] = \begin{bmatrix} 1 & 0 \\ 0 & 0 \\ 0 & 1 \end{bmatrix}, \quad (7.57)$$

$$\Psi_2 = [\bar{\mathbf{T}}_1 \quad \bar{\mathbf{T}}_4] = \begin{bmatrix} 1 & 0 \\ 0 & 0 \\ 0 & -1 \end{bmatrix}, \quad (7.58)$$

$$\Psi_3 = [\bar{\mathbf{T}}_3 \quad \bar{\mathbf{T}}_2] = \begin{bmatrix} 0 & 0 \\ 2 & 0 \\ 0 & 1 \end{bmatrix}, \quad (7.59)$$

$$\Psi_4 = [\bar{\mathbf{T}}_3 \quad \bar{\mathbf{T}}_4] = \begin{bmatrix} 0 & 0 \\ 2 & 0 \\ 0 & -1 \end{bmatrix}, \quad (7.60)$$

this gives the following σ_{\max, Ψ_k} 's:

$$\sigma_{\max, \Psi_k} = \begin{cases} 1, & \text{if } k = 1, 2, \\ 2, & \text{if } k = 3, 4, \end{cases} \quad (7.61)$$

By applying Theorem 7.2, we get $\sigma_{\min} = 0.5$. This means that one unit input can produce at least 0.5 unit force in any direction, $0.5 \|\bar{\mathbf{T}}\|_2 \leq \|\bar{\tau}\|_2$. Comparing with the result in Example 7.2 it is seen that Theorem 7.2 gives a 72% increase in the minimum gain.

Substituting all bidirectional thrusters with two unidirectional ones, Theorem 7.2 is not changed at all. However, it is guaranteed that there are no negative elements in Ψ_k . This implies that σ_{\min} actually is σ_{\inf} , the greatest lower bound on σ_{\min} . The following lemma then applies:

Lemma 7.1 *If $\bar{\mathbf{T}}_{i,j} \geq 0 \forall i, j$, the solution in Theorem 7.2 is the greatest lower bound on the gain from thrust to generalized forces.*

Proof. By the properties of the norms:

$$\begin{aligned}\|\Psi_k\|_2 &= \max_{\|\mathbf{b}\|_2=1} \|\Psi_k \mathbf{b}\|_2, \\ &= \sigma_{\max, \Psi_k}.\end{aligned}\quad (7.62)$$

Hence, there exist a \mathbf{b} , with $\|\mathbf{b}\|_2 = 1$ such that $\|\Psi_k \mathbf{b}\|_2 = \sigma_{\max, \Psi_k}$. It is then necessary to proof that this \mathbf{b} has all elements $b_i \geq 0$ such that the lower bound applies to the case with only positive thrusts. Let:

$$\mathbf{A} = [\mathbf{A}_1 \quad \mathbf{A}_2], \quad (7.63)$$

$$\mathbf{x}_+ = [\mathbf{x}_1^T \quad \mathbf{x}_2^T]^T, \quad (7.64)$$

$$\mathbf{x}_- = [\mathbf{x}_1^T \quad -\mathbf{x}_2^T]^T, \quad (7.65)$$

and assume all the elements of \mathbf{A}_1 , \mathbf{A}_2 , \mathbf{x}_1 and \mathbf{x}_2 are non negative. Then:

$$\begin{aligned}\mathbf{x}_+^T \mathbf{A}^T \mathbf{A} \mathbf{x}_+ &= [\mathbf{x}_1^T \quad \mathbf{x}_2^T] \begin{bmatrix} \mathbf{A}_1^T \\ \mathbf{A}_2^T \end{bmatrix} [\mathbf{A}_1 \quad \mathbf{A}_2] \begin{bmatrix} \mathbf{x}_1 \\ \mathbf{x}_2 \end{bmatrix}, \\ &= \mathbf{x}_1^T \mathbf{A}_1^T \mathbf{A}_1 \mathbf{x}_1 + 2\mathbf{x}_1^T \mathbf{A}_1^T \mathbf{A}_2 \mathbf{x}_2 + \mathbf{x}_2^T \mathbf{A}_2^T \mathbf{A}_2 \mathbf{x}_2,\end{aligned}\quad (7.66)$$

and:

$$\begin{aligned}\mathbf{x}_-^T \mathbf{A}^T \mathbf{A} \mathbf{x}_- &= [\mathbf{x}_1^T \quad -\mathbf{x}_2^T] \begin{bmatrix} \mathbf{A}_1^T \\ \mathbf{A}_2^T \end{bmatrix} [\mathbf{A}_1 \quad \mathbf{A}_2] \begin{bmatrix} \mathbf{x}_1 \\ -\mathbf{x}_2 \end{bmatrix}, \\ &= \mathbf{x}_1^T \mathbf{A}_1^T \mathbf{A}_1 \mathbf{x}_1 - 2\mathbf{x}_1^T \mathbf{A}_1^T \mathbf{A}_2 \mathbf{x}_2 + \mathbf{x}_2^T \mathbf{A}_2^T \mathbf{A}_2 \mathbf{x}_2.\end{aligned}\quad (7.67)$$

This leads to:

$$\mathbf{x}_+^T \mathbf{A}^T \mathbf{A} \mathbf{x}_+ - \mathbf{x}_-^T \mathbf{A}^T \mathbf{A} \mathbf{x}_- = 4\mathbf{x}_1^T \mathbf{A}_1^T \mathbf{A}_2 \mathbf{x}_2 \Rightarrow \quad (7.68)$$

$$\mathbf{x}_+^T \mathbf{A}^T \mathbf{A} \mathbf{x}_+ \geq \mathbf{x}_-^T \mathbf{A}^T \mathbf{A} \mathbf{x}_-. \quad (7.69)$$

Hence by dividing \mathbf{b} into positive and negative elements like in (7.65), it can be shown that the norm where the negative elements has changed sign is greater or equal to the norm with the negative elements. Hence, it is concluded that $\max_{\|\mathbf{b}\|_2=1} \|\Psi_k \mathbf{b}\|_2$ is found with equal sign on all the elements of \mathbf{b} if all elements of $\Psi_k \geq 0$. All elements of $\Psi_k \geq 0$, since $\bar{\mathbf{T}}_{i,j} \geq 0 \forall i, j$. ■

Example 7.4 *By substituting the bidirectional actuator in y direction with two unidirectional ones, Lemma 7.1 can be applied. We then have:*

$$\mathbf{B}_S = \begin{bmatrix} 1 & -0.5 & 0 & 0 \\ 0 & 0 & 1 & -1 \end{bmatrix}. \quad (7.70)$$

Γ remains unchanged and the \mathbf{T}_i 's becomes:

$$[\mathbf{T}_1 \quad \mathbf{T}_2 \quad \mathbf{T}_3 \quad \mathbf{T}_4] = \begin{bmatrix} 1 & 0 & 0 & 0 \\ 0 & 0 & 2 & 0 \\ 0 & 1 & 0 & 0 \\ 0 & 0 & 0 & 1 \end{bmatrix}.$$

The following Ψ_k 's are then found:

$$\Psi_1 = [\bar{\mathbf{T}}_1 \quad \bar{\mathbf{T}}_2] = \begin{bmatrix} 1 & 0 \\ 0 & 0 \\ 0 & 1 \\ 0 & 0 \end{bmatrix}, \quad (7.71)$$

$$\Psi_2 = [\bar{\mathbf{T}}_1 \quad \bar{\mathbf{T}}_4] = \begin{bmatrix} 1 & 0 \\ 0 & 0 \\ 0 & 0 \\ 0 & 1 \end{bmatrix}, \quad (7.72)$$

$$\Psi_3 = [\bar{\mathbf{T}}_3 \quad \bar{\mathbf{T}}_2] = \begin{bmatrix} 0 & 0 \\ 2 & 0 \\ 0 & 1 \\ 0 & 0 \end{bmatrix}, \quad (7.73)$$

$$\Psi_4 = [\bar{\mathbf{T}}_3 \quad \bar{\mathbf{T}}_4] = \begin{bmatrix} 0 & 0 \\ 2 & 0 \\ 0 & 0 \\ 0 & 1 \end{bmatrix}, \quad (7.74)$$

this gives the following σ_{\max, Ψ_k} 's:

$$\sigma_{\max, \Psi_k} = \begin{cases} 1, & \text{if } k = 1, 2, \\ 2, & \text{if } k = 3, 4, \end{cases} \quad (7.75)$$

By applying Theorem 7.2, we get $\sigma_{\min} = 0.5$. Since all actuators are unidirectional, Lemma 7.1 gives $\sigma_{\inf} = 0.5$. This means that one unit input can produce at least 0.5 unit force in any direction, $0.5 \|\bar{\mathbf{T}}\|_2 \leq \|\bar{\tau}\|_2$, and that it actually exist at least one generalized force where $0.5 \|\bar{\mathbf{T}}\|_2 = \|\bar{\tau}\|_2$. Compared with Theorem 7.1 and 7.2, Lemma 7.1 guarantees that the largest minimum gain is found.

Theorem 7.3 A minimum bound on the attainable set is given by either one of:

$$\|\bar{\tau}\|_2 \geq \sigma_{\min}, \quad (7.76)$$

$$\|\mathbf{S}\tau\|_2 \geq \sigma_{\min} \bar{T}_{\max}, \quad (7.77)$$

$$\|\tau\|_2 \geq \min(1, L_{typ}) \sigma_{\min} \bar{T}_{\max}. \quad (7.78)$$

Proof. Theorem 7.2 gives:

$$\frac{\|\bar{\tau}\|_2}{\|\bar{\mathbf{T}}\|_2} \geq \sigma_{\min} \Rightarrow \quad (7.79)$$

$$\|\bar{\tau}\|_2 \geq \sigma_{\min} \|\bar{\mathbf{T}}\|_2. \quad (7.80)$$

From Khalil (2000):

$$\|\bar{\mathbf{T}}\|_2 \geq \|\bar{\mathbf{T}}\|_\infty. \quad (7.81)$$

If one thruster operates at maximum thrust, $|\bar{\mathbf{T}}_j| = 1$, and hence $\|\bar{\mathbf{T}}\|_\infty = 1$. Using (7.80) and (7.81) then gives:

$$\begin{aligned} \|\bar{\tau}\|_2 &\geq \sigma_{\min} \|\bar{\mathbf{T}}\|_\infty, \\ &\geq \sigma_{\min}, \end{aligned} \quad (7.82)$$

which proofs (7.76).

Using the fact that:

$$\|\bar{T}_{\max} \bar{\tau}\| = |\bar{T}_{\max}| \|\bar{\tau}\|, \quad (7.83)$$

since $\bar{T}_{\max} \in \mathbb{R}$, and multiplying both sides of (7.82) with \bar{T}_{\max} gives:

$$\bar{T}_{\max} \|\bar{\tau}\|_2 \geq \sigma_{\min} \bar{T}_{\max} \Rightarrow \quad (7.84)$$

$$\|\bar{T}_{\max} \bar{\tau}\|_2 \geq \sigma_{\min} \bar{T}_{\max}. \quad (7.85)$$

Inserting (7.6) into (7.85) gives:

$$\|\mathbf{S}\tau\|_2 \geq \sigma_{\min} \bar{T}_{\max}, \quad (7.86)$$

which proofs (7.77).

By use of (7.17) the following result is obtained:

$$\begin{aligned} \|\mathbf{S}\tau\|_2 &\leq \sigma_{\max, \mathbf{S}} \|\tau\|_2, \\ \frac{1}{\sigma_{\max, \mathbf{S}}} \|\mathbf{S}\tau\|_2 &\leq \|\tau\|_2. \end{aligned} \quad (7.87)$$

Since \mathbf{S} is diagonal with 1's and $\frac{1}{L_{typ}}$'s on its diagonal, $\sigma_{\max, \mathbf{S}} = \max \left(1, \frac{1}{L_{typ}} \right)$. Hence:

$$\min \left(1, L_{typ} \right) \|\mathbf{S}\tau\|_2 \leq \|\tau\|_2. \quad (7.88)$$

By use of (7.77) and (7.88) the result is:

$$\begin{aligned} \|\tau\|_2 &\geq \min \left(1, L_{typ} \right) \|\mathbf{S}\tau\|_2, \\ &\geq \min \left(1, L_{typ} \right) \sigma_{\min} \bar{T}_{\max}. \end{aligned} \quad (7.89)$$

which proofs (7.78). ■

Example 7.5 Using Theorem 7.3 on our example gives the minimum attainable set: $\|\bar{\tau}\|_2 \geq 0.5$.

7.5 Avoiding singularites during design

When designing a DP vessel the vessel configuration in terms of placement of thrusters and division into power busses are important issues in order to maximize the operability and maneuverability of the vessel. Vessels with fixed, rotating, bi- and unidirectional thrusters are considered. One way of evaluating the

configuration is by finding the minimum gain from thruster forces to generalized forces. In the general case this can be found by solving the problem numerically for a set of generalized forces with length one. The numerical solution solves the problem for a set of generalized forces, since the number of generalized forces is infinite. The set should cover the entire region of generalized forces with reasonable accuracy. Comparing configurations with and without unidirectional thrusters, the unidirectional method should be used also for the cases with only bidirectional thrusters. By requiring that the thrust allocation problem is convex, analytical results can be obtained. This is presented in the following. If problems are discovered, the operability and maneuverability can be increased by better choice of thruster positions, e.g. move the tunnel thruster forward in order to increase the yaw moment from the thruster, installing larger thrusters, replacing fixed thrusters with azimuthing ones, increase the number of thrusters, and proper distribution of the thrusters among the power busses. In most designs the most cost-effective solution will be chosen, taking rules, investment, current costs, down time and operability into account.

7.5.1 Bidirectional thrusters

Both fixed and freely rotating thrusters are considered. Freely rotating thrusters are modeled as two orthogonal fixed bidirectional thrusters in the same location. In order to investigate the controllability of a vessel, the thruster configuration matrix $\mathbf{B}_A \in \mathbb{R}^{m \times n_f + 2n_r}$ is defined, where $n_f \in \mathbb{N}$ is the number of fixed thruster, and $n_r \in \mathbb{N}$ is the number of rotating azimuth thrusters. The relationship between thruster forces and generalized forces is:

$$\boldsymbol{\tau} = \mathbf{B}_A \mathbf{T}_G, \quad (7.90)$$

$$\mathbf{T}_{G,i} = \mathbf{T}_i \quad \forall i \in [1, n_f], \quad (7.91)$$

$$\mathbf{T}_{G,n_f+2i-1} = \mathbf{T}_{x,i} \quad \forall i \in [1, n_r], \quad (7.92)$$

$$\mathbf{T}_{G,n_f+2i} = \mathbf{T}_{y,i} \quad \forall i \in [1, n_r], \quad (7.93)$$

where $\mathbf{T}_G \in \mathbb{R}^{n_f + 2n_r}$ is a modified extended thrust vector, and the j 'th column of \mathbf{B}_A in the surge, sway and yaw case is defined as:

$$\mathbf{B}_{A,j} = \begin{cases} \begin{bmatrix} \cos \alpha_j \\ \sin \alpha_j \\ \mathbf{L}_{x,j} \sin \alpha_j - \mathbf{L}_{y,j} \cos \alpha_j \\ 1 \\ 0 \\ -\mathbf{L}_{y,j} \\ 0 \\ 1 \\ \mathbf{L}_{x,j} \end{bmatrix}, & \text{if } j \leq n_f, \\ \begin{bmatrix} 1 \\ 0 \\ -\mathbf{L}_{y,j} \\ 0 \\ 1 \\ \mathbf{L}_{x,j} \end{bmatrix}, & \text{if } j = n_f + 2i - 1, i < n_r, \\ \text{else .} & \end{cases} \quad (7.94)$$

Before the singular values are computed, the thruster configuration matrix is scaled according to:

$$\begin{aligned}\bar{\tau} &= \frac{1}{\bar{T}_{\max}} \mathbf{S} \mathbf{B}_A \text{diag}(\mathbf{T}_{G \max}) \text{diag}(\mathbf{T}_{G \max})^{-1} \mathbf{T}_G, \\ &= \mathbf{B}_G \bar{\mathbf{T}}_G,\end{aligned}\quad (7.95)$$

$$\mathbf{B}_G = \frac{1}{\bar{T}_{\max}} \mathbf{S} \mathbf{B}_A \text{diag}(\mathbf{T}_{G \max}), \quad (7.96)$$

$$\bar{\mathbf{T}}_G = \text{diag}(\mathbf{T}_{G \max})^{-1} \mathbf{T}_G, \quad (7.97)$$

where $\mathbf{B}_G \in \mathbb{R}^{m \times (n_f + 2n_r)}$ is the nondimensional thruster configuration matrix, and $\bar{\mathbf{T}}_G \in \mathbb{R}^{n_f + 2n_r}$ is the nondimensional thrust vector.

Since all the thrusters are bidirectional and either fixed or freely rotating, the rank of \mathbf{B}_G determines the controllability of the vessel. The minimum requirement for controllability is to have $\text{rank}(\mathbf{B}_G) = m$. Since all thrusters are bidirectional, the singular value decomposition method in Section 7.3 can be used to determine the minimum gain from thruster forces to generalized forces.

7.5.2 Unidirectional thrusters

It will in this section be shown how the results in Section 7.4 can be extended for use with any convex thruster configuration. The problem formulated in (7.20)-(7.23) is then substituted by a convex constrained thrust allocation problem like the one in Section 4.4. The formulation in cylindrical coordinates is used for the fixed thrusters, and the extended thrust formulation in Cartesian coordinates is used for the rotating thrusters. This way rotating thrusters are modeled by \mathbf{T}_x and \mathbf{T}_y subject to constraints. Since the vessel capability is considered, the response time of the thrusters interpreted as rate constraints are excluded. Only one magnitude constraint on each thruster is included, either by requiring that the thrust should be positive or negative. It is shown how the results on minimum gain from thruster forces to generalized forces and the estimate in Theorem 7.3 on the minimum attainable set can be extended to take convex limitations on thrust directions into account.

The directional constraints are modeled as:

$$-\sin(\alpha_{\min,j}) T_{xd,j} + \cos(\alpha_{\min,j}) T_{yd,j} \geq 0, \quad (7.98)$$

$$\sin(\alpha_{\max,j}) T_{xd} - \cos(\alpha_{\max,j}) T_{yd,j} \geq 0. \quad (7.99)$$

The directional constraints can be collected in a matrix $\mathbf{A} \in \mathbb{R}^{n_c \times n_f + 2n_r}$, where $n_c \in \mathbb{N}$ is the total number of constraints, together with the unidirectional constraints, and expressed as:

$$\mathbf{A} \bar{\mathbf{T}}_G \leq \mathbf{0}_{n_c \times 1}. \quad (7.100)$$

The problem to be solved is then:

$$\min \|\bar{\mathbf{T}}_{Gi}\|_2, \quad (7.101)$$

$$\Gamma_i = \mathbf{B}_G \bar{\mathbf{T}}_{Gi}, \quad (7.102)$$

$$\mathbf{A} \bar{\mathbf{T}}_{Gi} \leq \mathbf{0}_{n_c \times 1}, \quad (7.103)$$

where \mathbf{T} is given in (7.24). The following proposition is then proposed:

Proposition 7.1 Any $\bar{\mathbf{T}}_G = \Psi_k \mathbf{b}$ with $\mathbf{b}_i \geq 0$ will satisfy the inequality constraints (7.103), where Ψ_k is a $n \times m$ matrix whose column number i is either $\bar{\mathbf{T}}_{Gi}$ or $\bar{\mathbf{T}}_{Gi+m}$, and k indexes all the different combinations.

Proof. We start with:

$$\begin{aligned} \mathbf{A}\bar{\mathbf{T}}_G &= \mathbf{A}\Psi_k \mathbf{b}, \\ &= \mathbf{A} \sum_{i=1}^{2m} \mathbf{a}_i \bar{\mathbf{T}}_{Gi}, \\ &= \sum_{i=1}^{2m} \mathbf{a}_i \mathbf{A} \bar{\mathbf{T}}_{Gi}. \end{aligned} \quad (7.104)$$

Inserting (7.103) into (7.104) gives:

$$\begin{aligned} \mathbf{A}\bar{\mathbf{T}}_G &\leq \sum_{i=1}^{2m} \mathbf{a}_i \mathbf{0}_{n_c \times 1}, \\ &\leq \mathbf{0}_{n_c \times 1}. \end{aligned} \quad (7.105)$$

Hence, the inequality constrain is satisfied. ■

Theorem 7.4 Since Proposition 7.1 does not impose any extra constraint on Theorem 7.1 and 7.2, and Lemma 7.1, they are hence proofed valid for any convex thruster configuration.

When introducing the extended thrust formulation, Theorem 7.3 is changed to the following:

Lemma 7.2 A minimum bound on the attainable set is given by either one of:

$$\|\bar{\boldsymbol{\tau}}\|_2 \geq \frac{1}{\sqrt{2}} \sigma_{\min}, \quad (7.106)$$

$$\|\mathbf{S}\boldsymbol{\tau}\|_2 \geq \frac{1}{\sqrt{2}} \sigma_{\min} \bar{T}_{\max}, \quad (7.107)$$

$$\|\boldsymbol{\tau}\|_2 \geq \frac{1}{\sqrt{2}} \min(1, L_{typ}) \sigma_{\min} \bar{T}_{\max}. \quad (7.108)$$

Proof. The proof follows the proof of Theorem 7.3 with the exception that the maximum thrust limit is given by:

$$|\mathbf{T}_{G,i}| \leq 1 \quad \forall i = 1..n_f, \quad (7.109)$$

$$\mathbf{T}_{G,n_f+2i-1}^2 + \mathbf{T}_{G,n_f+2i}^2 \leq 1 \quad \forall i = 1..n_r. \quad (7.110)$$

Introducing the infinity norm inequality (7.109) can be substituted by:

$$\|\bar{\mathbf{T}}_G\|_\infty \leq 1, \quad (7.111)$$

and inequality (7.110) by:

$$\begin{aligned}\|\bar{\mathbf{T}}_G\|_\infty^2 + \|\bar{\mathbf{T}}_G\|_\infty^2 &\leq 1, \\ \|\bar{\mathbf{T}}_G\|_\infty &\leq \frac{1}{\sqrt{2}}.\end{aligned}\quad (7.112)$$

■

7.5.3 During faults

The effect of faults can be investigated by calculating the minimum gain from thruster forces to generalized forces without faults and with different faults. This way it is easily seen how a fault will affect the thrust producing capability. The method can also be used in the case of multiple thruster failures, caused by e.g. loss of a power bus. By calculating the minimum gain from thruster forces to generalized forces for all possible combinations of thrusters, the best way of splitting the system into power busses can easily be determined. Remember to use the same \bar{T}_{\max} , L_{typ} and computation method.

7.5.4 Design loop

In the following a suggestion for a design loop for determination of the thruster configuration is presented. The steps in the design loop are shown in Figure 7.3.

Step 1: Propose a thruster configuration

The first step is to propose a thruster configuration. The placement and capability of the different thrusters should be stated.

Step 2: Calculate minimum gain from thruster forces to generalized forces

In this step, the maneuverability of the proposed configuration with all thrusters working is investigated. This means that first, the average torque arm and the average maximum thrust have to be determined from (7.2) and (7.3), respectively. Then singular value decomposition, or Theorem 7.2 and 7.4 can be used to determine the minimum gain from thruster forces to generalized forces, and Theorem 7.3 or Lemma 7.2 can be used to determine a minimum attainable set.

Step 3: Calculate minimum gain for any single thruster failure

The capability of the thruster configuration is now further challenged in order to evaluate the performance under any single thruster failure. In order to calculate the minimum gain from thruster forces to generalized forces when subject to single thruster failure, the failing thruster is simply removed from the \mathbf{B}_G matrix and the minimum gain from thruster forces to generalized forces is computed.

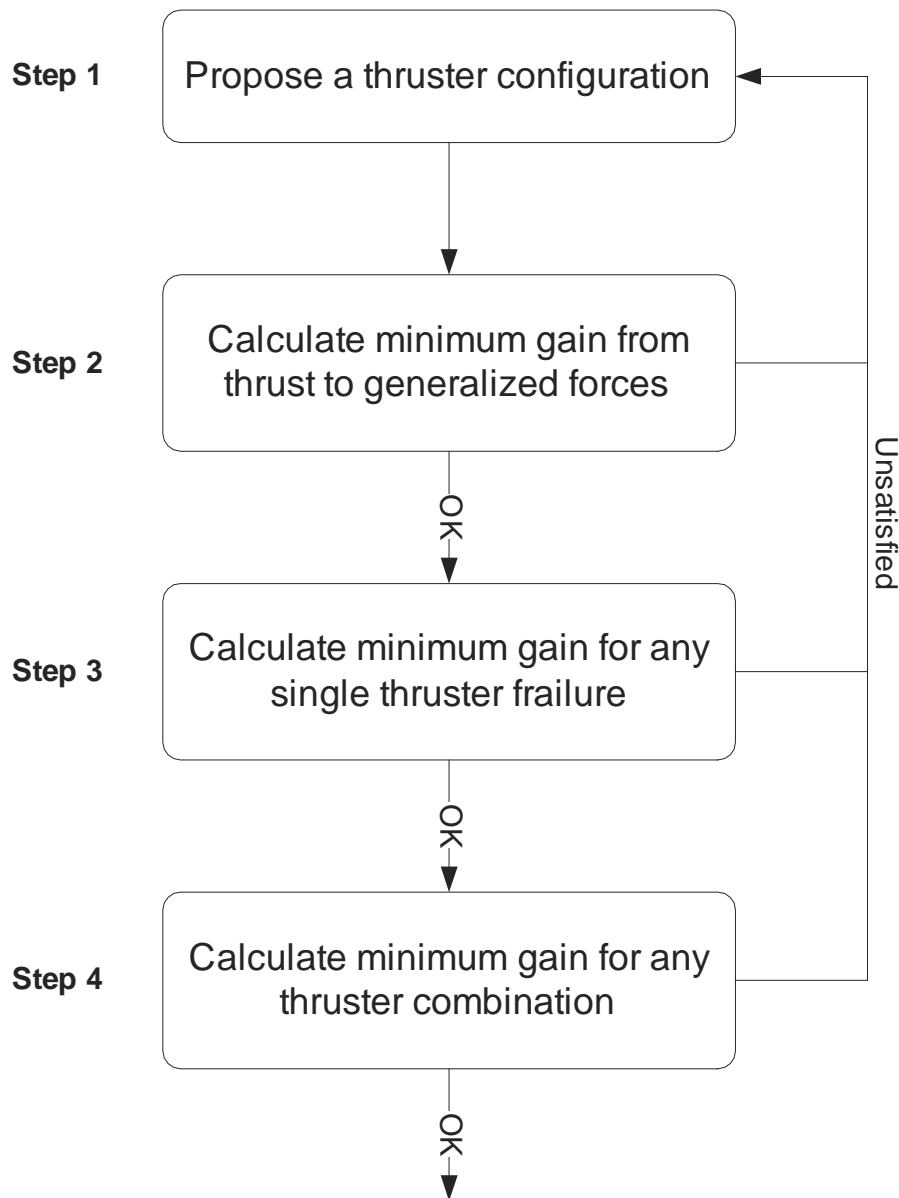


Figure 7.3: Flow chart for thruster configuration design.

Step 4: Calculate minimum gain for any thruster combination.

On vessels requiring a high degree of reliability it is a requisite that the vessel should be able to continue operation also subject to failure of a power bus. In order to find the best way of dividing the ship into two separate power busses, the minimum gain from thruster forces to generalized forces is computed for any combination of enabled thrusters. Any combination with insufficient minimum gain should be avoided by not allowing the failing thrusters to be on the same power bus.

7.6 Example with CyberShip III

The vessel configuration of CyberShip III is seen in Figure 4.4. Thruster number 1 is the tunnel thruster in the bow, thruster number 2 is an azimuthing thruster in front, and thruster number 3 and 4 are azimuthing thrusters positioned as typical main propulsors, port and starboard, respectively. The maximum thrusts are given in Table 4.2, and the exact position of the different thrusters are given in Appendix B.

7.6.1 Fixed bidirectional thrusters

In order to investigate the degree of singularity for different thruster directions, the singular values are computed as in Section 7.3 for all combinations of thrust directions. Since there are three rotating thrusters on CyberShip III, it is not possible to present the results in one plot. It is then chosen to make plots for different directions of the forward azimuth.

Equal maximum thrust

In the case when the maximum thrust of all the thrusters are equal, (7.4) reduces to:

$$\mathbf{B}_S(\alpha) = \mathbf{S}\mathbf{B}(\alpha). \quad (7.113)$$

The maximum thrusts are set to the mean of the values in Table 4.2. The minimum gains were plotted as functions of thrust direction 3 and 4, for different directions of thruster number 2. High minimum gains are considered to be good. In Figure 7.4 and 7.5 the best and worst plot, respectively, for the different directions of thruster number 2 are shown. It is seen that there are significant differences between the figures for both the areas with large and small minimum singular values.

In Figure 7.6 and 7.7 the effect of loosing the tunnel thruster is shown. In Figure 7.6 it is seen that the loss of the tunnel thruster causes a near singular configuration. This is because $\alpha_2 = 0$, and hence the ability to produce sway force and yaw moment in the front is lost. This means that the ship has practically only the two aft thrusters for sway and yaw control. In Figure 7.7 it is seen that when $\alpha_2 = 90[\text{deg}]$ the effect of loosing the tunnel thruster is almost none. This is because the azimuth thruster in this case easily can take over for

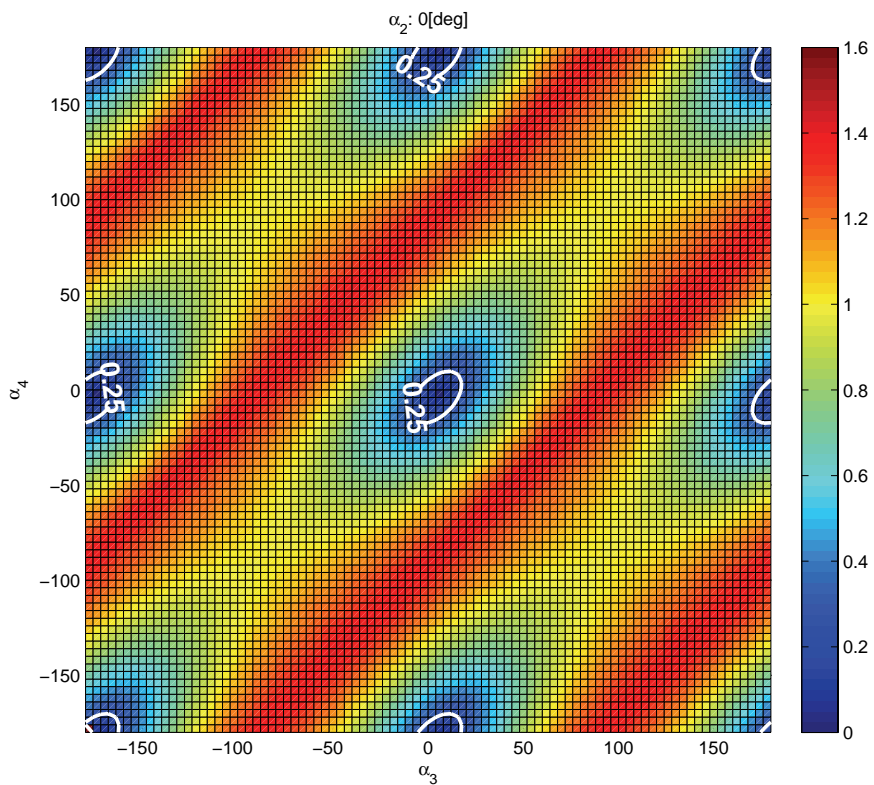


Figure 7.4: Minimum singular values for CyberShip III with equal maximum thrust and $\alpha_2 = 0[\text{deg}]$.

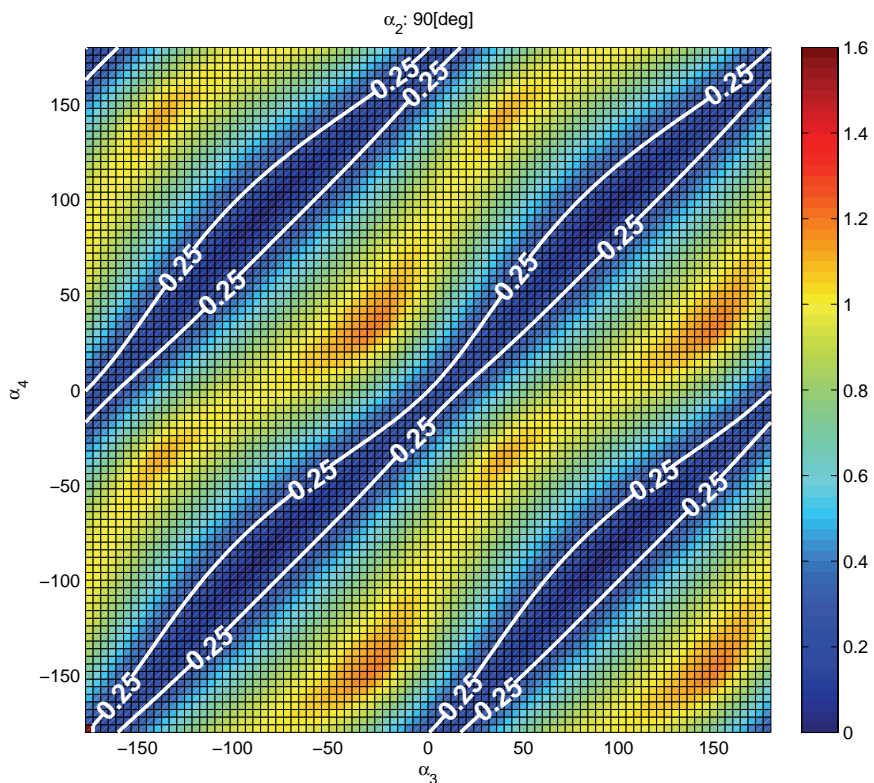


Figure 7.5: Minimum singular values for CyberShip III with equal maximum thrust and $\alpha_2 = 90[\text{deg}]$.

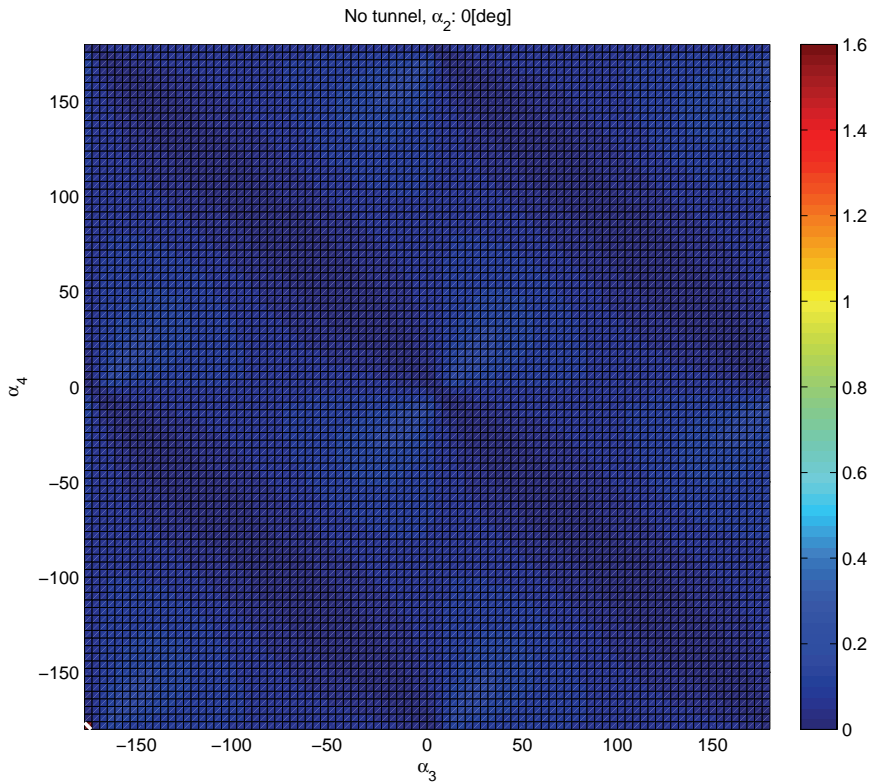


Figure 7.6: Minimum singular values for CyberShip III with equal maximum thrust, loss of tunnel thruster and $\alpha_2 = 0[\text{deg}]$.

the tunnel thruster, since they produce thrust in the same directions and are both positioned far in front of the centre of rotation.

In Figure 7.8 the effect of loosing the forward azimuth is seen. This plot is nearly identical to the ones in Figure 7.5 and 7.7. This is because the tunnel thruster and the azimuth thruster at 90[deg] easily can take over the task of the other.

In Figure 7.9 the effect of loosing the aft port thruster is shown. It is seen that this fault causes a completely different picture. (Notice the change of axis from α_3 to α_2 .) The ability to produce generalized forces are significantly reduced, but have acceptable values in some regions.

Comparing Figure 7.4-7.9 and computing the singular values for some new thruster directions, it is suggested to use a thruster configuration with $\alpha_2 = 35[\text{deg}]$, $\alpha_3 = -45[\text{deg}]$ and $\alpha_4 = 45[\text{deg}]$ if CyberShip III is to be operated with high maneuverability subject to single thruster failure, and all thrusters fixed and bidirectional. The singular values for this configuration subject to different single failures are given in Table 7.1.

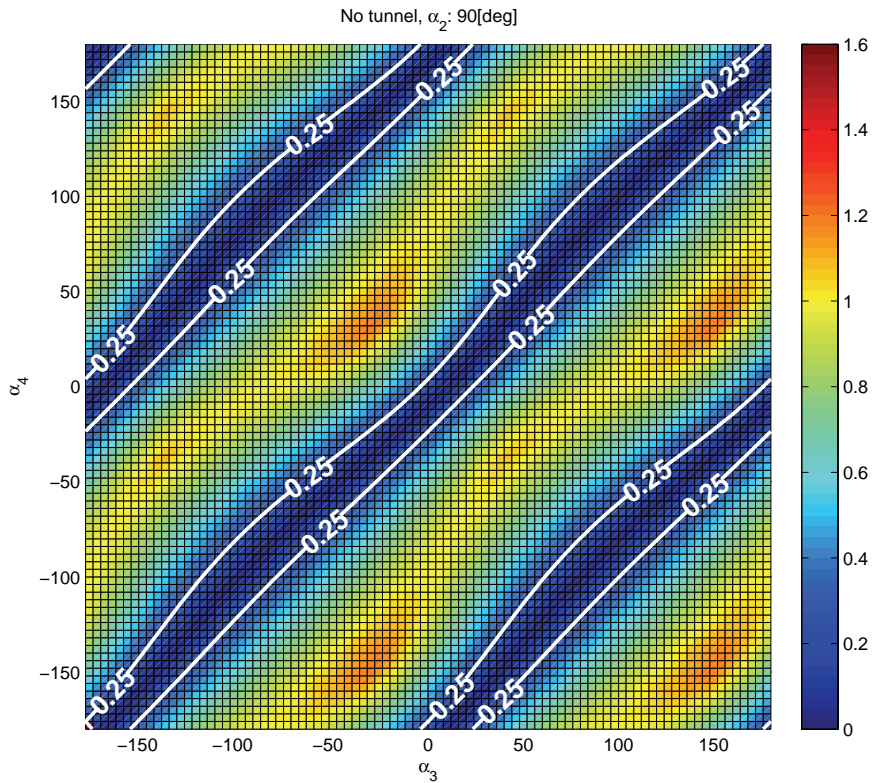


Figure 7.7: Minimum singular values for CyberShip III with equal maximum thrust, loss of tunnel thruster and $\alpha_2 = 90[\text{deg}]$.

Table 7.1: Singular values for different single failures with fixed bidirectional thrusters on CyberShip III. $\alpha_2 = 35[\text{deg}]$, $\alpha_3 = -45[\text{deg}]$ and $\alpha_4 = 45[\text{deg}]$.

Enabled thrusters	$\min(\text{svd}(\mathbf{B}_S))$
1 2 3 4	1.17
2 3 4	0.50
1 3 4	1.00
1 2 4	0.50
1 2 3	0.68

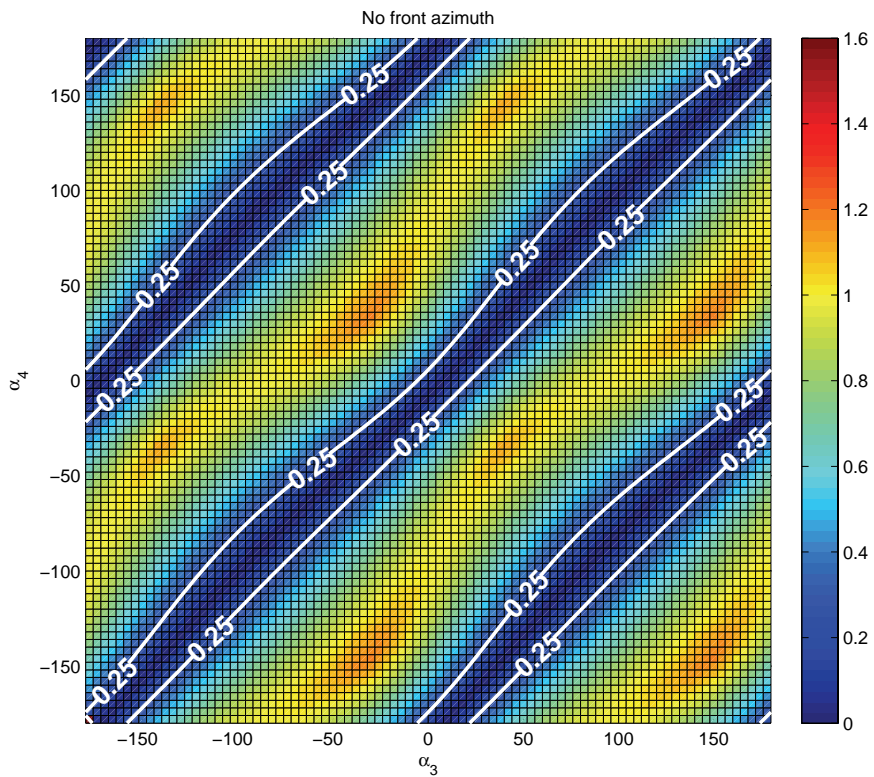


Figure 7.8: Minimum singular values for CyberShip III with equal maximum thrust and loss of forward azimuth.

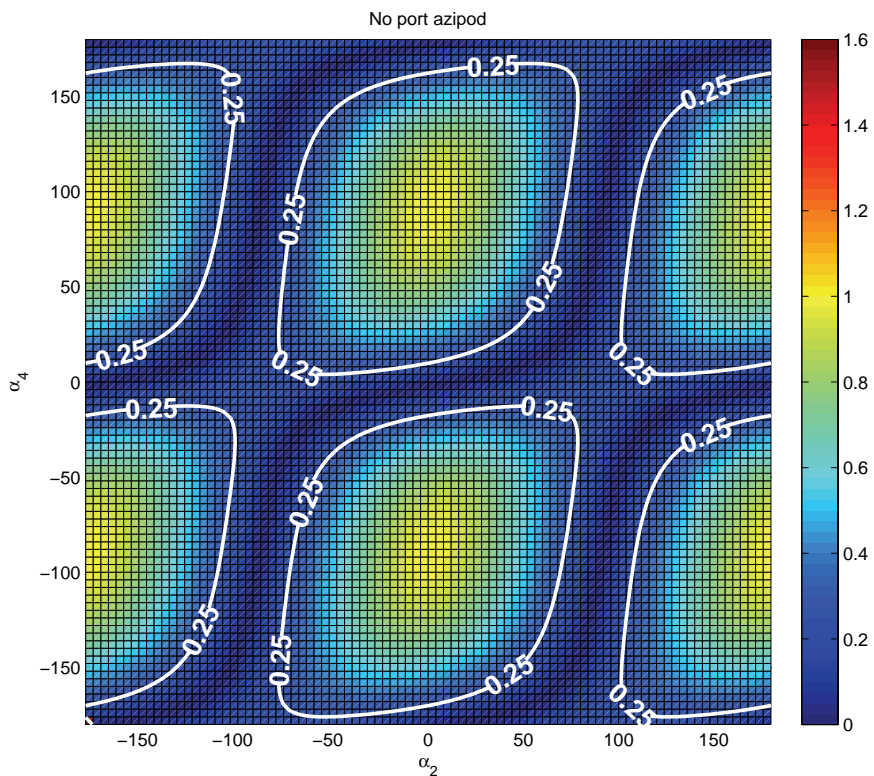


Figure 7.9: Minimum singular values for CyberShip III with equal maximum thrust and loss of port azipod.

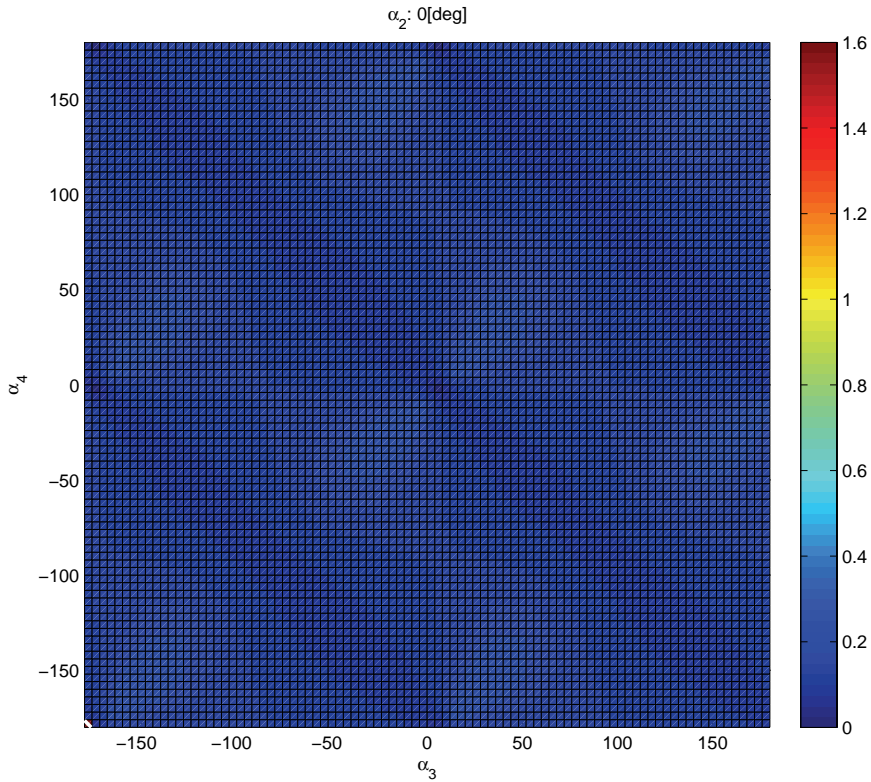


Figure 7.10: Minimum singular values for CyberShip III with model ship maximum thrusts and $\alpha_2 = 0[\text{deg}]$.

Different maximum thrust

On the model scale ship CyberShip III there are significant differences between the different maximum thrusts. In particular the tunnel thruster is very weak. In order to investigate the effect of the different maximum thrusts, the thruster configuration matrix is scaled according to (7.4) with the maximum thrusts taken from Table 4.2. Two of the resulting plots are shown in Figure 7.10 and 7.11 for the fault free case with $\alpha_2 = 0[\text{deg}]$ and $\alpha_2 = 90[\text{deg}]$, respectively. By comparing with Figure 7.4 and 7.5, it is seen that the new method of scaling catches the importance of low thrust on the tunnel thruster. Further, the best direction of thruster number 2 is no longer $0[\text{deg}]$, but $90[\text{deg}]$, which actually makes good sense by practical considerations, since the tunnel thruster is hardly able to produce any significant force.

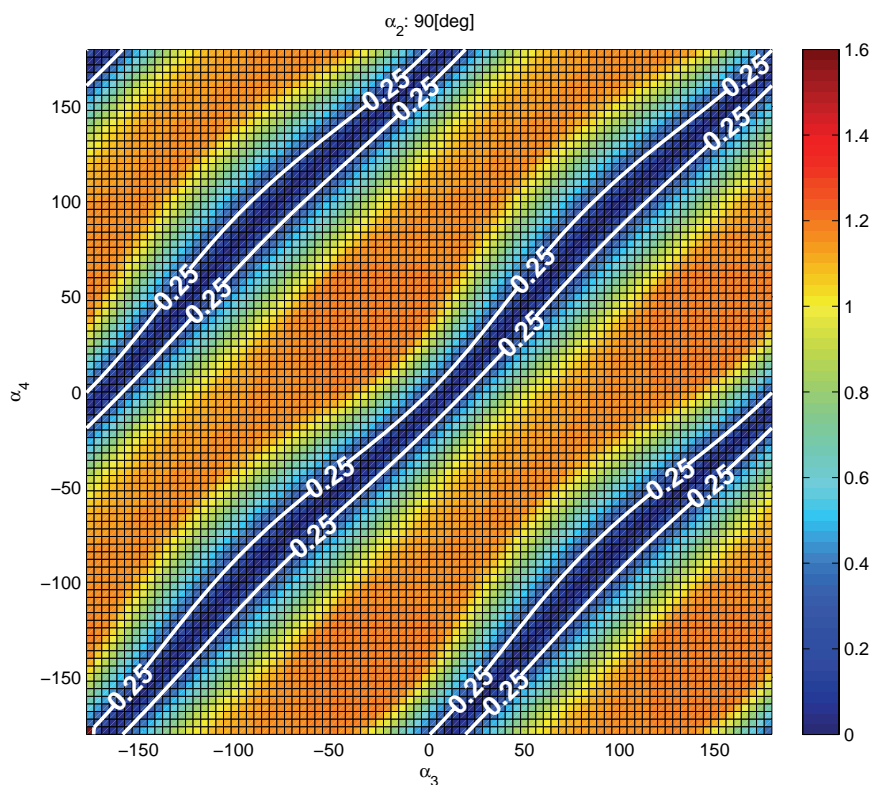


Figure 7.11: Minimum singular values for CyberShip III with model ship maximum thrusts and $\alpha_2 = 90[\text{deg}]$.

7.6.2 Fixed unidirectional thrusters

Here an example where the tunnel thruster is bidirectional and the others are unidirectional is presented. It is assumed equal maximum thrust of the different thrusters. The value used is the mean of the values in Table 4.2. The difference between the approximated solution based on Theorem 7.1 and improved solution by Theorem 7.2 is shown in Figure 7.12 and 7.13. It is seen that the simplified approach catches the main behavior of the gains.

7.6.3 Freely rotating thrusters

As stated in Section 7.5 the minimum requirement for controllability is $\text{rank}(\mathbf{B}_G) = m$. In the DP applications presented here $m = 3$, which means that three fixed or one fixed and one freely rotating thruster with appropriate directions and positions on a vessel can make the vessel controllable. In the following a design study of the thruster configuration on CyberShip III with freely rotating thrusters is presented. The steps of the design loop are shown in Figure 7.3 and described in Section 7.5.4.

Step 1

The vessel configuration with one bidirectional tunnel thruster and three freely rotating thrusters on CyberShip III are proposed. The cases with uni- and bidirectional rotating thrusters are equivalent, since the rotating thruster in both cases are modeled as two fixed orthogonal bidirectional thrusters. The thruster configuration can be seen in Figure 4.4, and the maximum thrusts are taken from Table 4.2.

Step 2

In order to calculate the minimum gain from thruster forces to generalized forces, the thruster configuration matrix has to be scaled. The thruster configuration matrix is given as:

$$\mathbf{B}_A = \begin{bmatrix} 0 & 1 & 0 & 1 & 0 & 1 & 0 \\ 1 & 0 & 1 & 0 & 1 & 0 & 1 \\ \mathbf{L}_{x,1} & -\mathbf{L}_{y,2} & \mathbf{L}_{x,2} & -\mathbf{L}_{y,3} & \mathbf{L}_{x,3} & -\mathbf{L}_{y,4} & \mathbf{L}_{x,4} \end{bmatrix}. \quad (7.114)$$

Using (7.2) and (7.3) give:

$$\bar{T}_{\max} = 8.9, \quad (7.115)$$

$$L_{typ} = 0.79. \quad (7.116)$$

The scaled thruster configuration matrix is then found from (7.96):

$$\mathbf{B}_G = \begin{bmatrix} 0 & 0.97 & 0 & 1.51 & 0 & 1.45 & 0 \\ 0.065 & 0 & 0.97 & 0 & 1.51 & 0 & 1.45 \\ 0.070 & 0 & 0.68 & 0.23 & -1.67 & -0.22 & -1.61 \end{bmatrix}. \quad (7.117)$$

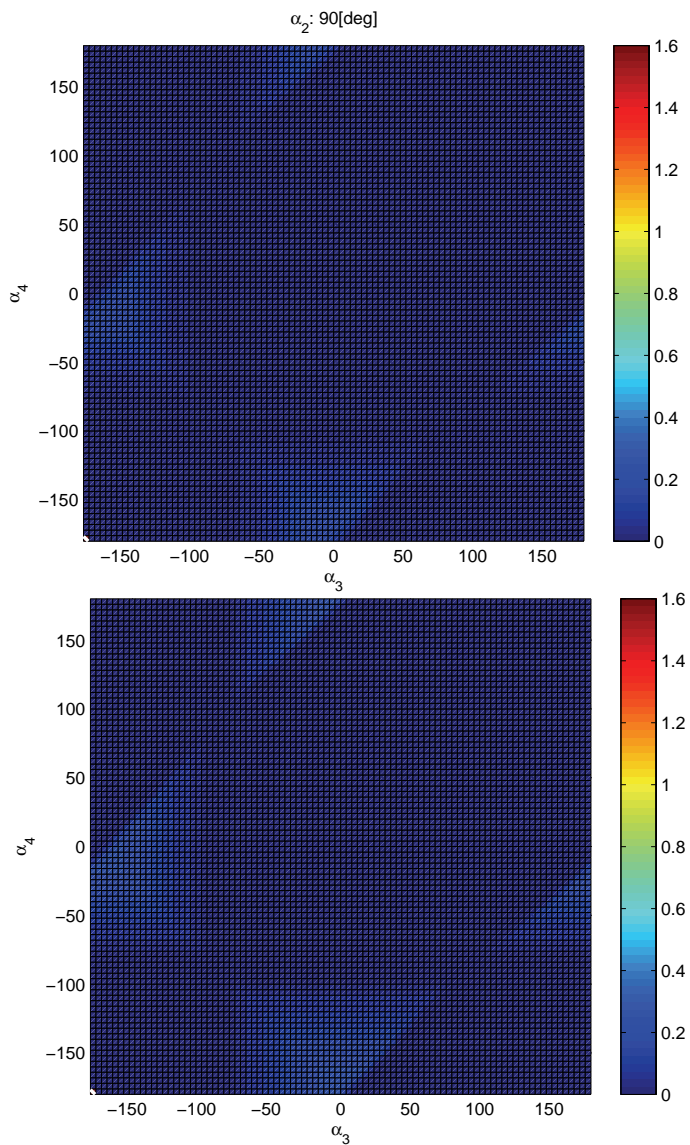


Figure 7.12: Comparison of minimum gain for fixed thrusters obtained by Theorem 7.1 (upper) and Theorem 7.2 (lower). The lower left corner is modified to get nice plots. $\alpha_2 = 90[\text{deg}]$.

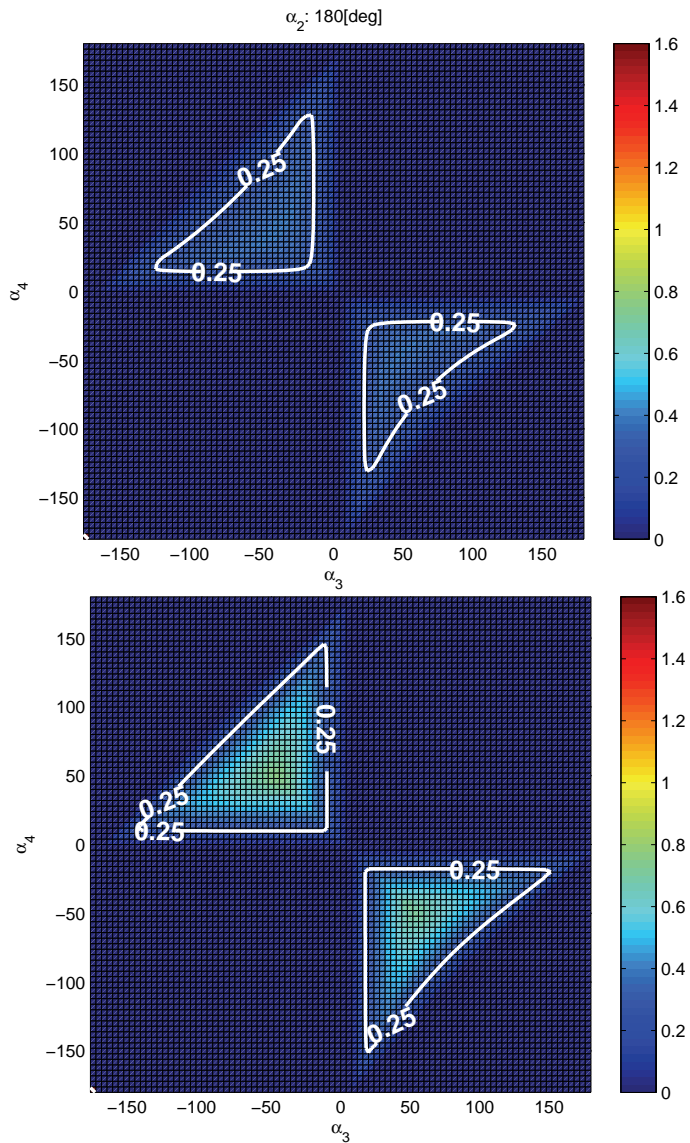


Figure 7.13: Comparison of minimum gain for fixed thrusters obtained by Theorem 7.1 (upper) and Theorem 7.2 (lower). The lower left corner is modified to get nice plots. $\alpha_2 = 180[\text{deg}]$.

The singular values are then found by singular value decomposition:

$$\boldsymbol{\sigma} = [3.1 \quad 2.3 \quad 1.20]^T. \quad (7.118)$$

The minimum singular value is then $\sigma_{\min} = 1.20$, which is an acceptable value. By applying Lemma 7.2 it can be concluded that the minimum attainable set is:

$$\begin{aligned} \|\boldsymbol{\tau}\|_2 &= \frac{1}{\sqrt{2}} 0.79 \cdot 1.20 \cdot 8.9, \\ &= 6.0. \end{aligned} \quad (7.119)$$

This means that the thrusters can produce any generalized force within a ball with radius 6.0.

Step 3

The minimum gain from thruster forces to generalized forces when subject to any single failure is computed. The resulting minimum singular values are given in Table 7.2 as row 2 to 5. It is seen that thruster configuration 134, that is failure on thruster number 2, has a low minimum gain from thruster forces to generalized forces. This fault is significantly worse than any other of the single failures, since the thrust producing capability of the tunnel thruster is low, and the tunnel thruster is the only thruster left working in front of the centre of gravity.

In this design example we will then have to go back to step 1 and propose a new thruster configuration. It is then proposed to install four equally power full thrusters, all with a maximum thrust of \bar{T}_{\max} (8.9[N]). Bare in mind that the maximum thrust on the aft thrusters are now reduced. In order to shorten this example, step 1 to 3 with the modified design are not presented, but the results are shown in the fourth column in Table 7.2. It is now seen that all single thruster failure scenarios have a minimum gain larger than 1.21. Then we move on to the next step.

Step 4

Assuming CS3 is a vessel requiring a high degree of reliability, it is a requisite that the vessel should be able to continue operation also subject to failure of a power bus. The minimum gain from thruster forces to generalized forces are computed for any combination of enabled thrusters. The result is seen in the fourth column in Table 7.2. It is obvious that having only one thruster at a power bus is impossible since the ship is not controllable with only one thruster operating. This can be seen from the second column in Table 7.2 where the rank of the thruster configuration matrix is less than three for all the configurations with only one thruster operating. When the rank of the thruster configuration matrix is less than three the thruster configuration is incapable of producing forces in all directions. Then it is time to investigate the thruster configurations with two thrusters in each bus. From the fourth column in Table 7.2 it is seen that

Table 7.2: Rank and singular values for different combinations of the thrusters on CyberShip III. The third column is for the actual thruster configuration on CS3, and the fourth column is for the modified thruster configuration with equal maximum thrust on all the thrusters.

Enabled thrusters	$\text{rank}(\mathbf{B}_G)$	$\min(\text{svd}(\mathbf{B}_G))$	$\min(\text{svd}(\mathbf{B}_G))$ $\mathbf{T}_{\max,i} = \bar{T}_{\max} \forall i$
1 2 3 4	3	1.20	1.73
1 2 3	3	1.17	1.40
1 2 4	3	1.17	1.40
1 3 4	3	0.23	1.41
2 3 4	3	1.19	1.21
1 2	3	0.02	0.20
1 3	3	0.09	0.99
1 4	3	0.09	0.99
2 3	3	1.17	1.19
2 4	3	1.17	1.19
3 4	3	0.22	0.15
1	1	—	—
2	2	—	—
3	2	—	—
4	2	—	—

thruster configuration 12 and 34 should be avoided, since these configurations have the smallest minimum gains from thrust to generalized forces. It is then concluded that by using 13 and 24, or 14 and 23 as power busses will guaranty a minimum gain from thruster forces to generalized forces of 0.99.

It is worth noticing that the findings in Table 7.2 matches with the experimental results on thruster failures presented in Section 6.5.3. Ranking the experimental results from worst to best we get the following thruster configurations: 12, 14, 34, 24, 134, 124, and 234. The only deviation from the table is that 24 and 134 has switched place. This is explained by the fact that the tunnel thruster, which is particularly weak, is operated away from its saturations point. Hence, the penalty imposed on this thruster by the thruster scaling is too hard. Investigations of dynamic performance when subject to different faults were also performed by Strømquist (2007). However, in the results of Strømquist (2007) the holding capability and not the maneuverability was investigated.

7.7 Singularity monitoring

Singularities can be monitored by one of the earlier presented methods for finding minimum gain from thruster forces to generalized forces. In order to monitor the instant degree of singularity, the fixed thruster approaches can be used. When using rotating thrusters, their ability to rotate should be taken into account. It is

then proposed to determine a minimum gain from thruster forces to generalized forces allowing the thrusters to rotate e.g. 5 seconds. The time should be significantly smaller than the response time of the DP controller. When choosing this time, it is important that none of the thrusters are capable of rotating more than $\pm 90[\text{deg}]$. This is because when solving the time-limited problem, one solves "the design problem" with sector constraints:

$$\alpha_{\min} = \alpha_0 - \dot{\alpha}_{\max} t_{\lim}, \quad (7.120)$$

$$\alpha_{\max} = \alpha_0 + \dot{\alpha}_{\max} t_{\lim}, \quad (7.121)$$

$$\alpha_{\max} - \alpha_{\min} \leq \pi_{n \times 1}, \quad (7.122)$$

where t_{\lim} is the time limit, and (7.120) ensures convexity. The result is that a minimum gain from thruster forces to generalized forces for the next t_{\lim} seconds are computed.

7.7.1 Monitoring singular direction

The solution to the singular value decomposition contains the vector in generalized forces that belongs to the minimum gain. Monitoring this vector in addition to the singular value may be of interest for captains. The general singular value decompositions is given as (Strang 1988):

$$\mathbf{X} = \mathbf{U}\mathbf{S}\mathbf{V}^T, \quad (7.123)$$

where $\mathbf{U} \in \mathbb{R}^{m \times m}$ is orthogonal, $\mathbf{S} \in \mathbb{R}^{m \times n}$ is diagonal and contains the singular values, and $\mathbf{V} \in \mathbb{R}^{n \times n}$ is orthogonal. It is common to order the solution such that the values of \mathbf{S} decreases down it's diagonal. This means that the most singular generalized force direction is the m 'th column of \mathbf{U} (see e.g. Skogestad and Postlethwaite (2007) for details on this). In the bidirectional case, discussed in Section 7.3 and 7.5.1, it is straight forward to find this direction, since it is a result of the singular value decomposition. However, for the unidirectional cases this is not straight forward.

Theorem 7.5 *For the minimum gain from thruster forces to generalized forces found in Theorem 7.2, the corresponding generalized force direction $\tau_{\sigma_{\min}}$ is given as:*

$$\tau_{\sigma_{\min}} = \Omega_k \mathbf{V}_1, \quad (7.124)$$

where Ω_k is the matrix of Γ_i 's corresponding to Ψ_k , \mathbf{V}_1 is the first column of the \mathbf{V} matrix from the singular value decomposition of Ψ_k , and k is the index of the most singular configuration.

Proof. According to Skogestad and Postlethwaite (2007) the input direction with the largest amplification is \mathbf{V}_1 . Hence:

$$\begin{aligned} \sigma_{\max, \Psi_k} &= \max_{\|\mathbf{b}\|_2=1} \left(\frac{\|\Psi_k \mathbf{b}\|_2}{\|\mathbf{b}\|_2} \right), \\ &= \|\Psi_k \mathbf{V}_1\|_2. \end{aligned} \quad (7.125)$$

Since Ψ_k is a matrix with $\bar{\mathbf{T}}_{Gi}$'s as columns, the elements of \mathbf{V}_1 , can be seen as the weighting of the different $\bar{\mathbf{T}}_{Gi}$'s. Since the different $\bar{\mathbf{T}}_{Gi}$'s are connected to different $\mathbf{\Gamma}_i$'s the \mathbf{V}_1 vector is also the weighting of the different $\mathbf{\Gamma}_i$'s. Hence, the direction with the smallest gain is given as:

$$\boldsymbol{\tau}_{\sigma_{\min}} = \boldsymbol{\Omega}_k \mathbf{V}_1. \quad (7.126)$$

■

Remark 7.2 *The result in (7.124) is equivalent with:*

$$\boldsymbol{\tau}_{\sigma_{\min}} = \mathbf{B}_G \boldsymbol{\Psi}_k \mathbf{V}_1. \quad (7.127)$$

This can be verified by using (7.102).

For the case with surge, sway and yaw control, it is further proposed to visualize the minimum gain direction as a projection of $\boldsymbol{\tau}_{\sigma_{\min}}$ in the surge and sway plane. The direction of the vector will then show the singular direction in the surge-sway plane, and the length of the vector will show the magnitude of the surge-sway force compared to the yaw moment. Further, the color of the vector can be used to show if the yaw force is positive or negative. The following equations applies:

$$\begin{aligned} \alpha_{\sigma_{\min}} &= \arctan2(\boldsymbol{\tau}_2, \boldsymbol{\tau}_1), \\ L_{\sigma_{\min}} &= \frac{\|\boldsymbol{\tau}_1 + \boldsymbol{\tau}_2\|}{\|\boldsymbol{\tau}\|}, \end{aligned}$$

where $\alpha_{\sigma_{\min}} \in \mathbb{R}$ is the projected direction of the most singular direction, and $L_{\sigma_{\min}} \in [0, 1] \in \mathbb{R}$ is the length of the vector. This way, $L_{\sigma_{\min}}$ is 1 if it is no yaw moment in the most singular direction, and 0 if the most singular direction is pure yaw. The arrows are red if the yaw force is positive, and blue if the yaw force is negative. Examples of such vectors are shown for $\boldsymbol{\tau}_{\sigma_{\min}} = [0.70, 0.70, 0.14]^T$, $\boldsymbol{\tau}_{\sigma_{\min}} = [0, -0.1, 0.99]^T$, and $\boldsymbol{\tau}_{\sigma_{\min}} = [-0.57, 0.57, -0.59]^T$ in Figure 7.14.

7.8 Real time singularity avoidance

So far the focus has been singularity monitoring and singularity avoidance during the design phase. However, in real operations with rotating azimuths it is not guaranteed that singularities are avoided. In that case real time singularity avoidance may be needed.

Normally the azimuth speed is about $12[\text{deg}/\text{s}]$ in full scale. This corresponds to the thrusters moving three grid lines in both directions during one time sample ($1.0[\text{s}]$) in Figure 7.4-7.13. Hence, at this azimuth speed singularities should not be a big problem. If the azimuth speed is slow, singularities can be avoided by introducing functions penalizing near singular configurations in the cost function. By including singularity avoidance in the optimization problem, the convexity of the problem is easily lost. Examples on this can be found in

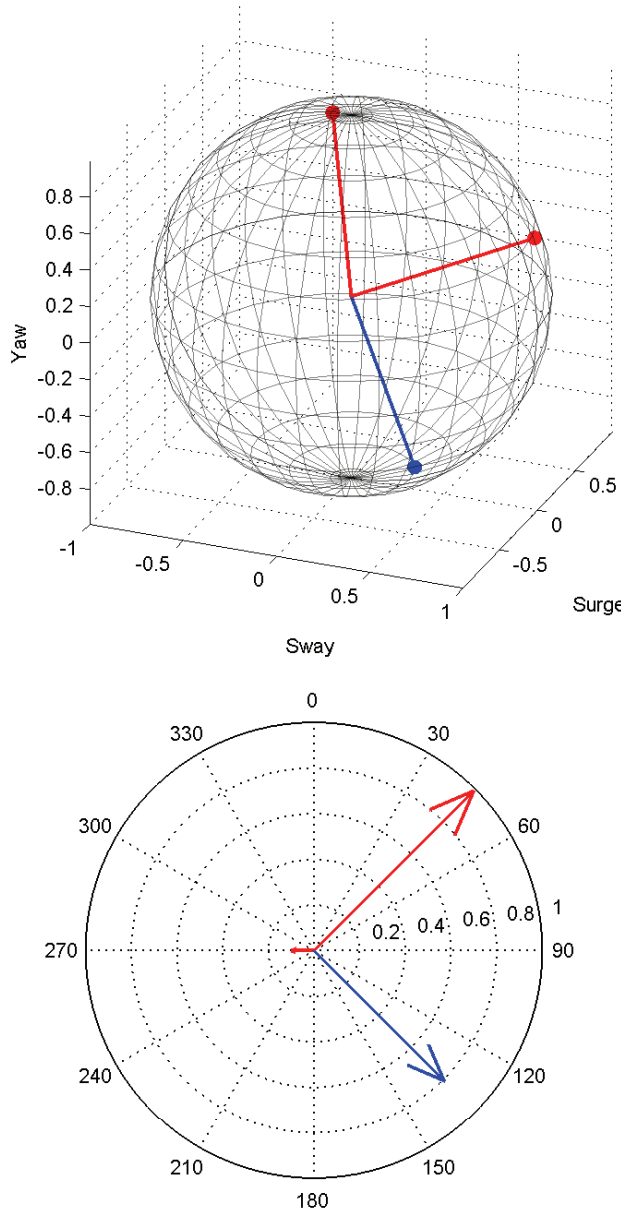


Figure 7.14: Example of visualization of different $\tau_{\sigma_{\min}}$ vectors. The upper plot is 3D and the lower plot is the projection in the surge-sway plane. In the lower plot the largest red vector is $\tau_{\sigma_{\min}} = [0.70, 0.70, 0.14]^T$, the smallest red vector is $\tau_{\sigma_{\min}} = [0, -0.1, 0.99]^T$, and the blue vector is $\tau_{\sigma_{\min}} = [-0.57, 0.57, -0.59]^T$. There are no relations between the vectors.

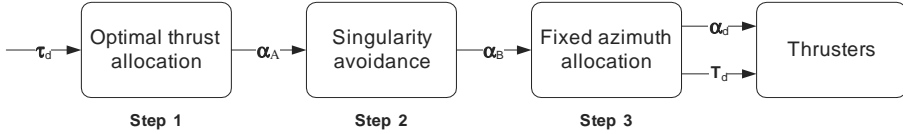


Figure 7.15: Block diagram of real time singularity avoidance.

Johansen et al. (2004) and Johansen (2004). Loosing the convexity is considered to be unwanted, since it significantly complicates and influences the solution method of the problem.

Another solution may be to fix or significantly constraint one or more rotating thrusters in order to ensure reserve capacity in all generalized force direction. Which sector the thruster should be constraint too can be found from plots like in Figure 7.4. If $\alpha_2 = 0$ and α_3 is constraint to $[50, 130]$ [deg], the controllability is seen to be large for all values of α_4 (bidirectional thrusters are assumed).

A third approach can be to deny the thrusters to rotate to near singular configurations. This can be done by monitoring the minimum gain, and deny the thrusters to rotate to positions with small minimum gains.

The advantage by use of singularity avoidance is that the vessel is capable of rapidly change generalized force direction and magnitude. The disadvantage is reduced maximum generalized forces. Depending on the variation in generalized force, singularity avoidance may both increase and decrease the power consumption. If the variations in generalized forces are small, singularity avoidance will increase the power consumption, since the thrusters are forced to operate away from the power optimal solution. On the other hand, if there are large variations in the generalized forces, the power consumption may be reduced with singularity avoidance. This is because operating at near singular configurations with small gain from thrust to generalized forces are avoided.

7.8.1 Avoiding small minimum gains

The idea in this approach is to only allow the thrusters to rotate if they are aiming for a configuration with a minimum gain larger than a given threshold σ_{lim} . The thrusters have to be allowed to pass through singular configurations as fast as possible in order to not lock the thrusters completely when the minimum allowed gain from thrust to generalized force is reached. Additionally dwell time can also be included. Then it is ensured that the thrusters have been operating with a minimum gain for some time, before the thrusters are allowed to move to the new configuration. The method is implemented by solving the thrust allocation problem in three steps as shown in Figure 7.15.

The first step runs independently of the other steps and always aims at finding the optimum, independently of any singularity avoidance. The first thrust direction solution is denoted $\alpha_A \in \mathbb{R}^n$.

The second step is to check for the degree of singularity in terms of the

minimum gain. If the minimum gain is above the threshold, and the dwell time is exceeded, the desired azimuth angle α_A is passed on to the third step unchanged. In all other cases, the previous azimuth angles (from the second step) are used. Mathematically this is formulated as:

$$\alpha_B(t) = \begin{cases} \alpha_A(t), & \text{if } \sigma_{\min} > \sigma_{\lim} \wedge t_2 > t_{\lim}, \\ \alpha_B(t - \Delta t), & \text{else ,} \end{cases} \quad (7.128)$$

where $\alpha_B \in \mathbb{R}^n$ is the desired azimuth directions in the second and third step, $t \in \mathbb{R}$ is time, $\Delta t \in \mathbb{R}$ is the time step, $t_2 \in \mathbb{R}$ is the time σ_{\min} has been larger than σ_{\lim} , and t_{\lim} is the dwell time limit.

The third step solves the fixed azimuth problem with α_B as given azimuth directions.

A weakness of this approach is the possibility of locking the thrusters in unfavorable directions when the path of α_A remains smaller than the minimum gain limit. This is because the method will not allow the thrusters to rotate before they are aiming for a configuration with sufficient minimum gain. However, the experiments seems to indicate that the path of α_A frequently has a minimum gain larger than the threshold. Anyway, a possible solution to the problem is to monitor the cost of the first and third solution and inform the captain if the difference is large for a long time. Other ways of overcoming this possible problem may be interesting subjects for further research. An improvement in this real time singularity avoidance method compared to previously presented results is the possibility of going through singular configurations if the system is aiming for a configuration with sufficient minimum gain. Also the requirement on minimum gain ensures that the thruster directions will not be very unfavorable.

7.9 Experimental validation of singularity avoidance in real time

Experiments were conducted with CyberShip III. A complete collection of figures for the presented runs are found in Appendix C. The sample time of the control system, including the thrust allocator was 0.20[s], corresponding to approximately 1[Hz] in full scale.

7.9.1 Run J: Minimum attainable set

In this case CS3 was operated in station keeping by use of a DP system with fixed thruster directions $\alpha_d = [90, 80, 26, 46][\deg]$ in order to demonstrate the theory. Due to the layout of CS3, the thrusters were allowed to produce both positive and negative thruster force. No waves were present. In Figure 7.16 the norm of the nondimensional generalized forces is plotted together with the minimum gain from thruster forces to generalized forces. It is seen that the deviations between desired and commanded generalized forces occur when the desired nondimensional generalized force magnitude exceeded the minimum gain. This is in accordance with the theory in Theorem 7.3.

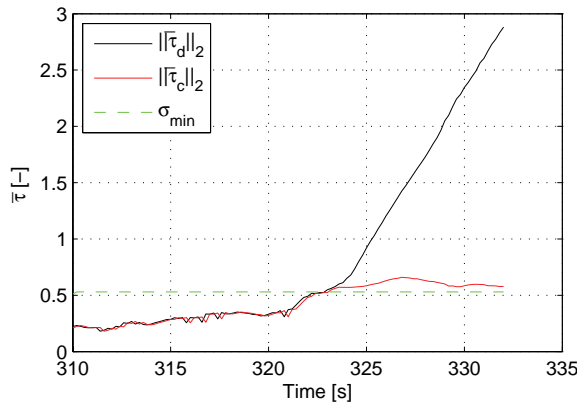


Figure 7.16: Plot of normalized generalized forces and minimum gain during Run J.

7.9.2 Run K: Avoiding small minimum gains

In this case CS3 was operated in station keeping by use of a DP system, with singularity avoidance as described in Section 7.8.1 included. Due to the layout of CS3, the thrusters were allowed to produce both positive and negative thrust in the third step when solving the thrust allocation problem. Otherwise, the configuration would have been singular most of the time. No waves were applied. Singularity avoidance was turned on at 659[s]. It is pointed out that the experiments demonstrated the capabilities of the method, and that the results are very dependent on the initial condition of the vessel and thrusters at which position change is initiated. In order to demonstrate singularity avoidance, the maximum azimuth speed of the thrusters were reduced to $\Delta\alpha_{\max} = 0.10 \cdot [1, 1, 1, 1]^T$. Further, $\sigma_{\lim} = 0.5$ and $t_{\lim} = 0$ were used. The first position change, 1.0[m] to port, is conducted without singularity avoidance, and the second, an additional 1.0[m] to port, with singularity avoidance. In Figure 7.17 it is seen that the positioning performance was best with singularity avoidance. The maximum deviation between desired an observed position is seen in Table 7.3. Roughly, the deviations are halved for the positions and quartered for the heading when applying singularity avoidance. In Figure 7.18 the generalized forces are plotted, showing a larger deviation between desired and commanded values without singularity avoidance. The maximum error between desired and commanded generalized force in the different directions are given in Table 7.4. The large deviation in sway force with singularity avoidance is caused by the thrusters rotating between two configurations with sufficient minimum gain. This can be seen in Figure 7.19 where the nondimensional generalized force magnitudes are plotted together with the minimum gain in order to demonstrate the minimum attainable set. It is seen that all deviations between desired and commanded generalized force occur when $\|\bar{\tau}_d\|_2 > \sigma_{\min}$. This means that as long as the

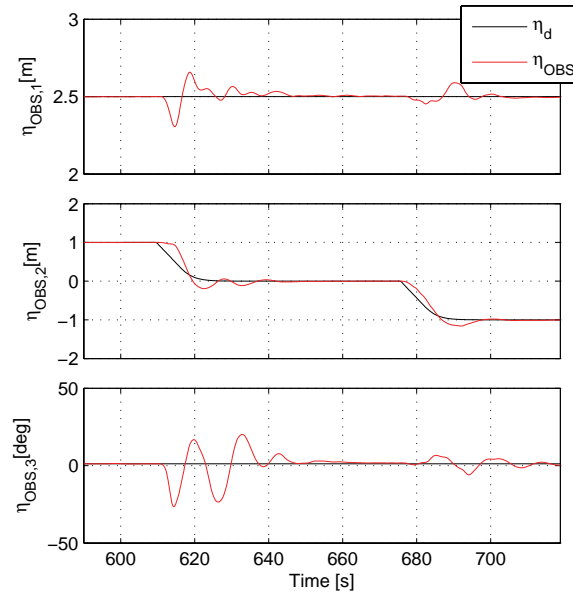


Figure 7.17: Plot of position and heading during Run K.

Table 7.3: Maximum deviation between desired and observed position with and without singularity avoidance during Run K.

Direction	Without singularity avoidance	With singularity avoidance	Unit
Surge	0.19	0.09	[m]
Sway	0.43	0.24	[m]
Yaw	28	7.1	[deg]

nondimensional desired generalized force is in the minimum attainable set, the thrust allocator is capable of commanding the desired generalized forces. This is in accordance with Theorem 7.3. In Figure 7.20 the minimum gain from the first and third step in the thrust allocation are shown. The deviations between the two curves are caused by the singularity avoidance actions. It is seen that reduced positioning performance correlates with small minimum gain in the third step. When singularity avoidance is turned on, $\sigma_{\min} < \sigma_{\lim}$ only if the thrusters are moving as fast as possible to a new configuration with $\sigma_{\min} > \sigma_{\lim}$. This has to be allowed in order to avoid locking the thrusters in unfavorable directions. In Figure 7.21 the power consumption with and without singularity avoidance is compared. It is seen that the average power consumption was reduced by 44% when singularity avoidance was included. This is because singularity avoidance ensures a readiness for changing environmental disturbances.

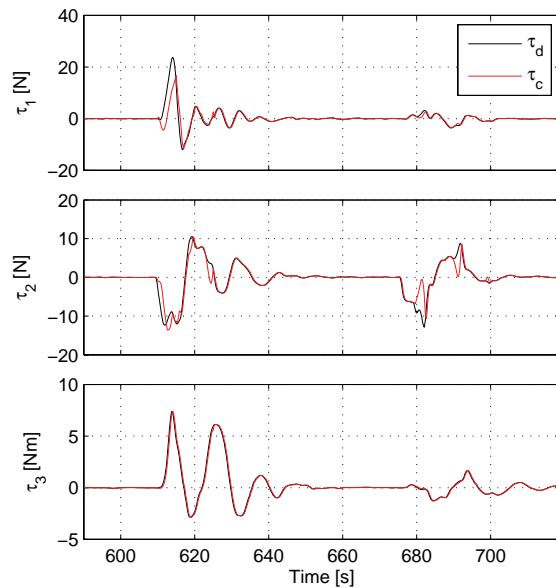


Figure 7.18: Plot of generalized forces during Run K.

Table 7.4: Maximum deviation between desired and commanded generalized force with and without singularity avoidance during Run K.

Direction	Without singularity avoidance	With singularity avoidance	Unit
Surge	12.5	1.6	[N]
Sway	7.1	10.8	[N]
Yaw	0.98	0.25	[Nm]

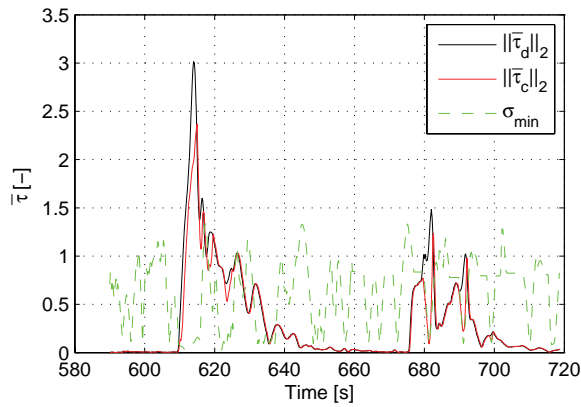


Figure 7.19: Nondimensional generalized forces and minimum singular value during Run K.

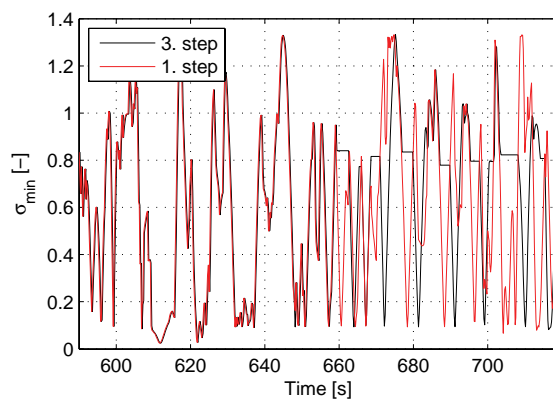


Figure 7.20: Minimum singular values from first and third thrust allocation step, see Figure 7.15, during Run K. The deviations between the two lines are caused by the singularity avoidance actions.

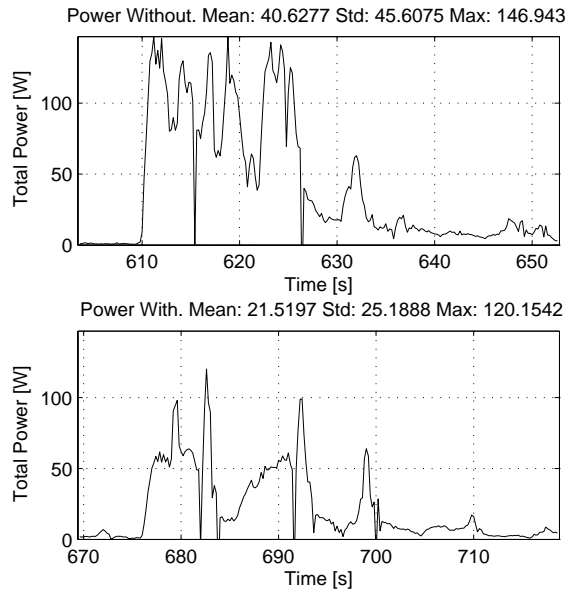


Figure 7.21: Power consumption during Run K.

7.9.3 Summary experiments

It was demonstrated that as long as the desired generalized force were inside the minimum attainable set, the thrusters were capable of producing the desired generalized force. Singularity avoidance in real time was shown to improve the positioning performance and reduce the power consumption. In order to avoid locking the thruster directions, rotation through regions with insufficient minimum gain was allowed. Going through such regions resulted in deviations between desired and commanded generalized force.

Chapter 8

Conclusions and recommendations

8.1 Conclusions

An overview of scaling laws for propellers, including the effects of ventilation and in-and-out-of water events was presented. A new parameter τ for comparison of different propellers and propulsion controllers under equal environmental conditions was proposed. The parameter could be used to determine the optimal pitch ratio and the optimal diameter of a particular propeller. When comparing different propellers or propulsion controllers, the parameter could be used to compare the efficiency and the thrust sensitivity. A quasi-static model of ventilating propellers was presented. The model was further developed into a dynamic model of ventilation and in-and-out-of water events. The model was verified by experiments with a ducted model scale propeller. The anti-spin thruster control action on consolidated controlled propellers should be taken care of by the shaft controller, due to the slow response time of the pitch actuator. Hence, it was found that results on anti-spin thruster control for fixed pitch propellers should applied to the shaft controller on consolidated controlled propellers. However, an important finding was that reducing the pitch ratio would reduce the likelihood and severity of ventilation, hence improving efficiency, safety and positioning accuracy.

Differences in the propulsion control problem for surface vessels and under-water vehicles were highlighted. The context of the propulsion control problem for low and moderate/high advance speeds were stated. Different propulsion controllers were presented and compared with respect to efficiency and thrust sensitivity by use of the τ parameter. Among the fixed pitch controllers, the combined controller showed the best performance. Among the consolidated controllers, the torque/shaft speed controller was the recommended controller, due to its simplicity and near optimal (with respect to power) performance in the whole operating range. Simulations were carried out in order to demonstrate

the theory on the different controllers.

The thrust allocation problem was stated and a literature review conducted. A convex linearly contained quadratic thrust allocator was proposed. The problem was formulated in cylindrical coordinates and converted to Cartesian coordinates. Further, it was proposed a way of taking both constraints on total power consumption and constraints on power bus consumption into account when solving the thrust allocation problem. The performance of the convex linearly constrained quadratic thrust allocator was demonstrated by experiments with a model ship.

Anti-spin thrust allocation was demonstrated. It was shown how the cost function could be modified in order to give a more correct penalty on the power consumption of the individual thrusters. This was necessary in order to be able to distribute the generalized forces on the most efficient thrusters, also when subject to ventilation. Different ways of accounting for ventilation by modification of the cost function and by modification of the thruster configuration matrix were proposed. It was argued that only modification of the cost function would give the desired performance of the anti-spin thrust allocator. The presented anti-spin thrust allocation strategy was, by experiments with a model ship, shown to reduce the power consumption, reduce the fluctuations in torque and power, and increase the positioning accuracy.

In stead of designing one "super allocator" capable of handling all eventualities, the possibility of doing switched thrust allocation was investigated. The idea was to design several allocators, all specialized at particular controller operating conditions, and switch among these in order to get a complete thrust allocation system. Examples with nonconvex linearly constrained quadratic thrust allocation, switching between fixed and rotating thrusters, and handling of thruster faults were proposed and the performance demonstrated by experiments with a model ship.

It was proposed how to scale the thruster configuration matrix before determination of the minimum gain from thruster forces to generalized forces. The terms bi- and unidirectional thrusters were defined, and the term local singularity was introduced. Determination of the minimum gain for bidirectional thrusters was presented. It was proposed a way of finding the minimum gain also for systems with unidirectional thrusters present. The method was valid for any thruster configuration with convex constraints on the azimuth directions. A design loop for evaluation of the maneuverability of the thruster configuration was proposed. The method evaluated the maneuverability under any single failure (either thruster or power bus). An extensive example with the theory applied to CyberShip III was presented. It was further shown how the most singular generalized force direction could be determined. Suggestions on how real time singularity avoidance could be done were presented. Experiments were conducted with CyberShip III in order to demonstrate the theory and an real time singularity avoidance method. The experiments showed improved efficiency and positioning accuracy.

8.2 Recommendations for future work

- This work is a scientific approach to the different problems. Although we have tried to include practical considerations, it has also sometimes been necessary to exclude them in order to get a manageable size on the investigated problems. This means that for all topics in this thesis an amount of work may be needed, before full scale implementation, in order to ensure safe and reliable performance.
- Investigating the effect of controllable pitch on ventilation and in-and-out-of water events, the results were obtained with a ducted propeller. Similar tests should also be performed for an unducted propeller, and the results compared with the ducted results.
- Full scale implementation of anti-spin thruster control is recommended as a final verification of the concept.
- A problem during the investigation of the different propulsion controllers was the lack of an adequate four quadrat thrust characteristic of a controllable pitch propeller. We recommend that such a model is developed and used for comparison of the different consolidated controllers.
- The lack of a model scale propeller with real time pitch actuation made it impossible to experimentally verify the results on consolidated controllers and anti-spin thruster control of consolidated controlled propellers. This is highly recommended to be carried out in the future.
- The commercial state of the art thrust allocators are vaguely described in the literature. It would indeed be very interesting to see a comparison of theoretical methods and state of the art commercial thrust allocators.
- The concept of anti-spin thrust allocation has shown the potential of significant power savings and reduced power fluctuations. It will be interesting to investigate if the implementation of such a system in full scale will be beneficial taking into account the low probability of experiencing severe ventilation and in-and-out-of water events.
- In the presented work on singularity avoidance, the main contribution lies in the capability of quantifying the degree of singularity. Some initial tests on singularity avoidance were performed. However, this is certainly a field for further research. Particularly the task of deciding how to switch between two configurations with sufficient minimum gain, when the region in between has insufficient minimum gain, is a challenging problem. Also the problem of determining the most efficient solution with a certain minimum gain would be interesting to look into.

Bibliography

- K. Andresen. Thrusters for auxiliary propulsion and manoeuverability. In *Ship Propulsion Systems - International multi-teamed conference*, Manchester, UK, Desember 2000.
- ATTC. Surface ventilated flows. In *17th American Towing Tank Conference*, volume 1, pages 185–187, Pasadena, California, June 1974.
- R. Bachmayer and L. L. Whitcomb. An open loop nonlinear model based thrust controller for marine thrusters. In *International Conference on Intelligent Robots and Systems*, pages 1817–1823, Maui, USA, October 2001.
- R. Bachmayer and L. L. Whitcomb. Adaptive parameter identification of an accurate nonlinear dynamical model for marine thrusters. *Journal of Dynamic Systems, Measurements, and Control*, 125(3):491–494, September 2003.
- R. Bachmayer, L. L. Whitcomb, and M. A. Grosenbaugh. An accurate four-quadrant nonlinear dynamical model for marine thrusters: theory and experimental validation. *Journal of Oceanic Engineering*, 25(1):146–159, January 2000.
- J. Bakkeheim, T. A. Johansen, Ø. N. Smogeli, and A. J. Sørensen. Lyapunov-based integrator resetting with appliction to marine thruster control. *IEEE Transactions on Control System Technology*, Accepted.
- L. Bakoutouzis. CPP systems optimisation requirements for automatic control. In *Maritime Technology 21st Century Conference*, pages III–2–1–III–2–19, Melbourne, November 1992.
- J. G. Balchen, N. A. Jensen, E. Mathisen, and S. Sælid. Dynamic positioning system based on kalman filtering and optimal control. *Modeling, Identification and Control*, 1(3):135–163, 1980b.
- J. G. Balchen, N. A. Jensen, and S. Sælid. Dynamic positioning using kalman filtering and optimal control theory. In *IFAC/IFIP Symposium on Automation in Offshore Oil Field Operation*, pages 183–186, Bergen, Norway, 1976.
- J. G. Balchen, N. A. Jensen, and S. Sælid. Dynamic positioning of floating vessels based on kalman filtering and optimal control. In *19th IEEE Conference on Decision and Control*, pages 852–864, New York, USA, 1980a.

- S. P. Berge and T. I. Fossen. Robust control allocation of overactuated ships; experiments with a model ship. In *Preprints IFAC Conference on Maneuvering and Control of Marine Craft*, pages 193–198, Brijuni, Croatia, 1997.
- P. I. Berntsen, O. M. Aamo, B. J. Leira, and A. J. Sørensen. Structural reliability-based control of moored interconnected structures. *Control Engineering Practice*, 16(4):495–504, 2008.
- M. Blanke. *Ship propulsion losses related to automatic steering and prime mover control*. PhD thesis, Technical University of Denmark, Lyngby, Denmark, 1981.
- M. Blanke, M. Kinnaert, J. Lunze, and M. Staroswiecki. *Diagnositis and Fault-Tolerant Control*. Springer, Berlin, Germany, 2003.
- M. Blanke, K. P. Lindegaard, and T. I. Fossen. Dynamic model for thrust generation of marine propellers. In *5th IFAC Conference on Manoeuvering and Control of Marine Craft*, pages 363–368, Aalborg, Denmark, August 2000.
- M. Blanke and P. Busk Nielsen. The marine governor. In *2nd International Conference on Maritime Communications and Control*, pages 11–20, London, UK, 1990.
- M. Blanke, L. Pivano, and T. A. Johansen. An effciency optimizing propeller speed control for ships in moderate seas - model experiments and simulation. In *Conference on Control Applications in Marine Systems*, Bol, Croatia, September 2007.
- F. Borrelli, A. Bemporad, M. Fodor, and D. Hrovat. An mpc/hybrid system approach to traction control. *IEEE Transactions on Control Systems Technology*, 14(3):541–552, May 2006.
- H. Brandt. Modellversuche mit Schiffspropellern an der Wasseroberfläche. *Schiff und Hafen*, 25(5 and 6):415–422 + 493–504, 1973.
- J. S. Carlton. *Marine Propellers and Propulsion*. Butterworth-Heinemann Ltd, Oxford, England, 1994.
- K. Chachulski, W. Kozetra, and J. Szczesniak. Optimal control system for propulsion unit with controllable pitch propeller. In *3rd IFAC Workshop on Control Applications in Marine Systems*, pages 332–337, 1995.
- C. Chu, Z. L. Chan, Y. S. She, and V. Z. Yuan. The 3-bladed JD-CPP series. Technical Report SA 19549, LIPS, Drunen, The Netherlands, October 1979.
- K. P. Fleischer. Untersuchungen über das zusammenwirken von Schiff und Propeller bei teilgetauchten Propellern. Technical Report 35/73, Forschungszentrum des deutschen schiffbaus, Hamburg, Germany, 1973.
- T. I. Fossen. *Guidence and Control of Ocean Vehicles*. John Wiley and sons, West Sussex, England, 1994.

- T. I. Fossen. *Marine Control Systems, Guidance, Navigation, and Control of Ships, Rigs and Underwater Vehicles*. Marine Cybernetics, Trondheim, Norway, 2002.
- T. I. Fossen and M. Blanke. Nonlinear output feedback control of underwater vehicle propellers using feedback from estimated axial flow velocity. *Journal of Oceanic Engineering*, 25(2):241–255, April 2000.
- T. I. Fossen and T. A. Johansen. A survey of control allocation methods for ships and underwater vehicles. In *14th IEEE Mediterranean Conference on Control and Automation*, Ancona, Italy, June 2006.
- T. I. Fossen and J. P. Strand. Nonlinear passive weather optimal positioning control system for ships and rigs: Experimental results. *Automatica*, 37(5):701–715, 2001.
- H. Fukuba, S. Morita, and T. Maeda. Simulation of NOx reduction by consolidated control of main engine and CPP. *Bulletin of Marine Engineering Society in Japan*, 24(1):21–27, February 1996.
- P. T-K. Fung and M. Gimble. Dynamic ship positioning using self-tuning kalman filter. *IEEE Transactions on Automatic Control*, 28(3):339–349, 1983.
- J. Garus. Optimization of thrust allocation in the propulsion system of an underwater vehicle. *International Journal of Applied Mathematics and Computer Science*, 14(4):461–467, 2004.
- R. W. L. Gawn. Effect of pitch and blade width on propeller performance. Technical report, Institution of Naval Architects, 1953.
- M. J. Gimble. Relationship between kalman and notch filters used in dynamic ship positioning systems. *Electronics Letters*, 14(13):399–400, 1978.
- M. J. Gimble and M. A. Jonhson. *Optimal Control and Stochastic Estimation. Theory and Applications*. John Wiley and Sons Ltd., 1989.
- M. J. Gimble, R. J. Patton, and D. A. Wise. The design of dynamic positioning systems using extended kalman filtering techniques. In *OCEANS'79*, pages 488–497, 1979.
- M. J. Gimble, R. J. Patton, and D. A. Wise. The design of dynamic positioning control systems using stochastic optimal control theory. *Optimal Control Applications and Methods*, 1:167–202, 1980.
- W. Guoqiang, J. Dashan, C. Meiliang, and S. Zhenbang. Propeller air ventilation and performance of ventilated propeller. In *Fourth international symposium on Practical Design of Ships and Mobile Units*, volume 1, pages 6–1–6–8, Varna, Bulgaria, October 1989.
- F. Gutsche. Einfluss der Tauchung auf Schrub und Wirkungsgrad von Schiffpropellern. *Schiffbauforschung*, 6(5/6):256–277, 1967.

- F. A. Gutsche and G. Schroeder. Freifahruersuche an Propellern mit festen und verstellbaren Flügeln 'voraus' und 'zurück'. *Schiffbauforschung*, 2(4), 1963.
- J. Hashimoto, E. Nishikawa, and Z. Li. An experimental study on propeller air ventilation and its induced vibratory forces. *Bulletin of Marine Engineering Society of Japan*, 11(1):11–21, March 1983.
- A. J. Healey, S. M. Rock, S. Cody, D. Miles, and J. P. Brown. Toward an improved understanding of thruster dynamics for underwater vehicles. *Journal of Oceanic Engineering*, 20(4):354–361, October 1995.
- J. P. Hespanha, D. Liberzon, and A. S. Morse. Hysteresis-based switching algorithms for supervisory control of uncertain systems. *Automatica*, 39(2):263–272, February 2003.
- J. P. Hespanha and A. S. Morse. Switching between stabilizing controllers. *Automatica*, 38(11):1905–1917, November 2002.
- IMO. Guidelines for vessels with dynamic positoning systems. Technical Report MSC/Circ.645, International Maritime Organization, London, 1994.
- ITTC. ITTC-recommended procedures, 7.5-02-03-01.4. Technical report, ITTC, 1999a.
- ITTC. The special committee on unconventional propulsors, surface piercing propellers. In *22th International Towing Tank Conference*, volume 2, pages 316–317, Seoul, South Korea and Shanghai, China, September 1999b.
- N. A. Jenssen and B. Realfsen. Power optimal thruster allocation. In *Dynamic Positioning conference*, Houston, USA, October 2006.
- T. A. Johansen. Optimizing nonlinear control allocation. In *Proceedings of 43rd IEEE Conference on Decision and Control*, pages 3435–3440, Paradise Island, Bahamas, 2004.
- T. A. Johansen, T. I. Fossen, and S. P. Berge. Constrained nonlinear control allocation with singularity avoidance using sequential quadratic programming. *IEEE Trans. Control Systems Technology*, 12:211–216, 2004.
- T. A. Johansen, T. I. Fossen, and P. Tøndel. Efficient optimal constrained control allocation via multiparametric programming. *Journal of Guidance, Control and Dynamics*, 28(3):506–515, May 2005.
- T. A. Johansen, T. P. Fuglseth, P. Tøndel, and T. I. Fossen. Optimal constrained control allocation in marine surface vessels with rudder. In *Proceedings of 6th Conference on Manoeuvering and Control of Marine Crafts*, Girona, Spainia, 2003.
- T. A. Johansen, T. P. Fuglseth, P. T. Tøndel, and T. I. Fossen. Optimal constrained control allocation in marine surface vessels with rudders. *Control Engineering Practice*, 2007.

- M. R. Katebi, M. J. Gimble, and Y. Zhang. H_∞ robust control design for dynamic ship positioning. In *IEEE Control Theory and Applications*, number 2 in 144, pages 110–120, 1997a.
- M. R. Katebi, Y. Zhang, and M. J. Gimble. Nonlinear dynamic ship positioning. In *13th IFAC World Congress*, number Q in 13, pages 303–380, 1997b.
- H. K. Khalil. *Nonlinear systems*. Prentice Hall, New Jersey, USA, 2000. Third edition.
- C. Kruppa. Testing of partially submerged propellers. In *13th International Towing Tank Conference*, volume 1, pages 761–775, Berlin/Hamburg, Germany, September 1972. Report of cavitation committee, appendix V.
- E. Lehn. Practical methods for estimation of thrust losses. Technical Report 513003.00.06, MARINTEK, Trondheim, Norway, January 1992.
- B. J. Leira, A. J. Sørensen, and C. M. Larsen. A reliability-based control algorithm for dynamic positioning of floating vessels. *Structual Safety*, 26(1):1–28, 2004.
- C. C. Liang and W. H. Cheng. The optimum control of thruster system for dynamically positioned vessels. *Ocean Engineering*, 31(1):97–110, January 2004.
- K. P. Lindegaard. *Acceleration Feedback in Dynamic Positioning*. PhD thesis, Norwegian University of Science and Technology, Trondheim, Norway, 2003.
- K. P. Lindegaard and T. I. Fossen. Fuel-efficient rudder and propeller control allocation for marine craft: Experiments with a model ship. *IEEE Trans. Control Systems Technology*, 11(6):850–862, November 2003.
- I. Lindfors. Thrust allocation method for the dynamic positioning system. In *10th International Ship Control Systems Symposium*, pages 3.93–3.106, Ottawa, Canada, 1993.
- K. Madsen and O. Tingleff. Robust subroutines for non-linear optimization. Technical Report NI-90-06, Technical University of Denmark, Denmark, 1990.
- M. Margaliot. Stability analysis of switched systems using variational principles: An introduction. *Automatica*, 42(12):2059–2077, December 2006.
- R. H. Middleton, G. C. Goodwin, D. J. Hill, and D. Q. Mayne. Design issues in adaptive control. *IEEE Transactions on Automatic Control*, 33(1):50–58, January 1988.
- K. J. Minsaas, H. J. Thon, and W. Kauczynski. Estimation of required thruster capacity for operation of offshore vessels under severe weather conditions. In *PRADS*, pages 411–427, Trondheim, Norway, June 1987.

- A. S. Morse. Supervisory control of families of linear set-point controllers—part 1: Exact matching. *IEEE Transactions on Automatic Control*, 41(10):1413–1431, October 1996.
- A. S. Morse. Supervisory control of families of linear set-point controllers—part 2: Robustness. *IEEE Transactions on Automatic Control*, 42(11):1500–1515, November 1997.
- A. S. Morse, D. Q. Mayne, and G. C. Goodwin. Applications of hysteresis switching in parameter adaptive control. *IEEE Transactions on Automatic Control*, 37(9):1343–1354, September 1992.
- R. A. Morvillo. Application of modern digital controls to improve the operational efficiency of controllable pitch propellers. In *SNAME Annual Meeting Technical Sessions*, pages 6–1–6–15, New York City, October 1996.
- D. T. Nguyen. *Design of hybride marine control systems for dynamic positioning*. PhD thesis, National University of Singapore, Singapore, 2005.
- T. D. Nguyen, A. J. Sørensen, and S. T. Quek. Design of hybrid controller for dynamic positioning from calm to extreme sea conditions. *Automatica*, 43(5):768–785, May 2007.
- T. D. Nguyen, A. J. Sørensen, and S. T. Quek. Multi-operational hybrid controller structure for station keeping and transit operations of marine vessels. *IEEE Transactions on Control System Technology*, 16(3):491–498, 2008.
- J. Nocedal and S. J. Wright. *Numerical optimization*. Springer, New York, 1999.
- NTNU. Marine system simulator, 2006. Computer program, www.cesos.ntnu.no/mss.
- N. Olofsson. *Force and flow characteristics of a partially submerged propeller*. PhD thesis, Chalmers University of Technology, Göteborg, Sweden, 1996.
- M. W. C. Oosterveld. Wake adapted ducted propellers. Technical Report No.345, Netherland ship model basin, Wageningen, Netherlands, 1970.
- M. G. Parsons and J. Y.-C. Wu. Limit cycles in diesel/controllable pitch propeller propulsion systems using load control. *International Shipbuilding Progress*, 32 (375):246–263, November 1985.
- J. A. M. Peterson and M. Bodson. Constrained quadratic programming techniques for control allocation. *Control Systems Technology*, 14(1):91–97, January 2006.
- K. Y. Pettersen, F. Mazenc, and H. Nijmeijer. Global uniform asymptotic stabilization of an underactuated surface vessel: Experimental results. *IEEE Transactions on Control System Technology*, 12(6):891–903, November 2004.

- L. Pivano. *Thrust Estimation and Control of Marine Propellers in Four-Quadrant Operations*. PhD thesis, Norwegian University of Science and Technology, Trondheim, Norway, 2008.
- E. Ruth. *Modelling and control of controllable pitch thrusters subject to large losses*. Master thesis, Department of Marine Technology, Norwegian University of Science and Technology, Trondheim, Norway, 2005.
- E. Ruth and Ø. N. Smogeli. Ventilation of controllable pitch thrusters. *Marine Technology and SNAME news*, 43(4):170–179, October 2006.
- E. Ruth, Ø. N. Smogeli, T. Perez, and A. J. Sørensen. Anti-spin thrust allocation for marine vessels. *IEEE Transactions on Control System Technology*, Accepted.
- E. Ruth, Ø. N. Smogeli, and A. J. Sørensen. Overview of propulsion control for surface vessels. In *7th IFAC Conference on Manoeuvring and Control of Marine Craft*, Lisbon, Portugal, September 2006.
- E. Ruth and A. J. Sørensen. Design of thruster configurations. In *International Marine Design Conference*, Trondheim, Norway, Submitted-a.
- E. Ruth and A. J. Sørensen. Singularities in marine control allocation with bi- and unidirectional thrusters. *Automatica*, Submitted-b.
- E. Ruth, A. J. Sørensen, and T. Perez. Thrust allocation with linear constrained quadratic cost function. In *Conference on Control Applications in Marine Systems*, Bol, Croatia, September 2007.
- F. Schanz. The controllable pitch propeller as an integral part of the ship's propulsion system. In *SNAME Annual Meeting*, number 6, pages 1–24, New York, November 1967.
- J. O. Scherer. Partially submerged and supercavitating propeller systems. In *18th general meeting of the American Towing Tank Conference*, volume 1, pages 161–166, Annapolis, Maryland, USA, August 1977.
- K. Schittkowski. qld.c, July 1992. Computer program.
- H. Shiba. Air-drawing of marine propellers. Technical report, Transportation technical research institute, Tokyo, Japan, August 1953.
- P. Sinding and S. V. Anderson. A force allocation strategy for dynamic positioning. In *Proceedings of the Eight International Offshore and Polar Engineering Conference*, pages 346–353, Montreal, Canada, May 1998.
- S. Skogestad and I. Postlethwaite. *Multivariable Feedback Control*. Wiley, West Sussex, England, 2007.
- S. Sælid, N. A. Jensen, and J. G. Balchen. Design and analysis of a dynamic positioning system based on kalman filtering and optimal control. *IEEE Transaction on Automatic Control*, 28(3):331–339, 1983.

- D. A. Smallwood and L. L. Whitcomb. The effect of model accuracy and thruster saturation on tracking performance of model based controllers for underwater robotic vehicles: Experimental results. In *International Conference on Intelligent Robots and Systems*, pages 1081–1087, Washington, USA, May 2002.
- Ø. N. Smogeli. *Control of Marine Propellers, From Normal to Extreme Conditions*. PhD thesis, Norwegian University of Science and Technology, Trondheim, Norway, 2006. <http://urn.nb.no/urn:nbn:no:ntnu:diva-1463>.
- Ø. N. Smogeli, L. Aarseth, E. S. Overå, A. J. Sørensen, and K. J. Minsaas. Anti-spin thruster control in extreme seas. In *6th IFAC Conference on Manoeuvering and Control of Marine Craft*, pages 221–226, Girona, Spain, September 2003.
- Ø. N. Smogeli, J. Hansen, A. J. Sørensen, and T. A. Johansen. Anti-spin control for marine propulsion systems. In *43rd IEEE Conference on Decision and Control*, Paradise Island, Bahamas, December 2004a.
- Ø. N. Smogeli, E. Ruth, and A. J. Sørensen. Experimental validation of power and torque thruster control. In *Joint 2005 International Symposium on Intelligent Control and 13th Mediterranean Conference on Control and Automation*, Limassol, Cyprus, 2005.
- Ø. N. Smogeli, A. J. Sørensen, and T. I. Fossen. Design of a hybrid power/torque thruster controller with loss estimation. In *IFAC Conference on Control Applications in Marine Systems*, Ancona, Italy, 2004b.
- Ø. N. Smogeli, A. J. Sørensen, and K. J. Minsaas. The concept of anti-spin thruster control. *Control Engineering Practice*, 16(4):465–481, April 2008.
- O. J. Sørdalen. Thrust allocation: Singularities and filtering. In *13th World Congress of IFAC*, volume Q, pages 369–374, San Francisco, USA, 1996.
- O. J. Sørdalen. Full sea trials with optimal thrust allocation. In *Preprints IFAC Conference on Maneuvering and Control of Marine Craft*, pages 177–182, Brijuni, Croatia, 1997a.
- O. J. Sørdalen. Optimal thrust allocation for marine vessels. *Control Engineering Practice*, 5:1223–1231, 1997b.
- A. J. Sørensen. *Marine Cybernetics, Modeling and Control*. Department of Marine Technology, NTNU, Trondheim, 2004.
- A. J. Sørensen, A. K. Ådnanes, T. I. Fossen, and J-P. Strand. A new method of thruster control in positioning of ships based on power control. In *4th IFAC Conference on Maneuvering and Control of Marine Craft*, Brijuni, Croatia, September 1997.

- A. J. Sørensen, B. Leira, J. P. Strand, and C. M. Larsen. Optimal setpoint chasing in dynamic positioning of deep-water drilling and intervention vessels. *Journal of Robust and Nonlinear Control*, 11:1187–1205, 2001.
- A. J. Sørensen, S. T. Quek, and T. D. Nguyen. Improved operability and safety of dp vessels using hybride control concept. In *OSV*, Singapore, 2005.
- A. J. Sørensen, S. I. Sagtun, and T. I. Fossen. The design of a dynamic positioning system using model-based control. *Control Engineering Practice*, 4(3):359–368, 1996.
- A. J. Sørensen and J. P. Strand. Positioning of small-waterplane-area marine constructions with roll and pitch damping. *Control Engineering Practice*, 8 (2):205–213, 2000.
- A. J. Sørensen, J. P. Strand, and H. Nyberg. Dynamic positioning of ships and floaters in extreme seas. In *OCEANS'02 MTS/IEEE*, Biloxi, MS, USA, 2002.
- H. R. Sørheim. *Dynamic positioning in Single Point - A Theoretical Analysis of Motions, and Design and Evaluation of an Optimal Control System*. PhD thesis, Norwegian University of Science and Technology, Trondheim, Norway, 1981.
- J. P. Strand. *Nonlinear Positioning Control Systems Design for Marine Vessels*. PhD thesis, Norwegian University of Science and Technology, Trondheim, Norway, 1999.
- J. P. Strand, A. J. Sørensen, and T. I. Fossen. Design of automatic thruster assisted position mooring systems for ships. *Modeling, Identification and Control*, 19(2):61–75, 1998.
- G. Strang. *Linear Algebra and its Applications*. Thomson Learning Inc., USA, 1988. Third edition.
- J. B. Strømquist. *Evaluation of Linearly Constrained Quadratic Thrust Allocation With Respect to Faults*. Master thesis, Norwegian University of Science and Technology, Trondheim, Norway, 2007.
- J. Strom-Jensen and R. R. Porter. Prediction of controllable-pitch propeller performance in off-design conditions. In *Third Ship Control Systems Symposium, Paper VII B-1*, 1972.
- T. L. Swanson. A generalized propulsion control logic. In *IEEE International Conference on Engineering in the Ocean Environment*, pages 723–727, Washington D.C., USA, September 1982.
- J. Tjønnås and T. A. Johansen. Optimizing nonlinear adaptive control allocation. In *IFAC World Congress*, Prague, Czech Republic, 2005.
- J. Tjønnås and T. A. Johansen. On optimizing nonlinear adaptive control allocation with actuator dynamics. In *7th IFAC Symposium on Nonlinear Control Systems*, Pretoria, South Africa, 2007.

- W. P. A. van Lammeren, J. D. van Manen, and M. W. C. Oosterveld. The Wageningen B-Screw series. In *SNAME*, number 8, 1969.
- H. Wagner. Über die Entstehung des dynamischen Auftriebes vom Tragflügeln. *Z.f.a.MM*, 5(1):17–35, Februar 1925.
- W. C. Webster and J. Sousa. Optimum allocation for multiple thrusters. In *Proc. International Society of Offshore and Polar Engineers Conference*, Brest, France, 1999.
- R. Whalley and M. Ebrahimi. Gas turbine propulsion plant control. *Naval Engineers Journal*, 114(4):79–94, Fall 2002.
- L. L. Whitcomb and D. R. Yoerger. Comparative experiments in the dynamics and model-based control of marine thrusters. In *MTS/IEEE Oceans Conference*, pages 1019–1028, San Diego, USA, October 1995.
- L. L. Whitcomb and D. R. Yoerger. Development, comparison, and preliminary experimental validation of nonlinear dynamic thruster models. *Journal of Oceanic Engineering*, 24(4):481–493, October 1999a.
- L. L. Whitcomb and D. R. Yoerger. Preliminary experiments in model-based thruster control for underwater vehicle positioning. *Journal of Oceanic Engineering*, 24(4):495–506, October 1999b.
- D. E. Winterbone. Adaptive multi-variable control of ship propulsion plant. In *3rd IFAC symposium on Ship Operation Automation*, pages 305–312, Tokyo, Japan, November 1980.
- D. R. Yoerger, J. G. Cooke, and J. E. Slotine. The influence of thruster dynamics on underwater vehicle behavior and their incorporation into control system design. *Journal of Oceanic Engineering*, 15(3):167–178, July 1990.
- K. Young-Bok, J. Byun, B. Jung, and J. Yang. Optimization control for fuel consumption of a ship propulsion system with CPP using decoupling and LMI approach. In *Control Applications in Marine Systems*, pages 315–320, Fukuoka, Japan, October 1998.

Appendix A

Experimental setup: Open water experiments

The open water tests of the ventilation model were conducted in the MCLab basin. The tests were performed with a fixed pitch propeller as it was no available test rig with a controllable pitch propeller. The tests were carried out 17-19 of October 2005 by Øyvind N. Smogeli and the author of this thesis. The information flow in the control system can be seen in Figure A.1.

A photo of the test setup, without the duct present, is shown in Figure A.2. It is possible to see the indication of the propeller as a metal piece between two red fittings. A photo of the propeller with duct, taken during the previously conducted cavitation tunnel results are shown in Figure A.3.

The main dimensions of the propeller, duct and motor are given in Table 2.3, 2.4 and A.1. The control of the propeller was done by a real-time computer (control PC) communicating with the motor drive. The real-time computer was able to control the propeller in shaft speed, torque and power control mode by sending a torque demand to the motor drive. The control system is illustrated in Figure A.1. The measured variables are shown in Table A.2. In order to vary the submergence, the whole propeller rig was moved up and down by the towing carriage.

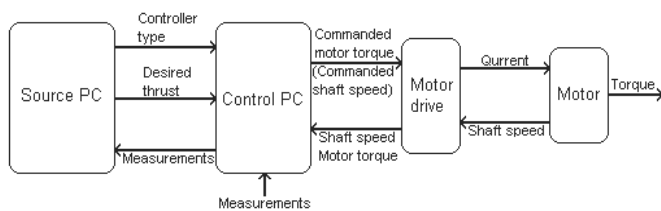


Figure A.1: Information flow in the physical control system.

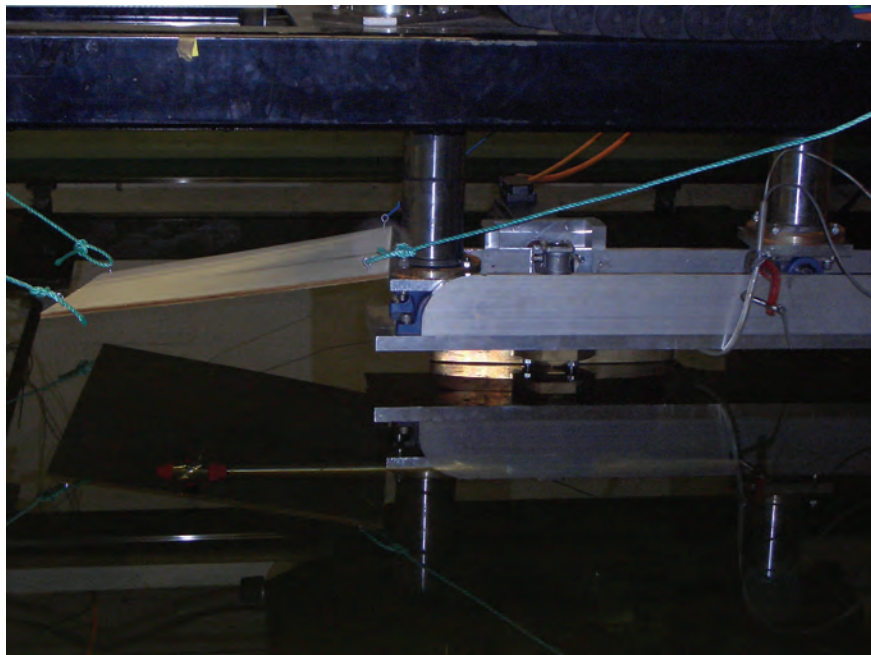


Figure A.2: Photograph of the test setup without the duct present.

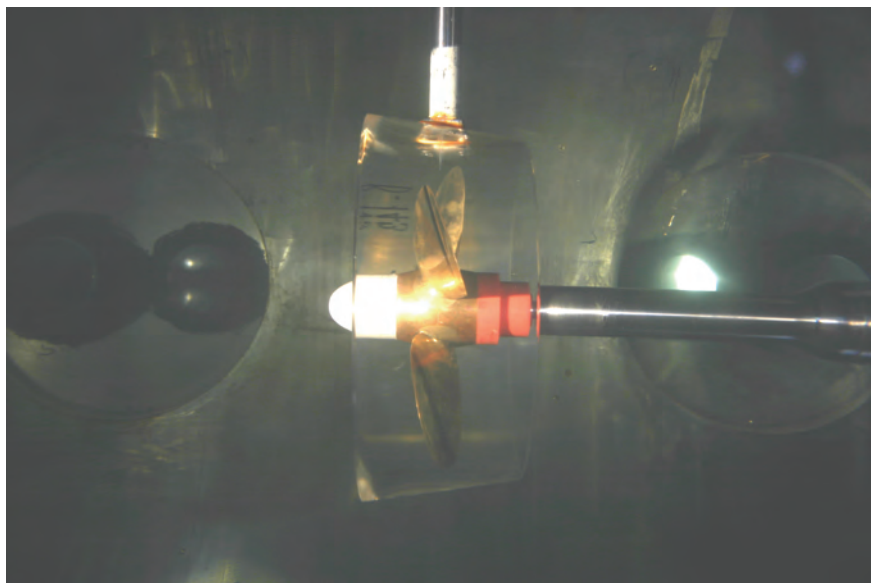


Figure A.3: Propeller with duct in the cavitation tunnel.

Table A.1: Motor data in experiment.

Type	Bosch MKD071-61	
Nominal motor speed	4500	[rev/min.]
Max. motor speed	6000	[rev/min.]
Torque at standstill	8.0	[Nm]
Theoretical maximum torque	32.0	[Nm]

Table A.2: Variables measured in the model tests.

Variable	Symbol	Unit
Shaft speed	n	[1/s]
Motor torque	Q_m	[Nm]
Propeller thrust	T_p	[N]
Propeller torque	Q_p	[Nm]

Appendix B

Experimental setup: CyberShip III

Experiments with CyberShip III were conducted in the MCLab basin. The tests where conducted from 25th of October to 15th of November. All parameters are given in SI units. Angles are given in radians. The control system ran at 5[Hz]. Two reference frames were used to formulate the guidance, navigation and control system: the body frame and the NED frame. For details on the reference frames see Fossen (2002). The main particulars of CyberShip III are given in Table 4.1.

B.1 Wave maker

The wave maker system consisted of a computer, an amplifier and the flap. The system used was the "DHI Wave Synthesizer". In the experiments regular sinusoidal waves were used in order to remove the random elements of waves generated by wave spectrums.

B.2 Measurements

The available measurements were: the shaft speed of the propellers, measured by the motor encoder, the azimuth angles, measured by potentiometers, the vessel position, measured by an optical system, motor voltage measured by differential amplifier, motor current measured by Hall effect, and joystick position.

B.2.1 Position measurement

For position measurements, the "Qualisys" system was used. The system consisted of four cameras and a computer. The cameras were positioned on the towing carriage and their position can be seen in Figure B.1. The "Qualisys Track Manager 1.9.260" software was used to deliver real time six degree of



Figure B.1: Picture of basin and positioning system.

freedom (surge, sway, heave, roll, pitch and yaw) position measurements. The system relied on markers positioned on the model. A picture of the positions of the markers on CyberShip III is seen in Figure B.2. The position measurement system was set to sample at 10[Hz].

B.2.2 Power measurements

Power measurements were build by the author of this thesis. A picture of a circuit board is shown in Figure B.3. This circuit measured the current and voltage of the forward thrusters. In Figure B.4 the results from the reference tests are shown. The green line shows the consumed power, the black line shows the developed power, and the red line shows the power consumed by the propeller. The equations are:

$$\mathbf{P}_C = \mathbf{v}_{RAW} \mathbf{i}_{RAW}, \quad (B.1)$$

$$\mathbf{P}_D = \mathbf{P}_C \eta_m(\mathbf{n}_{RAW}), \quad (B.2)$$

$$= 2\pi \mathbf{k}_{curr} \mathbf{i}_{RAW} \mathbf{n}_{RAW}, \quad (B.3)$$

$$\mathbf{P}_F = \text{diag}(\mathbf{a}) \mathbf{n}_{RAW} + b + \text{diag}(\mathbf{c}) \text{sign}(\mathbf{n}_{RAW}), \quad (B.4)$$

$$\mathbf{P}_P = \mathbf{P}_D - \mathbf{P}_F, \quad (B.5)$$

where $\mathbf{P}_C \in \mathbb{R}^4$ is the consumed power, $\mathbf{v}_{RAW} \in \mathbb{R}^4$ is the measured voltage, $\mathbf{i}_{RAW} \in \mathbb{R}^4$ is the measured current, $\mathbf{P}_D \in \mathbb{R}^4$ is the developed power, $\eta_m \in \mathbb{R}^4$ is the motor efficiency, $\mathbf{k}_{curr} \in \mathbb{R}^4$ is the torque constant of the motor, $\mathbf{P}_F \in \mathbb{R}^4$

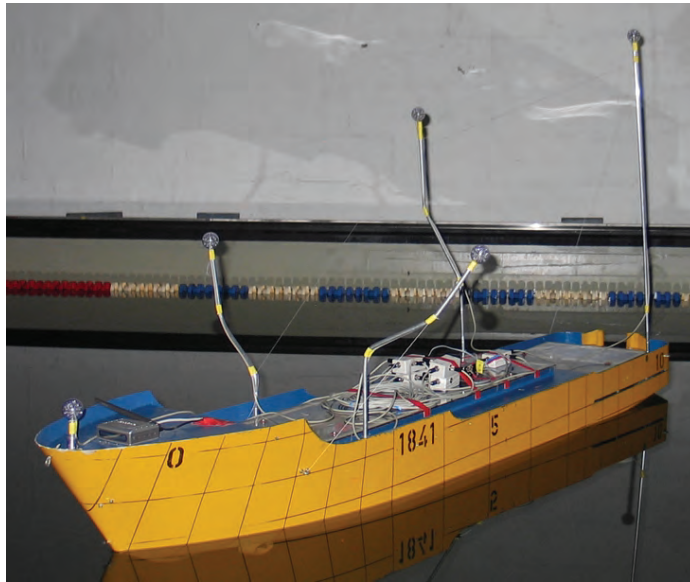


Figure B.2: Picture of CS3 with markers and forward trim.

is the power consumed by friction, $\mathbf{P}_P \in \mathbb{R}^4$ is the power consumed by the propeller, and $\mathbf{a} \in \mathbb{R}^4$, $\mathbf{b} \in \mathbb{R}^4$ and $\mathbf{c} \in \mathbb{R}^4$ are coefficients determined by running the propellers in air. It was chosen to use the developed power as background for calculating the weighting in the thrust allocator, and in the power measurements. This was because the consumed power was significantly affected by the efficiency of the motors. Particularly the aft thrusters operated at unfavorable conditions, and hence had an unrealistically low efficiency compared to the forward thrusters. The developed power was also used since this is the measurement available in full scale, and due to the fact that it was too difficult separate friction and propeller power for the tunnel thruster.

B.3 Control systems

The layout of the control system is seen in Figure B.5.

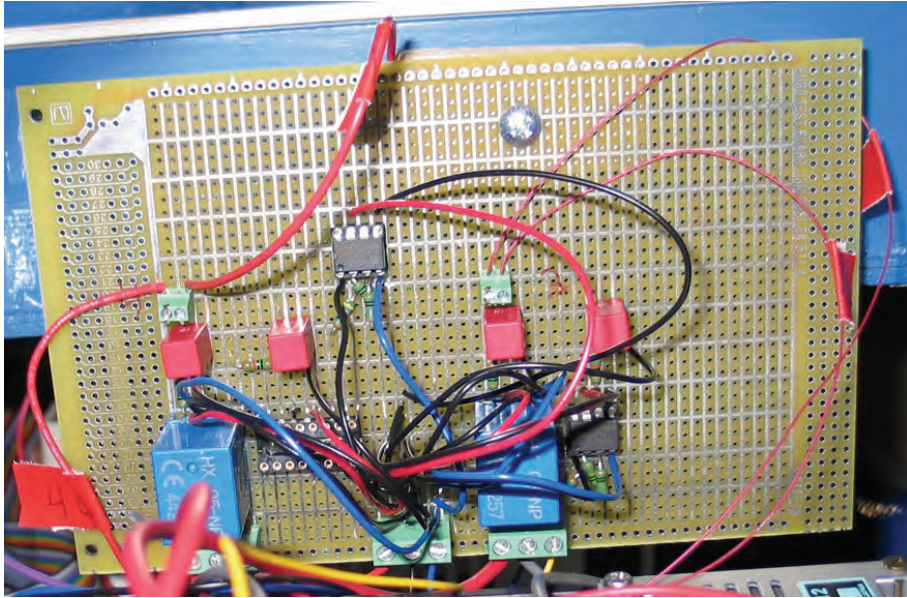


Figure B.3: Picture of circuit build by the author.

B.3.1 Position and velocity observer

The passive nonlinear observer for velocity and wave frequency motion in Fossen (2002) was used. The values of the parameters were:

$$\mathbf{M} = \begin{bmatrix} 75 & 0 & 0 \\ 0 & 77 & -1.07 \\ 0 & -1.07 & 14.7 \end{bmatrix}, \quad (\text{B.6})$$

$$\mathbf{D} = \begin{bmatrix} 6.9 & 0 & 0 \\ 0 & 19.3 & 0.59 \\ 0 & 0.59 & 6.8 \end{bmatrix}, \quad (\text{B.7})$$

$$\mathbf{A}_w = \begin{bmatrix} -2\lambda\omega_0 & \omega_0^2 \\ \mathbf{I}_{3 \times 3} & \mathbf{0}_{3 \times 3} \end{bmatrix}, \quad (\text{B.8})$$

$$\mathbf{C}_w = [\mathbf{I}_{3 \times 3} \ \mathbf{0}_{3 \times 3}], \quad (\text{B.9})$$

$$\mathbf{T} = \text{diag}(1, 1, 1) \cdot 10^7, \quad (\text{B.10})$$

$$\mathbf{K}_1 = \begin{bmatrix} 2\omega_0(\mathbf{I}_{3 \times 3} - \boldsymbol{\lambda}) \\ -2(\mathbf{I}_{3 \times 3} - \boldsymbol{\lambda})\omega_c\omega_0^{-1} \end{bmatrix}, \quad (\text{B.11})$$

$$\mathbf{K}_2 = \boldsymbol{\omega}_c, \mathbf{K}_3 = \text{diag}(25, 20, 25), \quad (\text{B.12})$$

$$\mathbf{K}_4 = \text{diag}(300, 300, 188), \boldsymbol{\lambda} = 0.1\mathbf{I}_{3 \times 3}, \quad (\text{B.13})$$

$$\omega_0 = 4.66\mathbf{I}_{3 \times 3}, \boldsymbol{\omega}_c = 1.22\omega_0. \quad (\text{B.14})$$

Although the mass of the vessel was 89[kg] (Table 4.1), it was observed

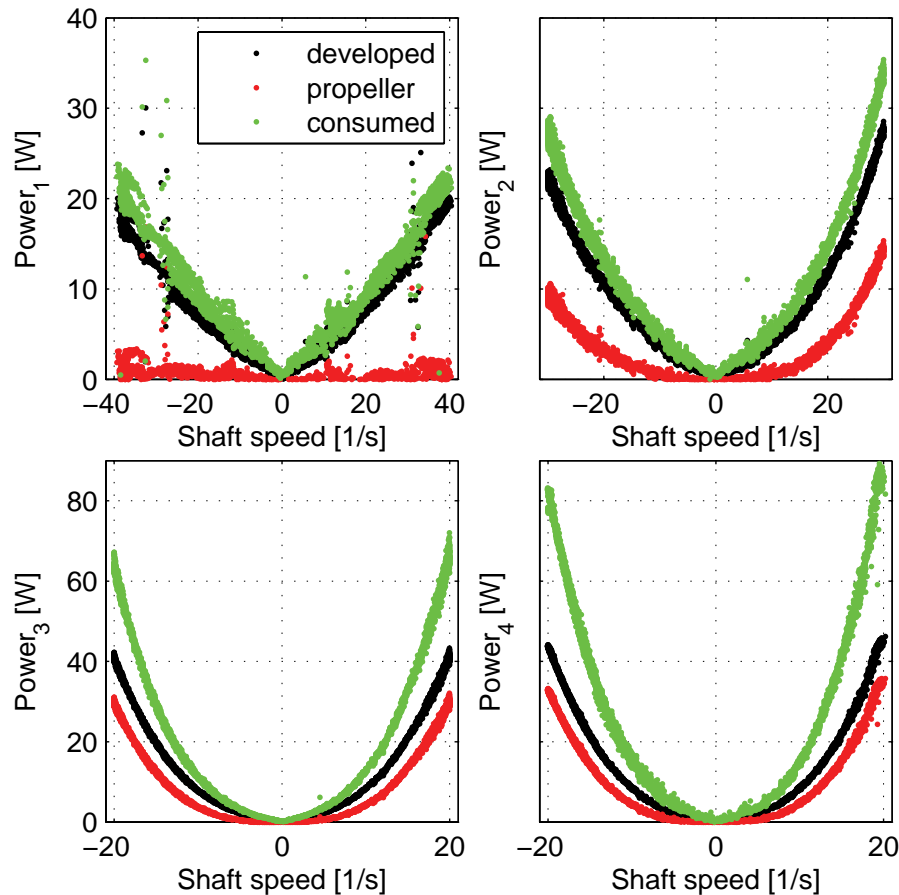


Figure B.4: Different types of power for the individual thrusters as function of shaft speed.

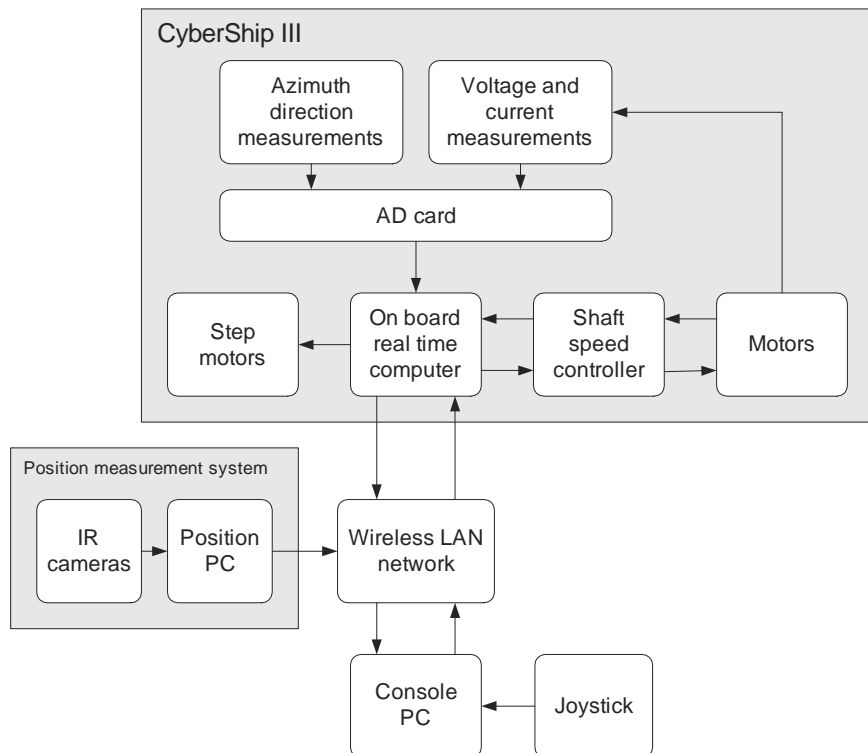


Figure B.5: Control system for CyberShip III.

that the specified parameters for the \mathbf{M} matrix gave better performance of the observer. However, in general we still recommend to start the tuning with a mass matrix containing both rigid body inertia and hydrodynamic added mass. With other combinations of tuning parameters this may have worked equally well.

B.3.2 Reference generator

The reference generator was a second order filter (Fossen 2002). The filter could be reset to the current position and speed. The vessel velocities generated by the reference generator were limited to $\pm 0.10[m/s]$. The filter frequency was set to $0.5[rad/s]$.

B.3.3 PID motion controller

The surge, sway and yaw position were controlled by a nonlinear PID controller (NTNU 2006):

$$\begin{aligned}\tau_d = & -\mathbf{K}_D \hat{\nu} + \mathbf{K}_P \mathbf{R}^T(\hat{\eta}_3)(\boldsymbol{\eta}_d - \hat{\boldsymbol{\eta}}), \\ & + \mathbf{K}_I \int_0^t \mathbf{R}^T(\hat{\eta}_3)(\boldsymbol{\eta}_d - \hat{\boldsymbol{\eta}}) dt,\end{aligned}\quad (\text{B.15})$$

where $\hat{\nu} \in \mathbb{R}^3$ is the estimated vessel velocity in the body frame, $\mathbf{R}^T(\eta_3) \in \mathbb{R}^{3 \times 3}$ is a rotation matrix for transformation between NED and body frame, $\hat{\boldsymbol{\eta}} \in \mathbb{R}^3$ and $\boldsymbol{\eta}_d \in \mathbb{R}^3$ are the estimated and desired vessel position the NED frame, and $t \in \mathbb{R}$ is the time. The PID motion controller gains were:

$$\mathbf{K}_D = \text{diag}(98, 89, 14), \quad (\text{B.16})$$

$$\mathbf{K}_P = \text{diag}(75, 77, 15), \quad (\text{B.17})$$

$$\mathbf{K}_I = \text{diag}(3.0, 3.1, 0.59). \quad (\text{B.18})$$

B.3.4 Thrust allocator

The thrust allocation parameters were:

$$\gamma = 1000, \quad (\text{B.19})$$

$$\mathbf{W}_v = \text{diag}(1, 1, 10), \quad (\text{B.20})$$

$$\mathbf{L}_x = [0.84, 0.76, -0.81, -0.81], \quad (\text{B.21})$$

$$\mathbf{L}_y = [0.0, 0.0, -0.11, 0.11], \quad (\text{B.22})$$

$$\mathbf{T}_{\min} = [-0.47, -4.7, -10.1, -9.0], \quad (\text{B.23})$$

$$\mathbf{T}_{\max} = [0.58, 8.7, 13.5, 13.0], \quad (\text{B.24})$$

$$\Delta \mathbf{T}_{\max} = -\Delta \mathbf{T}_{\min} = 0.2T_{\max}, \quad (\text{B.25})$$

$$\alpha_{\max} = +\infty, \alpha_{\min} = -\infty, \quad (\text{B.26})$$

$$\Delta \boldsymbol{\alpha}_{\max} = [1, 1, 1, 1] \cdot 0.21, \quad (\text{B.27})$$

$$\mathbf{T}_+ = \min(\mathbf{T}_{\max}, \mathbf{T}_0 + \Delta \mathbf{T}_{\max}), \quad (\text{B.28})$$

$$\mathbf{T}_- = \max(\mathbf{T}_{\min}, \mathbf{T}_0 + \Delta \mathbf{T}_{\min}), \quad (\text{B.29})$$

$$\boldsymbol{\alpha}_+ = \min(\boldsymbol{\alpha}_{\max}, \boldsymbol{\alpha}_0 + \Delta \boldsymbol{\alpha}_{\max}), \quad (\text{B.30})$$

$$\boldsymbol{\alpha}_- = \max(\boldsymbol{\alpha}_{\min}, \boldsymbol{\alpha}_0 - \Delta \boldsymbol{\alpha}_{\max}). \quad (\text{B.31})$$

In all tests but the anti-spin tests:

$$\mathbf{W}_u = \text{diag}(14, 1.2, 0.85, 0.87). \quad (\text{B.32})$$

In the anti-spin test:

$$\mathbf{W}_u = \text{diag}(6.62, 1.2, 0.90, 0.91). \quad (\text{B.33})$$

Different \mathbf{W}_u 's were used since the cost was calculated based on $\mathbf{T}^{3/2}$ in the anti-spin cases, compared to \mathbf{T}^2 in the other cases. The particular QP solver used, qld.c, was written by Schittkowski (1992).

B.3.5 Thruster control

Due to hardware limitations, the thrusts were controlled by shaft speed control (3.8). The parameters used in the shaft speed controller were:

$$\mathbf{K}_{Tc} = [0.36, 0.52, 0.42, 0.46], \quad (\text{B.34})$$

$$\mathbf{D} = [0.03, 0.06, 0.09, 0.09], \quad (\text{B.35})$$

$$\rho = 1000. \quad (\text{B.36})$$

B.3.6 Azimuth direction controller

The azimuth direction controller was a modified P controller. It was modified in order to avoid scattering due to noise in the $\boldsymbol{\alpha}_{RAW}$ measurements. This was done by letting the output be proportional to $\boldsymbol{\alpha}_{RAW,j}^2$ for $\boldsymbol{\alpha}_{RAW,j} \leq 3.3[\text{deg}]$:

$$\tilde{\alpha}_j = \alpha_{c,j} - \alpha_{RAW,j}, \quad (B.37)$$

$$steps_j = \begin{cases} 689 |\tilde{\alpha}_j| \tilde{\alpha}_j, & \text{if } \tilde{\alpha}_j \leq 0.058, \\ 40.1 \tilde{\alpha}_j, & \text{if } \tilde{\alpha}_j \geq 0.058, \end{cases} \quad (B.38)$$

where α_c is the commanded azimuth direction, $steps$ is the output to the step motor, and j indexes the different thrusters.

B.3.7 Ventilation detection

The ventilation detection method in Section 5.2 was modified in order to work with the current experimental setup. In anti-spin thruster control the sampling speed is in the order of hundreds of Hz . In our implementation the sampling speed was $5[Hz]$, in order to match a typical DP system. As a result of this, the torque was not observed, but simply calculated based on the measurements of current and shaft speed. The shaft speed was used in order to subtract the friction torque from the motor torque.

$$\mathbf{Q}_p(I_{RAW}, n_{RAW}) = \mathbf{Q}_m(I_{RAW}) - \mathbf{Q}_f(n_{RAW}), \quad (B.39)$$

$$\beta_Q(I_{RAW}, n_{RAW}) = \frac{\mathbf{Q}_p(I_{RAW}, n_{RAW})}{\mathbf{Q}_{nom}(n_{RAW})}, \quad (B.40)$$

where \mathbf{Q}_f is the friction torque. The criteria for detecting the ventilation start were:

$$|\mathbf{n}_{RAW,j}| > \mathbf{n}_{lim,j} = \begin{cases} 5, & \text{if } j = 3, 4, \\ 50, & \text{else,} \end{cases} \quad (B.41)$$

$$\beta_{Q,j} < \beta_{Q,on,j} = 0.5, \quad (B.42)$$

$$\dot{\mathbf{n}}_j > \dot{\mathbf{n}}_{lim,j} = -10, \quad (B.43)$$

where $\dot{\mathbf{n}}_{lim} \in \mathbb{R}^4$ is the minimum allowed change in \mathbf{n}_{RAW} . The limitation in (B.43) was introduced in order to avoid detecting ventilation if the shaft speed of the propeller was rapidly reduced. The values of $n_{lim,j}$ was chosen such that ventilation was never detected on the forward thrusters. For thruster number 1 this was done because the physical design of the thruster made ventilation detection very difficult and because the maximum thrust was very low compared to the others. For thruster number 2 ventilation detection was denied because the thruster was deeply submerged under the hull and was hence assumed to never experience ventilation.

The criterion for detecting the ventilation stop was:

$$\beta_{Q,j} > \beta_{Q,off,j} = 0.8. \quad (B.44)$$

The ventilation flag ζ_j changed to 1 if (B.41)-(B.43) were true, and changed to 0 if (B.44) was true. Else the value of the ventilation parameter was held. Equations (5.16)-(5.18) were used to modify the cost function.

Appendix C

Experimental Results: CyberShip III

This chapter contains supplementary figures to the results already presented in Chapter 4, 5, 6 and 7. An overview of the tests are presented in Table C.1.

Table C.1: Overview of model tests with CyberShip III.

Run	Waves		What is tested
	Amplitude	Period	
A	0.06[m]	0.8[s]	Station keeping, convex linearly constrained quadratic thrust allocator
B	–	–	Joystick, convex linearly constrained quadratic thrust allocator
C	0.04[m]	0.8[s]	Anti-spin thrust allocation, redistribution
D	0.06[m]	0.8[s]	Anti-spin thrust allocation, power reduction and smoothing
E	0.03[m]	0.8[s]	Anti-spin thrust allocation, positioning accuracy
F	0.03[m]	0.8[s]	Maneuvering, nonconvex linearly constrained quadratic thrust allocator
G	0.04[m] 0.00[m]	0.8[s] –	Switching between fixed and rotating thrusters dependent on environment
H	0.03[m]	0.8[s]	Thrust failures
I	0.03[m]	0.8[s]	Azimuth failures
J	–	–	Minimum attainable set
K	–	–	Avoiding small minimum gains

C.1 Run A: Station keeping, convex.

The main results from this run is found in Section 4.5.1. In Figure C.1 it is seen that the thrust allocator commands the desired generalized force. In Figure C.2 the thrust directions are shown. It is clearly seen that the thrusters start to rotate at 826[s]. It is also seen that the rate limitations in the thrust allocator ensures that the azimuth mechanism keeps up with it's desired signal. In Figure C.3 the thruster forces are shown. The peaks at 828[s] are caused by the thrusters rotating through near singular configurations, requiring an enormous amount of thruster force.

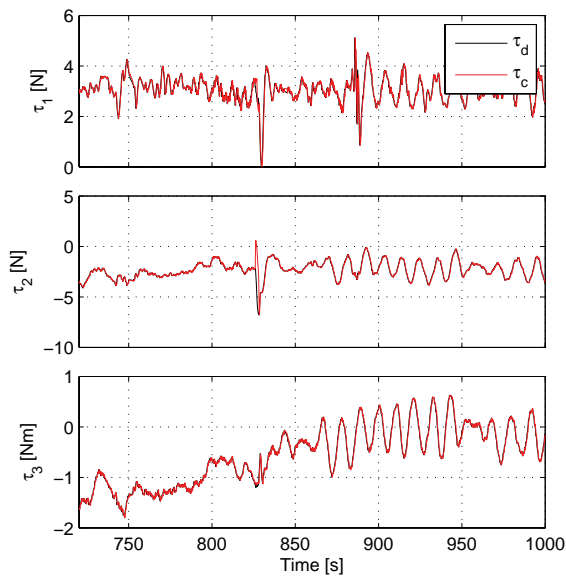


Figure C.1: Generalized force during Run A.

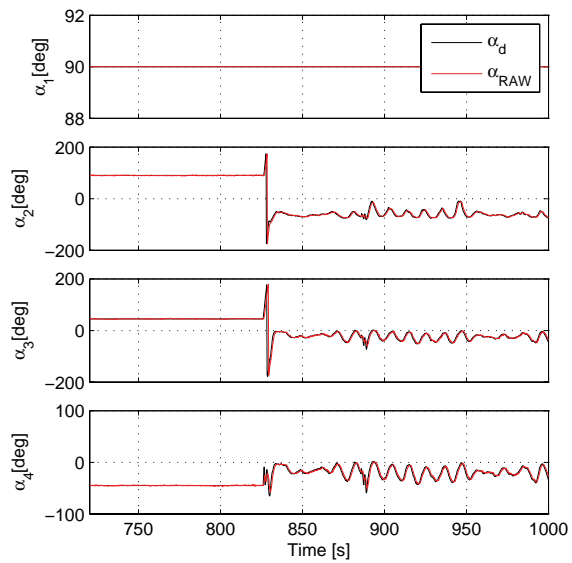


Figure C.2: Thrust directions during Run A.

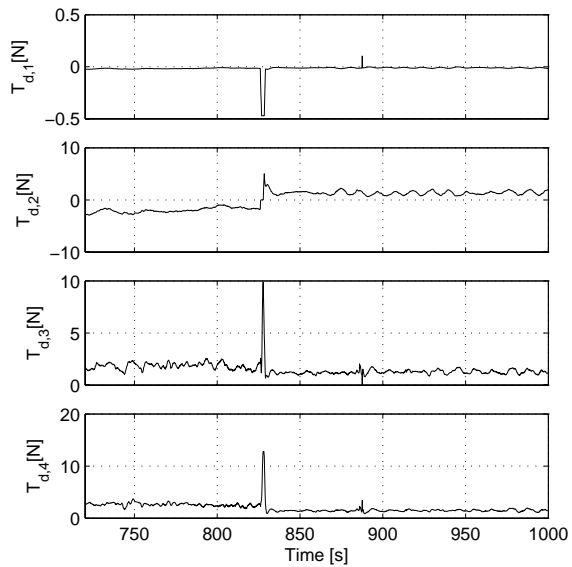


Figure C.3: Thruster forces during Run A.

C.2 Run C: Anti-spin thrust allocation, thrust redistribution

The main results from this run is found in Section 5.3.1. In Figure C.4 the thrust directions are seen to behave as expected.

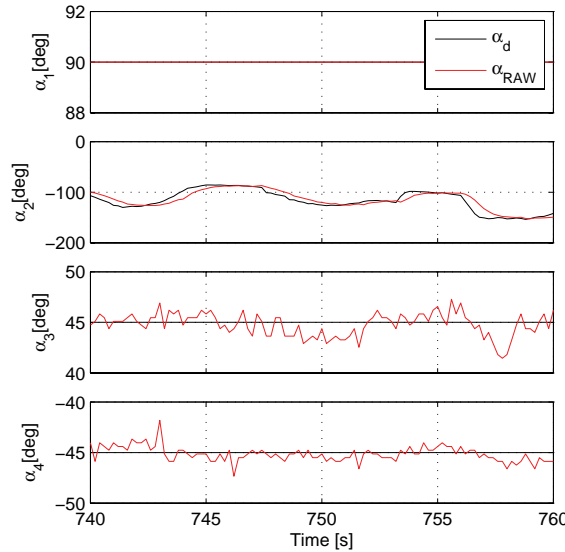


Figure C.4: Thrust directions during Run C.

C.3 Run D: Anti-spin thrust allocation, power saving

The main results from this run is found in Section 5.3.2. In Figure C.5 it is seen that when anti-spin thrust allocation is turned on, it is a significant reduction in the desired generalized surge force. This is due to the increased efficiency of the thrusters and this is the main reason for the power saving. In Figure C.6 the thrust directions are seen. The thrust direction on thruster number two is close to 180[deg] in order to counteract the mean environmental load.

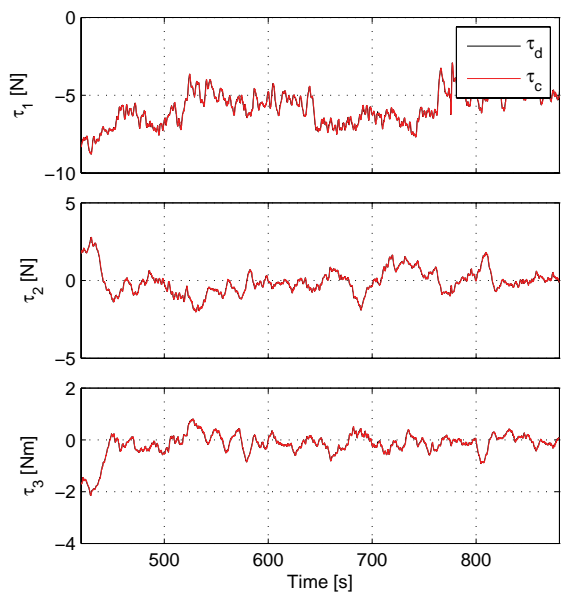


Figure C.5: Generalized forces during Run D.

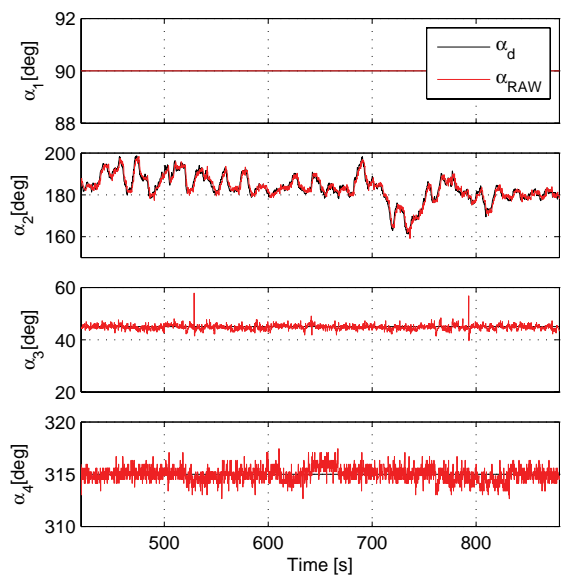


Figure C.6: Thrust directions during Run D.

C.4 Run E: Anti-spin thrust allocation, positioning performance

The main results from this run is found in Section 5.3.3. In Figure C.7 it is seen that the thrust allocator commands the desired generalized force. In Figure C.8 it is seen that thruster number two rotates much during the maneuver. This is because thruster number two is the only azimuthing thruster. In Figure C.9 the power consumption during maneuvering (when the desired heading is changing) is shown. Since the propellers are ventilated only a small amount of time, the differences in power consumption with and without anti-spin thrust allocation are not significant. However, both the mean power consumption and the standard deviation are reduced by around six percent when anti-spin thrust allocation is used.

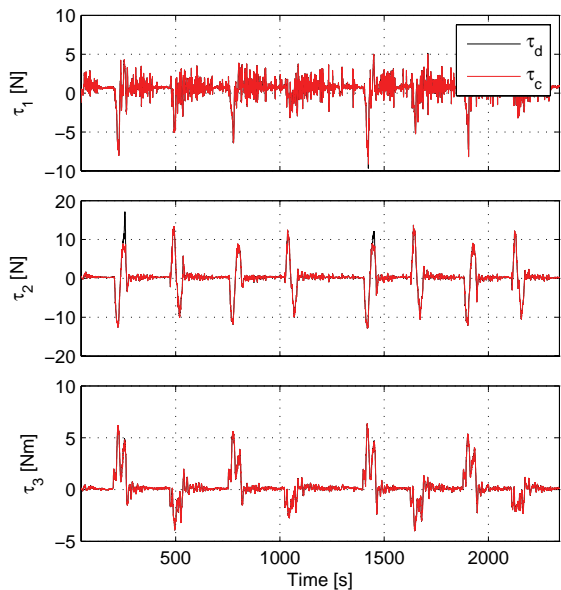


Figure C.7: Generalized forces during Run E.

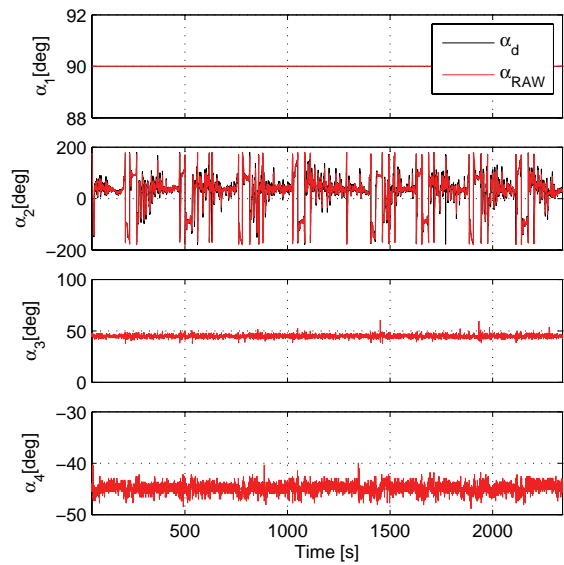


Figure C.8: Thrust directions during Run E.

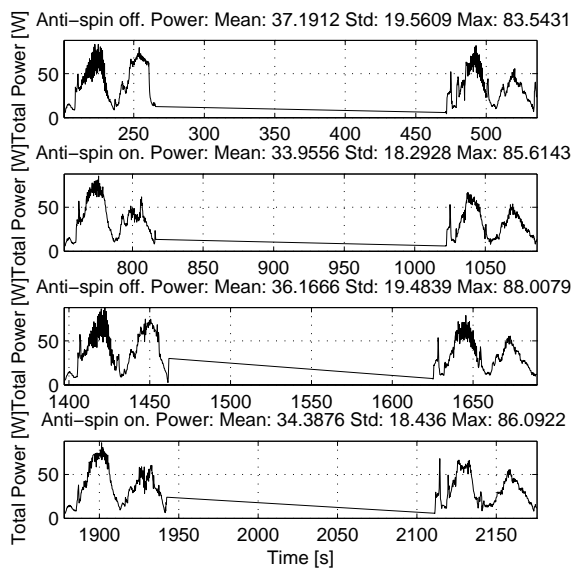


Figure C.9: Power during Run E.

C.5 Run F: Maneuvering, nonconvex.

The main results from this run is found in Section 6.5.1. In Figure C.10 it is seen that the vessel follows the desired path. In Figure C.11 the thruster forces are shown. By comparing with Figure 6.5 it is seen that the fluctuations in the thruster forces seem to coincide with the fluctuations in thrust directions. This is probably caused by near singular configurations.

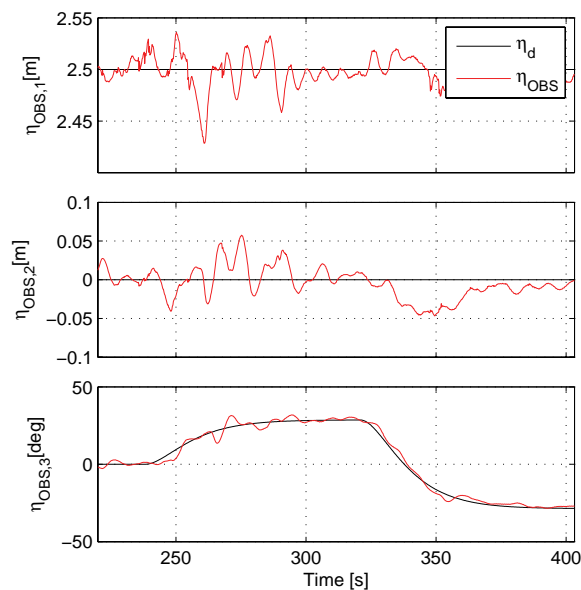


Figure C.10: Position and heading during Run F.

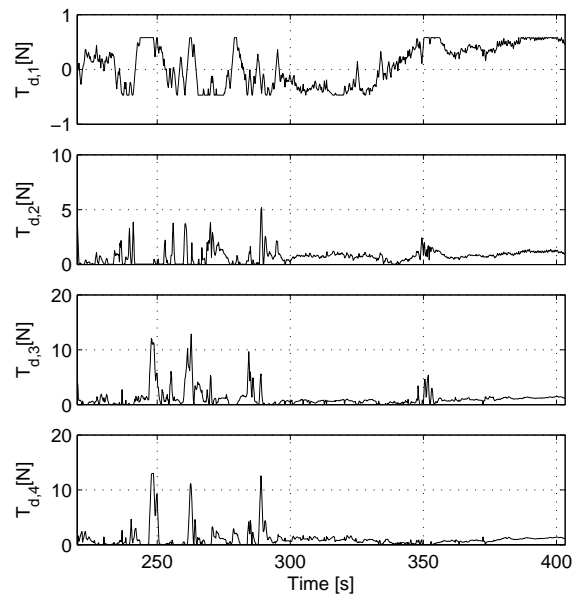


Figure C.11: Thruster forces during Run F.

C.6 Run G: Switching between fixed and rotating trusters

The main results from this run is found in Section 6.5.2. In Figure C.12 the position and heading is shown. It is seen that the positioning accuracy is very good, except during the start and stop of the waves, where the performance is acceptable. The deviations during start and stop of the waves are caused by the response time of the integrator in the motion controller.

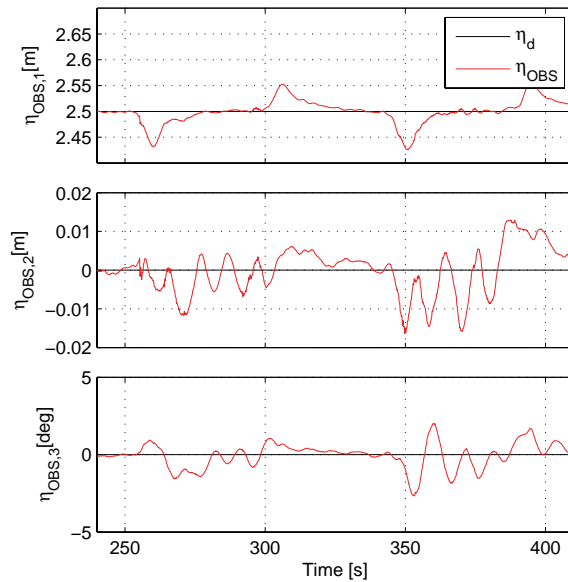


Figure C.12: Position and heading during Run G.

C.7 Run H: Thrust failures

The main results from this run is found in Section 6.5.3. In Figure C.13 the thrust directions are shown. It is seen that during thruster failures, the azimuthing capability are more actively used than under normal operation.

C.8 Run I: Azimuth failures

The main results from this run is found in Section 6.5.4. In Figure C.14 the thruster forces are seen. No general conclusions can be drawn from this plot, since the behavior is strongly dependent on the azimuth directions when the azimuth mechanism fails.

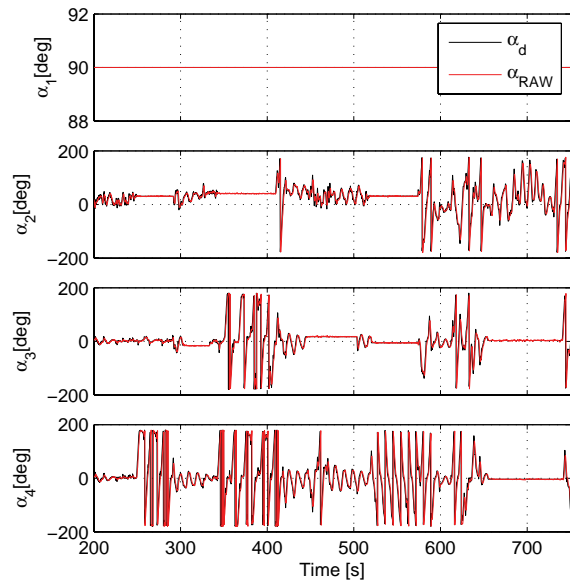


Figure C.13: Thrust directions during Run H.

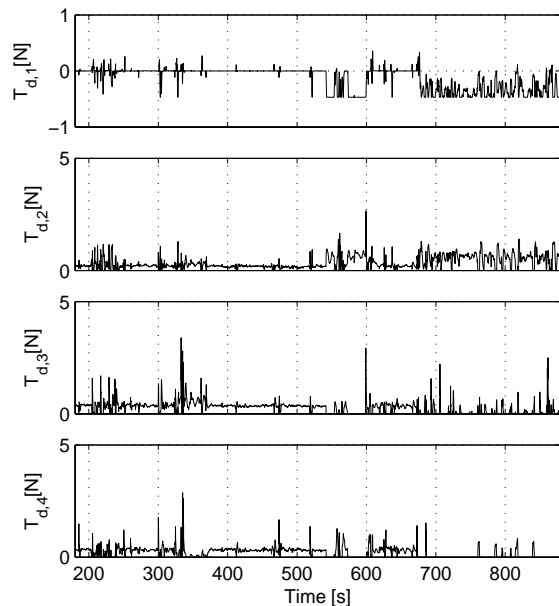


Figure C.14: Thrust forces during Run I.

C.9 Run J: Minimum attainable set

The main results from this run is found in Section 7.9.1. In Figure C.15 it is seen that the vessel looses both position and heading when the desired generalized force no longer can be provided. In Figure C.16 it is seen that the large $\|\tau_d\|$ are caused by the surge and sway forces, whereas the allocator provides the desired yaw force. This is because the yaw force has a higher weight in the thrust allocator than the surge and sway forces. In Figure C.17 it is seen that some of the thruster becomes saturated when trying to provide an unrealistic large desired generalized force.

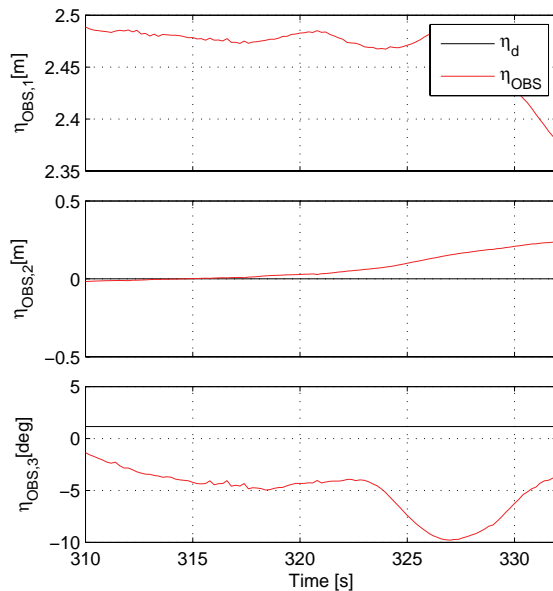


Figure C.15: Position during Run J.

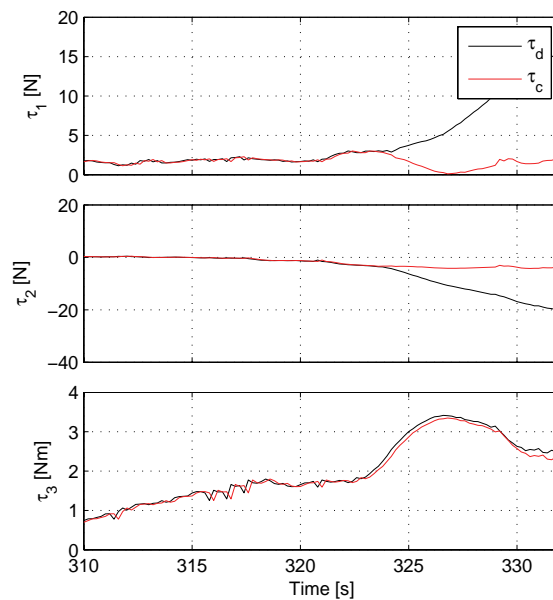


Figure C.16: Generalized forces during Run J.

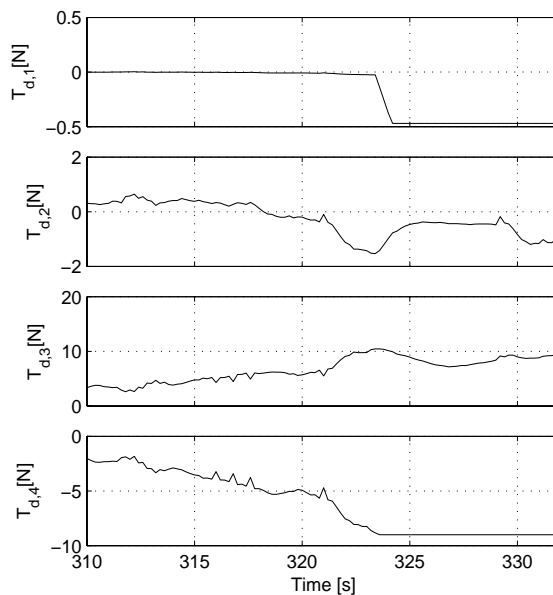


Figure C.17: Thrust forces during Run J.

C.10 Run K: Avoiding small minimum gains

The main results from this run is found in Section 7.9.2. In Figure C.18 the thrust directions are shown. It is seen that turning on singularity avoidance introduces step like behavior. This is because the thrusters are looked from further rotation when the minimum gain becomes too small until the minimum gain becomes large enough again. In Figure C.19 it is seen that the thruster forces are significantly smaller with singularity avoidance. This is because the thrusters does not operate long periods at low minimum gains.

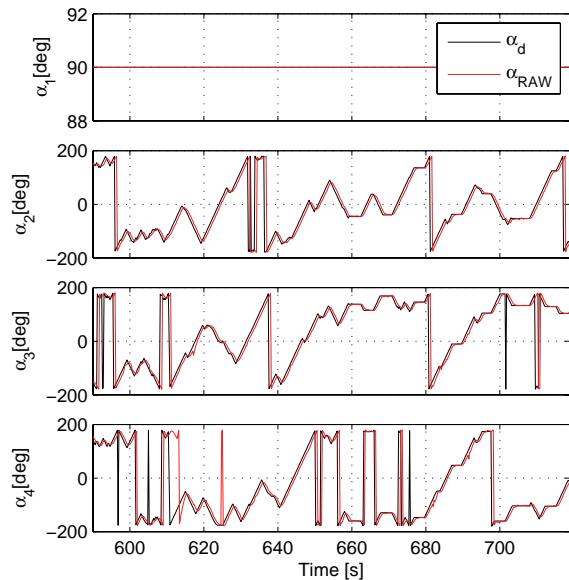


Figure C.18: Thrust directions during Run K.

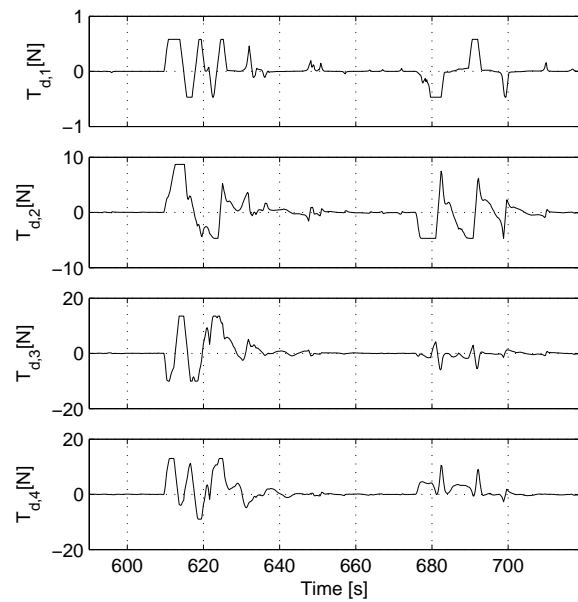


Figure C.19: Thrust forces during Run K.

Appendix D

Convergence of modified cost function

In this appendix the convergence of the $\left\| \frac{\mathbf{w}_u}{\sqrt[4]{|\mathbf{T}_{d,prev}|}} \mathbf{T}_d \right\|_2^2$ term in (5.1) for the special case with two actuators ($a = 2$), one controlled direction ($b = 1$), and a constant generalized force ($\tau_d = \text{constant}$) is shown analytically. First the optimum is found analytically, then it is shown that the iterative solution converges to the optimum.

D.1 Finding the equilibrium analytically

Assume the iterations in (5.1) subject to (4.11)-(4.13) have converged. Then the optimization problem becomes:

$$\min_{T_1, T_2} \left(|T_1|^{3/2} + a |T_2|^{3/2} \right), \quad (\text{D.1})$$

subject to:

$$T_1 + T_2 = \tau, \quad (\text{D.2})$$

$$a > 0. \quad (\text{D.3})$$

The solution to this minimization problem can be found analytically by using the equality constraint to remove T_2 from the cost function. The equality constraint gives:

$$T_2 = \tau - T_1. \quad (\text{D.4})$$

Substituting (D.4) into the cost function (D.1) gives:

$$\min_{T_1} |T_1|^{3/2} + a |\tau - T_1|^{3/2}. \quad (\text{D.5})$$

The minimization problem is solved by finding its extrema. The extrema are found by differentiating the cost and set this expression equal to zero:

$$\frac{\partial}{\partial T_1} \left(|T_1|^{3/2} + a |\tau - T_1|^{3/2} \right) = 0 \Rightarrow \quad (\text{D.6})$$

$$\frac{3}{2} \sqrt{|T_1|} \text{sign}(T_1) - a \frac{3}{2} \sqrt{|\tau - T_1|} \text{sign}(\tau - T_1) = 0 \Rightarrow \quad (\text{D.7})$$

$$\begin{aligned} \sqrt{|T_1|} \text{sign}(T_1) &= a \sqrt{|\tau - T_1|} \text{sign}(\tau - T_1) \Rightarrow \\ |T_1| &= a^2 |\tau - T_1| \Rightarrow \\ T_1^2 &= a^4 (\tau - T_1)^2 \Rightarrow \\ (a^4 - 1) T_1^2 - 2a^4 \tau T_1 + a^4 \tau &= 0 \Rightarrow \\ T_1 &= \frac{a^2}{a^2 + 1} \tau \vee T_1 = \frac{a^2}{a^2 - 1} \tau. \end{aligned} \quad (\text{D.8})$$

Due to the squares taken when solving the problem, it has to be investigated if both solutions are the actual solutions. This is done by inserting the solutions in the left side of (D.7). For $T_1 = \frac{a^2}{a^2 + 1} \tau$ the result is:

$$\begin{aligned} &\frac{3}{2} \sqrt{|T_1|} \text{sign}(T_1) - a \frac{3}{2} \sqrt{|\tau - T_1|} \text{sign}(\tau - T_1) \\ &= \frac{3}{2} \sqrt{\left| \frac{a^2}{a^2 + 1} \tau \right|} \text{sign}\left(\frac{a^2}{a^2 + 1} \tau\right) - a \frac{3}{2} \sqrt{\left| \tau - \frac{a^2}{a^2 + 1} \tau \right|} \text{sign}\left(\tau - \frac{a^2}{a^2 + 1} \tau\right), \\ &= \frac{3}{2} \sqrt{\left| \frac{a^2}{a^2 + 1} \tau \right|} \text{sign}(\tau) - a \frac{3}{2} \sqrt{\left| \frac{1}{a^2 + 1} \tau \right|} \text{sign}(\tau), \\ &= \frac{3}{2} \text{sign}(\tau) \left(\sqrt{\left| \frac{a^2}{a^2 + 1} \tau \right|} - \sqrt{\left| \frac{1}{a^2 + 1} \tau \right|} \right), \\ &= 0. \end{aligned} \quad (\text{D.9})$$

For $T_1 = \frac{a^2}{a^2 - 1} \tau$ the result is:

$$\begin{aligned} &\frac{3}{2} \sqrt{|T_1|} \text{sign}(T_1) - a \frac{3}{2} \sqrt{|\tau - T_1|} \text{sign}(\tau - T_1) \\ &= \frac{3}{2} \sqrt{\left| \frac{a^2}{a^2 - 1} \tau \right|} \text{sign}\left(\frac{a^2}{a^2 - 1} \tau\right) - a \frac{3}{2} \sqrt{\left| \tau - \frac{a^2}{a^2 - 1} \tau \right|} \text{sign}\left(\tau - \frac{a^2}{a^2 - 1} \tau\right), \\ &= \frac{3}{2} \sqrt{\left| \frac{a^2}{a^2 - 1} \tau \right|} \text{sign}\left(\frac{a^2}{a^2 - 1} \tau\right) - a \frac{3}{2} \sqrt{\left| \frac{1}{a^2 - 1} \tau \right|} \text{sign}\left(\frac{-1}{a^2 - 1} \tau\right), \\ &= \frac{3}{2} \sqrt{\left| \frac{a^2}{a^2 - 1} \tau \right|} \text{sign}\left(\frac{a^2}{a^2 - 1} \tau\right) + \frac{3}{2} \sqrt{\left| \frac{a^2}{a^2 - 1} \tau \right|} \text{sign}\left(\frac{1}{a^2 - 1} \tau\right), \\ &= \frac{3}{2} \sqrt{\left| \frac{a^2}{a^2 - 1} \tau \right|} \left(\text{sign}\left(\frac{a^2}{a^2 - 1} \tau\right) + \text{sign}\left(\frac{1}{a^2 - 1} \tau\right) \right), \end{aligned}$$

$$\begin{aligned}
&= \frac{3}{2} \sqrt{\left| \frac{a^2}{a^2 - 1} \tau \right|} \left(\text{sign}\left(\frac{1}{a^2 - 1} \tau\right) + \text{sign}\left(-\frac{1}{a^2 - 1} \tau\right) \right), \\
&> 0.
\end{aligned} \tag{D.10}$$

Hence it is concluded that the extremum is:

$$T_1 = \frac{a^2}{1+a^2} \tau, \tag{D.11}$$

$$T_2 = \frac{1}{1+a^2} \tau. \tag{D.12}$$

To verify that the extremum is a minimum, the cost function is differentiated twice:

$$\begin{aligned}
&\frac{\partial^2}{\partial T_1^2} \left(|T_1|^{3/2} + a |\tau - T_1|^{3/2} \right) \\
&= \frac{\partial}{\partial T_1} \left(\frac{3}{2} \sqrt{|T_1|} \text{sign}(T_1) - a \frac{3}{2} \sqrt{|\tau - T_1|} \text{sign}(\tau - T_1) \right), \\
&= \left(\frac{3}{4} \frac{1}{\sqrt{|T_1|}} \text{sign}(T_1) \text{sign}(T_1) + a \frac{3}{4} \frac{1}{\sqrt{|\tau - T_1|}} \text{sign}(\tau - T_1) \text{sign}(\tau - T_1) \right), \\
&= \frac{3}{4\sqrt{|T_1|}} + \frac{3a}{4\sqrt{|\tau - T_1|}} > 0 \quad \forall a > 0.
\end{aligned} \tag{D.13}$$

Since the second derivative is positive, the extremum is a minimum.

D.2 The iterative solution

Another way to solve this problem is by formulating it as an iterative quadratic problem:

$$\min_{T_{1,k}, T_{2,k}} \frac{T_{1,k}^2}{\sqrt{|T_{1,k-1}|}} + a \frac{T_{2,k}^2}{\sqrt{|T_{2,k-1}|}}, \tag{D.14}$$

subject to:

$$T_{1,k} + T_{2,k} = \tau, \tag{D.15}$$

$$a > 0, \tag{D.16}$$

$$\tau = \text{constant}, \tag{D.17}$$

where k indexes the different time steps. We now want to show that the iterative solution converges to the analytical solution. We start by finding the equilibrium and continue by showing that the iterative solution converges to the equilibrium monotonically.

D.2.1 Finding the equilibrium

The solution to the problem $\min_x \mathbf{x}^T \mathbf{W} \mathbf{x}$, $\mathbf{A} \mathbf{x} = \mathbf{b}$ is known to be $\mathbf{x} = \mathbf{W}^{-1} \mathbf{A}^T (\mathbf{A} \mathbf{W}^{-1} \mathbf{A}^T)^{-1} \mathbf{b}$. By defining:

$$\mathbf{x} = \begin{bmatrix} T_{1,k} \\ T_{2,k} \end{bmatrix}, \quad (\text{D.18})$$

$$\mathbf{W} = \begin{bmatrix} \frac{1}{\sqrt{|T_{1,k-1}|}} & 0 \\ 0 & \frac{a}{\sqrt{|T_{2,k-1}|}} \end{bmatrix}, \quad (\text{D.19})$$

$$\mathbf{A} = \begin{bmatrix} 1 & 1 \end{bmatrix}, \quad (\text{D.20})$$

$$\mathbf{b} = \tau. \quad (\text{D.21})$$

The solution is:

$$\begin{aligned} \begin{bmatrix} T_{1,k} \\ T_{2,k} \end{bmatrix} &= \mathbf{W}^{-1} \mathbf{A}^T (\mathbf{A} \mathbf{W}^{-1} \mathbf{A}^T)^{-1} \mathbf{b}, \\ &= \begin{bmatrix} \frac{|T_{1,k-1}|}{|T_{1,k-1}| + \frac{1}{a} \sqrt{|\tau - T_{1,k-1}| |T_{1,k-1}|}} \\ \frac{\frac{1}{a} \sqrt{|\tau - T_{1,k-1}| |T_{1,k-1}|}}{|T_{1,k-1}| + \frac{1}{a} \sqrt{|\tau - T_{1,k-1}| |T_{1,k-1}|}} \end{bmatrix} \tau. \end{aligned} \quad (\text{D.22})$$

From (D.22) it is seen that if $k = 0$ is the initial condition, $\frac{T_{1,k}}{\tau}, \frac{T_{2,k}}{\tau} \in \langle 0, 1 \rangle$, $\forall k \geq 1$ independently of $T_{1,0}$ and $T_{1,0}$.

Define the function f :

$$f = \frac{T_{1,k} - T_{1,k-1}}{\tau}, \quad (\text{D.23})$$

$$= \frac{T_{1,k-1}}{T_{1,k-1} + \frac{1}{a} \sqrt{T_{1,k-1} (1 - T_{1,k-1})}} - \frac{T_{1,k-1}}{\tau}. \quad (\text{D.24})$$

To reduce the required space in the computations $\frac{T_{1,k-1}}{\tau}$ is substituted with x such that the following function is investigated:

$$f = \frac{x}{x + \frac{1}{a} \sqrt{x(1-x)}} - x \wedge x \in \langle 0, 1 \rangle, a > 0, \quad (\text{D.25})$$

where x is assumed to be in the range $\langle 0, 1 \rangle$, since this will always be the case after the first iteration.

It is desirable to find the equilibrium points of the mapping (D.22). This is done by solving $f = 0$:

$$f = 0 \Rightarrow \quad (\text{D.26})$$

$$\begin{aligned} \frac{x}{x + \frac{1}{a} \sqrt{x(1-x)}} - x &= 0 \Rightarrow \\ x \left(\frac{1}{x + \frac{1}{a} \sqrt{x(1-x)}} - 1 \right) &= 0. \end{aligned} \quad (\text{D.27})$$

Hence $x = 0$ is a solution (but it is required that $x > 0$), further:

$$\begin{aligned}
 \frac{1}{x + \frac{1}{a}\sqrt{x(1-x)}} - 1 &= 0 \Rightarrow \\
 x + \frac{1}{a}\sqrt{x(1-x)} &= 1 \Rightarrow \\
 \left(-\frac{1}{a}\sqrt{x(1-x)}\right)^2 &= (x-1)^2 \Rightarrow \\
 \frac{1}{a^2}x(1-x) &= x^2 - 2x + 1 \\
 &\Downarrow \\
 x - x^2 &= (x^2 - 2x + 1)a^2 \\
 &\Downarrow \\
 (a^2 + 1)x^2 - (2a^2 + 1)x + a^2 &= 0 \Rightarrow \\
 x &= \frac{(2a^2 + 1) \pm \sqrt{(2a^2 + 1)^2 - 4(a^2 + 1)a^2}}{2(a^2 + 1)}, \\
 &= \frac{(2a^2 + 1) \pm \sqrt{4a^4 + 4a^2 + 1 - 4a^4 - 4a^2}}{2(a^2 + 1)}, \\
 &= \frac{(2a^2 + 1) \pm 1}{2(a^2 + 1)}, \\
 &= \frac{2(a^2 + 1)}{2(a^2 + 1)} \vee \frac{2a^2}{2(a^2 + 1)}, \\
 &= 1 \vee \frac{a^2}{(a^2 + 1)}. \tag{D.29}
 \end{aligned}$$

Hence the solutions are:

$$x = \begin{cases} 0 \\ 1 \\ \frac{a^2}{(a^2+1)} \end{cases}. \tag{D.30}$$

Taking the constraints on x into account, it is only one solution:

$$x = \frac{a^2}{(a^2 + 1)}. \tag{D.31}$$

This solution is equal to the one found in (D.11) for the analytical problem (D.1)-(D.3). This means that the equilibrium point of the iterative solution is the analytical solution.

D.2.2 Convergence

We now investigate if the iterations approaches the equilibrium by investigating $g = \frac{T_{1,k} - T_{eq,1}}{T_{1,k-1} - T_{eq,1}}$, where $T_{eq,1}$ is the equilibrium point of T_1 :

$$g = \frac{T_{1,k} - T_{eq,1}}{T_{1,k-1} - T_{eq,1}}, \quad (\text{D.32})$$

$$= \frac{\frac{T_{1,k-1}}{T_{1,k-1} + \frac{1}{a}\sqrt{(\tau - T_{1,k-1})T_{1,k-1}}} \tau - T_{eq,1}}{T_{1,k-1} - T_{eq,1}},$$

$$= \frac{\frac{x}{x + \frac{1}{a}\sqrt{x(1-x)}} - \frac{a^2}{a^2+1}}{x - \frac{a^2}{a^2+1}},$$

$$= \frac{\frac{x}{x + \frac{1}{a}\sqrt{x(1-x)}} - \frac{a^2}{a^2+1}}{x - \frac{a^2}{a^2+1}},$$

$$= \frac{\frac{(a^2+1)x}{x + \frac{1}{a}\sqrt{x(1-x)}} - a^2}{(a^2+1)x - a^2},$$

$$= \frac{\frac{(a^2+1)x - a^2(x + \frac{1}{a}\sqrt{x(1-x)})}{x + \frac{1}{a}\sqrt{x(1-x)}}}{(a^2+1)x - a^2},$$

$$= \frac{(a^2+1)x - a^2(x + \frac{1}{a}\sqrt{x(1-x)})}{\left(x + \frac{1}{a}\sqrt{x(1-x)}\right)((a^2+1)x - a^2)}, \quad (\text{D.33})$$

$$= \frac{\left(x + \frac{1}{a}\sqrt{x(1-x)}\right)(a^2x + x - a^2) + (a^2+1)x - (a^2x + x)\left(x + \frac{1}{a}\sqrt{x(1-x)}\right)}{\left(x + \frac{1}{a}\sqrt{x(1-x)}\right)(a^2x + x - a^2)},$$

$$= \frac{\left(x + \frac{1}{a}\sqrt{x(1-x)}\right)(a^2x + x - a^2) - (a^2x + x)\left(x + \frac{1}{a}\sqrt{x(1-x)} - 1\right)}{\left(x + \frac{1}{a}\sqrt{x(1-x)}\right)(a^2x + x - a^2)},$$

$$= 1 - \frac{(a^2x + x)\left(x + \frac{1}{a}\sqrt{x(1-x)} - 1\right)}{\left(x + \frac{1}{a}\sqrt{x(1-x)}\right)(a^2x + x - a^2)},$$

$$= 1 - \frac{(a^2x + x)}{x + \frac{1}{a}\sqrt{x(1-x)}} \cdot \frac{x + \frac{1}{a}\sqrt{x(1-x)} - 1}{a^2x + x - a^2}. \quad (\text{D.34})$$

It is seen that the first fraction is positive:

$$\frac{(a^2x + x)}{\left(x + \frac{1}{a}\sqrt{x(1-x)}\right)} > 0 \quad \forall x \in \langle 0, 1 \rangle, a > 0. \quad (\text{D.35})$$

The behavior of the last fraction has to be investigated further. We start by looking at the numerator. First the zero crossings of the numerator is found:

$$\begin{aligned} 0 &= \left(x + \frac{1}{a} \sqrt{x(1-x)} - 1 \right) \Rightarrow \quad (D.36) \\ \left(\frac{1}{a} \sqrt{x(1-x)} \right)^2 &= (1-x)^2 \Rightarrow \\ x(1-x) &= a^2(1-x)^2 \Rightarrow \\ x &= a^2(1-x) \Rightarrow \\ x &= 1 \vee \frac{a^2}{a^2+1}. \end{aligned} \quad (D.37)$$

This shows that the only zero crossing is for $x = \frac{a^2}{a^2+1}$. We then find the sign of the numerator by investigating the derivative of the numerator:

$$\begin{aligned} &\frac{\partial}{\partial x} \left(x + \frac{1}{a} \sqrt{x(1-x)} - 1 \right) \\ &= 1 + \frac{1-2x}{2a\sqrt{x(1-x)}}, \end{aligned} \quad (D.38)$$

evaluating the derivative at the zero crossing gives:

$$\begin{aligned} &\frac{\partial}{\partial x} \left(x + \frac{1}{a} \sqrt{x(1-x)} - 1 \right)_{x=\frac{a^2}{a^2+1}} \\ &= 1 + \frac{1-2\frac{a^2}{a^2+1}}{2a\frac{a}{a^2+1}}, \\ &= 1 + \frac{a^2+1-2a^2}{2a^2}, \\ &= 1 + \frac{1-a^2}{2a^2}, \\ &= \frac{1}{2} \left(1 + \frac{1}{a^2} \right). \end{aligned} \quad (D.39)$$

The derivative at the zero crossing is larger than zero, and hence the numerator is negative for $x < \frac{a^2}{a^2+1}$ and positive for $x > \frac{a^2}{a^2+1}$. We then continue by investigating the denominator. First the zero crossing of the denominator is found:

$$(a^2x + x - a^2) = 0 \Rightarrow \quad (D.40)$$

$$x = \frac{a^2}{a^2+1}. \quad (D.41)$$

Then the derivative of the denominator at the zero crossing is computed:

$$\frac{\partial}{\partial x} (a^2x + x - a^2) = (a^2 + 1). \quad (D.42)$$

This shows that the derivative of the denominator is positive. It can then be concluded that the denominator is negative for $x < \frac{a^2}{a^2+1}$ and positive for $x > \frac{a^2}{a^2+1}$. Hence the numerator and the denominator have the same sign all the time, and hence the fraction will always be positive (except at the zero crossing which is the equilibrium):

$$\begin{aligned} \frac{\left(x + \frac{1}{a}\sqrt{x(1-x)} - 1\right)}{(a^2x + x - a^2)} &> 0 \\ \forall x \in \langle 0, 1 \rangle \setminus \frac{a^2}{a^2+1}, a > 0. \end{aligned} \quad (\text{D.43})$$

Combining (D.34), (D.35) and (D.43) it is then seen that:

$$\frac{T_{1,k} - T_{eq,1}}{T_{1,k-1} - T_{eq,1}} < 1 \quad \forall x \in \langle 0, 1 \rangle \setminus \frac{a^2}{a^2+1}, a > 0. \quad (\text{D.44})$$

Since we have not considered absolute values of the distance to equilibrium, we also need to show that $\frac{T_{1,k} - T_{eq,1}}{T_{1,k-1} - T_{eq,1}} > -1$ to account for the case where $T_{1,k}$ and $T_{1,k-1}$ might be on different sides of $T_{eq,1}$. We start from (D.33):

$$\begin{aligned} g &= \frac{(a^2 + 1)x - a^2 \left(x + \frac{1}{a}\sqrt{x(1-x)}\right)}{\left(x + \frac{1}{a}\sqrt{x(1-x)}\right)((a^2 + 1)x - a^2)}, \\ &= \frac{(a^2 + 1)x - a^2 - a^2 \left(x + \frac{1}{a}\sqrt{x(1-x)} - 1\right)}{\left(x + \frac{1}{a}\sqrt{x(1-x)}\right)((a^2 + 1)x - a^2)}, \\ &= \frac{(a^2 + 1)x - a^2 \left(x + \frac{1}{a}\sqrt{x(1-x)}\right)}{\left(x + \frac{1}{a}\sqrt{x(1-x)}\right)((a^2 + 1)x - a^2)}, \\ &= \frac{x - a^2 \left(\frac{1}{a}\sqrt{x(1-x)}\right)}{\left(x + \frac{1}{a}\sqrt{x(1-x)}\right)((a^2 + 1)x - a^2)}, \\ &= \frac{x - a\sqrt{x(1-x)}}{\left(x + \frac{1}{a}\sqrt{x(1-x)}\right)((a^2 + 1)x - a^2)}, \\ &= \frac{1}{\left(x + \frac{1}{a}\sqrt{x(1-x)}\right)} \frac{x - a\sqrt{x(1-x)}}{((a^2 + 1)x - a^2)}, \end{aligned} \quad (\text{D.45})$$

$$\frac{1}{\left(x + \frac{1}{a}\sqrt{x(1-x)}\right)} > 0 \quad \forall x \in \langle 0, 1 \rangle, a > 0. \quad (\text{D.47})$$

where the first fraction are larger than zero:

Further the sign of the second fraction is investigated. For the numerator we find the zero crossing:

$$x - a\sqrt{x(1-x)} = 0 \Rightarrow \quad (\text{D.48})$$

$$\begin{aligned} x^2 &= \left(a\sqrt{x(1-x)}\right)^2 \Rightarrow \\ x^2 &= a^2x(1-x) \Rightarrow \\ (a^2+1)x^2 &= a^2x \Rightarrow \\ x &= 0 \vee \frac{a^2}{(a^2+1)}, \end{aligned} \quad (\text{D.49})$$

where $x = \frac{a^2}{(a^2+1)}$ is the only solution satisfying the x constrains. The derivative in the equilibrium is:

$$\begin{aligned} &\frac{\partial}{\partial x} \left(x - a\sqrt{x(1-x)} \right)_{x=\frac{a^2}{(a^2+1)}} \\ &= \left(1 - \frac{a(1-2x)}{2\sqrt{x(1-x)}} \right)_{x=\frac{a^2}{(a^2+1)}}, \\ &= 1 - \frac{a \left(1 - 2\frac{a^2}{(a^2+1)} \right)}{2\frac{a}{a^2+1}}, \\ &= 1 - \frac{(a^2+1-2a^2)}{2}, \\ &= 1 - \frac{(1-a^2)}{2}, \\ &= \frac{1}{2}(1+a^2), \end{aligned} \quad (\text{D.50})$$

hence the derivative is larger than zero, which implies that the numerator is negative for $x < \frac{a^2}{a^2+1}$ and positive for $x > \frac{a^2}{a^2+1}$. Hence the numerator and the denominator always have the same sign, resulting in that the fraction always is positive:

$$\begin{aligned} \frac{x - a\sqrt{x(1-x)}}{((a^2+1)x - a^2)} &> 0 \\ \forall x &\in \langle 0, 1 \rangle \setminus \frac{a^2}{a^2+1}, a > 0. \end{aligned} \quad (\text{D.51})$$

By combining (D.46), (D.47), and (D.51) it is seen that:

$$\frac{T_{1,k} - T_{eq,1}}{T_{1,k-1} - T_{eq,1}} > 0 \quad \forall x \in \langle 0, 1 \rangle \setminus \frac{a^2}{a^2+1}, a > 0. \quad (\text{D.52})$$

Hence, it can be concluded by using (D.44) and (D.52) that:

$$\begin{aligned} \frac{T_{1,k} - T_{eq,1}}{T_{1,k-1} - T_{eq,1}} &\in \langle 0, 1 \rangle \\ \forall T_{1,k-1}, T_{2,k-1} &\in \langle 0, \tau \rangle \setminus \frac{a^2}{a^2 + 1} \tau, a > 0. \end{aligned} \quad (\text{D.53})$$

This means that the distance to the equilibrium is monotonically decreasing and hence the iterations will always approach the equilibrium at $T_1 = \frac{a^2}{a^2 + 1} \tau$ as long as the conditions (D.15)-(D.17) are satisfied.

R A P P O R T E R
UTGITT VED
INSTITUTT FOR MARIN TEKNIKK
(tidligere: FAKULTET FOR MARIN TEKNIKK)
NORGES TEKNISK-NATURVITENSKAPELIGE UNIVERSITET

- UR-79-01 Brigt Hatlestad, MK:
The finite element method used in a fatigue evaluation of fixed offshore platforms. (Dr.Ing. Thesis)
- UR-79-02 Erik Pettersen, MK:
Analysis and design of cellular structures. (Dr.Ing. Thesis)
- UR-79-03 Sverre Valsgård, MK:
Finite difference and finite element methods applied to nonlinear analysis of plated structures. (Dr.Ing. Thesis)
- UR-79-04 Nils T. Nordsve, MK:
Finite element collapse analysis of structural members considering imperfections and stresses due to fabrication. (Dr.Ing. Thesis)
- UR-79-05 Ivar J. Fylling, MK:
Analysis of towline forces in ocean towing systems. (Dr.Ing. Thesis)
- UR-80-06 Nils Sandmark, MM:
Analysis of Stationary and Transient Heat Conduction by the Use of the Finite Element Method. (Dr.Ing. Thesis)
- UR-80-09 Sverre Haver, MK:
Analysis of uncertainties related to the stochastic modelling of ocean waves. (Dr.Ing. Thesis)
- UR-85-46 Alf G. Engseth, MK:
Finite element collapse analysis of tubular steel offshore structures. (Dr.Ing. Thesis)
- UR-86-47 Dengody Sheshappa, MP:
A Computer Design Model for Optimizing Fishing Vessel Designs Based on Techno-Economic Analysis. (Dr.Ing. Thesis)
- UR-86-48 Vidar Aanesland, MH:
A Theoretical and Numerical Study of Ship Wave Resistance. (Dr.Ing. Thesis)
- UR-86-49 Heinz-Joachim Wessel, MK:
Fracture Mechanics Analysis of Crack Growth in Plate Girders. (Dr.Ing. Thesis)
- UR-86-50 Jon Taby, MK:
Ultimate and Post-ultimate Strength of Dented Tubular Members. (Dr.Ing. Thesis)
- UR-86-51 Walter Lian, MH:
A Numerical Study of Two-Dimensional Separated Flow Past Bluff Bodies at Moderate KC-Numbers. (Dr.Ing. Thesis)
- UR-86-52 Bjørn Sortland, MH:
Force Measurements in Oscillating Flow on Ship Sections and Circular Cylinders in a U-Tube Water Tank. (Dr.Ing. Thesis)
- UR-86-53 Kurt Strand, MM:
A System Dynamic Approach to One-dimensional Fluid Flow. (Dr.Ing. Thesis)

UR-86-54 <u>Arne Edvin Løken</u> , MH:	Three Dimensional Second Order Hydrodynamic Effects on Ocean Structures in Waves. (Dr.Ing. Thesis)
UR-86-55 <u>Sigurd Falch</u> , MH:	A Numerical Study of Slamming of Two-Dimensional Bodies. (Dr.Ing. Thesis)
UR-87-56 <u>Arne Braathen</u> , MH:	Application of a Vortex Tracking Method to the Prediction of Roll Damping of a Two-Dimension Floating Body. (Dr.Ing. Thesis)
UR-87-57 <u>Bernt Leira</u> , MR:	Gaussian Vector Processes for Reliability Analysis involving Wave-Induced Load Effects. (Dr.Ing. Thesis)
UR-87-58 <u>Magnus Småvik</u> , MM:	Thermal Load and Process Characteristics in a Two-Stroke Diesel Engine with Thermal Barriers (in Norwegian). (Dr.Ing. Thesis)
MTA-88-59 <u>Bernt Arild Bremsdal</u> , MP:	An Investigation of Marine Installation Processes - A Knowledge - Based Planning Approach. (Dr.Ing. Thesis)
MTA-88-60 <u>Xu Jun</u> , MK:	Non-linear Dynamic Analysis of Space-framed Offshore Structures. (Dr.Ing. Thesis)
MTA-89-61 <u>Gang Miao</u> , MH:	Hydrodynamic Forces and Dynamic Responses of Circular Cylinders in Wave Zones. (Dr.Ing. Thesis)
MTA-89-62 <u>Martin Greenhow</u> , MH:	Linear and Non-Linear Studies of Waves and Floating Bodies. Part I and Part II. (Dr.Techn. Thesis)
MTA-89-63 <u>Chang Li</u> , MH:	Force Coefficients of Spheres and Cubes in Oscillatory Flow with and without Current. (Dr.Ing. Thesis)
MTA-89-64 <u>Hu Ying</u> , MP:	A Study of Marketing and Design in Development of Marine Transport Systems. (Dr.Ing. Thesis)
MTA-89-65 <u>Arild Jæger</u> , MH:	Seakeeping, Dynamic Stability and Performance of a Wedge Shaped Planing Hull. (Dr.Ing. Thesis)
MTA-89-66 <u>Chan Siu Hung</u> , MM:	The dynamic characteristics of tilting-pad bearings.
MTA-89-67 <u>Kim Wikstrøm</u> , MP:	Analysis av projekteringen for ett offshore projekt. (Licentiat-avhandling)
MTA-89-68 <u>Jiao Guoyang</u> , MR:	Reliability Analysis of Crack Growth under Random Loading, considering Model Updating. (Dr.Ing. Thesis)
MTA-89-69 <u>Arnt Olufsen</u> , MK:	Uncertainty and Reliability Analysis of Fixed Offshore Structures. (Dr.Ing. Thesis)
MTA-89-70 <u>Wu Yu-Lin</u> , MR:	System Reliability Analyses of Offshore Structures using improved Truss and Beam Models. (Dr.Ing. Thesis)
MTA-90-71 <u>Jan Roger Hoff</u> , MH:	Three-dimensional Green function of a vessel with forward speed in waves. (Dr.Ing. Thesis)
MTA-90-72 <u>Rong Zhao</u> , MH:	Slow-Drift Motions of a Moored Two-Dimensional Body in Irregular Waves. (Dr.Ing. Thesis)

MTA-90-73 <u>Atle Minsaas</u> , MP:	Economical Risk Analysis. (Dr.Ing. Thesis)
MTA-90-74 <u>Knut-Aril Farnes</u> , MK:	Long-term Statistics of Response in Non-linear Marine Structures. (Dr.Ing. Thesis)
MTA-90-75 <u>Torbjørn Sotberg</u> , MK:	Application of Reliability Methods for Safety Assessment of Submarine Pipelines. (Dr.Ing. Thesis)
MTA-90-76 <u>Zeuthen, Steffen</u> , MP:	SEAMAID. A computational model of the design process in a constraint-based logic programming environment. An example from the offshore domain. (Dr.Ing. Thesis)
MTA-91-77 <u>Haagensen, Sven</u> , MM:	Fuel Dependant Cyclic Variability in a Spark Ignition Engine - An Optical Approach. (Dr.Ing. Thesis)
MTA-91-78 <u>Løland, Geir</u> , MH:	Current forces on and flow through fish farms. (Dr.Ing. Thesis)
MTA-91-79 <u>Hoen, Christopher</u> , MK:	System Identification of Structures Excited by Stochastic Load Processes. (Dr.Ing. Thesis)
MTA-91-80 <u>Haugen, Stein</u> , MK:	Probabilistic Evaluation of Frequency of Collision between Ships and Offshore Platforms. (Dr.Ing. Thesis)
MTA-91-81 <u>Sødahl, Nils</u> , MK:	Methods for Design and Analysis of Flexible Risers. (Dr.Ing. Thesis)
MTA-91-82 <u>Ormberg, Harald</u> , MK:	Non-linear Response Analysis of Floating Fish Farm Systems. (Dr.Ing. Thesis)
MTA-91-83 <u>Marley, Mark J.</u> , MK:	Time Variant Reliability under Fatigue Degradation. (Dr.Ing. Thesis)
MTA-91-84 <u>Krokstad, Jørgen R.</u> , MH:	Second-order Loads in Multidirectional Seas. (Dr.Ing. Thesis)
MTA-91-85 <u>Molteberg, Gunnar A.</u> , MM:	The Application of System Identification Techniques to Performance Monitoring of Four Stroke Turbocharged Diesel Engines. (Dr.Ing. Thesis)
MTA-92-86 <u>Mørch, Hans Jørgen Bjelke</u> , MH:	Aspects of Hydrofoil Design: with Emphasis on Hydrofoil Interaction in Calm Water. (Dr.Ing. Thesis)
MTA-92-87 <u>Chan Siu Hung</u> , MM:	Nonlinear Analysis of Rotordynamic Instabilities in High-speed Turbomachinery. (Dr.Ing. Thesis)
MTA-92-88 <u>Bessason, Bjarni</u> , MK:	Assessment of Earthquake Loading and Response of Seismically Isolated Bridges. (Dr.Ing. Thesis)
MTA-92-89 <u>Langli, Geir</u> , MP:	Improving Operational Safety through exploitation of Design Knowledge - an investigation of offshore platform safety. (Dr.Ing. Thesis)
MTA-92-90 <u>Sævik, Svein</u> , MK:	On Stresses and Fatigue in Flexible Pipes. (Dr.Ing. Thesis)

MTA-92-91 <u>Ask, Tor Ø.</u> , MM:	Ignition and Flame Growth in Lean Gas-Air Mixtures. An Experimental Study with a Schlieren System. (Dr.Ing. Thesis)
MTA-86-92 <u>Hessen, Gunnar</u> , MK:	Fracture Mechanics Analysis of Stiffened Tubular Members. (Dr.Ing. Thesis)
MTA-93-93 <u>Steinebach, Christian</u> , MM:	Knowledge Based Systems for Diagnosis of Rotating Machinery. (Dr.Ing. Thesis)
MTA-93-94 <u>Dalane, Jan Inge</u> , MK:	System Reliability in Design and Maintenance of Fixed Offshore Structures. (Dr.Ing. Thesis)
MTA-93-95 <u>Steen, Sverre</u> , MH:	Cobblestone Effect on SES. (Dr.Ing. Thesis)
MTA-93-96 <u>Karunakaran, Daniel</u> , MK:	Nonlinear Dynamic Response and Reliability Analysis of Drag-dominated Offshore Platforms. (Dr.Ing. Thesis)
MTA-93-97 <u>Hagen, Arnulf</u> , MP:	The Framework of a Design Process Language. (Dr.Ing. Thesis)
MTA-93-98 <u>Nordrik, Rune</u> , MM:	Investigation of Spark Ignition and Autoignition in Methane and Air Using Computational Fluid Dynamics and Chemical Reaction Kinetics. A Numerical Study of Ignition Processes in Internal Combustion Engines. (Dr.Ing. Thesis)
MTA-94-99 <u>Passano, Elizabeth</u> , MK:	Efficient Analysis of Nonlinear Slender Marine Structures. (Dr.Ing. Thesis)
MTA-94-100 <u>Kvålsvold, Jan</u> , MH:	Hydroelastic Modelling of Wetdeck Slamming on Multihull Vessels. (Dr.Ing. Thesis)
MTA-94-102 <u>Bech, Sidsel M.</u> , MK:	Experimental and Numerical Determination of Stiffness and Strength of GRP/PVC Sandwich Structures. (Dr.Ing. Thesis)
MTA-95-103 <u>Paulsen, Hallvard</u> , MM:	A Study of Transient Jet and Spray using a Schlieren Method and Digital Image Processing. (Dr.Ing. Thesis)
MTA-95-104 <u>Hovde, Geir Olav</u> , MK:	Fatigue and Overload Reliability of Offshore Structural Systems, Considering the Effect of Inspection and Repair. (Dr.Ing. Thesis)
MTA-95-105 <u>Wang, Xiaozhi</u> , MK:	Reliability Analysis of Production Ships with Emphasis on Load Combination and Ultimate Strength. (Dr.Ing. Thesis)
MTA-95-106 <u>Ulstein, Tore</u> , MH:	Nonlinear Effects of a Flexible Stern Seal Bag on Cobblestone Oscillations of an SES. (Dr.Ing. Thesis)
MTA-95-107 <u>Solaas, Frøydis</u> , MH:	Analytical and Numerical Studies of Sloshing in Tanks. (Dr.Ing. Thesis)
MTA-95-108 <u>Hellan, øyyvind</u> , MK:	Nonlinear Pushover and Cyclic Analyses in Ultimate Limit State Design and Reassessment of Tubular Steel Offshore Structures. (Dr.Ing. Thesis)
MTA-95-109 <u>Hermundstad, Ole A.</u> , MK:	Theoretical and Experimental Hydroelastic Analysis of High Speed Vessels. (Dr.Ing. Thesis)

MTA-96-110 <u>Bratland, Anne K.</u> , MH:	Wave-Current Interaction Effects on Large-Volume Bodies in Water of Finite Depth. (Dr.Ing. Thesis)
MTA-96-111 <u>Herfjord, Kjell</u> , MH:	A Study of Two-dimensional Separated Flow by a Combination of the Finite Element Method and Navier-Stokes Equations. (Dr.Ing. Thesis)
MTA-96-112 <u>Æsøy, Vilmar</u> , MM:	Hot Surface Assisted Compression Ignition in a Direct Injection Natural Gas Engine. (Dr.Ing. Thesis)
MTA-96-113 <u>Eknes, Monika L.</u> , MK:	Escalation Scenarios Initiated by Gas Explosions on Offshore Installations. (Dr.Ing. Thesis)
MTA-96-114 <u>Erikstad, Stein O.</u> , MP:	A Decision Support Model for Preliminary Ship Design. (Dr.Ing. Thesis)
MTA-96-115 <u>Pedersen, Egil</u> , MH:	A Nautical Study of Towed Marine Seismic Streamer Cable Configurations. (Dr.Ing. Thesis)
MTA-97-116 <u>Moksnes, Paul O.</u> , MM:	Modelling Two-Phase Thermo-Fluid Systems Using Bond Graphs. (Dr.Ing. Thesis)
MTA-97-117 <u>Halse, Karl H.</u> , MK:	On Vortex Shedding and Prediction of Vortex-Induced Vibrations of Circular Cylinders. (Dr.Ing. Thesis)
MTA-97-118 <u>Igland, Ragnar T.</u> , MK:	Reliability Analysis of Pipelines during Laying, considering Ultimate Strength under Combined Loads. (Dr.Ing. Thesis)
MTA-97-119 <u>Pedersen, Hans-P.</u> , MP:	Levendefiskteknologi for fiskefartøy. (Dr.Ing. Thesis)
MTA-98-120 <u>Vikestad, Kyrre</u> , MK:	Multi-Frequency Response of a Cylinder Subjected to Vortex Shedding and Support Motions. (Dr.Ing. Thesis)
MTA-98-121 <u>Azadi, Mohammad R. E.</u> , MK:	Analysis of Static and Dynamic Pile-Soil-Jacket Behaviour. (Dr.Ing. Thesis)
MTA-98-122 <u>Ulltang, Terje</u> , MP:	A Communication Model for Product Information. (Dr.Ing. Thesis)
MTA-98-123 <u>Torbergsen, Erik</u> , MM:	Impeller/Diffuser Interaction Forces in Centrifugal Pumps. (Dr.Ing. Thesis)
MTA-98-124 <u>Hansen, Edmond</u> , MH:	A Discrete Element Model to Study Marginal Ice Zone Dynamics and the Behaviour of Vessels Moored in Broken Ice. (Dr.Ing. Thesis)
MTA-98-125 <u>Videiro, Paulo M.</u> , MK:	Reliability Based Design of Marine Structures. (Dr.Ing. Thesis)
MTA-99-126 <u>Mainçon, Philippe</u> , MK:	Fatigue Reliability of Long Welds Application to Titanium Risers. (Dr.Ing. Thesis)
MTA-99-127 <u>Haugen, Elin M.</u> , MH:	Hydroelastic Analysis of Slamming on Stiffened Plates with Application to Catamaran Wetdecks. (Dr.Ing. Thesis)

MTA-99-128 <u>Langhelle, Nina K.</u> , MK:	Experimental Validation and Calibration of Nonlinear Finite Element Models for Use in Design of Aluminium Structures Exposed to Fire. (Dr.Ing. Thesis)
MTA-99-129 <u>Berstad, Are J.</u> , MK:	Calculation of Fatigue Damage in Ship Structures. (Dr.Ing. Thesis)
MTA-99-130 <u>Andersen, Trond M.</u> , MM:	Short Term Maintenance Planning. (Dr.Ing. Thesis)
MTA-99-131 <u>Tveiten, Bård Wathne</u> , MK:	Fatigue Assessment of Welded Aluminium Ship Details. (Dr.Ing. Thesis)
MTA-99-132 <u>Søreide, Fredrik</u> , MP:	Applications of underwater technology in deep water archaeology. Principles and practice. (Dr.Ing. Thesis)
MTA-99-133 <u>Tønnesen, Rune</u> , MH:	A Finite Element Method Applied to Unsteady Viscous Flow Around 2D Blunt Bodies With Sharp Corners. (Dr.Ing. Thesis)
MTA-99-134 <u>Elvekrok, Dag R.</u> , MP:	Engineering Integration in Field Development Projects in the Norwegian Oil and Gas Industry. The Supplier Management of Norne. (Dr.Ing. Thesis)
MTA-99-135 <u>Fagerholt, Kjetil</u> , MP:	Optimizeringsbaserte Metoder for Ruteplanlegging innen skipsfart. (Dr.Ing. Thesis)
MTA-99-136 <u>Bysveen, Marie</u> , MM:	Visualization in Two Directions on a Dynamic Combustion Rig for Studies of Fuel Quality. (Dr.Ing. Thesis)
MTA-2000-137 <u>Storteig, Eskild</u> , MM:	Dynamic characteristics and leakage performance of liquid annular seals in centrifugal pumps. (Dr.Ing. Thesis)
MTA-2000-138 <u>Sagli, Gro</u> , MK:	Model uncertainty and simplified estimates of long term extremes of hull girder loads in ships. (Dr.Ing. Thesis)
MTA-2000-139 <u>Tronstad, Harald</u> , MK:	Nonlinear analysis and design of cable net structures like fishing gear based on the finite element method. (Dr.Ing. Thesis)
MTA-2000-140 <u>Kroneberg, André</u> , MP:	Innovation in shipping by using scenarios. (Dr.Ing. Thesis)
MTA-2000-141 <u>Haslum, Herbjørn Alf</u> , MH:	Simplified methods applied to nonlinear motion of spar platforms. (Dr.Ing. Thesis)
MTA-2001-142 <u>Samdal, Ole Johan</u> , MM:	Modelling of Degradation Mechanisms and Stressor Interaction on Static Mechanical Equipment Residual Lifetime. (Dr.Ing. Thesis)
MTA-2001-143 <u>Baarholm, Rolf Jarle</u> , MH:	Theoretical and experimental studies of wave impact underneath decks of offshore platforms. (Dr.Ing. Thesis)
MTA-2001-144 <u>Wang, Lihua</u> , MK:	Probabilistic Analysis of Nonlinear Wave-induced Loads on Ships. (Dr.Ing. Thesis)

MTA-2001-145 <u>Kristensen, Odd H.</u> , Holt, MK:	Ultimate Capacity of Aluminium Plates under Multiple Loads, Considering HAZ Properties. (Dr.Ing. Thesis)
MTA-2001-146 <u>Greco, Marilena</u> , MH:	A Two-Dimensional Study of Green-Water Loading. (Dr.Ing. Thesis)
MTA-2001-147 <u>Heggelund, Svein E.</u> , MK:	Calculation of Global Design Loads and Load Effects in Large High Speed Catamarans. (Dr.Ing. Thesis)
MTA-2001-148 <u>Babalola, Olusegun T.</u> , MK:	Fatigue Strength of Titanium Risers - Defect Sensitivity. (Dr.Ing. Thesis)
MTA-2001-149 <u>Mohammed, Abuu K.</u> , MK:	Nonlinear Shell Finite Elements for Ultimate Strength and Collapse Analysis of Ship Structures. (Dr.Ing. Thesis)
MTA-2002-150 <u>Holmedal, Lars E.</u> , MH:	Wave-current interactions in the vicinity of the sea bed. (Dr.Ing. Thesis)
MTA-2002-151 <u>Rognbakke, Olav F.</u> , MH:	Sloshing in rectangular tanks and interaction with ship motions. (Dr.Ing. Thesis)
MTA-2002-152 <u>Lader, Pål Furset</u> , MH:	Geometry and Kinematics of Breaking Waves. (Dr.Ing. Thesis)
MTA-2002-153 <u>Yang, Qinzheng</u> , MH:	Wash and wave resistance of ships in finite water depth. (Dr.Ing. Thesis)
MTA-2002-154 <u>Melhus, Øyvin</u> , MM:	Utilization of VOC in Diesel Engines. Ignition and combustion of VOC released by crude oil tankers. (Dr.Ing. Thesis)
MTA-2002-155 <u>Ronæss, Marit</u> , MH:	Wave Induced Motions of Two Ships Advancing on Parallel Course. (Dr.Ing. Thesis)
MTA-2002-156 <u>Økland, Ole D.</u> , MK:	Numerical and experimental investigation of whipping in twin hull vessels exposed to severe wet deck slamming. (Dr.Ing. Thesis)
MTA-2002-157 <u>Ge, Chunhua</u> , MK:	Global Hydroelastic Response of Catamarans due to Wet Deck Slamming. (Dr.Ing. Thesis)
MTA-2002-158 <u>Byklum, Eirik</u> , MK:	Nonlinear Shell Finite Elements for Ultimate Strength and Collapse Analysis of Ship Structures. (Dr.Ing. Thesis)
IMT-2003-1 <u>Chen, Haibo</u> , MK:	Probabilistic Evaluation of FPSO-Tanker Collision in Tandem Offloading Operation. (Dr.Ing. Thesis)
IMT-2003-2 <u>Skaugset, Kjetil Bjørn</u> , MK:	On the Suppression of Vortex Induced Vibrations of Circular Cylinders by Radial Water Jets. (Dr.Ing. Thesis)
IMT-2003-3 Chezhian, Muthu	Three-Dimensional Analysis of Slamming. (Dr.Ing. Thesis)

IMT-2003-4 Buhaug, Øyvind	Deposit Formation on Cylinder Liner Surfaces in Medium Speed Engines. (Dr.Ing. Thesis)
IMT-2003-5 Tregde, Vidar	Aspects of Ship Design: Optimization of Aft Hull with Inverse Geometry Design. (Dr.Ing. Thesis)
IMT-2003-6 Wist, Hanne Therese	Statistical Properties of Successive Ocean Wave Parameters. (Dr.Ing. Thesis)
IMT-2004-7 Ransau, Samuel	Numerical Methods for Flows with Evolving Interfaces. (Dr.Ing. Thesis)
IMT-2004-8 Soma, Torkel	Blue-Chip or Sub-Standard. A data interrogation approach of identity safety characteristics of shipping organization. (Dr.Ing. Thesis)
IMT-2004-9 Ersdal, Svein	An experimental study of hydrodynamic forces on cylinders and cables in near axial flow. (Dr.Ing. Thesis)
IMT-2005-10 Brodkorb, Per Andreas	The Probability of Occurrence of Dangerous Wave Situations at Sea. (Dr.Ing. Thesis)
IMT-2005-11 Yttervik, Rune	Ocean current variability in relation to offshore engineering. (Dr.Ing. Thesis)
IMT-2005-12 Fredheim, Arne	Current Forces on Net-Structures. (Dr.Ing. Thesis)
IMT-2005-13 Heggernes, Kjetil	Flow around marine structures. (Dr.Ing. Thesis)
IMT-2005-14 Fouques, Sebastien	Lagrangian Modelling of Ocean Surface Waves and Synthetic Aperture Radar Wave Measurements. (Dr.Ing. Thesis)
IMT-2006-15 Holm, Håvard	Numerical calculation of viscous free surface flow around marine structures. (Dr.Ing. Thesis)
IMT-2006-16 Bjørheim, Lars G.	Failure Assessment of Long Through Thickness Fatigue Cracks in Ship Hulls. (Dr.Ing. Thesis)
IMT-2006-17 Hansson, Lisbeth	Safety Management for Prevention of Occupational Accidents. (Dr.Ing. Thesis)
IMT-2006-18 Zhu, Xinying	Application of the CIP Method to Strongly Nonlinear Wave-Body Interaction Problems. (Dr.Ing. Thesis)
IMT-2006-19 Reite, Karl Johan	Modelling and Control of Trawl Systems. (Dr.Ing. Thesis)
IMT-2006-20 Smogeli, Øyvind Notland	Control of Marine Propellers. From Normal to Extreme Conditions. (Dr.Ing. Thesis)
IMT-2007-21 Storhaug, Gaute	Experimental Investigation of Wave Induced Vibrations and Their Effect on the Fatigue Loading of Ships. (Dr.Ing. Thesis)
IMT-2007-22 Sun, Hui	A Boundary Element Method Applied to Strongly Nonlinear Wave-Body Interaction Problems. (PhD Thesis, CeSOS)

IMT-2007-23 Rustad, Anne Marthine	Modelling and Control of Top Tensioned Risers. (PhD Thesis, CeSOS)
IMT-2007-24 Johansen, Vegar	Modelling flexible slender system for real-time simulations and control applications.
IMT-2007-25 Wroldsen, Anders Sunde	Modelling and control of tensegrity structures. (PhD Thesis, CeSOS)
IMT-2007-26 Aronsen, Kristoffer Høye	An experimental investigation of in-line and combined in-line and cross flow vortex induced vibrations. (Dr.avhandling, IMT)
IMT-2007-27 Zhen, Gao	Stochastic response analysis of mooring systems with emphasis on frequency-domain analysis of fatigue due to wide-band processes. (PhD-thesis CeSOS).
IMT-2007-28 Thorstensen, Tom Anders	Lifetime Profit Modelling of Ageing Systems Utilizing Information about Technical Condition. Dr.ing. thesis, IMT.
IMT-2008-29 Berntsen, Per Ivar B.	Structural Reliability Based Position Mooring. PhD-Thesis, IMT.
IMT-2008-30 Ye, Naiquan	Fatigues Assessment of Aluminium Welded Box stiffener Joints in ships. Dr.ing.-Thesis, IMT.
IMT-2008-31 Radan, Damir	Integrated Control of Marine Electrical Power Systems. PhD-Thesis, IMT.
IMT-2008-32 Norum, Viggo L.	Analysis of Ignituin and Combustion in Otto Lean-Burn Engines with Prechambers. Dr.ing. thesis, IMT.
IMT-2008-33 Pákozdi, Csaba	A Smoothed Particle Hydrodynamics Study of Two-dimensional Nonlinear Sloshing in Rectangular Tanks. Dr.ing.thesis, IMT.
IMT-2008-34 Grytøy, Guttorm	A Higher-Order Boundary Element Method and Applications to Marine Hydrodynamics. Dr.ing. Thesis, IMT.
IMT-2008-35 Drummen, Ingo	Experimental and Numerical Investigation of Nonlinear Wave-Induced Load effects in Containerships Considering Hydroelasticity. PhD-Thesis. CeSOS.
IMT-2008-36 Skejic, Renato	Maneuvering and Seakeeping of a Singel Ship and of Two Ships in Interaction. PhD-Thesis. CeSOS.
IMT-2008-37 Harlem, Alf	An Age-Based Replacement Model for Repairable Systems with Attention to High-Speed Marine Diesel Engines. PhD-Thesis, IMT.

IMT-2008-38 Alsos, Hagbart S.	Ship Grounding. Analysis of Ductile Fracture, Bottom Damage and Hull Girder Response. PhD-thesis, IMT.
IMT-2008-39 Graczyk, Mateusz	Experimental Investigation of Sloshing Loading and Load Effects in Membrane LNG Tanks Subjected to Random Excitation. PhD-thesis, CeSOS.
IMT-2008-40 Taghipour, Reza	Efficient Prediction of Dynamic Response for Flexible and Multi-body Marine Structures. PhD-thesis, CeSOS.